School of Pharmacy
Division of Molecular Therapeutics and Formulations

Evaluation of lipid liquid crystalline phase particles as drug delivery vectors
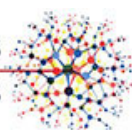
Rachael M. Xerri BSc.

March 2021

Thesis submitted to the University of Nottingham
for the degree of
Doctor of Philosophy

CRODA

CDT in Advanced Therapeutics
and Nanomedicines

Abstract

Lipids, of the glyceride sub-species, are amphiphilic molecules that will self-assemble in aqueous conditions. Based on the lipid's critical packing parameter (CPP), i.e., the ratio between the lipid tail length, tail volume and the lipid head area, the lipids may self-assemble into different liquid crystalline phases, such as lamellar or cubic phases. Such phases may then be stabilised into discrete nanoparticles in an aqueous suspension through the utilisation of a polymer, namely here poloxamers. These stabilised liquid crystalline particles have many of the advantages of liposomes (one of the most used lipid nanoparticle formulations) such as biocompatibility and the ability to encapsulate both hydrophobic and hydrophilic moieties. Liquid crystalline phases additionally offer an improved stability of the formulation's physicochemical properties and API stability during storage and *in vivo* compared to other lipid nanoparticle formulations; increasing the shelf-life of formulations and offering a wide variety of formulation administration strategies i.e. intravenous, intramuscular, oral. The primary types of liquid crystalline phases found within the literature, particularly for pharmaceutical applications, are cubosomes and hexasomes, formed from cubic phases and hexagonal phases respectively.

Explored here is the ability of liquid crystalline phase nanoparticles to encapsulate various active pharmaceutical ingredients (APIs) for drug delivery applications. Initial studies focused on the development of a robust formulation, examining both on the utilisation of the biocompatible lipid glycerol monooleate, and the commonly used poloxamer polymer. The development of a novel particle

fabrication protocol, based on controlled mixing of the formulation's constituent components, that could forego the use of high energy techniques, or the utilisation of a solvent was undertaken and achieved. Upon the establishment of this base formulation (utilising glycerol monooleate (Cithrol^{TM}) and poloxamer 407 (Synperonic^{TM} F127) in a water suspension) the focus moved towards the encapsulation of a range of active pharmaceutical ingredients (including Amitriptyline, Imipramine, Progesterone, Hydrocortisone, Budesonide and Propofol).

15 different APIs were encapsulated into the base formulation. These new formulations were then evaluated by high performance liquid chromatography for their encapsulation efficiency (EE); this varied greatly, with the highest EE being observed for Amitriptyline where an EE of 96.4% was achieved. Pearson regressing analysis of API loading showed an increased loading could be achieved with a lower API molecular weight, polar surface area and a lower number of hydrogen bonding capabilities. API release was also evaluated, in these studies it was found that liquid crystalline phases exhibit a staggered release of APIs. No significant trend could be identified between APIs and their rate of release, however a potential link between API release and the API's logD has been found during comparison of API release profiles.

Final investigations explored the impact of API loading upon the liquid crystalline phase as early studies revealed a confirmation shift in the liquid crystalline phase to phases existing with a lesser curvature upon the incorporation of an API, as displayed by a shift from an inverse hexagonal phase to an inverse cubic phase, as

observed by small angle x-ray scattering and cryo-transmission electron microscopy. The degree of API loading altered the packing, it was found that with an increased concentration of API within the system a greater change in the critical packing parameter was observable. However, this degree of change was also dependent upon the physicochemical properties of the API. Analysis was performed comparing the different physicochemical properties of APIs and how this effected the packing of components within the formulation. Here it was found that an APIs LogS, polar surface area and API loading had significant influence upon the liquid crystalline phase structuring. The liquid crystalline structure and changes within it can be analysed with cryo-transmission electron microscopy, with allows the visualisation on the nano-scale of a particle's morphology, structuring, and size; or, by small angle x-ray scattering which allows in-depth characterisation of the lipid phase behaviour.

Acknowledgements

I would like to thank my supervisors, Snow Stolnik, Mischa Zelzer, Giuseppe 'Beppe' Mantovani, Paul Smith, James Humphry, and Steve Mellor. You each contributed so much to this journey and gave me some great stories to tell. Thank you David Scurr, you were part of my whole PhD journey, thank you for being the way you are and for the support you gave.

Croda have been a fantastic sponsor throughout this project. I would thank both Croda and the healthcare team for their support of the project and support in my personal development. I could not have asked for a better industrial sponsor.

I would like to thank the CDT family. You all supported me when I needed it and gave me some great memories. Thank you to all of those at the University of Nottingham and Boots Science Building for the support and friendship. To those at the University of Bristol, particularly Chris Brasnett and Dr Annela Seddon for all the support in SAXS studies. To Chris Parmenter and all those who supported me at the NMRC, thank you, your friendship and tutelage made me a half decent microscopist. We shared so much joy and so many headaches sat in the dark with the microscope. A special mention to the Diamond team, Mischa, Oran, there were some strange conversations at 2 am but it was definitely a highlight of my PhD! Claudia, you are one in a million, you gave fantastic support and meaningful friendship.

I would like to thank all my family for all their support, especially my mum whom without a doubt deserves a lot of the credit for me starting and being able to pursue this PhD journey. Grandad, thank you for all the tips, Grandma, thank you for telling Grandad to shut up. Boo, thanks for the competition to be the highest achieving sibling, encouraging me to do a PhD.

Of course, I couldn't not mention Buster, Bewsa, Nejna and Xaghra; thank you for keeping me sane. Ich glaube, ich spinne!

Contents

Abbreviations

ADME   -   Absorption, Distribution, Metabolism and Excretion

API   -   Active pharmaceutical ingredient

CPP   -   Critical packing parameter

Cryo-TEM   -   Cryo transmission electron microscopy

DLS   -   Dynamic light scattering

DOMA   -   Dioctadecyldimethylammonium bromide

DOPC   -   1,2-Dioleoyl-sn-glycero-3-phosphocholine

DOPE   -   1,2-Dioleoyl-sn-glycero-3-phosphoethanolamine

DOPS   -   1,2-Dioleoyl-sn-glycero-3-phospho-L-serine

EE   -   Encapsulation efficiency

EO (PEO)   -   (Poly) Ethylene oxide

F   -   Flake

FFT   -   Fast Fourier Transform

GMO   -   Glycerol monooleate

H_{II} -   Inverse hexagonal phase

HP   -   High purity

I.M.   -   Intramuscular

I.V.   -   Intravenous

Ia3d	-	Gyroid cubic phase
Im3m	-	Primitive cubic phase
L	-	Liquid
LC	-	Liquid crystalline
LNP	-	specific abbreviation given in the literature for RNA lipid nanoparticles
mL	-	Millilitre
mM	-	Milli molar
MWCO	-	Molecular weight cut-off
nm	-	Nanometre
P	-	Paste
PEG	-	Polyethylene glycol
Pn3m	-	Double diamond cubic phase
PO (PPO)	-	Poly (propylene oxide)
RES	-	Reticuloendothelial System
RNA	-	Ribonucleic acid
SAXS	-	small angle x-ray scattering
SF127	-	Synperonic^{TM} F127
siRNA	-	Small interfering RNA
^{TM}	-	Trademark

Chapter 1: Introduction

Including the aims and objectives

1. Introduction

Glycerol monooleate (GMO) is a simple lipid with interesting capabilities in forming liquid crystalline phases. It consists of a single eighteen-carbon fatty acid chain attached to a glycerol head group. The relative size of the head group and tail and the molecule's amphiphilic nature allow this lipid to self-assemble into a variety of lyotropic liquid crystalline phases upon mixing with water. These include the diamond cubic, gyroid cubic, lamellar, and inverse hexagonal phases. The use of additives additional to the GMO allows five additional phases to be formed: bicelles, vesicles, primitive cubic, micellar cubic and sponge phases (1). These liquid crystalline phases may be stabilised into nanoparticle suspensions through the utilisation of a stabiliser; the most common stabiliser is poloxamer 407, often referred to by its trademarked names: Pluronic™ F127 or Synperonic™ F127.

In pharmaceutical research liquid crystalline phase particle research is gaining momentum due to its increased loading potential of hydrophobic/lipophilic active pharmaceutical ingredients (API) and greater stability as compared to non-internally ordered/structured lipid nanoparticles i.e., liposomes and micelles. Further benefits of these particles are their size and ability to enhance API delivery, permeation, and retention, allowing for a more efficacious formulation (2–4).

New API molecules are constantly being proposed for a variety of diseases; this in combination with the pre-existing library of APIs offer enormous potential to treat the many known diseases. Unfortunately, many of these APIs never reach the clinic due to inherent instabilities, propensity to degrade or be destroyed *in vivo*, poor

solubility, off target side effects and more. Some of these API limitations are detailed as follows:

- **API metabolised or degraded prior to therapeutic effect** – enzymes within the body may metabolise specific bonds within the chemical structure of the API, e.g., esterase and protease enzymes may hydrolyse ester bonds. Alternatively, the pH range an API may be exposed to is broad, for example orally delivered APIs may be exposed to a pH range of 1.0 to 7.5 within the gastrointestinal tract (5); this could alter, or degrade, the API chemical structure detrimentally, leading the API to have a decrease or loss in therapeutic activity.

- **Inappropriate distribution of API within the body** – most drug targets will be localised to a defined region of the body, e.g., the tumour microenvironment. Non-encapsulated APIs have the potential to be distributed throughout the body via the cardiovascular network or the lymph system. Because of this, often the dose at the site of action is a fraction of the dose administered, with fractions of the initial dose being distributed throughout much of the body. Potentially resulting in off-target side-effects (6).

- **Inability to formulate** – this may be due the API being insoluble e.g., biopharmaceutics classification system (BCS) classes II and IV or having a poor stability in biocompatible suspension media.

To overcome these limitations a range of strategies have been used:

- The use of prodrugs can both improve the ability to formulate a drug and/or improve the pharmacokinetics and bioavailability of the drug. Put simply a prodrug is a precursor to the active drug molecule, the prodrug may then

undergo conversion within the biological environment into its active form. A prodrug may be used to improve the solubility of drugs by adding some polar moieties. Alternatively the additional moieties may be utilised for increasing drug targeting or decreasing toxicity within the body (7).

- The use of a **targeting motif** attached directly to the drug (as with prodrugs), or more commonly the drug may be designed in such a way as to innately target a specific organ or tissue without an additional prodrug type modification (8,9) .

- **Administration directly** to the desired site via injection, localised administration of a bulk phase/cream, or microneedle administration (10–13).

- Use of **nanoparticles**, including:

  - Iron-oxide nanoparticles

  - Gold nanoparticles

  - Silica nanoparticles

  - Polymeric nanoparticles

  - Lipid nanoparticles (14)

Of these strategies it is the lipid nanoparticle route is to investigate further as a delivery medium for APIs requiring a vehicle for delivery to the site of action.

1.1. <u>Lipid Nanoparticles</u>

Lipids, known commonly as fats, are biomolecules of great utility in the realm of pharmaceuticals and biologics. They have a host of biological functions including

energy storage, cell signalling, and as structural components, such as in cell membranes. Most lipid nanoparticles form via self-assembly.

Lipid self-assembly is the process in which amphiphilic molecules may orientate with each other (when above the critical micellar concentration), based primarily on hydrophobic and hydrophilic interactions, to form kinetically favourable structures when in an aqueous environment. Hydrophobic regions of the molecules, i.e., lipid tails, will pack together through Van der Waals interactions, whilst the hydrophilic regions of the molecules, i.e., the lipid head groups, will preferentially face the aqueous environment, in turn shielding the hydrophobic regions.

Nanoparticles are considered by International Union of Pure and Applied Chemistry (IUPAC) to be a particle sub 500 nm in diameter; it is this size that affords nanoparticles their desirable properties for drug delivery. This is because size modification, as well as parameters such as nanoparticle surface charge can be utilised for passive organ targeting (15). When comparing a bulk lipid phase, and a nanoparticle form of the same phase, the particle form has a vastly larger surface area to volume ratio. This property may allow rapid diffusion of substance out of the nanoparticles (16,17).

In respect of nanoparticle utilisation within pharmaceutical research lipid nanoparticles have been used for therapeutic treatment (next section) and as a tool for diagnostics. Diagnostic examples focus on cancer diagnostics with liposomes being radiolabelled or loaded with imaging agent, these liposomes may accumulate at tumour sites via the enhanced permeation and retention of the tumour microenvironment (18,19). Additionally, lipid nanoparticles can be utilised for active targeting using an external targeting motif, this can be advantageous when trying to

deliver the imaging agent, or indeed an API, to a particular cell line with a unique molecule on its cell membranes surface. One such example of this is the work of Parhiz *et al.*, they functionalised lipid nanoparticles with a platelet-endothelial cell adhesion molecule. This functionalisation enhanced the formulations localisation by 200 times, and increased subsequent luciferase transfection by 25 times (20).

1.1.1. Lipid Nanoparticle Drug Delivery

Lipid nanoparticles for drug delivery applications is an emerging field. Although not the first lipid formulation to be approved, the first liposome formulation, Doxil®, was approved by the FDA in 1995 for the treatment of cancer(21). This formulation offered a prolonged circulation time of the API (doxorubicin) and avoidance of the RES due to the use of PEGylated particle surface. The formulation also achieved high and stable remote loading of doxorubicin and showed enhanced API release at the tumour site (21,22). In more recent applications mRNA lipid nanoparticles (LNPs) have been used in the field of vaccines. Most notably as part of the RNA based SARS-CoV-2 vaccines developed by BioNTech and Moderna, of which regulatory approval has been granted (23,24). The LNPs enable the delivery of mRNA and modRNA which otherwise may be degraded by RNAses, or other factors present *in vivo,* such as changing pH. Furthermore, the LNPs are biocompatible and so do not have an adverse effect on healthy cells. LNPs are formed of ionizable lipids, helper lipids and cholesterol; these lipids in combination with RNA will form an amorphous core with RNA pockets, encapsulated by an ordered lipid bilayer membrane. The primary issue reported with LNPs is an instability, hence a long-term stability (i.e. longer than 1 month) requirement to store the LNP formulations at -80˚C (23,25).

The Doxil® and coronavirus vaccine examples of lipid nanoparticle formulations are the most prominent and well known within the field, but they are not exclusive. Many other formulations exist because of the following benefits:

- **Biocompatibility** – lipids are common biomolecules, with many lipids being degradable due to the hydrolysis of ester bonds, allowing for the degradation of lipid nanoparticles. Lipids may then be converted into a smaller, useable molecule (e.g., acetyl coenzyme A) or incorporated within biological structures (e.g., cellular membrane), finally to be excreted via the liver and kidneys (26,27).

- **Appropriate size** – the technology which is utilised in the production of lipid nanoparticles allows for the manipulation of the particle size and size distribution. Common methods of manipulation include sonication and extrusion, both of which can decrease the distribution of particle size, as well as target a desired size by altering the method parameters. The review of Samaridou *et al*. (15) discusses the importance of lipid nanoparticle size on particle distribution and size very well; to summarise: particles of size below 110 nm are required for I.V. administration (28). When examining particle sizes between 80 – 360 nm smaller particles preferentially went to the liver whilst larger particles were uptake by macrophages (29). This particle distribution based on size can be utilised for passive organ targeting.

- **Drug loading** – due to glyceride-type lipids being amphiphilic molecules, when they arrange into an ordered structure to form a nanoparticle, hydrophobic regions, and contrasting hydrophobic region are formed, enabling the loading of both hydro-phobic and –phillic APIs to be loaded within their structure.

Unlike the commercial lipid nanoparticle formulations such as liposome, LNP and micelle formulations, internally structured lipid particles offer many advantages. Internally structured particles contain an ordered internal organisation of lipid molecules. The following advantages of internally structure lipid nanoparticles have specifically been reported for cubosome and hexasome internally structured liquid crystalline particles.

- **Stability during storage** – when being stored at room temperature there have been reports of particles being stable for prolonged periods of time, e.g. 4 weeks (30) and 3 months (31,32)

- **Increased drug loading compared to liposomes**– particularly of poorly soluble APIs (33). Similarly, to all other lipid nanoparticles there is the potential for hydro-phobic/-phillic drug loading; however, due to the internal structuring there is a larger area of hydrophobic structuring, and with this comes an increased potential for hydrophobic drug packing compared to hollow particle formulations, such as liposomes.

- **Ability to encapsulate and deliver large APIs** – a diverse range of molecules have been encapsulated within liquid crystalline particles, including peptides and RNA (34–36).

- **Stability within the gastrointestinal tract** – of great utility to the pharmaceutical field is the observed potential of internally structured nanoparticles to be utilised in oral drug delivery (37,38). Oral drug delivery has a higher patient compliance as compared with injectable and intravenous administration and can negate the requirement of a health care professional for formulation administration.

- **Enhanced permeation of APIs through mucosal and skin membranes** - for dermal, transdermal and transmucosal delivery (39,40).

Further detail on the nature of cubosome and hexasome particles is discussed in the following sections.
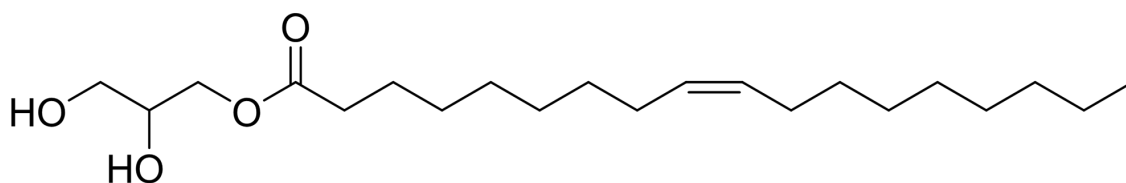
1.1.2. Glycerol Monooleate (GMO)

Figure 1.1.1: Chemical structure of glycerol monooleate (GMO). Formula: $C_{21}H_{42}O_4$; Molar mass: 358.57 g/mol; Density: 970 kg/m³; Solubility in water: Insoluble. The region on the left is the hydrophilic head group, and the fatty acid chain on the right being hydrophobic, as such this is an amphiphilic molecule.

Glycerol monooleate (Figure 1.1.1), chemically named 1-(cis-9-Octadecenoyl)-*rac*-glycerol, and otherwise commonly known as monoolein and monooleate, is the primary base component in a majority internally structured lipid nanoparticles (4,41,42). GMO is not the only lipid used in the literature, phytantriol is a common alternative, it may be the molecule of choice for several reasons:

- **Enzymatically degradable,** via lipolysis by esterase enzymes which cleave GMO at the ester bond. GMO has been shown to be a substrate of lipase enzymes (43).

- **Prior use** in cosmetic, food and pharmaceutical products (44).

- **Readily available**, with multiple vendors (e.g., Sigma-Aldrich, Alfa Chemistry, and Croda).

- **Biocompatible**, GMO does not elicit an immune response (45).

Alternatively, to GMO the synthetic molecule phytantriol has been used as the primary component to form liquid crystalline phases. Phytantriol and GMO are analogous to each other within the formulations in the literature, however only one experimental paper was found to show a direct comparison (46).
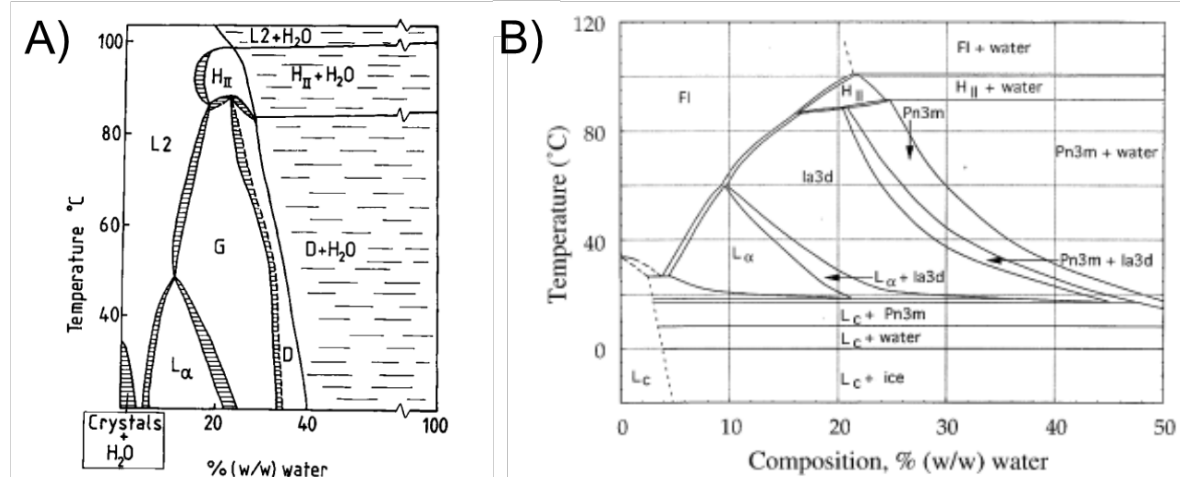

Figure 1.1.2: Example liquid crystalline phase diagrams for glycerol monooleate; both diagrams indicate a phase assignment per a specific water to glycerol monooleate ratio at a designated temperature. A) In this diagram: G denoted gyroid, D denotes diamond, Lα denotes lamellar phase, HII denotes [inverse] hexagonal phase and L2 denotes inverse micellar phase (47). B) In this diagram Lc denotes lamellar crystalline, Lα denotes lamellar liquid crystalline, Ia3d denotes gyroid cubic phase, Pn3m denotes diamond cubic phase, HII denotes [inverse] hexagonal and Fl denotes fluid isotropic (48) Differences can be seen at the phase boundaries (i.e. phase transitions being

reported to occur at different temperatures), this may be due to different purity profile of the glycerol monooleate or differences in the methodology.

It is the amphiphilic nature of GMO that is the principal factor that leads to its desirability for use in assembling lipid structures i.e., lipid nanoparticles. The inter-molecular interactions between the polar and non-polar regions of the GMO molecule led to its self-assembly into different phases (Figure 1.2.3), which may exist as a bulk phase or as discrete particles. The nature of this phase is highly dependent on the conditions of formation, including the temperature and solvent composition. Some evidence of this is illustrated in Figure 1.1.2 where changes can be observed based on the temperature and percentage presence of water. Of the phases detailed there are two key types of phase that have been identified in the literature with some frequency in respect to the pharmaceutical field, but not limited to: inverse hexagonal phase particles, dubbed hexasomes; and cubic phase particles (Figure 1.2.3 and Figure 1.2.4), dubbed cubosomes, these particles have differentiating properties and characteristics, as discussed in the following Sections 1.2.1 and 1.2.2.

1.2. Internally Structured Lipid Nanoparticles

Glyceride-type lipid molecules primarily form into multi-molecule self-assembled structures due to the hydrophilic and hydrophobic interactions amongst the head groups and tail groups of the lipids. Depending on the cross-sectional area of the head and tail groups a multitude of different structures can be formed. If the head group and tail group have the same structural width then the resulting mesophase structure will have no curvature, leading to the formation of a 'flat' bilayer, or lamellar

phase. However, often the lipid molecules have unequal head to tail widths; when these lipids then interact to form a mesophase structure there is a resulting curvature (Figure 1.2.1). The mesophase curvature can be predicted numerically through the critical packing parameter (Figure 1.2.2) and can lead to the formation of an array of liquid crystalline phases/structures (Figure 1.2.3), as well as a variety of different particles (Figure 1.2.4). Liquid crystalline is the term given to the mesophase that sits between the liquid and solid crystalline phases. Liquid crystalline phases will flow like liquids, yet the molecules within may orientate themselves in a crystal-like manner. There are three subcategories of liquid crystals, thermotropic, metallotropic and lyotropic (49). Lipid liquid crystalline phases fall under the definition of lyotropic. Lyotropic LCs undergo phase transitions as a function of the temperature and concentration of the liquid-crystal molecules in their solvent (i.e., water) (1,50,51).
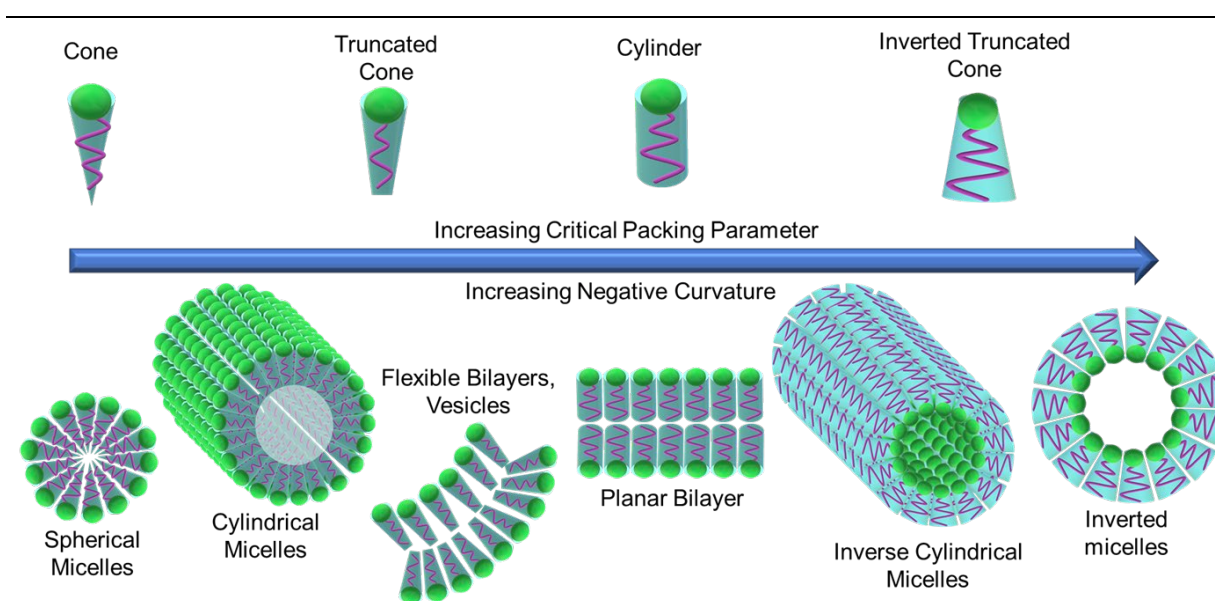

Figure 1.2.1: Schematic showing the variance in structure produced by lipids with varying head to tail ratios. This shows the importance of the lipid molecule morphology on the resultant phase formed. Figure inspired by Kulkarni *et al.*, 2011(1)**.**
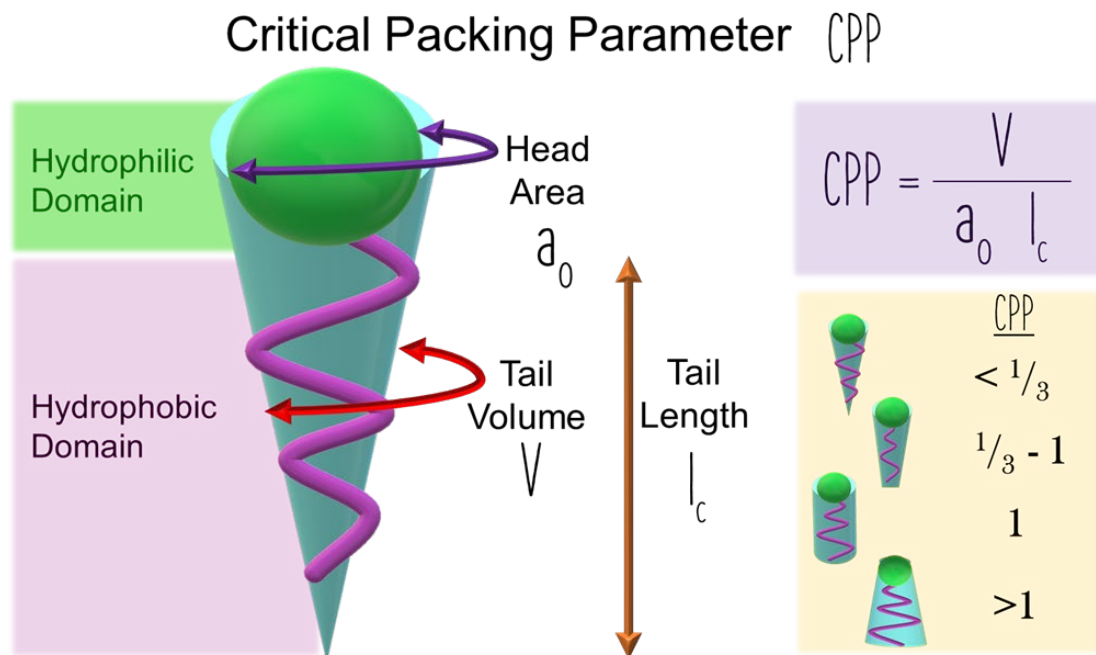
Figure 1.2.2. Overview of the critical packing parameter (CPP) calculation. CPP is determination through the relationship between tail length, tail volume and head group area of an amphiphilic molecule.
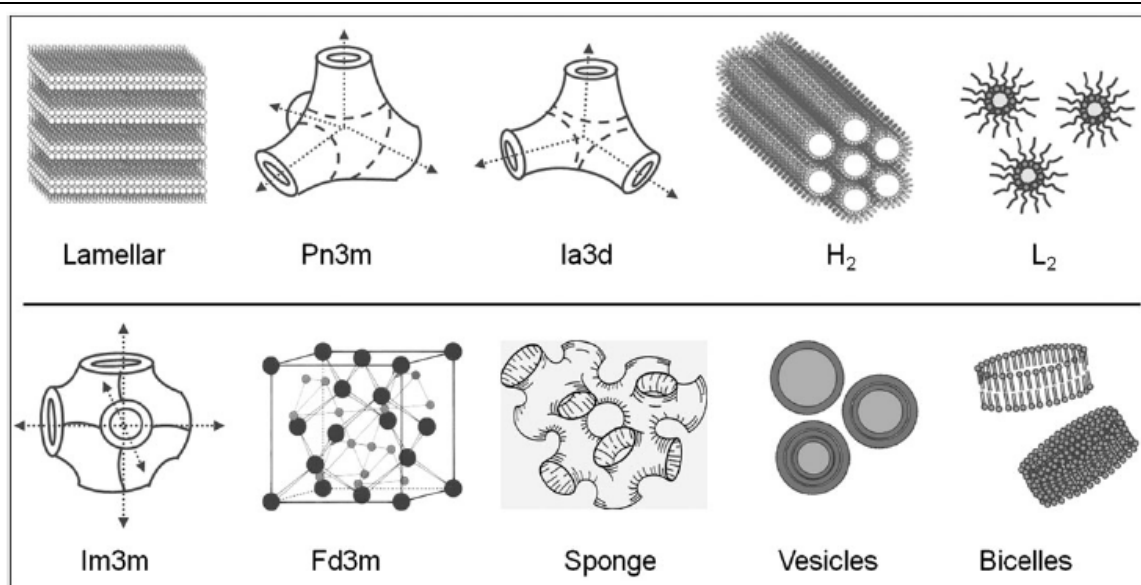
Figure 1.2.3. Depictions of the phases/structures which glycerol monooleate can form. The top five phases can be formed solely by glycerol monooleate and water. The bottom five however contain phases which require glycerol monooleate, water, and an additive. Image taken from Kulkarni *et al*., 2011(1).

The manufacturing of liquid crystalline formulations focuses upon the self-assembly of the constituent components, primarily through hydrophobic and hydrophilic interactions. The manufacturing protocols within the literature can be sub-categorised into top-down and bottom-up (52). In the top-down process a bulk liquid crystalline phase is formed, then dispersed into a nanoparticle suspension. This dispersion uses high energy, high shear methods that have two disadvantages, the first being scalability; for examples the use of ultrasonication has been used (52,53), this technique is currently not available for large-scale pharmaceutical manufacturing. The second disadvantage is that such high energy methods could be highly damaging to APIs, in particular biological APIs. The bottom-up manufacturing protocols, also known as the hydrotrope method, disperses the consitiuent

components in a hydrotrope, typically ethanol, and then this solution will be

combined with an aqueous phase to enable a nucleation type assembly of the liquid

crystalline structure (35,52,54). Disadvantages with the hydrotrope protocol lie in the

requirement for a solvent. This solvent must be safe *in vivo*, and/or be removed

depending on the final hydrotrope concentration. There may be scalability concerns

also due to the use of potentially high volumes of volatile solvents. The final

consideration is how a hydrotrope may interact with an API. Some APIs may be

degraded by hydrotrope solvent or may be insoluble with either the hydrotrope or

aqueous phase – resulting in an inability to formulate such APIs. The disadvantages

of both the top-down and bottom-up manufacturing route for liquid crystalline

particles limit the progression of these formulations to a large-scale clinical setting.

Work to overcome these limitations and more background as to the manufacturing

protocols within the literature is discussed in Chapter 3.

The characterisation of liquid crystalline particles is alike to lipid nanoparticles.

The most common and high throughput characterisation techniques are sizing

techniques utilising light scattering; this includes dynamic light scattering (DLS) and

(semi-high throughput) nanoparticle tracking analysis (NTA) (55,56). However, such

techniques only provide fundamental information about size distribution profiles.

More advanced techniques are typically required for liquid crystalline particle

analysis to attain an understanding of the liquid crystalline structure. The two primary

techniques for this are cryo-TEM and SAXS (57,58).

Electron microscopy is a technique in which one may visualise a sample or

feature by way of detecting changes in the electron density at the detector, once said

electrons have passed through (transmission) or been reflected off a sample

(scanning). Within the categories of scanning and transmission there are again more

variations that enable the acquisition of different data or can enable the visualisation of different samples.

Cryogenic electron microscopy (cryo-EM) techniques are becoming increasingly more common within the literature due to overcoming some of the limitations of more general electron microscopy. In cryo-EM the water within a sample remains *in situ*, whilst in non-cryogenic microscopy the water is removed from samples. Maintaining water *in situ* is vital in the imaging of many types of lipid and amphiphilic self-assembled nanoparticles; this is because the presence of water is required to maintain the hydrophobic-hydrophilic interactions to maintain the particle structure (59). The most used cryo-EM method for lipid nanoparticles and liquid crystalline phases is cryo-transmission electron microscopy (Cryo-TEM). Cryo-TEM of lipid nanoparticles typically achieves a maximum resolution or 1 to 5 nm (60), with a dependence upon the instrument and sample. Some sample limitations include sample degradation from the electron beam and/or the sample being too thick on the grid for the electron beam to pass through. In respect to liquid crystalline phases, it is possible to elicit information about the 2-dimensional particle shape, particle size, sample homogeneity (in terms of all mentioned characteristics), and crucially, it may provide information about the liquid crystalline phase. Cryo-TEM is one of the few techniques that achieves the sub-5 nm resolution required to observe liquid crystalline phases, and in some cases, identify which phase is present.

Furthermore, with the use of a fast Fourier transform (FFT) it is possible to condense the structural information over a designated area of a cryo-TEM micrograph into repeating units of structure. Generally, the literature reports distances of repeating structure (also known as d-spacing) in liquid crystalline phases to be 5 – 20 nm (61–63). The pattern of an FFT can then subsequently be

used to determine the phase identity, but also the d-spacing. The d-spacing is the distance between repeating units of structure. Further to the use of cryo-TEM, cryo-electron tomography (CET) has been used for cubosome characterisation. CET is a highly advanced characterisation technique which utilises cryo-TEM to image structures/particles from multiple orientations. These images are then resolved to generate a 3-dimensional structure of superior detail to stand alone cryo-TEM techniques (64). An addition cryo-EM technique used in the literature to generate 3-dimensional images is cryo-field emission scanning electron microscopy (Cryo-FESEM). This technique has been used to show spinning top conformations/outer morphologies of hexasomes, however a lower resolution is achieved compared to cryo-TEM and CET (65–67). Furthermore, no detail as to the nature of the liquid crystalline phase within the particle is attainable with cryo-FESEM or other SEM techniques.
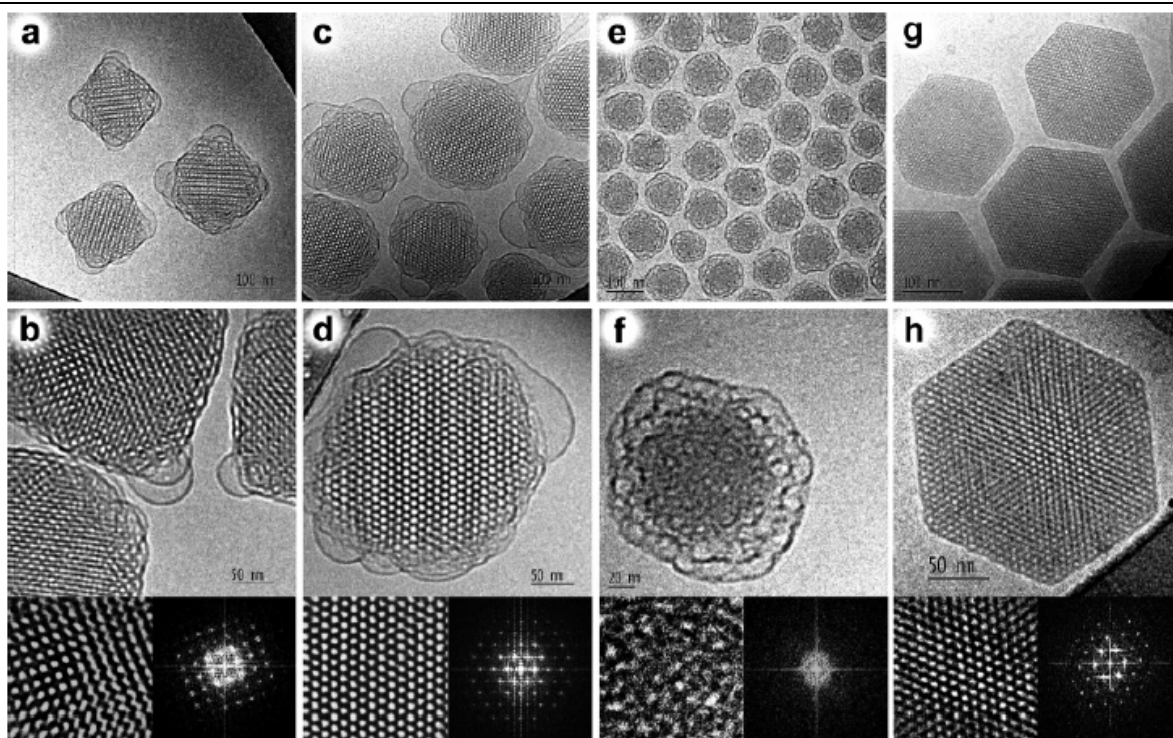
Figure 1.2.4: Cryo transmission electron microscopy images of selected lipid liquid crystalline phase nanoparticles (60). A-D show cubosomes, E and F show spongisomes, G and H show hexasomes.

To identify the specific liquid crystalline phase formed small angle x-ray scattering is typically performed. This technique directs an x-ray beam through a sample, which is scattered by liquid crystalline structure, it is this scattering which is recorded by a detector and translated into a scatter plot. Ordered structures produce distinct scattering patterns which are well known in the literature and are displayed in Figure 1.2.5. SAXS is further discussed in Chapter 5.
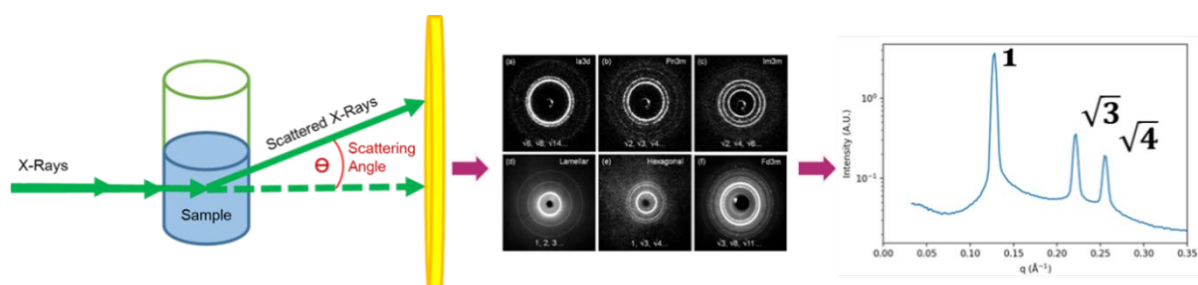
Figure 1.2.5: X-ray scattering patterns for structured lipid liquid crystalline phases. Typically, a cross section of these patterns is taken of intensity against a measure of distance, which is a function of the scattering angle, to form a XY graph. The rings of intensity translate as Bragg peaks on this graph, with the peak spacing ratio assignments being displayed in conjunction with X-ray scattering detector images. The SAXS the detector patterns are taken from (1).

An additional characterisation technique includes polarising light microscopy (16,68). This technique is not appropriate for all types of liquid crystalline phases, for example due to the birefringence of cubic phases polarising light microscopy will not reveal structural information, however this technique is compatible with hexagonal phases. Many other techniques have also been used within the literature for liquid crystalline characterisation but the forementioned are the most common and valuable in direct characterisation of the particle's properties.

Many lipid nanoparticle structures can be formed solely through the singular, such as eggPC liposomes (69), or dual use of lipid species, such as RNA lipid nanoparticles (LNP) which utilise cationic lipids, helper lipids, cholesterol, and the RNA payload (23). (e.g., cholesterol is utilised in liposome formulations to increase stability (70)) The utilisation of multiple lipid species in the RNA LNPs facilitates

factors such as RNA encapsulation and facilitates the formation of stable, spherical particles. Similarly, there may be the requirement for additional chemical species, either to form one of the specific liquid crystalline structures, to stabilise the structure into nanoparticles, to aid API encapsulation, or a combination of said reasons. The primary, or most used lipid in the formation of lipid liquid crystalline particles is glycerol monooleate (GMO), which has the innate ability to form liquid crystalline phases. These phases will then require the use of an additional polymeric species to stabilise the phase into discrete nanoparticles (71), the use of non-polymeric stabilising entities is rare and discussed later. Commonly used for this purpose are polyethylene oxide–polypropylene oxide–polyethylene oxide (PEO-PPO-PEO) tri-block copolymers. These are known under a variety of names: chemically as poloxamer, under the BASF trademark as Pluronic™, and under the Croda trademark as Synperonic™. Forthwith, in this thesis these copolymers shall be referred to as Synperonic due to Croda being the supplier of the polymer to be used.

The described internally structured liquid crystalline particles may be used in their bulk form. There are some limitations when using a bulk phase as opposed to a particle suspension/emulsion. When comparing a bulk lipid phase, and a nanoparticle form of the same phase, the particle form has a vastly larger surface area to volume ratio. This property may allow rapid diffusion of substance out of the nanoparticles (16,17). To consider further is the application of the material, bulk liquid crystalline phase materials are highly viscous (17) and so this may limit their application in the field of drug delivery, for example they may be used for a topical application, however, they would be unsuitable for I.V or I.M. administration. I.V. and I.M. administration would enable the treatment of systemic diseases or the treatment of diseased tissues that are not surface accessible, for example a tumour in the

pancreas or a diseased heart. This rationale would apply to the choice to focus the efforts here on the particle forms of the liquid crystalline phases and not the bulk phases i.e. cubosomes rather than bulk cubic phases.

It is of note that within the literature some refer to liquid crystalline particle formulations being emulsions (17,72) with others referring to the formulations as suspension (38,73), and others as dispersions (33,74). Emulsions are defined as a liquid disperse systems in which the dispersed phase is composed of a liquid distributed throughout a vehicle in which it is immiscible. However, liquid crystalline phases sit in the boundary between a liquid and a (solid) crystal phase; therefore, formulations may also be described as a suspension. A suspension is defined in simple terms as a dispersion or a solid material in a liquid phase. A dispersion is defined as one substance (with one phase) is dispersed within another substance or phase (75). The categorisation of a liquid crystalline particle system as a dispersion is indeterminate due to the water channels, the liquid crystalline phase is not discrete from what would be the dispersion medium and so it is unclear if a liquid crystalline particle formulation would meet the definition of a dispersion. Therefore, given the ambiguity within the literature I have therefore selected to use the term suspension.
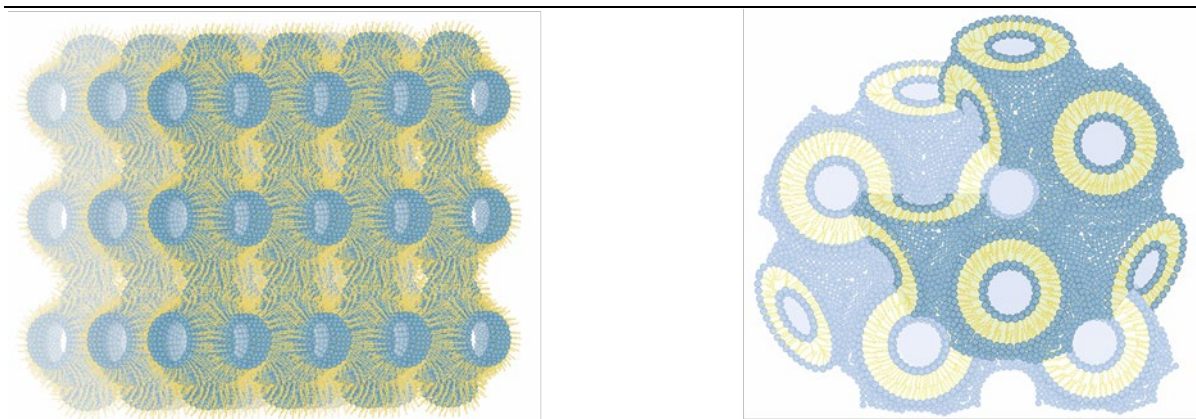
1.2.1. Cubosomes

Figure 1.2.6. Primitive (left) and diamond (right) cubic phases. Blue regions represent the hydrophilic head groups of the lipids; the yellow regions represent the hydrophobic tails of the lipids.

Cubosomes are dispersed cubic phase formed either *via* the self-assembly of its base components, or via the dispersion of a bulk cubic phase into a suspension medium. Although a relatively new field of study, with what is considered the founding paper being published in 1989 by K. Larsson (50), this paper is highly cited in the field and introduced liquid crystalline phases and GMO as a lipid capable of forming such liquid crystalline phases.

A cubic phase can be subcategorised into several different cubic phases, each with a discrete difference in their 3D conformation. These include the bicontinuous cubic phases: diamond (Pn3m), primitive (Im3m), gyroid (Ia3d) (Figure 1.2.6); and the discontinuous micellar cubic phase (Fd3m and Fm3m). The formation of these different phases may be due to different compositions and or different fabrication conditions i.e., temperature (Figure 1.1.2). The bicontinuous cubic phases

feature non-intersecting water channels throughout the structure, whilst the micellar cubic phases contain discrete pockets of water. It is these water channels or pockets that may enable an improved drug loading of amphiphilic or hydrophilic APIs (42,76–78).

Many promising results have been reported in the literature as to the usability of cubosomes in drug delivery. Primarily it is their ability to encapsulate a range of APIs including: amphotericin B (79), Aspirin (72), Docetaxel (80), Flurbiprofen (81), Capsaicin (3) and siRNA (34); this is most promising for future investigation and utilisation of these particles. Further to this is the exhibition that these particles have potential to be utilised for oral administration (30,37,79,82). The ability to administer formulations orally is advantageous to improve patient compliance and reduce the need for healthcare professionals to administer the medicine, as compared to medicines requiring I.V. or I.M. administration.

1.2.2. Hexasomes
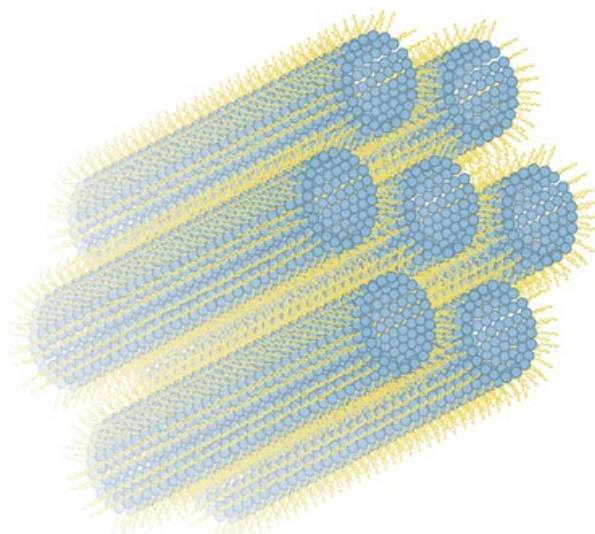
Figure 1.2.7. Cartoon of a H$_{II}$ inverse hexagonal phase. Blue regions represent the hydrophilic head groups of the lipids; the yellow regions represent the hydrophobic tails of the lipids.

Hexasomes consist of hexagonal phase. The hexagonal phase is formed when the CPP of the structure forming molecular components of a formulation is slightly increased from the CPP forming cubic phases. There are two types of hexagonal phase, the normal hexagonal phase (H$_I$) and the inverse hexagonal phase (H$_{II}$). Both normal and inverse hexagonal phases consist of cylinders orderly packed together. In the more commonly identified inverse hexagonal phase the lipid head groups face the inside of the cylinders, encapsulating a water channel (Figure 1.2.7). The reverse is true for the H$_I$ hexagonal phase. Dependent on the type of hexagonal phase, the lipid molecules may have one of two orientations. When observing the hexagonal phase, the X, Y plane has a uniform appearance, or

pattern, whilst the Z plane is different, whereas the cubic phases appear uniformly in both X, Y and Z planes.

The water channels of the hexagonal phases may offer the same possibilities as with cubosomes in encapsulating amphiphilic and hydrophilic APIs (42,76–78). The nature of the water channels in hexasomes and cubosomes leads to the advantages set out for encapsulating various APIs, most desirably encapsulating poorly soluble APIs. Additionally, however, these water channels may alter the solvent accessible surface area. Limited work examines the impact of water channel properties on the rate of API release, but comparison between liposomal and lamellar particle API release and the release of API from liquid crystalline particles featuring water channels shows a slowed release of API in the later particles. One possibility for this is that the water channels enable the steady diffusion of APIs out of the structures as opposed to burst release which is commonly seen with liposome and multi-lamellar particles (83,84).

Within the academic/research literature multiple examples of hexasomes being utilised for drug delivery can be found. They have been used for the *in vitro* delivery of Progesterone (40), Cyclosporine A (85), desmopressin (86), irinotecan (32) and cinnarizine (38).

1.2.3. Spongisomes
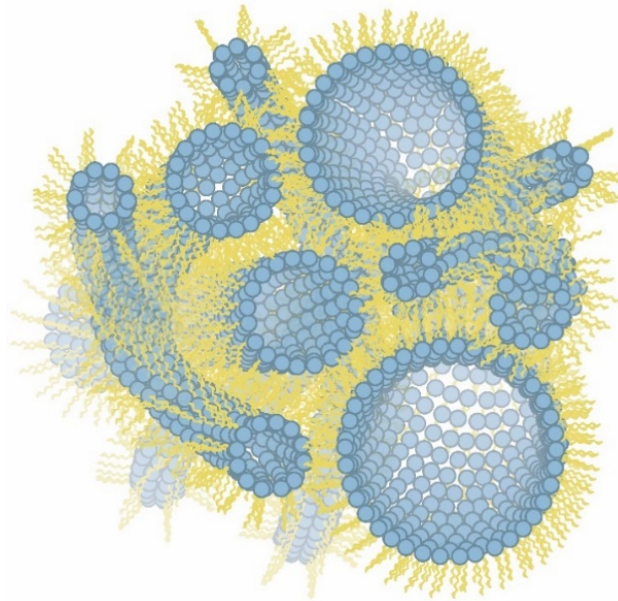
Figure 1.2.8. Illustration of the structure of a sponge phase. Blue regions represent the hydrophilic head groups of the lipids; the yellow regions represent the hydrophobic tails of the lipids.

As opposed to hexasomes and cubosomes which are characterised by ordered internal structures, spongisomes are characterised by the disorder in the said internal structure. Sponge phases are formed when the CPP of the system is below that of cubic phases, sitting between cubic and lamellar liquid crystalline phases. The defining feature of a sponge phase is the presence of two bicontinuous nonintersecting water channels. These water channels however have a random orientation and directionality. In the literature the research of sponge phases has taken place primarily as part of protein crystallography research. In such research sponge phases are used for the crystallography of membrane proteins[66][67].

The formation of sponge phases in the literature has required organic solvents in combination with GMO and water (89). However, Valldeperas *et al*. used a combination of diglycerol monooleate, Capmul GMO-50 (a mixture of mono-, di-, and tri-glycerides), polysorbate 80 and water to form discrete nanoparticles; here the authors state that such sponge phase particles hold potential for drug delivery, but do not demonstrate such drug delivery capabilities (90) Interestingly, Valldeperas *et al.* offers a route of formulation avoiding the requirement of ethanol, eliminating the potential drawbacks of ethanol utilisation detailed in the previous sections. Few examples can be found for the drug delivery applications of sponge phases, one such example however is the use of (bulk) sponge phase for the transdermal delivery of 5-aminolevulinic acid (91). Due to the identified possibility the work conducted here will give some attention to sponge phases as a potential vector for drug delivery.

1.2.4. Synperonic™ HP

Synperonics contain a central, hydrophobic poly (propylene oxide) block flanked by two hydrophilic poly (ethylene oxide) units (Figure 1.2.9), Producing an ABA type symmetrical triblock copolymer. These polymers may, in isolation of with other excipients, form micelles. These micelles can be utilised as drug delivery systems; however, more commonly these polymers are used in combination with other excipients (92,93), as with the liquid crystalline particles detailed within this work.
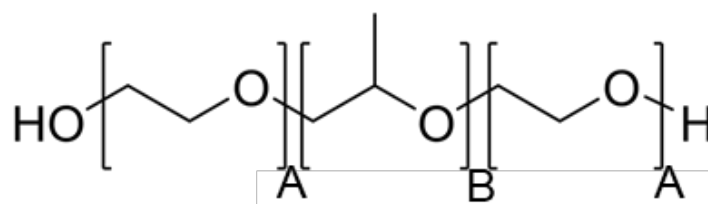
Figure 1.2.9: Structure of the PEO-PPO-PEO triblock copolymer, known under the trade names Synperonic^TM and Pluronic^TM, or the chemical name Poloxamer.

Synperonics^TM can be sub-classified based on their physical form into flake, paste or liquid; this is dependent upon the ratio of PEO to PPO (Figure 1.2.10). The differing physical forms offer differing advantages for Synperonic to be utilised in a range of purposes, including as a dispersant, a detergent, a lubricant, wetting agent, emulsifier, defoaming agent, and as a solubiliser. A selection of Synperonics^TM are used within the pharmaceutical and health care industries (94,95). There are numerous examples of Synperonic^TM PE F127 /poloxamer 407/ Pluronic^TM F127 being used to stabilise liquid crystalline formulations, with over 50 examples being found within the academic literature (52,68,96). Other Synperonics (under various trade names) have been utilised for this purpose too, for example F68 (97) and F108 (98) have been used in the literature for cubosome formulations.
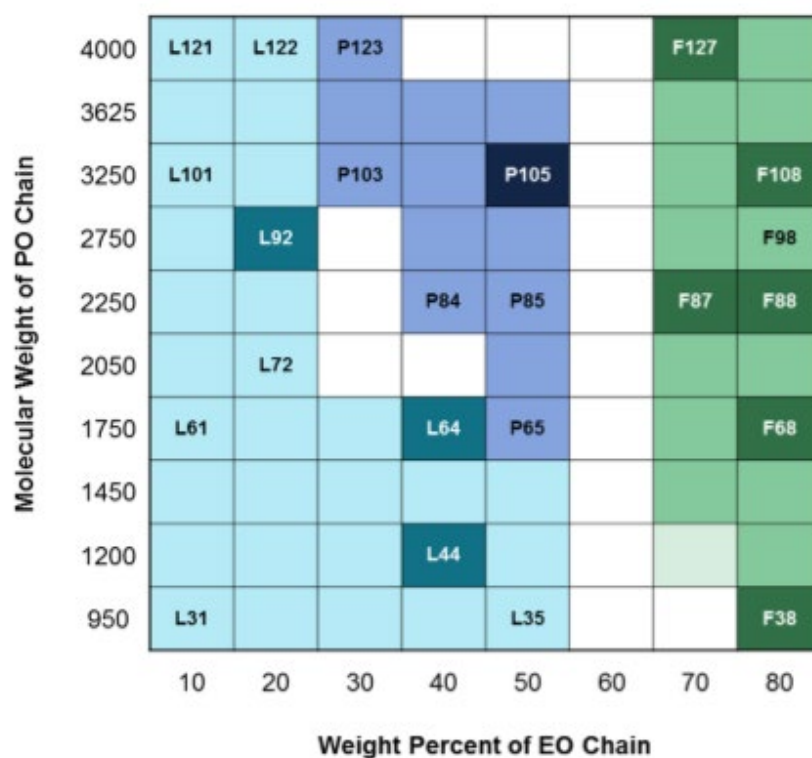
Figure 1.2.10: Naming scheme of Synperonics^{TM}/Pluronics^{TM} based on the PPO and PEO percentage and weight ratios (as reported by the various suppliers). The light blue with the prefix L- represents liquid Synperonics. The medium blue with the prefix P- represents paste Synperonics and the green with the prefix F- represents flake Synperonics. Highlighted Synperonics indicate those used in this work.

It has been suggested that Synperonics may increase permeability of the cell membrane to allow API entrance into the cell; however, this permeabilization can be detrimental to the cell's health (99,100). This may be concern when progressing to *in vitro* and *in vivo* studies as a formulation may have an inherent toxicity from the nanoparticle, regardless of the API. Furthermore, there is the question of Synperonics' fate once they have been internalised into the cell. Alakhova *et al*.

showed that cell-internalised Pluronic localised to, and impaired the respiratory function of mitochondria in multidrug resistant cancer cells, however this was desirable as it aided the induction of cellular apoptosis (101). Therefore, it should be considered if an apoptotic function or possible cellular toxicity is desirable or acceptable in such a formulation. Various studies have been performed on this category of chemicals: Magnusson *et al*. found Pluronic F68 induced phospholipidosis in rats (102). Johnston and Miller analysed a greater range of Pluronics administered via injection to muscle tissues, a key conclusion here was the Pluronic toxicity was proportional to their lipophilicity - the more lipophilic the more toxic. They deemed Pluronic F88 and F127 had a suitably low toxicity to merit their use in formulations, whilst Pluronics P105 and P123 showed some toxicity that could prove inhibitory to their use in pharmaceutical formulations (103).

A review of the literature in relation to Synperonics and their *in vitro* behaviours showed some differences in behaviour based upon the PPO:PEO ratio. Haemolysis, measured through a membrane lysis assay, occurs at a slower rate with an increasing amount of hydrophilic PEO relative to the hydrophobic PPO (104). Although haemolysis is a non-desirable and toxic event it may have a link to how a Synperonic may facilitate cellular uptake. The work of Redhead *et al.* discussed the reduced cytotoxicity of Pluronic F127 compared to L64, compared to the highly cytotoxic L61 and similarly to Nawaz *et al*. discussed how varying the PPO:PEO ratio can alter cell membrane interactions (105).

One further consideration is the orientation of the Synperonic in relation to the liquid crystalline phase. Their proposed integration into the liquid crystalline structure is depicted in Figure 1.2.11, and is as described in the literature (4,66,106). Therefore, particles would outwardly display a PEG coating. The most notable

benefit of this would be that the particles would have an innate stealth capability once administered. However, a possible disadvantage of PEG like molecules, such as Synperonics, is the reported immunogenicity of PEG. Recently approved LNP coronavirus vaccine formulations have been reported to elicit allergic reactions, this is thought to be a reaction due to the presence of PEG in formulations (107). As Synperonics possess highly similar poly (ethylene oxide) chains there is the potential for immunogenicity, however there is no clear research to show Synperonics to be highly immunogenic.
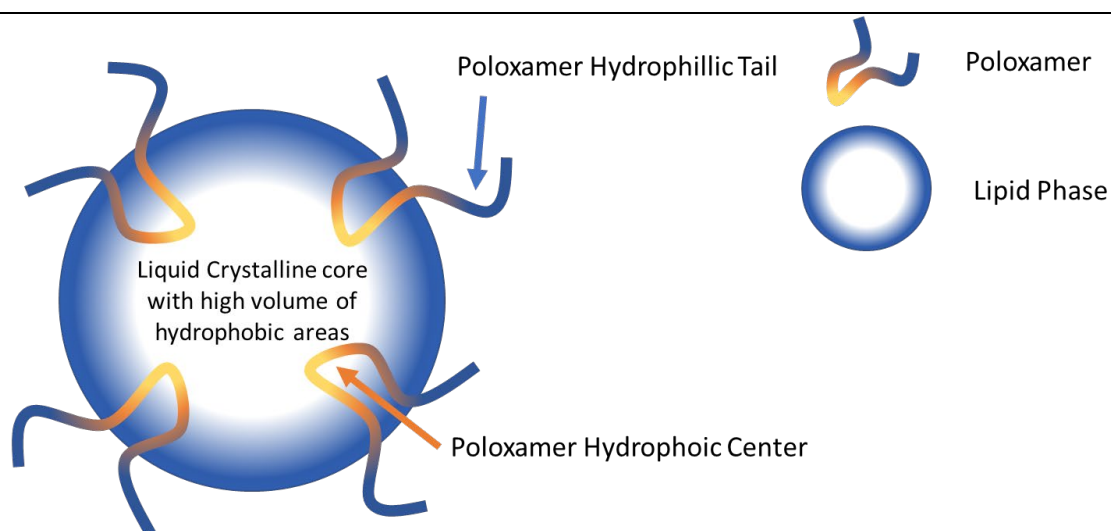
Figure 1.2.11. Schematic of the proposed mechanism of poloxamer/Synperonic^{TM} incorporation into lipid liquid crystalline phase nanoparticles. (Based off of (4,66,106).)

Alternatively, to Synperonics a variety of alternative stabilising compounds have been utilised.   Examples include PEG-lipid conjugates (108), e.g. DOPE-PEG$_{2000}$ (109), and GMO-PEG (34) and acrylamide-PEG (110) conjugates (34). Tweens 20, 40, 60 and 80 have also been utilised as stabilising species (31,97).

Additional, more varied and less common examples of Synperonic alternatives include Cremophor (31), β-casein (111) and ethoxylated phytosterols (86). All these literature examples showed a promising particle characteristic for the formulation's respective function.

Furthermore, in a bid to design a pH-responsive liquid crystalline nanocarrier Chountoulesi *et al*. utilised the stimuli-responsive amphiphilic block copolymer poly(2-(dimethylamino)ethyl methacrylate)-*b*-poly(lauryl methacrylate) (PDMAEMA-b-PLMA) as a stabiliser (112). This utilisation of a pH responsive stabilizing molecule enabled improved on-target site API release.

This work exclusively focused on the utilisation of Synperonics due to the support of Croda and prominence of Synperonics being used within the literature.

1.2.5. Organic Solvents use in Liquid Crystalline Phase Manufacturing

Organic solvents, particularly ethanol, are featured in the literature primarily due to their use in the hydrotrope fabrication protocol (described in Chapter 3). Briefly, this protocol dissolved the lipid components in a hydrotrope, commonly ethanol, this lipid-hydrotrope mix is combined with water to allow a bottom-up liquid crystalline phase/particle formation. The use of ethanol can significantly impact the nature of the phase formed by GMO. Ethanol acts at the partition between the lipid and water, effectively flattening the lipid head groups at the surface, increasing the lipid packing parameter (4). This drives the formation of alternative liquid crystalline phases (i.e., a hexagonal phase forming lipid may form a cubic phase in the presence of ethanol). However, the utilisation of ethanol or other solvents may result

in some drawbacks, particularly due to potential toxicity at higher concentrations of ethanol; therefore, the solvent should be at a low concentration, or be removed prior to the formulation's utilisation for drug delivery. Preliminary experiments conducted within the work presented here showed that the removal of ethanol resulted in the removal of any structural effect the ethanol had.

Further detail about liquid crystalline fabrication can be found in chapter 3.

1.2.6. Suspension Medium

Within the literature there is little variation found as to the suspension medium or buffer. The most utilised suspension medium is water, specifically milli-Q water.

The only alternative suspension medium identified within the literature was 11 mM phosphate buffer at pH 7 (109).

1.2.7. Additional formulation components

Some liquid crystalline nanoparticle formulations utilise additional components. The use of additional lipid species to glycerol monooleate liquid crystalline phases has been explored by multiple researchers, primarily in fundamental research to understand phase behaviour. For example, Cherezov *et al*. explored bulk GMO phases which formed a Pn3m phase; to this phase they added the lipids DOPE, DOPC, DOPS and cholesterol at a 10% mol ratio to the GMO, these resulted in the transition from the Pn3m to H_{II}, to Lα to Im3m and Lα and to Im3m L_c combined respectively (Figure 1.2.3) (113). Beyond this fundamental research in phase behaviour understanding, some researchers incorporated

secondary lipids to enhance the encapsulation of the API. For example the inclusion of the cationic lipids DOTAP (34) and DOMA (109) allowed to improve the encapsulation of siRNA.

Although no secondary lipid species will be used in this work it is important to highlight works showing how the incorporation of secondary species can influence the liquid crystalline phase. This can also provide an indication as to how secondary species, either a lipid and/or an API, may influence the nature of the liquid crystalline phase.

A discussion as to the inclusion of APIs into liquid crystalline phase particles is included in Chapter 4, and briefly in the following sections.

1.3. <u>**Aims and Objectives.**</u>

The overarching aim of this PhD project was to develop lipid particles with capabilities to encapsulate poorly soluble drugs for drug delivery applications. Based on the literature LC phase particles were identified as a potentially attractive lipid nanoparticle for the delivery of soluble APIs. Aiming to utilise current literature to develop a formulation focused on the use of glycerol monooleate, trade name Cithrol^{TM} and Synperonic^{TM}. Using these materials, an optimal composition and fabrication process to produce a LC phase particle formulation will be designed. Adaptation of the composition and fabrication process to manipulate particle size and other particle physicochemical properties will be explored to produce a formulation capable of being utilised for a range of administration routes, e.g., I.V., I.M. and oral.

With a target identify a fabrication procedure and composition that negates many of the harsh processes used in the literature to fabricate a favourable formulation.

Understanding how the self-assembled internal structure may be affected through the changing of the formulating parameters, such as temperature changes, changing the ratios of water to lipid, and the addition of other chemical species, i.e., different Synperonics.

Upon the development of a formulation and fabrication procedure the aim is to screen a variety of APIs to ascertain the effectiveness of LC particles for drug delivery applications. Effectiveness will be assessed by:

- The ability for LC particle to load APIs, as a measure of drug loading and encapsulation efficiency

- The capabilities of particles to release drug at a desired rate.

These abilities will predictably change dependent on an API's physiochemical properties. Hence developing an understanding as to which API physicochemical properties are the most consequential in affecting drug loading, encapsulation efficiency and drug release. This is in the aim to produce a profile for which APIs may best benefit from formulation into liquid crystalline particles. In order to achieve this a diverse range of APIs will be studied based on their varying physicochemical properties e.g., differing molecular weight, solubility in terms of LogS and differing numbers of aromatic rings, and not for the API's specific application.

Chapter 2: Methodology

Reported in this Chapter are all the materials used in the study. This Chapter will also describe methods and instrumentation used in conducting the experiments.

2. Methodology

2.1. <u>Materials</u>

Croda International Plc. (Goole, UK) supplied Glycerol monooleate at 92% purity (supplier specified) under the trade name Cithrol^{TM} HP GMO, and Synperonic^{TM} HP/PEs. Synperonic^{TM} HP/PE F127 is the predominantly used Synperonic in this study, details of all the Synperonics featured in this study can be found in Table 2.1.1 and the APIs used in the study and the suppliers can be found in Table 2.1.2. All solvents and dyes were sourced from Sigma-Aldrich (U.K.) and used without further purification. Milli-Q water was sourced in-house at 18.2 MΩ•cm.

Table 2.1.1: List of the Synperonics used in this study including details about their form i.e., liquid (L), flake (F) or paste (P); their molecular weight, and the average number of propylene oxide (PO) and ethylene oxide (EO) units within each of the different Synperonics^{TM}. Values are based on average MW and so are inexact rounded values.

Synperonic	Form	Molecular Weight (g mol^{-1})	Number of EO Units	Number of PO Units
31	L	1100	3	17
44	L	2200	20	23
64	L	2900	26	30
92	L	3650	17	50
105	P	6500	74	56
38	F	4700	85	16

87	F	7700	123	40
68	F	8400	153	29
88	F	11400	207	39
127	F	12600	200	65
108	F	14600	265	50

Table 2.1.2: List of all the active pharmaceutical ingredients used in this study with their supplier and supplier reported purity.

Active Pharmaceutical Ingredient	Supplier	Supplier Reported Purity (%)
Amitriptyline Hydrochloride	Sigma-Aldrich	≥98
Beclomethasone	Sigma-Aldrich	≥99
Budesonide	Croda (non-commercial)	≥99
Chloroquine Diphosphate salt	Sigma-Aldrich	≥98.5
Chlorpromazine Hydrochloride	Sigma-Aldrich	≥98
Clomipramine Hydrochloride	Sigma-Aldrich	≥98
Cyclosporine A	LC Laboratories	≥98.5
Dexamethasone	TRC	≥97
β-Estradiol	Sigma-Aldrich	≥98
Fenofibrate	Sigma-Aldrich	≥99
Glipizide	Sigma-Aldrich	≥96
Haloperidol	TRC	≥99
Haloperidol Decanoate	TRC	≥98
Hydrocortisone	Sigma-Aldrich	≥98
Imipramine Hydrochloride	Sigma-Aldrich	≥99
Mefenamic acid	Sigma-Aldrich	≥98.5
Menadione	Sigma-Aldrich	≥98
Mometasone Furoate	Sigma-Aldrich	≥99
Nortriptyline Hydrochloride	Sigma-Aldrich	≥98
Progesterone	Sigma-Aldrich	≥99
Propofol	LC Laboratories	≥97
Quinine Hydrochloride Dihydrate	Sigma-Aldrich	≥98
Tolbutamide	Sigma-Aldrich	≥97
Trazodone Hydrochloride	Sigma-Aldrich	≥99

2.2. <u>Particle Fabrication Methodologies</u>

Described briefly is the method established post the optimisation work carried out in Chapter 3. Each Chapter contains a more detailed particle fabrication section.

2.2.1. Fabrication of Liquid Crystalline Particles

The Cithrol and Synperonic F127 were combined in a 6:1 w/w ratio, respectively, in a glass vial. The vial was then heated to 65 °C on a hot plate until the material appeared homogenously molten. Milli-Q water (56:3 water: Cithrol w/w) at 65 °C was added drop wise to the molten mixture, whist being stirred with magnetic stirrer at 300 rpm at 65 °C. Formulations were then allowed a day sealed at room temperature to stabilise prior to analysis. Final formulations appeared homogenous and semi-opaque. Some formulations exhibited flocculation; this is described later in the relevant cases.

2.3. <u>Particle Analysis Methodologies</u>

2.3.1. Small angle x-ray scattering experiments for liquid crystalline phase identification.

SAXS is a technique which allows the acquisition of data which may then be used in combination with defined models described within the literature to identify the internal structure of a particle. The background of this technique and the described models can be found within section 1.2. in chapter 1 as well as in chapter 5.

2.3.1.1. *Ganesha SAXS*

This work was performed in collaboration with Mr Chris Brasnett and his supervisor, Dr Annela Seddon at the University of Bristol, Department of Physics. 50 µl of each sample was loaded into 1.5 mm borosilicate glass capillaries. Scattering patterns were captured via a SAXSLAB Ganesha 300XL instrument in a q-range of 0.015–0.65 Å^{-1}, with an exposure time of 30 minutes per sample. This exposure time was used to acquire a good signal to noise ratio. Data was processed via the processes detailed by the white paper produced by our collaborators: Identifying lipid mesophases from a set of Small-Angle X-Ray Scattering (SAXS) peaks by Christopher Brasnett and Annela Seddon (University of Bristol). Due to limited availability this white paper is attached at the end of this document.

2.3.1.2. *Diamond B21 beamline SAXS*

SAXS measurements were conducted at the Solution State SAXS B21 beam line at Diamond Light Source on the Harwell Campus, Didcot, UK. This beamline measures at a resolution range of 0.0031 to 0.38 Å-1 using a flux of ~1012 photons per second. It operates in a fixed camera length configuration (4.014 meters) at 12.4 keV.

The bioSAXS (EMBL Arinax sample handling) robot was used to automate data collection from a 96-well plate. The samples are loaded by the bioSAXS robot into a temperature controlled (20 ˚C) quartz cell capillary (1.8 mm internal diameter) enclosed in a vacuum chamber. The vacuum chamber is utilised to avoid parasitic scattering for X-ray scattering measurements (as is also the case with the Ganesha lab-based instrument). The data acquisition duration was 20 seconds, with sampling taking approximately 2 minutes. A beam of wavelength λ = 13.1 keV (~0.94644 Å)

with a beam size at the sample of 1 mm × 1 mm was used. Images were captured using a Pilatus 2 m detector. Data processing (background subtraction, radial averaging) was performed using the dedicated beamline Scatter software integrated to the instrument operating system.

2.3.1.3. *SAXS Data Analysis*

Peaks were manually identified using SasView 5.0 software, the location of each peak was recorded and inputted into the following spreadsheet to identify peaks with ratios fitting one of the known liquid crystalline phases (Table 2.3.1, Table 2.3.2 and Table 2.3.3). The white sheet as detailed in section 2.3.1.1 was used to develop this methodology for analysis.

Table 2.3.1: Table of the predefined Bragg peak ratios for the commonly occurring liquid crystalline phases.

Phase	Peak ratios/model
Hexagonal	$1 : \sqrt{3} : \sqrt{4} : \sqrt{7} : \sqrt{12} \ldots$
Gyroid (Ia3d)	$\sqrt{6} : \sqrt{8} : \sqrt{14} : \sqrt{16} : \sqrt{18} \ldots$
Diamond (Pn3m)	$\sqrt{2} : \sqrt{3} : \sqrt{4} : \sqrt{6} : \sqrt{8} \ldots$
Primitive (Im3m)	$\sqrt{2} : \sqrt{4} : \sqrt{6} : \sqrt{8} \ldots$
Lamellar	$1 : 2 : 3 : 4 : 5 \ldots$
Cubic Micellar (fcc)	$\sqrt{3} : \sqrt{4} : \sqrt{8} : \sqrt{11} : \sqrt{12} \ldots$

Table 2.3.2: Snapshot of the spreadsheet with the formulas used to calculate peak ratios. The number letter combinations i.e., 'C5' represents the cell ID within the excel spreadsheet.

	Peak				
	1	2	3	4	5
Å $^{-1}$ of Peak					
1	2*3.141/C4	2*3.141/D4	2*3.141/E4	2*3.141/F4	2*3.141/G4
√2	C5*SQRT(2)	D5*SQRT(2)	E5*SQRT(2)	F5*SQRT(2)	G5*SQRT(2)
√3	C5*SQRT(3)	D5*SQRT(3)	E5*SQRT(3)	F5*SQRT(3)	G5*SQRT(3)
√4	C5*SQRT(4)	D5*SQRT(4)	E5*SQRT(4)	F5*SQRT(4)	G5*SQRT(4)

Table 2.3.3: Snapshot of the spreadsheet with example data used to calculate peak ratios with model data. In the example data in this snapshot a co-existence of a primitive (blue) and a diamond (orange) phase has been highlighted.

	Peak						
	1	2	3	4	5	6	7
Å $^{-1}$ of Peak	0.077123	0.103217	0.109496	0.126241	0.13405	0.145688	0.178705
1	81	61	57	50	47	43	35
√2	115	86	81	70	66	61	50
√3	141	105	99	86	81	75	61
√4	163	122	115	100	94	86	70
√5	258	192	181	157	148	136	111
√6	200	149	141	122	115	106	86

2.3.2. Cryo-Transmission Electron Microscopy (Cryo-TEM)

Cryo-TEM is a technique that allows for the direct visualisation of nanoparticles in an as near to native state situation as possible with current technology. The cryogenic nature of the measurement allows for water molecule to be held in situ during the measurement meaning the hydrophobic and hydrophilic

interactions necessary for the liquid crystalline structure are maintained. Analysis of cryo-TEM micrographs can allow one to ascertain particle size, outer morphology, and internal structure. Further FFT analysis can be a helpful tool in internal structure identification. Further explanation as to the selection, background, and application of cryo-TEM can be found in section 1.2. in chapter 1.

2.3.2.1. *Cryo-Transmission Electron Microscopy Sample Preparation*

Holey carbon grids (Agar Scientific, U.K.) were prepared via plasma discharge (Fishione, Model 1020 Plasma Cleaner) for 10 seconds at 5 mA. Grids were loaded with 3 μL of sample at the production concentration; the sample was incubated in a humidity-controlled chamber for 1 minute prior to being blotted and freeze plunged into liquid ethane. This process was performed using the Gatan cryo-plunge 3 system. Samples were then stored in liquid nitrogen at ~ -196 ˚C or transferred for analysis instantaneously. Sample application volume and incubation time on the grid were optimised through trial and error. The selected 3 μL and 1 minute incubation led to the most appropriate particle concentration on the grid for imaging. If the particle concentration is low then representative particles may not be identified, however, if the concentration is too high then particles may overlap leading to an inability to perform single particle analysis. Samples were freeze-plunged into liquid ethane as this reduces the number of ice crystals formed due to no Leiden-Frost effect.

2.3.2.2. *Cryo-Transmission Electron Microscopy Sample Analysis*

Prepared sample grids were loaded into a Gatan 626 cryo-TEM holder under liquid nitrogen. The samples were analysed under cryo-conditions (~ -180 ˚C) using a US1000 CCD camera and Digital Micrograph GMS 3 operating software on a JEOL 2100Plus instrument at 200 kV. Micrographs were captured at exposure times of 2–64 seconds at doses below 10 e/A^2. Parameters such as magnification, spot size, brightness, and the use of the high-contrast aperture was variable between samples and was variable and dependent upon the following factors:

- The presence and thickness of ice

- The size of the particles in the X. Y plane

- The thickness of the particle in the Z plane

- Filament condition/beam intensity without adjustments

- Z-height of the sample

It was found that focusing into the middle of the particle (in terms of z-height) was more appropriate than focusing on the particle surface to ascertain a good micrograph of the liquid crystalline structure. Due to the higher amount of material that the beam had to penetrate a longer image acquisition time was used. This increases the electron dose upon the sample; however, samples were robust enough to withstand beam damage for micrograph acquisition.

2.3.2.3. *Cryo-Transmission Electron Microscopy Micrograph Analysis*

Micrograph enhancement (contract/brightness) was performed using ImageJ software. This software was additionally used to conduct fast Fourier transform (FFT) or inverse FFT analysis upon micrographs.

2.3.3. Dynamic Light Scattering

DLS allows for the measurement of particle size in its native state using the Stokes-Einstein equation. DLS offers advantages over cryo-TEM as it is representative considered to be more representative. This is because DLS will measure thousands of particles at once whilst with cryo-TEM a highly limited number of particles may typically be analysed in one micrograph, depending on the magnification. Furthermore, DLS is a high throughput technique (10 minute measurement time and 1 minute samples preparation) whereas cryo-TEM is considered low throughput with a single sample taking between 2 and 8 hours in total for sample preparation and analysis.

A Zetasizer Nano ZS (Malvern, UK) was used to determine particle hydrodynamic size. A machine determined number of measurements were taken at 173° backscatter with auto attenuation. For standard sizing 3 measurements were taken per sample.

2.4. <u>Analysis of Drug Loading and Drug Release</u>

2.4.1. Dye/API encapsulation

Dye or API was weighed as solid material directly into scintillation vials (with the Cithrol and Synperonic). In the event the weight of dye required fell below the scale's accuracy a stock solution was made utilising a solvent e.g., acetone or ethanol; the appropriate volume of the stock was transferred into a scintillation vial. The solvent used was given time to evaporate (~1 day for volumes up to 200 µl) before adding the Cithrol (300 mg) and Synperonic F127 (50 mg) into the vial. The procedure was then followed as described in Section 2.2.1.. Samples were not extruded unless stated otherwise.

2.4.2. Removal of unencapsulated API

Free drug was removed after the 24-hour particle formation period. Free drug removal was performed using Amicon® Ultra-Centrifuge filters (Sigma, U.K.) device with a 300 KDa molecular weight cut off membrane. Free API/drug would pass through the membrane during centrifugation whilst the particles with encapsulated API/dye would remain on the top. Devices were centrifuged at 4,000 x g (swing bucket) for 20 minutes. The sample was removed from the top of the device for use in further experiments.

2.4.3. Encapsulation efficiency and drug loading

A calibration curve was produced for each API analysed by dissolving fixed amounts of API into isopropanol and performing a serial dilution in isopropanol (w/w).

Calibration curve samples (Chapter 4 supplementary information), and formulation samples, were diluted 1:20 in isopropanol, dissolving the LC structure, and analysed via high-performance liquid chromatography (HPLC) using an Agilent 1200 system with a C18 column (see supporting information in Chapter 4).

API loading and encapsulation efficiency were calculated via the following equations:

Equation 2.4.1:

$$API\ loading\ (\%) = \left(\frac{weight\ of\ entrapped\ drug}{weight\ of\ Cithrol\ carrier}\right) \times 100$$

Equation 2.4.2:

$$API\ encapsulation\ efficiency\ (\%)$$
$$= \left(\frac{Weight\ of\ drug\ loaded\ in\ sample}{Weight\ of\ drug\ added\ to\ formulation}\right) \times 100$$

2.4.4. API Release

API release was measured through dialysis using a slide-a-lyzer dialysis system (ThermoFischer, U.K., Figure 2.4.1). As API is released from the nanoparticles in the donor cup it may in principle diffuse though the semi-permeable dialysis membrane into the receptor medium.
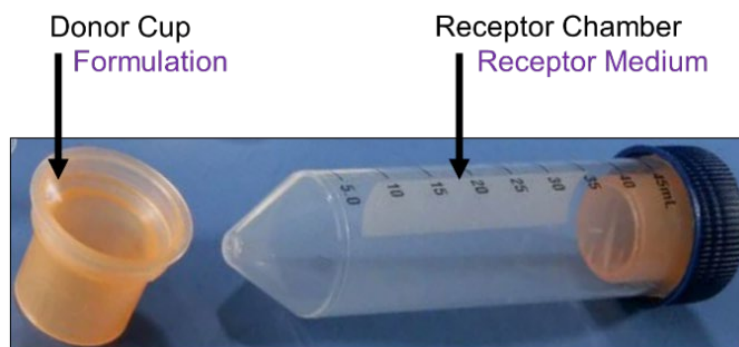
Figure 2.4.1: Image of slide-a-lyzer dialysis device.

1 ml of formulation was placed into a slide-a-lyzer dialysis device (as the donor). The receptor medium was a 1% Tween 20 (Croda, U.K.) in water solution. Tween 20 was used in order to solubilise free API, overcoming the inherent insolubility of the hydrophobic/poorly water-soluble APIs. Samples were analysed via RP HPLC and quantified using the same method described in the encapsulation efficiency and API loading section.

2.5. <u>Correlation analysis</u>

2.5.1. Pearson regression analysis

Pearson regression analysis was performed using GraphPad Prism 8.1.2 software. A more detailed description can be found in the relevant Chapters.

Chapter 3: Development of a Cithrol liquid crystalline phase particle formulation

Several methodologies have been identified for the fabrication of liquid crystalline phases within the literature. Developed here is a novel protocol capable of encapsulating APIs whilst avoiding high energy input processes, such as heat cycles. A formulation was developed here based upon the usage of Cithrol^{TM} HP GMO and Synperonic^{TM} materials.

3. Development of a Cithrol liquid crystalline phase particle formulation

3.1. <u>Introduction</u>

Lipid liquid crystalline particle fabrication focuses upon the self-assembly of the constituent molecules. The constituent molecular components, i.e., the lipid and polymer stabiliser, will self-assemble in the presence of water. In low water concentrations a bulk phase may be formed, but in excess water a particle suspension will form (51). The different methodologies in fabricating the liquid crystalline particles are as such to control the kinetics of this self-assembly procedure. Methodologies to fabricate liquid crystalline phase particles are based around two pathways, the top-down path, or the bottom-up pathway.

- **Top-down.** The top-down method involves the formation and then dispersion of a bulk phase. The bulk phase is typically a clear, rigid gel. The dispersion of the bulk phase requires a high energy input method, typically sonication (64,114,115), homogenisation (77), shearing (53), or less commonly spray drying (37,116).

- **Bottom-up.** The bottom-up method is a process designed to have the constituent lipid and polymer stabiliser components of the formulation self-assemble directly into particles ranging from nm to micron size (64,117). Within the literature this method is typically called the hydrotrope method (35,51).

Additional possibilities to achieve desirably low particle size, (of sub-200 nm to achieve a desirable particle distribution *in vivo* and high cellular up-take) include rapid-mixing of formulation components for 6 minutes at 6000 rpm; followed by the use of a microfluidizer (high pressure homogeniser) for 8 cycles and 35 MPa of pressure. However, in this protocol formulations were filtered at 0.45 µm (30), indicating that this protocol was not completely efficient at achieving the desirable particle size distribution. Post filtering however cubosome formulations were produced with mean particle diameters of 90.4 and 91.3 nm. Therefore, one may eliminate high pressure homogenisation as an efficient option for tailoring particle size.

Kim *et al.* used a methodology alike to the traditional method to form liposomes. Here a thin-film was formed from the constituent lipids and hydrated with an aqueous solution of siRNA. The hydration process was allowed 2 days for complete hydration (temperature not specified), then formulations were sonicated for 6 minutes at 20 kHz. Although cryo-TEM and SAXS data is presented for these formulations showing the formation of cuboplexes (cubosomes containing RNA) there is no direct particle size reported and there is significant variation in particle size and morphology observable in the cryo-TEM images (34). This may suggest that this fabrication protocol does not produce monodisperse particles; however, the protocol is seemingly compatible with incorporation of siRNA. Later work by Kim *et al*. demonstrated the use of microfluidics to form cuboplexes of a comparable formulation to the earlier works by Kim *et al*.. Using microfluidics with a herringbone chip the lipid phase, containing lipid dissolved in ethanol was mixed with the siRNA containing water phase. Microfluidics enabled the rapid, turbulent mixing of all components. The ethanol was subsequently removed through rotary evaporation.

Again limited particle size data was presented, however it was reported that cuboplexes formed through this procedure were 'around 75 nm' (118), suggesting that this protocol may form particles of a desirable size for I.M. and I.V. drug delivery; however no PDI or particle size distribution data is reported and so the suitability of this protocol for forming monodisperse, homogeneous formulations is unknown.

After this initial fabrication of particles, through either top-down or bottom-up methods, an additional process is often used to manipulate particle size and include sonication, homogenisation, shearing, heat cycles, and mechanical stirring. Barauskas *et al.* showed a direct comparison of particle size once preformed particles go through 2 hours mechanical mixing, homogenisation, and heat treatment at 125°C; data was presented as size distribution plots and cryo-TEM. This showed that untreated particles had micron size (1-10 μm), this was reduced to ~800 nm after 2 hours mixing. Heat treatment reduced the particle size to ~500 nm, whilst homogenisation reduced the average particle size to ~100 nm. However, the cryo-TEM showed a significant loss of the liquid crystalline structure within the particles. This also showed the formation of liposomes and membrane blebbing post homogenisation (119). Reviewing the use of heat cycles shows uniform particle formation, but, these heat cycles, some of which include the use of high pressure, could have a highly detrimental and degrading impact on encapsulated APIs. One examples as to how heat treatment can result in the formation of uniform and clearly structured particles can be seen in Figure 1.2.4, these particles underwent a 20 minute heat treatment at 125°C to improve the particle size and uniformity (60).

The use of Cithrol is central to the development of this base formulation which may then be utilised to encapsulate various APIs for drug delivery purposes. Therefore, it is alternative formulation composition parameters that will be explored

in this work, secondarily to the fabrication procedure. Such parameters to be explored is the formulation's water content, (Figure 1.1.2) and Synperonic content. The specific Synperonic, based upon the PEO:PPO ratio and molecular weight variation found within the umbrella of the chemical family of Synperonics, used to stabilise the liquid crystalline phase into particles could also be considered.

Identified in the literature is an awareness of how crucial the PPO:PEO ratio of Synperonics can be in determining their biological activity. There are two parameters of immediate importance regarding a Synperonic's activity when selecting them as part of a formulation. The first consideration is their toxicity, although as previously discussed in section 1.2.4 many Synperonics are already used in pharmaceutical formulations. The second consideration is how a Synperonic based particle coating may affect particle cellular uptake and behaviour *in vitro* and *in vivo*. As both considerations will also be related to other particle properties the approach was taken to examine the suitability of the different Synperonics as part of the formulation. One example of why it is important to consider the toxicity of Synperonic as part of a formulation and not as a lone entity is given in the work of Murgia *et al*.. Their studies lead them to propose that, although F127 is non-cytotoxic, GMO promotes its internalisation. Upon the Synperonic's internalisation its amphiphilic nature exerts a toxic effect upon the mitochondrial and nuclear membranes (120). Then each formulation candidate may be screened for their properties *in vitro* and *in vivo* in work additional to the body of work presented here.

3.2. <u>**Experimental**</u>

The materials used in this Chapter are as described in Chapter 2.

3.2.1. Nanoparticle Preparation

3.2.1.1. *Production of lipid liquid crystalline nanoparticles*

Cithrol (300 mg) and Synperonic (50 mg) were weighted into a scintillation vial, this vial was then placed upon a hot plate at 65 °C with a magnetic stirrer (12 mm stirrer bar, 400 rpm), once both components had melted and appeared homogenous milli-Q water (5.65 mL, preheated to 65 °C) was added at a constant rate via the aid of a syringe pump. This was performed at a constant stir rate of 400 rpm at 65 °C, stirring was stopped 10 minutes after the water addition, samples were then stored at room temperature and analysed after 1 day.

3.2.1.2. *Production via the use of a hydrotrope*

Cithrol (300 mg) and Synperonic (50 mg) were weighted into a scintillation vial, this vial was then placed upon a hot plate at 65°C until the material was molten and visually homogenous. The desired amount of ethanol (as the hydrotrope) was added and swirled until visually homogenous. Milli-Q water (5.65 mL, preheated to 65°C) was added instantaneously via the rapid expulsion of water from a syringe. Slow water addition resulted in a heterogeneous formulation whilst rapid water addition resulted in homogenous translucent formulations.

3.2.1.3. *Post-production sample manipulations*

Further processing of the sample after the initial production phases can aid liquid crystalline phase formation and/or to reduce the particle size and size

dispersity. This was performed immediately after the production processes detailed in the following sections.

3.2.1.3.1. Sonication (Not performed on all samples)

Formulations were sonicated inside glass vials in a sonicating water (Elma Elmasonic S100H) bath for 1 hour under a constant frequency.

3.2.1.3.2. Extrusion (Not performed on all samples)

An Avanti Mini-Extruder was used (Avanti Polar Lipids, U.S.A). A 200 nm pore-size polycarbonate filter was used (pre-soaked in milli-Q water), with 21 passes through the filter. Extrusion was conducted at room temperature. The mini-Extruder was used as per the supplier's instructions.

3.3. <u>Results and Discussion</u>

Within the literature it is indicated that lipid liquid crystalline particle formulations were utilised and analysed after 24 hours (121). As such this period was investigated, as displayed in Figure 3.3.1. This investigation found that formulations kept at room temperature (25°C) required 20 hours to stabilise in terms of particle size, whilst formulations kept at 35 °C stabilised at a quicker rate, regarding particle size, but temperature led to the same size particles being formed. To overcome this variability in the first 20 hours all samples were allowed 24 hours at room temperature before analysis, use, or post fabrication manipulation. Although SAXS analysis was not performed at this stage to understand the kinetics of the liquid crystalline phase assembly, it is possible the lipid self-assembling into liquid crystalline structures takes a period of hours; this could attribute to the variability in the particle size over the first 1000 minutes/16 hours.
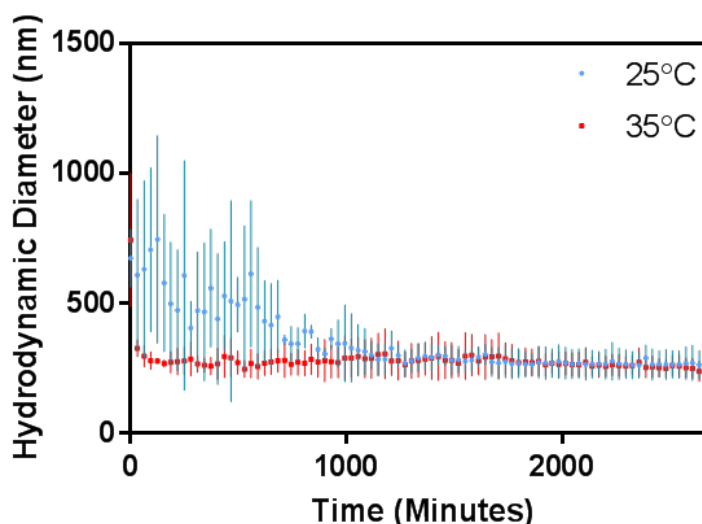
Figure 3.3.1: Average particle hydrodynamic diameter, as analysed by DLS) versus time following the liquid crystalline fabrication procedure. Samples were kept and analysed at 25 and 35 °C. N = 3, mean ± standard deviation.

Investigations into the ratios of lipid to stabilising polymer (Synperonic) to water were conducted to find a ratio with minimal excess Synperonic, whilst maintaining a stable particle formulation. The initial baseline formulation contained: 300 mg GMO, 100 mg Synperonic and 9.6 ml water; this was selected through a review of the literature. The first parameter investigated was the possibility to increase the concentration of lipid and surfactant component in the formulation. Therefore, formulations were produced at different ratios of water to Cithrol and Synperonic components. The resulting formulations were analysed though SAXS to understand the impact of these changes in the ratio of the components upon the liquid crystalline phase. As shown in Figure 3.3.2 and Figure 3.3.3 (inverse) hexagonal phase is consistently observed with the same peak ratios in terms of q, showing no distinctive change in the liquid crystalline phase characteristics, i.e. which phase is formed, and/or, the lattice parameter of the formed phase. In all samples the lattice parameter was 5.6 nm ± 0.5 nm. The relatively high error is as a result of the error in the exact q value of the peak maxima and not a reflection upon the degree of variance between samples. This indicates that the addition of extra water molecules into the system does not correlate to a difference in the repeating units of structure; following this it could therefore be assumed that the increasing amount of water does not increase the number of water molecules within the liquid crystalline structure. This conclusion however is applicable for the given range, within the literature it is documented that increasing water content of formulations can lead to structural swelling, leading to larger lattice parameters, and in some cases phase shifts (108). However, what can be observed is the change in the shape of the baseline. This baseline is resulting from the scattering of other

structures made from the lipid and surfactant present in the sample, such as micelles, liposomes, or free molecules; the height of the baseline, after the background subtraction at the lower q, is related to the amount of these non-liquid crystalline species. It is challenging to make conclusions as to the relative concentration of these species within the formulation due to SAXS being semi-concentration dependent.

Visual observations of samples showed an increase in viscosity and opaqueness with a decrease in the water volume. Combining the visual characteristics along with indications from the SAXS as to the presence of secondary species the 5.6 ml volume of water was selected per 400 mg of the solid formulation components (total of lipid and surfactant mass together).
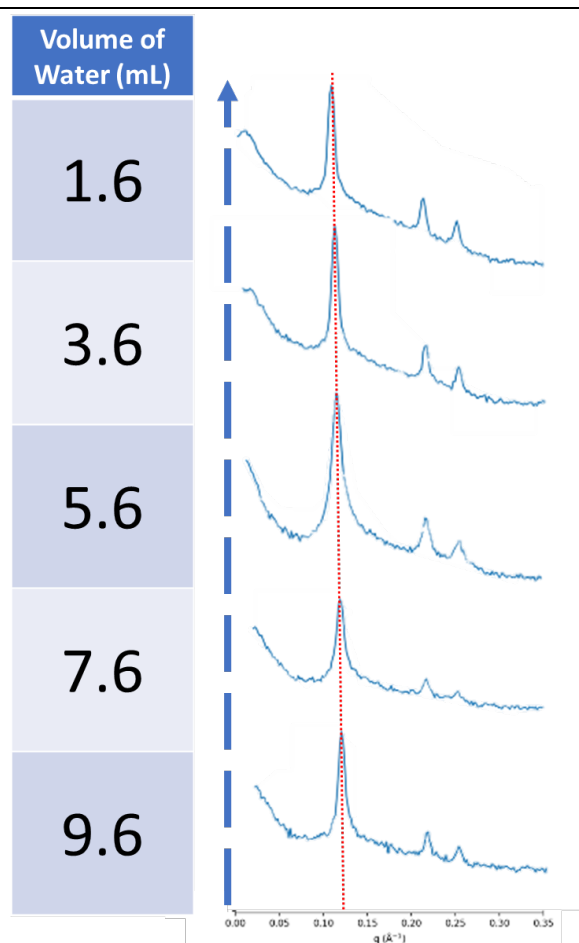
Figure 3.3.2: Dependence of water content on lipid liquid crystalline phase particle formation, as analysed by SAXS. All samples were produced with 300 mg of Cithrol^{TM}, 100 mg of Synperonic^{TM} F127 and volume of water as specified within the figure. SAXS profiles stacked to show minimal changes in q.

Post the establishment of an ideal water to lipid and surfactant ratio, an investigation into the ideal ratio of Synperonic was considered. The ideal ratio would achieve a stable particle formation (expected to be achieved with higher Synperonic concentrations) but contain as few Synperonic micelles/free Synperonic as possible. As Synperonic has the potential to have adverse effects on the formulation suitability for drug delivery due to their potential toxicity, as well as potentially hindering cellular

uptake it would be desirable to minimise the amount of Synperonic present within the formulation (104,105). However, through initial experiments and review of the literature Synperonic or similar surface-active polymers are essential in the formation of discrete nm sized particles as opposed to large micron sized liquid crystalline particles or aggregates. Beyond the potential adverse implications, such as toxicity, of having higher proportions of Synperonic within the particle structure SAXS revealed the presence of Synperonic micelles. These micelles and their increasing concentration can be observed at the lower end of q (x-axis) (Figure 3.3.3), where an increased scattering signal/increased slope can be observed. Furthermore, at the higher concentrations of Synperonic the intensity of the hexagonal phase peaks significantly decreases relative to the baseline scattering, indicating the Synperonic disrupts the liquid crystalline phase. As SAXS indicates high Synperonic micelle concentrations and hexagonal phase disruption formulations containing 100 mg or higher of Synperonic relative to the 300 mg of glycerol monooleate were discounted from future formulations. Upon comparison of the 10 and 50 mg Synperonic formulations the signal from the formulation containing less Synperonic has more noise in the SAXS traces, this noise and less distinct peaks may be due to any changes in the liquid crystalline phases. Such variability may arise due to the non-homogenous distribution of Synperonic and the presence of bulk/large particle/aggregates of liquid crystalline phase. As such the 50 mg Synperonic per 300 mg of glycerol monooleate was selected to go forward.
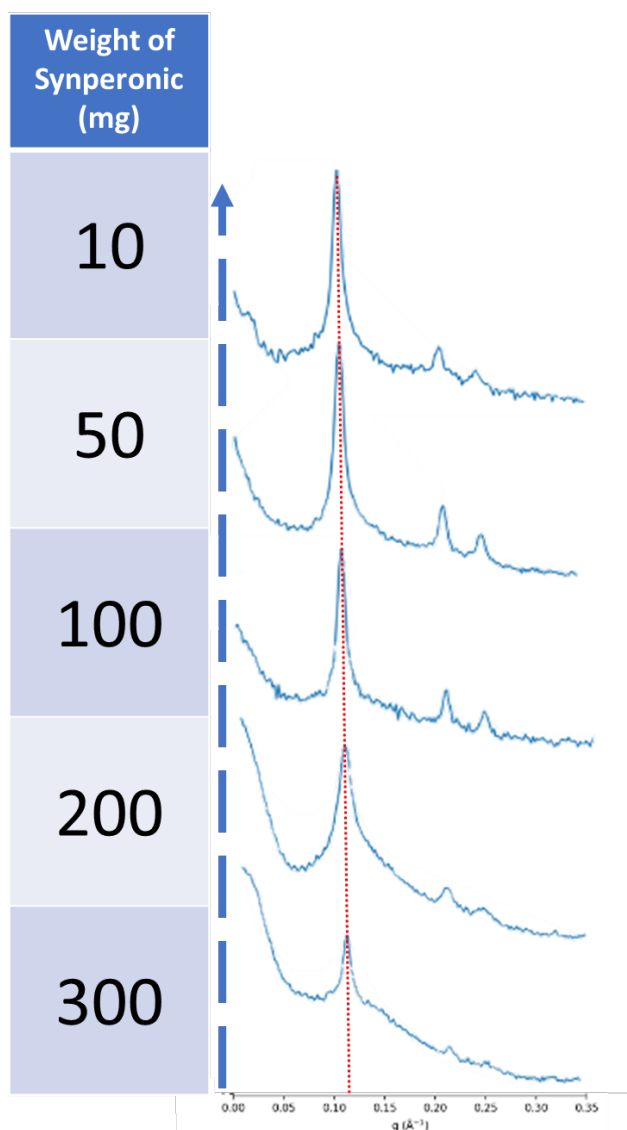
Figure 3.3.3: Effect of increased amounts of Synperonic^{TM} F127 present in the formulation, as analysed by SAXS. Formulations are prepared from 300 mg of Cithrol^{TM} and 5.6 mL of water. SAXS profiles stacked to show minimal changes in q; however, changes in the scattering intensity at low q (left of the red dashed line). A higher slope indicates more scattering of non-liquid crystalline species.

Visual observation (Figure 3.3.4) of liquid crystalline formulations containing different Synperonic species showed variability in that some formulations, such as the formulation containing Synperonic L44 where there is a high degree of flocculation observable. These samples were then analysed by SAXS to examine the influence of different Synperonics upon the liquid crystalline phase (Figure 3.3.5). This analysis showed that although the different Synperonics effected the sample scattering profile it was generally inconsequential (L92 being an exception) in its effect on the liquid crystalline phase (i.e., hexagonal phase) but was consequential in increasing the scattering present from non-liquid crystalline structures within the formulation (Figure 3.3.5). For instance, Synperonic L92 has the lowest ratio of PEO:PPO of the Synperonic^{TM} screened (Figure 1.2.9), this Synperonic disrupts the formation of the hexagonal liquid crystalline phase as observed by SAXS (Figure 3.3.5). Further analysis would be required to identify the nature of the particles present in this formulation, i.e., liposomes, spongisomes, etc. From the micrograph shown in Figure 3.3.6 it can be observed that changing the Synperonic in this case to P105 can induce the formation of many liposomes, but observable hexasomes (only a single representative micrograph is shown here) are perfectly hexagonal.

As Synperonics have varying interactions with cells regarding uptake and toxicity (104,105) the ability to form the lipid liquid crystalline phase particle formulations with different Synperonics may be vital in progressing formulations through to *in vitro* and *in vivo* testing .

Still, the presence of micron size particles would need to be analysed. This analysis would be pertinent due to the multimodal size distribution identified during DLS analysis (Figure 3.3.7) showing a high variability in particle size with this given fabrication procedure. But the particle size distribution does appear influenced by the

Synperonic used within the formulation. This size change is a function of altered

particles formation kinetics, where the PPO:PEO ratio may be significant as higher

ratios of PPO would increase the number of hydrophobic interactions with the GMO)

and changing of the polymer length on the particle surface.

The diverse and overlapping populations of particle sizes displayed in Figure

3.3.7 and Table 3.3.1 mean any discussion as to a link between particle size

distribution and the nature of the Synperonic is vague and inconclusive. To better

understand this a fabrication protocol that produces a monodisperse size distribution

with a low PDI would be required. Although this is possible with the extrusion method

of fabrication it would be inappropriate to use to study the effect of different

Synperonics on particle size. This is because extrusion manually manipulates

particle size, reducing the effect of any particle size changes based on the

formulation composition.
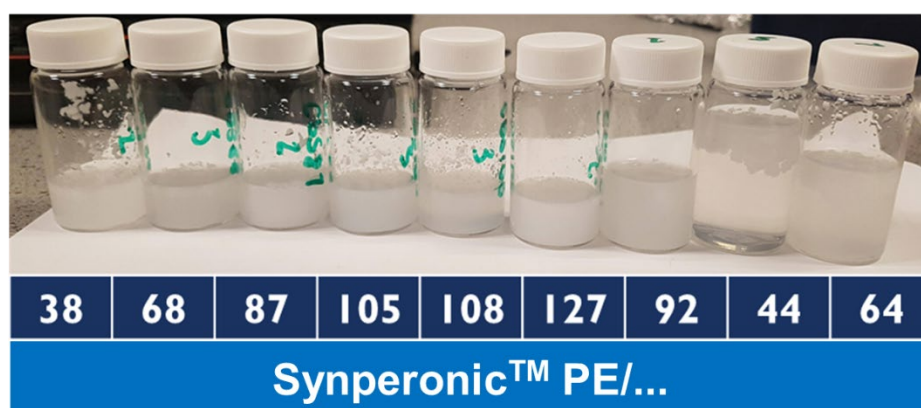
Figure 3.3.4: Examples of the physical appearances of hexasomes formed from different Synperonic™s. w/w/w ratio (mg:mg:mg) of Cithrol™: Synperonic™: Water was constant at 6:1:113. Sample volume inconsistent due to variation in the minimal weighable about of each Synperonic™.
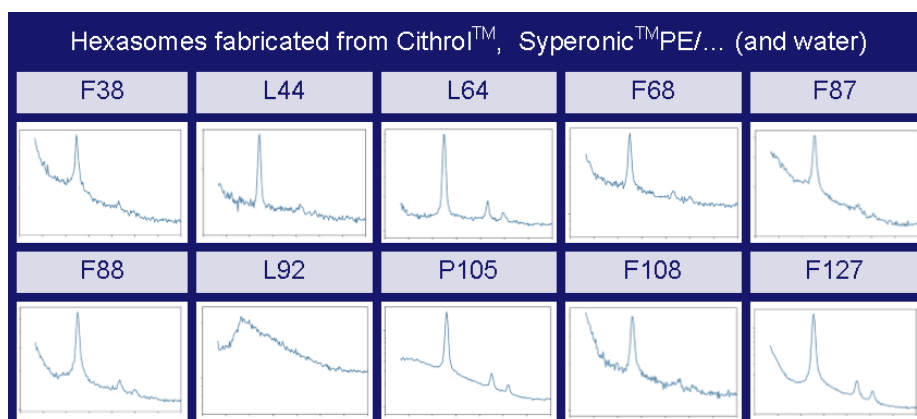
Figure 3.3.5: Small angle x-ray (SAXS) profiles for a range of formulations containing the varying Synperonics. w/w/w ratio (mg:mg:mg) of Cithrol^{TM}: Synperonic^{TM}: Water was constant at 6:1:113.
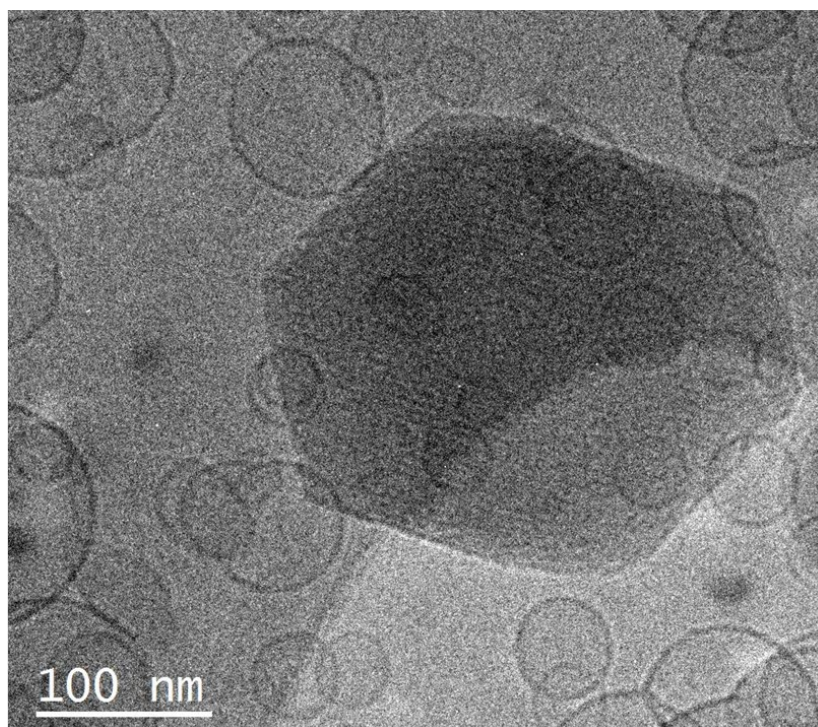
Figure 3.3.6: Cryo-transmission electron microscopy image of hexasome produced using Synperonic^{TM} PE/P105, the outer hexagonal shape can be

seen in conjunction with the striations indicative of a hexagonal phase. Additionally, smaller spherical liposomes can be seen. Formulation is 300 mg of Cithrol^{TM}, 50 mg of Synperonic^{TM} P105 and 5.65 mL water.
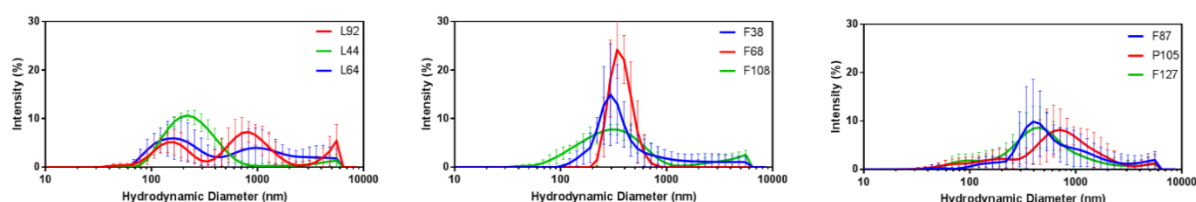
Figure 3.3.7: Particle size distribution profiles from dynamic light scattering of hexasomes made with different Synperonics. N = 3 ± S.D. w/w/w ratio (mg:mg:mg) of Cithrol^{TM}: Synperonic^{TM}: Water was constant at 6:1:113.

To overcome the presence of these multimodal particle size distribution in formulations produced when different Synperonics were utilised, a selection of formulations were examined as to their characteristics post extrusion. These samples were extruded using a 200 nm filter. In all cases the particle size was lower than 200 nm with the majority having a desirable PDI of below 0.2. All samples were monomodal and formulations became visibly homogeneous. This indicates formulations produced from 6 Synperonics (Table 3.3.1) may be manipulated to have desirable size profiles to take forward for testing.

Table 3.3.1: Average hydrodynamic particle size by DLS for hexasomes made with differing Synperonics (as shown in Figure 3.3.4), and then extruded as detailed in section 3.2.1.3.2.

Synperonic^{TM}	Z. Average (d. nm) ± standard deviation (Polydispersity index) **Before extrusion**	Z. Average (d. nm) ± Standard deviation (nm) (Polydispersity index) **After extrusion with a 200 nm filter**
F38	353.4 ± 46.9 (0.36)	115.2 ± 2.16 (0.19)
F68	358.7 ± 20.6 (0.24)	136.0 ± 1.07 (0.10)
F87	482.5 ± 118.9 (0.51)	138.7 ± 2.67 (0.17)
P105	407.6 ± 64.8 (0.66)	124.1 ± 2.18 (0.21)
F108	282.1 ± 6.9 (0.50)	143.6 ± 1.55 (0.17)
F127	348.3 ± 68.1 (0.57)	165.8 ± 2.07 (0.22)

Figure 3.3.8: Photographs of sample following extrusion of hexasomes produced using various flake Synperonic^{TM}s. w/w/w ratio (mg:mg:mg) of Cithrol^{TM}: Synperonic^{TM}: Water was constant at 6:1:113. Formulations were extruded using an Avanti mini-extrude with a 200 nm membrane.
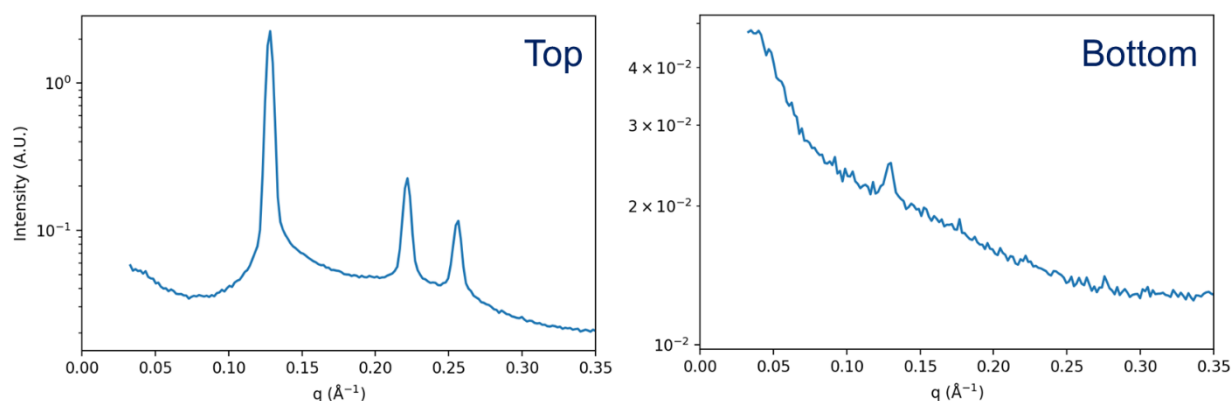
Figure 3.3.9. Comparison of SAXS profiles from flocculated hexasome formulations, a profile is shown for the top and bottom of the sample (300 mg Cithrol™, 50 mg Synperonic™ F127 and 5.65 mL water).

Extrusion has been shown to manipulate the particle size of formulations, producing monomodal particle distributions to a tailored maximum particle size. However, of question is what this extrusion does to the structural properties of the liquid crystalline phase particles. Therefore, SAXS analysis was performed on pre- and post-extruded samples (Figure 3.3.10). Further to this sonication was considered as a method for controlling particle size as this was identified as a possibility from the literature (64,114,115). Particle size analysis showed both extrusion, sonication, and a combination of both techniques reduce the particle size and polydispersity of a formulation. extrusion would be the preferable technique for producing a monodisperse formulation as this technique produces the lowest PDI (Table 3.3.2). Sonication, both alone and in combination with extrusion reduce the PDI relative to the untreated sample, but not compared to extrusion, this is likely due

to sonication producing several smaller particles, producing a smaller particle skew/tail on the particle size distribution of sonicated samples, relatively increasing the PDI compared to extruded samples. These smaller particles would not be removed or manipulated through extrusion, whilst seemingly extrusion does not result in the formation in such a significant number of smaller particles; additionally, extrusion will reduce the polydisperse particle size from un-processed particles to the precise pre-selected filter size (200 nm in this case). Therefore, in selecting a type of post-production sample manipulation to alter particle size distribution DLS analysis strongly indicates extrusion is preferable. However, it would be important to note that current technology does not allow large scale extrusion and other parameters to control size should be investigated if this liquid crystalline particle technology were to be upscaled.

Table 3.3.2: Average hydrodynamic particle diameter analysed by DLS of formulations sonicated, extruded (200 nm membrane) and sonicated then extruded post-fabrication. Hexasome formulation made with 300 mg Cithrol^{TM}, 50 mg Synperonic^{TM} F127 and 5.65 mL water.

Post-production Processing	Z. Average (d. nm) ± standard deviation (Polydispersity index)
None	540.9 ± 37.6 (0.342)
Sonication	196.3 ± 3.8 (0.286)
Extrusion	188.0 ± 7.6 (0.176)
Sonication & Extrusion	176.9 ± 4.1 (0.233)
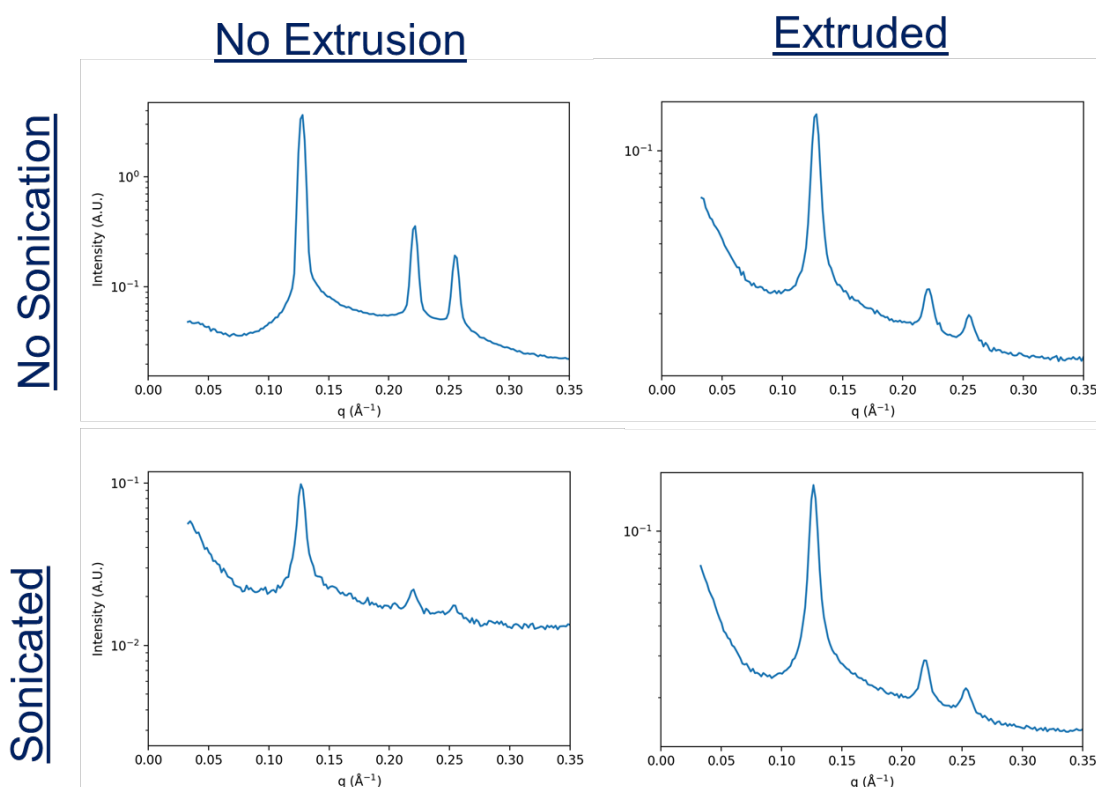
Figure 3.3.10: Comparison of the effects of sonication and extrusion on the internal hexagonal phase of hexasomes produced with   300 mg Cithrol™, 50 mg Synperonic™ F127 and 5.65 mL water. No significant change in q can be observed indicating no change in the characteristics of the hexagonal phase. Changes in intensity between plots is not directly comparable with the given experimental design; however, the changes in the slope at low q indicates a higher presence of liposomes or micelles. Sonication and extrusion both increase the concentration of liposomes and micelles relative to the concentration of the liquid crystalline phase.

3.3.1. Morphological Analysis

Cryo-TEM is one of the few applicable techniques here that may be used to understand the particles' outer morphology on a nanometre scale, i.e., the shape of the particle. Further to this it is possible to use cryo-TEM to determine the internal morphology of particles, with the assistance of FFT analysis, however, this is less definitive compared to SAXS. This is because of limited cryo-TEM micrograph resolution (typically a maximum resolution of 2-10 nm may be achieved), both in theoretical terms and practical terms. Although atomic resolution using cryo-TEM has been achieved (122), this is not routinely achievable due to practical considerations including: the compatibility of the sample with cryo-TEM and the instrument capabilities. Furthermore cryo-TEM gives a less representative overview of the particle population compared to SAXS. This is due to cryo-TEM micrographs generally showing a small number of particles, dependent upon the magnification and particle concentration, whilst SAXS analyses the combined scattering of all particles within the X-ray path, the scattering profiles of which are averaged out upon the signal collection on the recorder.

The utilisation of cryo-TEM techniques for lipid particle analysis is becoming increasingly more frequent within the literature, with the key characteristics to identifying a liposome being well defined, i.e., a dark ring structure, typically spherical, with an internal particle contrast being like the contrast outside of the particle. However, the utilisation of cryo-TEM for liquid crystalline particle analysis is less frequent and appears to be utilised primarily to give a visual reference of the particle characteristics (59). Proposed here however is the possibility to utilise cryo-TEM to a higher potential to directly identify liquid crystalline phases when SAXS

analysis may not be possible. Cryo-TEM may be best utilised in the analysis of hexagonal phase liquid crystalline particle, i.e., hexasomes, because of the following factors:

i)   Two orientations can be observable across the sample specimen, with one orientation showing pores, looking down the end of the ordered bilayer cylinders: with the other orientation showing stripes, observing the top, long side of the bilayer cylinders.

ii)   Particles appears homogenous in density aside from the pattern visible from the structuring. There should be no increase in density at the perimeter of the particle. A high-density perimeter, looking like an 'O', (signified by the darker ring) is indicative of a liposome.

iii)   The particles outer macrostructure can be informative as to the nature of the internal structure, hexasomes may exhibit a hexagonal macrostructure, as cubosomes may exhibit a cubic macrostructure. However, this is a non-exclusive rule, both hexasomes and cubosomes may have a spherical or slightly irregular particle shaped.
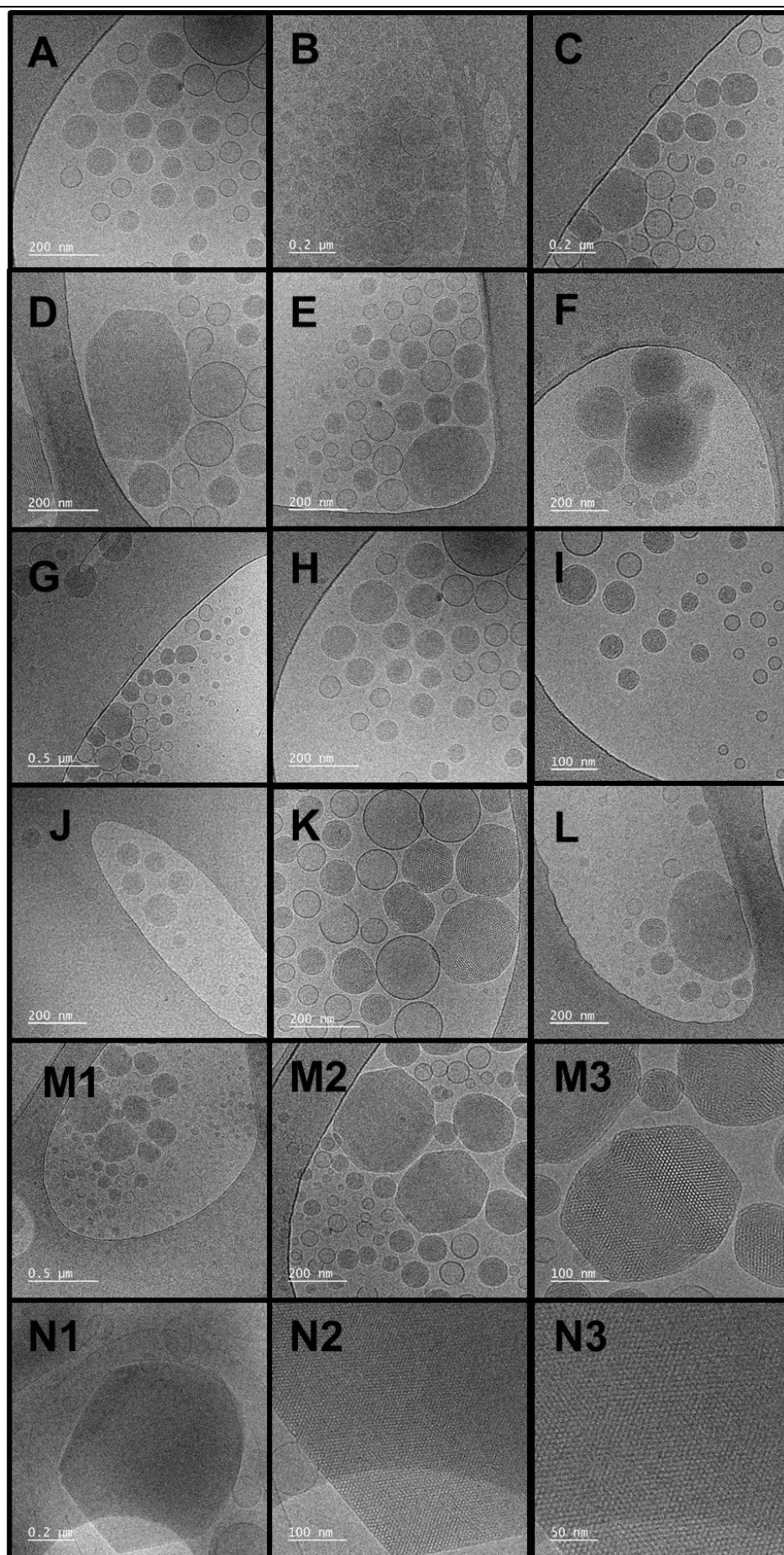
Figure 3.3.11: Cryo transmission electron microscopy images of hexasomes produced using Synperonic™ F127. A to L shows a selection of particles observed with both hexasomes and liposomes being present. Micrograph series M and N show the same features imaged with increasing magnifications.
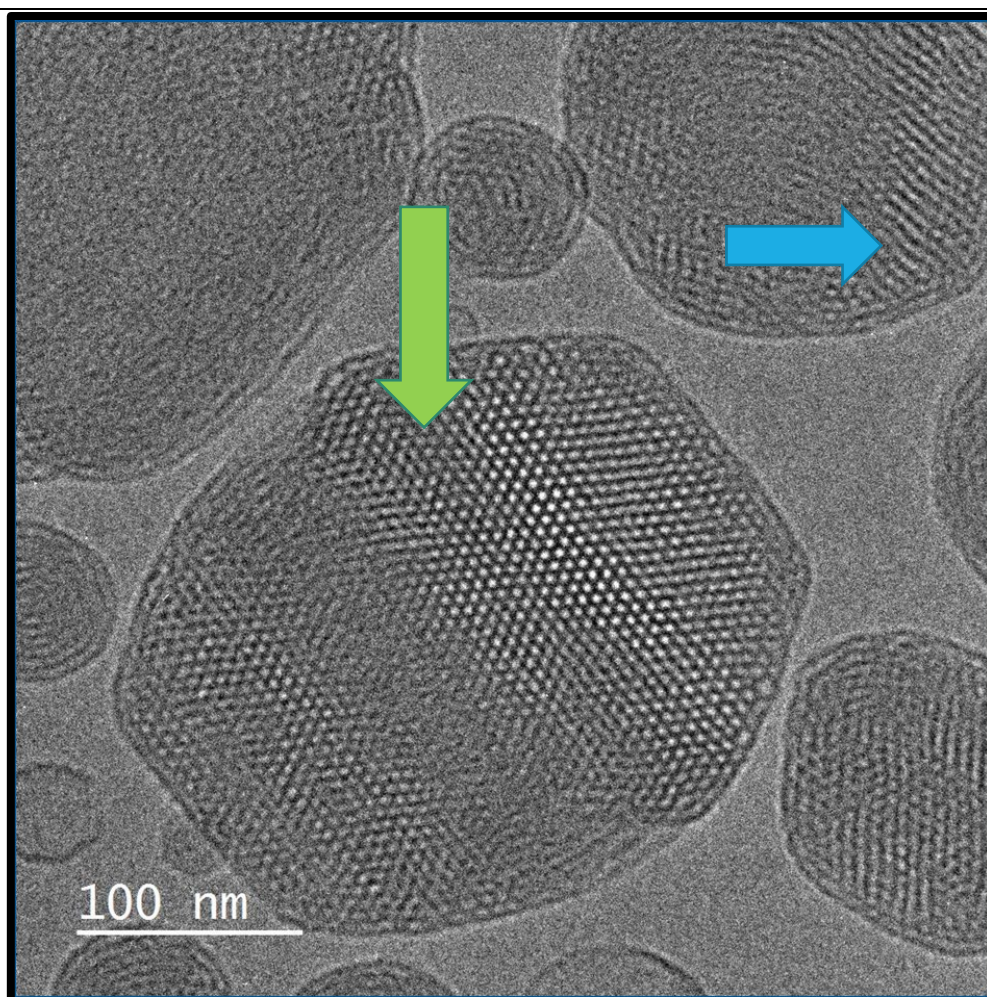
Figure 3.3.12: Higher magnification image of hexasomes (Figure 3.3.11. micrograph M3) made producing 6:1 Cithrol™: Synperonic™ F127. Two different orientations of the hexagonal phase can be seen, as indicated by the arrows. The green arrows show the pores/ ends of the lipid cylinders whilst the blue arrow shows the long side of these cylinders (Figure 1.2.7).
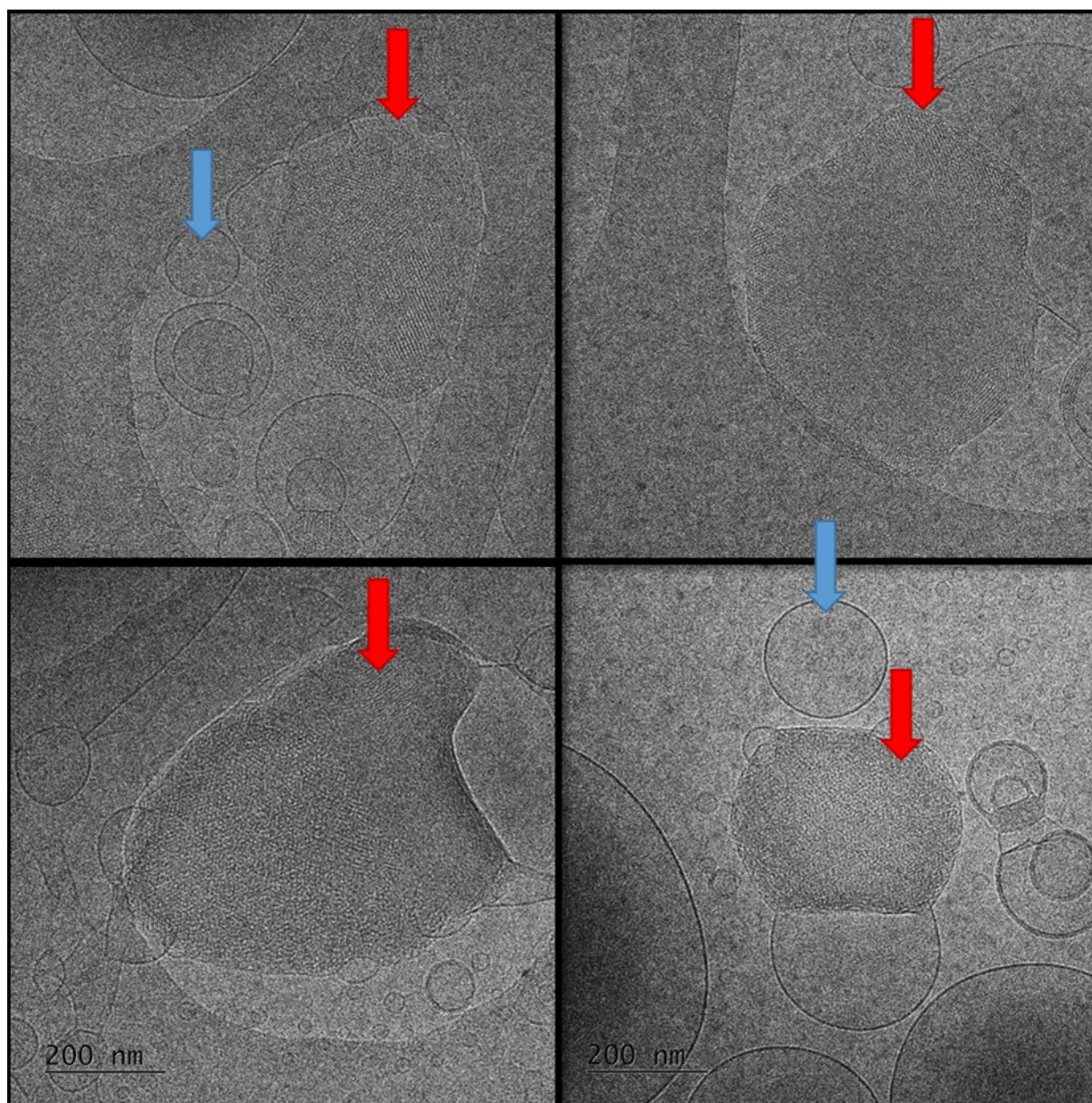
Figure 3.3.13: Cryo-transmission electron microscopy image of cubosomes produced using 300 mg of Cithrol™ GMO, 50 mg of Synperonic™ F127, 5.65 ml Milli-Q water and 1.5 ml of ethanol. A combination of liposomes (blue arrows) and cubosomes (red arrows) can be observed.

Via cryo-TEM it is possible to define a sample as hexasomes primarily due to variable orientations that may be observed. However, this type of phase identification would require additional FFT analysis to determine the presence of alternative phases, such as the cubic phases. Cubic phase particles, i.e., cubosomes have no variation between orientations, and minimal variation between cubic phases can be observed with cryo-TEM, which further would increase the need for FFT analysis compared with identifying hexasomes. Furthermore, there are multiple variations of cubic phase, including primitive, gyroid, discontinuous and diamond. These different cubic phases are well defined by SAXS, where the discrete differences may be easily distinguished. The FFT profiles of the cubic phases and any difference however are not defined in the literature and the development of such analysis was beyond the aim of this work and instead SAXS was relied upon for distinguishing between the different cubic phases.

Although the preference in this study was to avoid the use of ethanol, the use of ethanol in formulations was briefly explored here due to its use in the literature during the hydrotrope fabrication protocols (74,123). It was found that the relative content of ethanol used had a significant effect not only in the visual characteristics of the formulation, but also in measured characteristics, such as particle size. Three liquid crystalline phases were identified, across these preparations using ethanol, through SAXS analysis: diamond cubic, [inverse] hexagonal, and sponge phase. The parameter which is key between these phases is the proportion of ethanol used in each formulation. With increasing relative content of ethanol, the following trend in the liquid crystalline phases has been observed:

Hexagonal < Diamond Cubic < Sponge

as determined by SAXS (Figure 3.3.14: SAXS analysis of what ethanol containing samples prepared using when using a hydrotrope. A) shows a hexagonal phase (HII), B) shows a diamond phase (Pn3m) and C) shows a sponge phase (L3). Each formulation prepared from 300 mg CithrolTM HP GMO (glycerol monooleate), 50 mg SynperonicTM 127). These phases have all been featured within literature both as their bulk forms, but also in the particulate forms (72,90). Some differences between these phases in relation to drug delivery applications may include API loading and subsequent release. When producing a cubic or sponge phase particles from GMO, Synperonic and water there is the requirement of a fourth species, the use of ethanol in combination with these may therefore be required. The use of ethanol however may have a detrimental effect on any active pharmaceutical ingredient, particularly biologics (124). Furthermore, in the event ethanol is utilised during the formulation process, it may need to be removed if the ethanol content is above what is medically accepted, but upon dialysis and subsequent ethanol removal the formulation reverts to its native hexagonal phase (data not shown due to poor signal to noise).
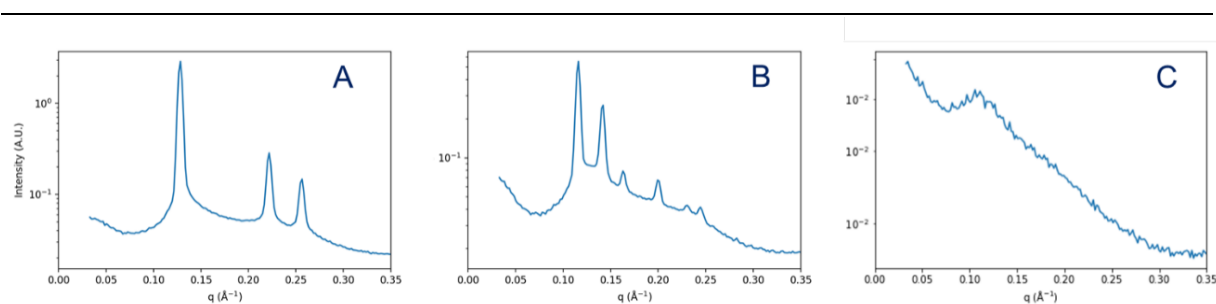
Figure 3.3.14: SAXS analysis of what ethanol containing samples prepared using when using a hydrotrope. A) shows a hexagonal phase (H$_{II}$), B) shows a diamond phase (Pn3m) and C) shows a sponge phase (L$_3$). Each formulation prepared from 300 mg Cithrol^{TM} HP GMO (glycerol monooleate), 50 mg Synperonic^{TM} 127, ratios or water: ethanol (v/v a) 1:0 b) 10:1 c) 5:1)

Review of the formulations in which hexasome were formed with comparison to the phase diagrams and formulations in the literature (47) our results were not complimentary. With the composition of GMO (Cithrol^{TM} >92% pure GMO), Synperonic F127 and water ratios at 65˚C used formulations should have formed cubosomes. Therefore, an investigation was conducted to identify the reason as to why hexasomes were formed over cubosomes. In partnership with Dr A. Seddon's lab Danisco company sourced glycerol monooleate was analysed and found to form a diamond cubic phase. This is consistent with what is reported within the literature (47). When the same procedure was conducted using Croda's Cithrol^{TM} HP GMO a hexagonal phase was formed. Therefore, the hexagonal phase formation can be attributed directly because of utilising Croda's product. The most apparent difference between Croda's (>92% pure) and Danisco's (>98% pure) glycerol monooleate products are the purity profiles, not only in percentage purity but also the makeup of these impurities (as specified by the supplier). Due to hexasomes sharing many of the properties of cubosomes it is at this stage non-consequential to form hexasomes as opposed to cubosomes. These experiments to show the innate packing of Cithrol to be hexagonal followed closely the protocol set out in (125).

3.3.2. Stability Analysis

Colloidal stability analysis was performed using two techniques: DLS and SAXS. DLS allows the assessment of any changes within particle size; whilst SAXS can identify a loss of liquid crystalline phase or any change in it via comparison of

the scattering pattern versus storage time. Both techniques will indicate instabilities in the particle structure through measuring the changes in the structure over time.

Analysis of the internal structure by showed no change in the nature on the internal phase after 2 months storage at room temperature of the base formulation (300 mg Cithrol, 50 mg Synperonic F127 and 5.65 mL water) (Figure 3.3.15). Not only is the hexagonal phase maintained (peak q ratio), but the q of the peaks remains the same. This shows that the internal arrangement of the lipids remained consistent, including the lattice parameter. The only observable change here is in the relative intensity, with peak intensity having a proportionality to the amount of structural occurrence. The experimental design here was not set up to be able to quantify changes in intensity, however, if the reduction in intensity of the sample on storage is real, and not because of discrete changes in the measurement parameters, such as beam intensity, then it may be concluded that there is a reduction in the amount of x-ray scattering structure in the sample. Complementary to this is the work of Ali *et al*., where cubosome particle size studies showed consistent particle size and PDI over a 4 week window, however no SAXS data was reported in relation to particle internal structure stability (30).
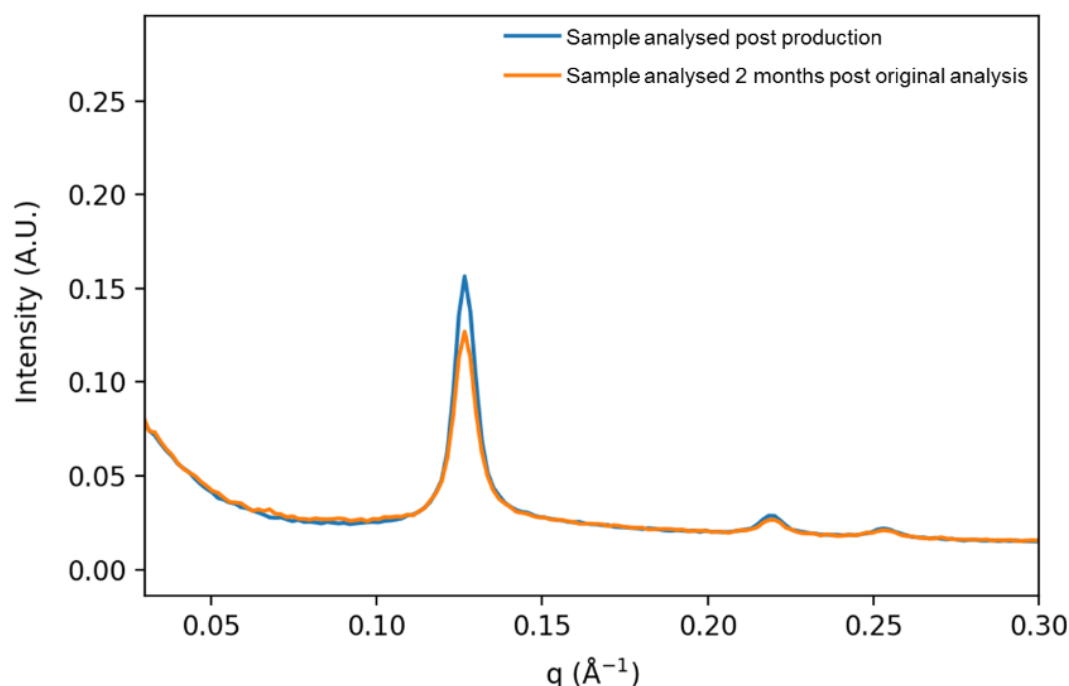
Figure 3.3.15: Small angle x-ray scattering overlay of the base formulation (300 mg Cithrol™, 50 mg Synperonic™ F127 and 5.65 mL water) post-production and post two months storage at room temperature (~20°C) in a sealed capillary.

Formulation stability was further analysed through temperature ramp studies, to understand how a change in the environmental temperature impacts upon the structure of the particles within the formulations (Figure 3.3.16). Between 15 and 55 °C there is no significant change in the average particle size. This indicates that particles are colloidally stable, at least when exposed for a short time (2-minute equilibration time for each 1 °C increase in temperature prior to measurement) to these temperatures. The clinical significance of this is that it shows there would be no significant change in particle size at biologically relevant temperatures. Further differential scanning calorimetry and SAXS studies would be needed to better

understand any changes within the system with increasing temperature, particularly as the phase temperature of the primary lipid component sits between storage and analysis temperature and the biological temperature. Therefore, it would be of value to understand how changing temperature (post-production) may affect the structure of the particles, such an investigation would be best achieved through SAXS analysis due to the ability to control particle size.

A change in the structure of the particles, particularly regarding the internal phase, due to change in temperature may result in the premature release of the API load, or an altered release profile as a function of the nature of the internal phase. This analysis however would be dependent on the formulation, including the specific API and ratio of API to Cithrol, as will be discussed in Chapter 5.
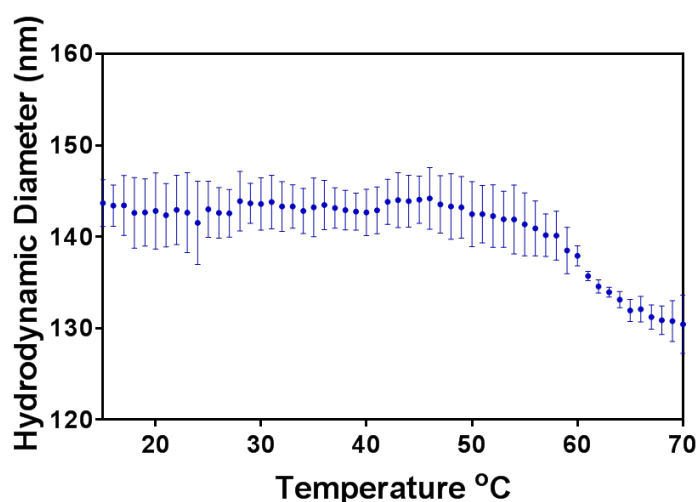
Figure 3.3.16: Size stability, as analysed by DLS, of an extruded (200 nm filter) hexasome formulation (300 mg Cithrol™, 50 mg Synperonic™ F127 and 5.65 mL water) in the15 to 70°C temperature range. The temperature was increased by 1°C and then the sample was allowed 6 minutes to equilibrate prior to measurements being taken. 3 measurements were taken at each temperature point. This experiment was run in triplicate, mean ± S.D.

Particle stability against dilution is crucial as it can be required to achieve an appropriate formulation concentration for administration, and, post-administration, dependent upon the route the formulation will be diluted within the body's fluids i.e., blood. If particles are subject to changing biophysical properties, or even disassembly, upon dilution, they may prematurely release their API cargo. Alternatively, other characteristics such as size may change, a factor that could change the fate of a particle once administered e.g., particle may accumulate in the lungs as opposed to the liver following I.V. administration. Measuring particle stability against dilution is problematic as samples may fall below the minimum concentration required for analysis. Below in Figure 3.3.17 shows particle size analysis. The formulation was diluted 1 in 10, with a serial dilution, up to a 1 in 1000 dilution. This showed an insignificant decrease in the particle size, despite the observable changes in the particle size profile. However, at the lowest particle concentration the data quality was compromised by the low particle concentration, and analysis of subsequent dilutions was not possible to due instrument limitations. This may prove relevant if this formulation was to be utilised for I.V. applications. The average person has 4.5 to 5.7 L of blood in their body, if a central value of 5 L were to be taken and a dose volume of 1 ml at the 3 mg/ml concentration then the concentration in the blood would be ~ 0.0006 mg/ml. Indications from Figure 3.3.17 would be that particles are stable at this concentration, however this does not account for other environmental factors introduced by the blood.
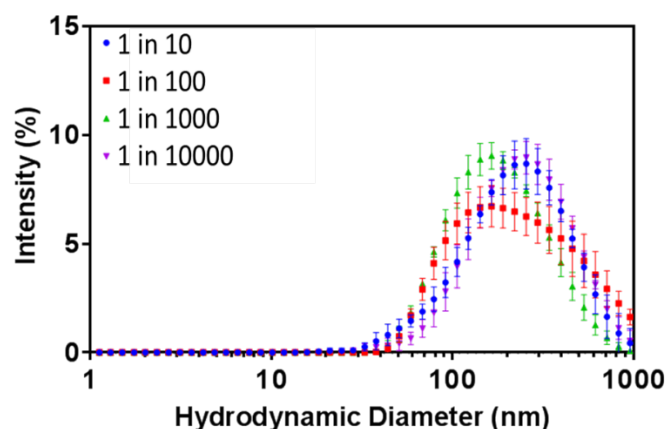
Figure 3.3.17: Changes in particle size distribution, as assessed by DLS, after the formulation has been diluted in water. The initial hexasome formulation was extruded (200 nm filter). Hexasomes were fabricated from 300 mg Cithrol™, 50 mg Synperonic™ F127 and 5.65 mL water. Dilution was performed via a serial dilution. N = 3 ± standard deviation.

3.4. <u>Conclusion</u>

The glycerol monooleate provided by Croda (Cithrol GMO) has a propensity to form a hexagonal phase when fabricated into liquid crystalline phase with Synperonic F127 and excess water at 65 ˚C. This is likely because Cithrol has a purity of ~92% whereas much of the literature utilises glycerol monooleate with a purity of/or exceeding 98%. Therefore, it is believed that this hexagonal phase formation is due to the purity of the glycerol monooleate, or due to the specific nature of said impurities (i.e., oleic acid) this has shown to be a significant factor as to which liquid crystalline phase has been formed. Later experiments detailed in Chapter 5 indicate the significance of how secondary species within the structure of the

particles can manipulate the phase being formed. The most likely reason for this and most likely impurity causing this is the oleic acid impurity, (supplier reported). The oleic acid may pack within the fatty acid tails of the glycerol monooleate, increasing the average tail volume, whilst actively decreasing the average head area as indeed the oleic acid lacks a lipid head group (126). To conclude, the Croda Cithrol^{TM} HP GMO has a propensity to form a hexagonal phase formulation.

During investigations into the different methodologies to produce liquid crystalline phase particles the utilisation of ethanol was explored for its role in the hydrotrope method. Both hexagonal, sponge and cubic phase lipid liquid crystalline nanoparticles have been produced here dependent upon the utilisation of ethanol within the formulation; with an increasing proportion of ethanol leading to a decrease in the critical packing parameter. Subsequently in this work however, methodologies not requiring ethanol were utilised, both to avoid the risk of API degradation through solvents, remove/not introduce the need to remove ethanol from the final formulation, and to avoid the additional structural changes that arise with the incorporation and removal of ethanol.

Stability studies showed the formulation's internal structure remained unchanged over 2 months at room temperature. Size stability experiments in the 15-70°C range showed no change in particle size up to 55°C, above this temperature a decrease in particle size was observed. A future study here may be to assess if changes occur in the internal liquid crystalline structures, via SAXS, at these increasing temperatures. Formulation stability against dilution studies indicated a stable particle size up to a 1 in 1000 dilution, however measurements at further dilutions was limited due to technique/instrument sensitivity.

The characteristics identified and discussed within the three-liquid crystalline (cubic, hexagonal and sponge) phases formed are all desirable as a drug delivery system when they are in their discrete particulate form. Identified in this work are methods in which one can manipulate which phase is formed and change particle size through formulation and fabrication parameters, for example with extrusion. As such, each formulation may be tailored based on the disease to be treated. Evidence here and within the literature suggests a broad range of APIs may be incorporated, including small molecular weight drugs, peptides, proteins, nucleic acids etc.

3.5. <u>Supplementary information</u>

No supplementary information has been included for this Chapter.

Chapter 4: Evaluation of liquid crystalline phase particles to encapsulate active pharmaceutical ingredients.

Presented here is the process and success in encapsulating 15 APIs. The highest encapsulation efficiency of 96.4% was achieved with the small molecular weight drug Amitriptyline. Subsequent analysis of the API loading versus the API physicochemical characteristics showed molecular weight, polar surface area, and the number of hydrogen bonding capabilities were significant factors impacting an API's drug loading.

API release studies were conducted showing a sustained release profile in line with the literature. Preliminary analysis indicates a link between the rate of API release and an API's logD.

4. Evaluation of the capabilities of liquid crystalline phase particles for active pharmaceutical ingredient encapsulation

Covid-19 Impact Statement

Scheduled HPLC analysis of the samples containing a further 8 different APIs and samples exploring varying API loading targets were negatively impacted, along with the corresponding API release studies, due to the COVID19 restrictions, as HPLC studies were to be conducted at Croda.

4.1. Introduction

Recently LC phase particles have been investigated in the field of drug delivery; most examples of this feature cubosomes (cubic phase particles), some examples being given by Faria *et al*., (127) who utilised cubosomes for the delivery of elesclomol (mitochondrial anticancer drug) and Boge *et al*., (128) who used cubosomes for the topical delivery of antimicrobial peptide LL-37. There are some examples of hexasomes being used, such as reports by Negrini and Mezzenga, (78) who encapsulated phloroglucinol in hexasomes. These liquid crystalline particles are attractive due to their biocompatible components and reported ability to encapsulate hydrophobic and amphiphilic drugs (129–131), exhibition of sustained release and ability to protect APIs from degradation (85). Interestingly, in some cases other particles have been encapsulated into cubosomes, such as magnetic nanoparticles (73).

Cubosomes has been documented to enable drug delivery following oral, topical, buccal (132), mucosal, transdermal (85), ophthalmic (81), intravenous (85),

nasal (54,85), intraarticular and intraduodenal routes, *in vivo* and *in vitro* models. Hexasomes have been reported for intravenous infusion, transdermal (85), transmucosal, intravenous (133) and oral delivery (38). No literature was identified for instances in which spongisomes were used for drug delivery, however an example of sponge phases being used for transdermal drug delivery was found (91) (discussed in Chapter 1).

LC phase particles consist of an intricate network of lipid bilayers, this, along with the presence of Synperonic in formulations has been reported to give particles stability during storage (85) (Chapter 3). Additionally, this intricate network offers an increased hydrophobic volume and hydrophilic surface area capable of encapsulating hydrophobic or amphiphilic APIs compared to liposomes.

This Chapter focuses on how the LC phase particles encapsulate a variety of APIs; whilst Chapter 5 later explores the LC phase characteristics are altered upon the inclusion of API molecules. API inclusion/encapsulation and subsequent release will be analysed to identify any correlation between physiochemical characteristics. In the future, these studies may be utilised to improve the API's bioavailability through its solubilisation into the LC structure. This work aims to produce LC phase particles which can encapsulate new APIs with predictable effects upon the LC phase, API loading, and API release profile. To do so, a broad range of APIs with varying physiochemical properties (i.e. molecular weight, LogP and number of aromatic rings) (Table 4.1.1) were encapsulated to identify which API characteristics are most influential in inducing a given LC phase in LC nanoparticles, API loading and API release profile.

The loading of APIs into the LC structure is could be expected to change the particle's LC phase, as many studies in the literature have already documented, examples of the introduction of secondary species inducing phase shifts (134). The effect of secondary lipid species and other guest molecules, including tetradecane (135), peptide KALP31 (136), and sucrose (136), have previously been identified to induce a phase transition.

To ascertain the capabilities of the developed formulation for API encapsulation 15 different APIs were encapsulated. These included amphiphilic drugs, hydrophobic drugs, and a peptide API. These APIs were selected for their varying physicochemical properties e.g., molecular weight, solubility, ability to form hydrogen bonds etc... (Table 4.1.1) as opposed to their clinical function or clinical need for their formulation. The differing physicochemical properties then would allow for the determination of which physicochemical properties held the most significant in determining a given APIs encapsulation efficiency. A general criterion was set out for the selection of APIs in that they should be hydrophobic or amphiphilic and not vary too significantly in molecular weight, i.e., all APIs should be considered low molecular weight drugs. However, it should be acknowledged that conclusions from this study therefore are only applicable to APIs fitting this criterion. Discussed in section 4.3 are some of the potential clinical benefits that may arise from these APIs being encapsulated into liquid crystalline formulations fabricated in this study.

Table 4.1.1. The physicochemical properties of the APIs encapsulated into the liquid crystalline formulations in sections 4.4 and 4.5. information was sourced from www.go.drugbank.com, May 2020.

Active Pharmaceutical Ingredient	Molecular Weight (gmol^{-1})	# Aromatic Rings	Heterogeneity	# Rotatable Bonds	# Hydrogen Bonds	LogP	LogD pH (at 7.4)	Solubility	Polarizability (Å^3)	Van der Waals Volume (Å^3)	Van der Waals surface area (Å^2)	Solvent accessible surface area Å^2)	Polar Surface Area Å^2)
Amitriptyline HCl	313.9	2.0	0.0	3.0	1.0	4.8	2.5	-2.6	35.3	282.8	457.2	529.7	3.2
Budesonide	430.5	0.0	1.0	4.0	6.0	2.7	2.7	-4.7	45.5	405.4	641.2	535.8	93.1
Chloroquine	319.0	2.0	1.0	8.0	3.0	3.9	0.9	-3.7	38.1	312.6	528.4	597.8	28.2
Chlorpromazine HCl	354.0	2.0	1.0	4.0	2.0	4.5	2.7	-5.3	36.0	284.7	456.7	499.6	6.5
Clomipramine HCl	314.0	2.0	1.0	4.0	2.0	4.9	3.1	-4.6	36.5	299.7	494.4	520.9	6.5
Cyclosporine	1202.6	0.0	1.0	15.0	12.0	3.6	3.6	-6.5	127.9	1217.9	2029.1	1323.9	279.0
Dexamethasone	392.5	0.0	0.0	2.0	5.0	1.7	1.7	-4.0	39.6	362.1	565.5	435.4	94.8
Estradiol	272.4	1.0	0.0	0.0	2.0	3.8	3.7	-4.0	31.3	269.7	436.6	395.1	40.5
Fenofibrate	360.8	2.0	0.0	7.0	3.0	5.3	5.3	-5.9	38.2	325.4	533.6	643.5	52.6
Glipizide	445.6	2.0	1.0	6.0	6.0	1.4	0.5	-0.1	45.1	394.5	650.5	747.3	130.2
Haloperidol	375.9	2.0	1.0	6.0	3.0	3.7	2.9	-3.7	39.5	337.8	545.1	562.9	40.5
Haloperidol Decanoate	530.1	2.0	1.0	16.0	3.0	7.9	7.0	-7.5	58.0	515.3	856.5	919.8	46.6
Hydrocortisone	362.5	0.0	0.0	2.0	5.0	1.3	1.3	-3.0	35.3	347.3	556.5	424.3	94.8
Imipramine HCl	316.9	2.0	1.0	4.0	2.0	4.3	2.5	-2.0	34.7	285.7	477.9	502.7	6.5
Mefenamic acid	241.3	2.0	0.0	3.0	3.0	5.4	2.2	-0.6	26.9	226.0	361.6	440.7	49.3
Menadione	172.0	1.0	0.0	0.0	2.0	1.9	1.9	-3.1	18.7	152.3	227.4	326.3	34.1
Mometasone Furoate	512.4	1.0	1.0	5.0	4.0	5.1	5.1	-6.5	51.4	450.9	689.6	528.8	93.8
Nortriptyline HCl	263.0	2.0	0.0	3.0	1.0	4.4	1.6	-4.2	33.4	265.0	433.7	488.0	12.0
Progesterone	314.5	0.0	0.0	1.0	2.0	4.2	4.2	-5.6	36.5	321.0	524.4	423.7	34.1
Propofol	178.3	1.0	0.0	2.0	1.0	4.2	4.2	-3.5	21.9	192.6	331.1	405.1	20.2
Quinine HCl	324.0	2.0	3.0	4.0	4.0	2.5	0.9	-2.8	38.4	310.1	484.8	468.4	45.6
Tolbutamide	270.0	1.0	0.0	4.0	3.0	2.3	1.4	-3.8	27.8	244.8	421.1	554.1	75.3
Trazodone	371.0	3.0	3.0	5.0	4.0	3.1	3.0	-3.8	39.2	327.0	501.7	552.0	42.4

4.2. **Experimental**

Materials used here are as reported in Chapter 2. Particle characterisation techniques are as reported in Chapter 2. All formulations were produced with 300 mg Cithrol, 50 mg Synperonic F127 and 5.65 mL of water. Dye or API was added to this at a w/w calculated in relation to the Cithrol. Formulations were allowed a day to stabilise at room temperature prior to the removal of free dye or API.

4.2.1. Dye or API encapsulation

The dye riboflavin was used as a model API for assay development; Nile Red was used to study the ability to encapsulate APIs in hydrophobic pockets, Nile Red was selected for this due to its solvachromatic properties. Dye or API was weighed as solid material directly into scintillation vials (with the Cithrol and Synperonic). In the event the weight of dye required fell below the scale's accuracy a stock solution was made utilising a solvent e.g., acetone or ethanol; the appropriate volume of the stock was transferred into a scintillation vial. The solvent used was given time to evaporate (~1 day for volumes up to 200 µl) before adding the Cithrol (300 mg) and Synperonic F127 (50 mg) into the vial. The procedure was then followed as described in section 3.2.1.1.. Samples were not extruded unless stated otherwise.

4.2.1.1.1. Unencapsulated dye removal

Size separation, and hence free dye removal, was performed using GE Healthcare size separation PD10 columns. Columns were washed through with the elution medium, milli-Q water, prior to use. Multiple sample aliquots were collected

and analysed both visually and via dynamic light scattering to identify which sample fractions contained particles and which contained free dye.

4.2.1.1.2. Unencapsulated API removal

Free API removal was performed using Amicon® Ultra-Centrifuge filters (Sigma Aldrich, U.K.) device with a 300 KDa molecular weight cut-off membrane. Devices were centrifuged at 4,000 x g (swing bucket) for 20 minutes at ambient temperature. Sample was taken from the top of the device for storage and analysis.

4.2.1.2. *Dye Release*

In this investigation a 3.5 kDa dialysis membrane (Sigma Aldrich, U.K.) was used. 5 mL of the 7.5 mL collected from the size separation columns was used. Fraction selection was based on DLS measurements. If it were to be assumed there was no loss of lipid material, the concentration of particles was 40 mg/mL with a total of 200 mg of GMO in samples used for dialysis. The dialysis medium was milli-Q water, with a volume of 200 mL. Beakers were kept in a gyrating water bath at 37°C with no to minimal exposure to light (vials were individually wrapped and kept in a dark environment within the water bath).

4.2.1.3. *Dye (Riboflavin) Quantification*

A calibration curve was produced via serial dilution. 200 µL of each sample was loaded into a 96 well black nucleon plate (ThermoFischer, U.K.) in triplicate. Dye containing hexasome, and dye-free hexasome (control) samples were analysed.

Plates were then analysed by a TECAN plate reader. An excitation of λ = 445 nm and emission of λ = 520 nm was used for Riboflavin measurements.

4.2.2. API Loading and Release Analysis

API loading analysis was performed as reported in section 2.4

4.2.3. Correlation Analysis

The Pearson regression analysis was carried out using GraphPad Prism 8 software. Physicochemical properties of each API were compiled into Table 4.1.1. The physicochemical property values were cross analysed using Pearson regression analysis with values obtained for API loading (w/w and mol/mol were both analysed) when a 10% API loading (w/w) was targeted.

4.3. **Results and Discussion**

4.3.1. Dye Encapsulation Studies

Once the liquid crystalline formulation protocol was established, as described in Chapter 3, initial groundwork investigation was performed to establish this formulation's capabilities to encapsulate an API and subsequently release it. A variety of dyes were explored in preliminary investigations to examine the potential of liquid crystalline phase particles to encapsulate guest molecules. Reported here is the dye explored most comprehensively in this body of work, Riboflavin, also known

as Vitamin B$_2$. Riboflavin is a fluorescent molecule allowing for rapid dye quantification through fluorescence spectroscopy.
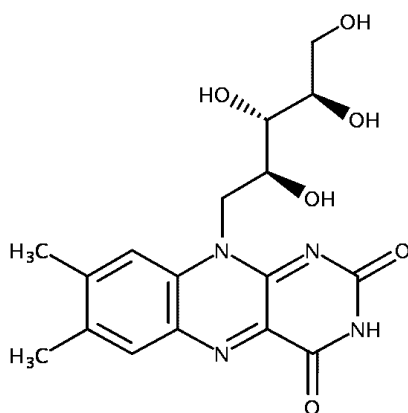
Figure 4.3.1: Chemical structure of Riboflavin 7,8-Dimethyl-10-[(2S,3S,4R)-2,3,4,5-tetrahydroxypentyl]benzo[g]pteridine-2,4-dione; Formula: C$_{17}$H$_{20}$N$_4$O$_6$. MW: 376.37 g·mol^{-1}. Excitation l = 445 nm and emission l = 520 nm.

Riboflavin was encapsulated into liquid crystalline formulations at increasing w/w percentages (Riboflavin: GMO) of 5, 10, 25 and 50% (Figure 4.3.2). This showed a non-linear trend in the dye loading relative to the quantity of dye added to the formulation. Data suggest a maximum dye loading has been reached between 5 and 25% of dye loading as at higher percentages the amount of encapsulated dye does not increase. More investigation would be required to find the maximum loading however due to large increments in percentage dye increase used in this study. Subsequent dye release analysis indicated a potential quenching effect of the liquid crystalline particle structure upon the dye, this may be because of the dense lipid structure not allowing the transmittance of fluorescence. This became evident when conducting dye release studies as shown in Figure 4.3.3 where a significantly higher

amount of dye is released from the formulation than what was calculated to be encapsulated.
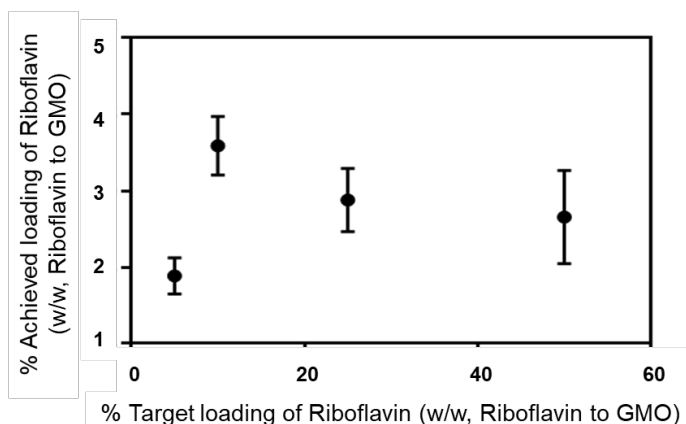
Figure 4.3.2: Achieved % loading Riboflavin versus targeted Riboflavin in the base hexasome formulation (300 mg Cithrol™, 50 mg Synperonic™ F127 and 5.65 mL water). The values were calculated using the equation of the line of best fit in the calibration graph (Figure 4.5.1).
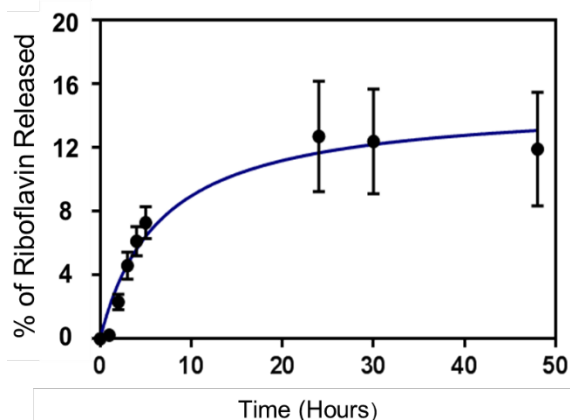
Figure 4.3.3: Dye release profile of Riboflavin from hexasomes produced with 300 mg Cithrol™, 50 mg Synperonic™ F127 and 5.65 mL water and 50 mg of Riboflavin; unencapsulated dye was removed though the use of PD10 size separation columns. Formulation was dialysed into water using a MWCO 3.5 kDa dialysis membrane. N = 3 ± S.D.

Riboflavin containing hexasomes were dialysed into water (3.5 kDa MWCO membrane) (Figure 4.3.3), this showed dye release lasting an excess of 5 hours, with a plateau being observed from 24 hours onward. The steady, controlled like, release of Riboflavin would indicate non-burst release (burst release being the immediate release of molecules encapsulated within structures, where upon the decay of the structure all encapsulated molecules are released instantaneously). This release profile is likely due to the gradual release of dye through diffusion or decay of the cylinders within the hexagonal phase. Here, speculated is that cylinders on the outer regions of the hexasome particle will likely rapidly release their dye load, whilst the inner cylinders releasing their dye at a delayed rate/time.

The dialysis medium volume was calculated based upon the value of dye encapsulated when comparing to the calibration, however, the quenching resulted in a lower amount of dye being assumed than what was present, and so it is probable that the dialysis medium reached saturation before all the dye was fully released.

This preliminary investigation as to dye release has been promising and enabled the use of fluorescence studies prior to research progression into model API encapsulation which requires HPLC analysis for API quantification.

Baseline particle characterisation was performed on the Riboflavin containing formulations to establish methods to assess the influence of guest molecule(s) incorporation upon the particle characteristics. DLS particle sizing (Figure 4.3.4) and examination of changes in the internal structure using SAXS (Figure 4.3.5) methods were selected. Data shown in Figure 4.3.4 is for formulations containing a targeted 10% w/w of Riboflavin to Cithrol. Comparing particle size distribution of empty and

Riboflavin loaded hexasomes shows that particles are still formed in the presence of dye and that there is no significant change in the particle size distribution upon the addition of dye.

Internal structure analysis (Figure 4.3.5) showed the maintenance of the hexagonal phase, but with a discrete increase in the lattice parameter. The lattice parameter is the measure in size of each repeating unit of structure. The *d*-spacing in the control hexasomes is 5.68 nm, and 5.74 nm with Riboflavin encapsulated, indicating potentially that dye incorporation does not impact the internal architecture. The incorporation of Riboflavin into the liquid crystalline structure could have the potential to increase the distances between neighbouring lipids, which in turn may increase the lattice parameter.
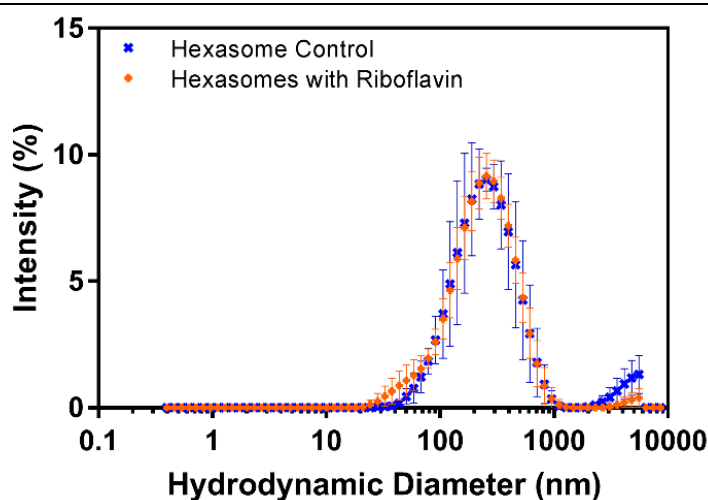
Figure 4.3.4: Overlay comparing particle size distribution, by DLS analysis, of comparable formulations of 'empty' hexasomes and hexasomes containing the dye Riboflavin (300 mg Cithrol™, 50 mg Synperonic™ F127 and 5.65 mL water, the dye containing sample contained 30 mg of Riboflavin).
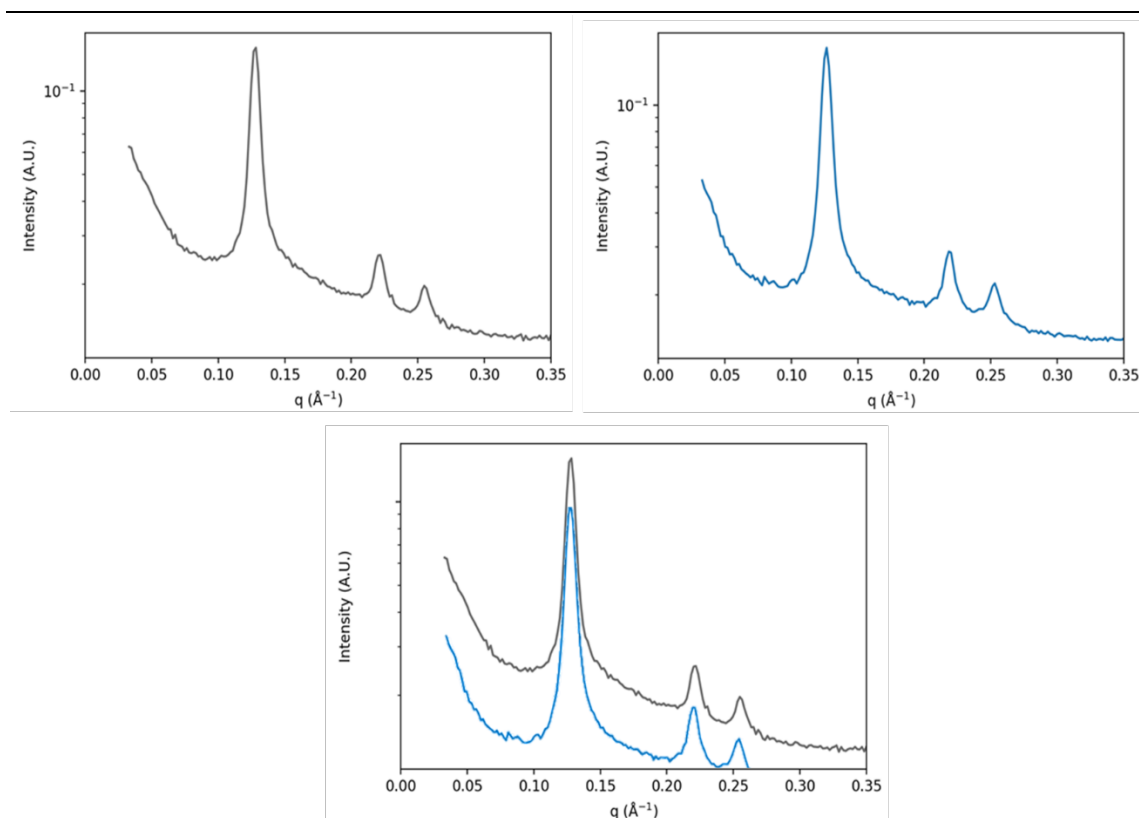
Figure 4.3.5. Comparison of the small angle x-ray scattering (SAXS) profiles of hexasomes containing Riboflavin (right) and 'empty' hexasomes (left) (300 mg Cithrol™, 50 mg Synperonic™ F127 and 5.65 mL water, the dye containing sample contained 30 mg of Riboflavin). Below is an offset overlay of the two spectra.

Key limitations in the dye-based studies related to the poor measurement of encapsulated dye. Dye was not adequately released from the liquid crystalline structure for fluorometric quantification. Adaption of the protocol to release the dye fully from the structures was not achieved as this required significant solvent dilution of the sample. Such significant dilution with a solvent (i.e. ethanol) lead to a dye concentration outside/below of the linear calibration range. Upon switching to HPLC analysis for APIs however this was overcome. HPLC offered an increased sensitivity

and lower limit of detection for APIs and so a greater solvent dilution could be performed. This dilution released all or near to all encapsulated API. Hence, an overall limitation in the quantification of molecules encapsulated in liquid crystalline particles is that the inherent stability of the particles leads to the requirement of high dilution to solubilise the structure – releasing the API cargo.

It may be imagined hydrophobic APIs will pack within hydrophobic micro-domains, investigations using the solvatochromic dye Nile Red showed the preferential partition of dye into a highly hydrophobic domain, alike to a pure ethanol environment (Figure 4.3.6). The hydrophobic micro-domain area will be limited, leading to a theoretical maximum loading within the liquid crystalline structure. In differing solvent systems, the maximum emissions wavelength of Nile Red shifts, as shown here by altering the ratios of water to ethanol. These wavelengths can then be compared to the emission spectra of hexasome encapsulated Nile Red; in hexasomes the local environment of Nile Red is comparable that in pure ethanol environment. This experiment therefore presents evidence that APIs may pack comfortably into a purely hydrophobic environment within the hexagonal phase structure of hexasomes. This consideration is helpful in determining the suitability of hexasomes for the encapsulation of solvent sensitive/hydrophobic environment sensitive APIs. This could be investigated further with small angle neutron scattering (SANS) experiments.
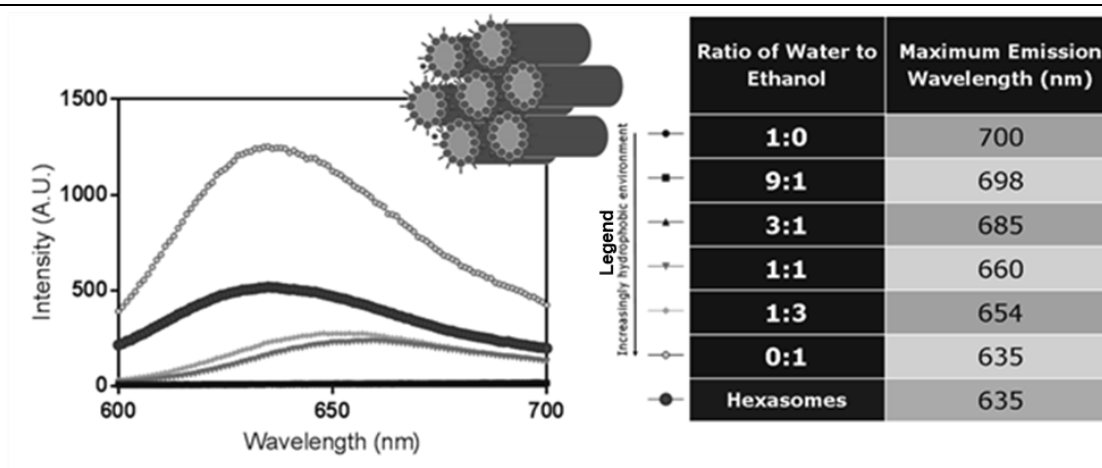
Figure 4.3.6. Analysis of API loading location within hexasomes (300 mg Cithrol™, 50 mg Synperonic™ F127, 5.65 mL water and 3 mg of Nile red) via the use of the solvatochromic dye Nile Red. λ_{ex} = 552 nm.

4.3.2. API Encapsulation Studies

Initially the aim was to investigate the ability of formulated liquid crystalline particles to encapsulate APIs. The initial study with Riboflavin as a model API, gave the initial proof of encapsulation capabilities. Subsequently a range of differing APIs were encapsulated. These APIs were selected both for a potential clinical need but primarily because of their physicochemical profiles. Figure 4.3.7 displays the encapsulation (drug loading values) for a selection of APIs. APIs were all formulated within the liquid crystalline nanoparticles (300 mg Cithrol, 50 mg Synperonic F127 and 5.65 mL water) at the same initial w/w 10% loading (API to GMO).
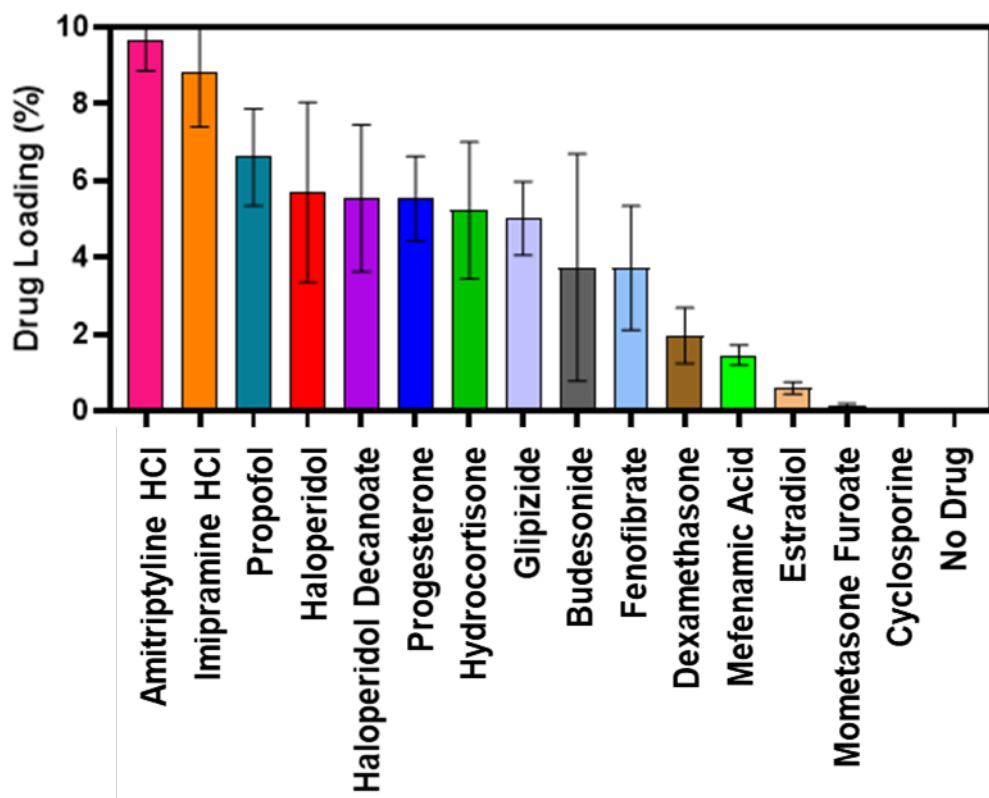
Figure 4.3.7. API encapsulation into the lipid liquid crystalline phase formulations. Each API was loaded at a targeted 10% w/w of API to GMO (300 mg Cithrol™, 50 mg Synperonic™ F127 and 5.65 mL water). API loading was quantified by HPLC; Drug loading is expressed as w/w of API to GMO. Error bars= 1 S.D. n= 3, N= 3. The targeted drug loading was 10%, therefore a drug loading of 10% represents a 100% encapsulation efficiency.

As can be observed in Figure 4.3.7 there is high variability in API loading and encapsulation efficiency. The variability between repeat samples and repeat measurements from the same sample (3 aliquots of sample was taken for analysis) was investigated. It was found that sample flocculation, which was variable between formulations, led to highly variable encapsulation efficiencies being shown due to the limited ability to take a homogeneous sample aliquot for HPLC analysis.

Measurements of a Propofol-containing sample showed that the flocculant contained substantially more API than the lower non-flocculated sample (Figure 4.3.8). SAXS analysis (Figure 3.3.9.) also showed that this flock contained a significantly higher abundance of the ordered liquid crystalline phase.
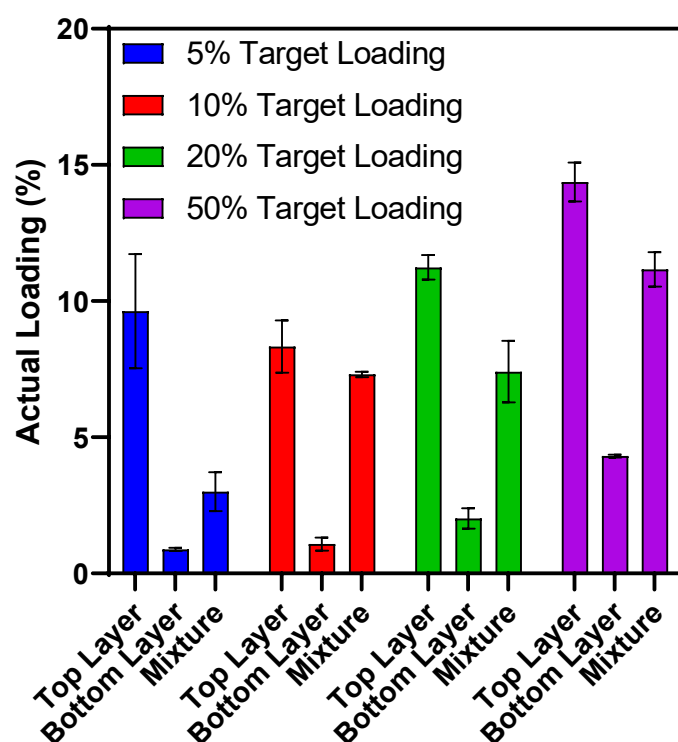
Figure 4.3.8: Analysis of Propofol loading (w/v) across the different layers of the formulation (300 mg Cithrol™, 50 mg Synperonic™ F127 and 5.65 mL water, with 15, 30, 60 and 150 mg of Propofol). 'Mixture' denotes sample taken from freshly vortexed sample that on visual observation appeared homogeneous; 'Top Layer' denotes sample taken from flocculated layer consisting mainly of liquid crystalline formulation, 'Bottom Layer' denotes formulation layer under flocculated material and contains mostly non-ordered particles, as confirmed by SAXS. N=3 ± S.D. A preferential loading of API into the top layer can be observed, increasing the drug loading in the top layer relative to the targeted loading across the whole sample.

The variability between loading of the different APIs was investigated through Pearson regression analysis (Figure 4.3.9). For this analysis both API loading reported as mg of what per mg of what, and as mol per mol was used. Physicochemical properties for each API were gathered (Table 4.1.1) and compared to the API loading data. This analysis (Figure 4.3.9) highlighted strong correlations between API loading and the following API's molecular descriptors and physicochemical properties: hydrogen bonding capacity, polar surface area, molecular weight, and, to less extent, polarizability, Van der Waals volume, Van der Waals surface area, and solvent surface area. These parameters are discussed in the following text with the reasons proposed to correlations observed. To confirm the proposed reasoning, further computational work would be desirable, as well as investigation into wider panel of APIs to strengthen the trends observed.
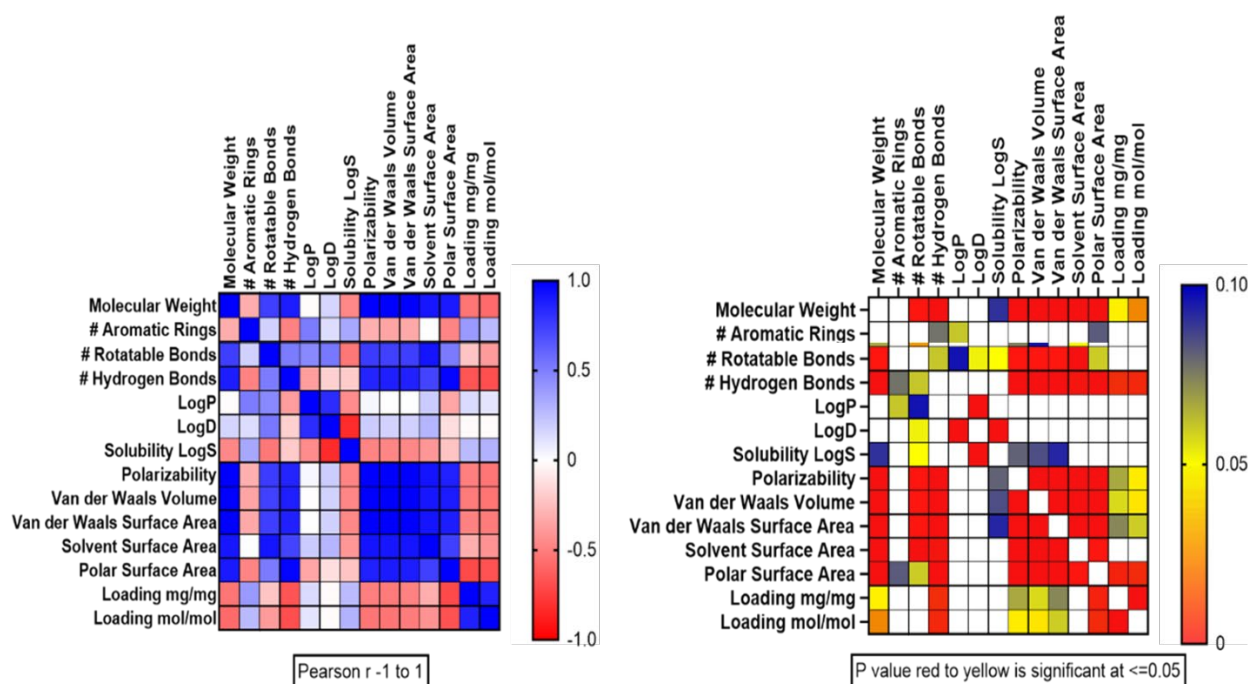
Figure 4.3.9: Pearson regression analysis examining the correlation between the physicochemical properties of APIs and their loading into hexasomes (300 mg Cithrol^{TM}, 50 mg Synperonic^{TM} F127, 5.65 mL water and 30 mg of API). The plot on the left indicates the directionality of the trend, i.e., red shows an inverse relationship whilst blue shows a positive relationship. The plot on the right indicates the significance of the trends identified through the Pearson regression analysis. The 15 APIs and their loadings were included in this analysis.

The hydrogen bonding capabilities, or number of hydrogens bonds, refers to the number of moieties within the API structure that have the capabilities of being a hydrogen bond acceptor or donor. An inverse relationship was identified between the API loading and number of hydrogen bonding moieties. The trend was most significant when the number of hydrogen bond donors and acceptors was combined

rather than when they were treated as individual parameters. Those API molecules with hydrogen bonding capabilities may interact more with the suspension medium of the particles, in this case water, reducing the preference for the API molecule to situate itself between the lipid tail groups during the self/assembly of the particles.

The polar surface area of a molecule refers to the surface area of a molecule from its polar functional groups. The relationship is like the relationship between API loading and hydrogen bonding. As polar surface area increases API loading decreases. As the particle suspension medium in this instance is polar (water), the more polar molecules may preferentially interact with the suspension medium rather than the non/polar tail groups of the GMO - whilst the non/polar APIs may preferentially pack within the non/polar tails.

Polarizability can give an indication as to how an API may interact with neighbouring molecules. An increase in the polarizability of an API may result in dipole–dipole or charge–dipole interactions between high-polarity API molecules and associated molecules (137). However, there is an inverse correlation observed between an API's polarizability and the API loading into liquid crystalline particles. This may indicate non-preferential interactions between GMO, and/or Synperonic, and an increasingly polarizable API, or preferential interactions between increasingly polarisable APIs themselves; such preferential interactions may reduce API loading due to APIs precipitating or otherwise aggregating.

As an API's molecular weight increases the API's loading decreases. Larger molecules disrupt the structure of the particle in which it has been encapsulated within more, meaning when the nanoparticle structure self assembles the structure may preferentially assemble away from the large API. Also, when observing Figure

4.3.9 it is observable that many other parameters have a strong correlation with molecular weight, such as the previously mentioned polar surface area and number of hydrogen bonding. Therefore, the correlation observed between molecular weight and API loading may in fact primarily be a composite, due to the associated increase in other critical parameters for API loading when there is an increase in the molecular weight.

Van der Waals surface area, or total molecular surface area (TSA), is the theoretical sum of the atomic van der Waals surfaces. As such, the van der Waals surface area is highly linked to the solvent surface area. Whilst the van der Waals volume is the volume of the space inside the van der Waals molecular surface. These parameters all have an inverse relationship to API loading, as these parameters increase, API loading decreases. This can be ascribed to each of these parameters being a descriptor for API size, and as with an increasing MW, an increasing size would lead to a greater disruption of the liquid crystalline phase, this is somewhat supported when reviewing the effect Cyclosporine incorporation has on the liquid crystalline phase, as compared to the smaller APIs (Chapter 5). With many formulation strategies it may be expected that an increase in these size parameters may decrease API loading, but an additional consideration with liquid crystalline formulations is that an increasing API surface area or volume would then result in a greater change in the particle structure, reducing the compatibility of API loading within such structures.
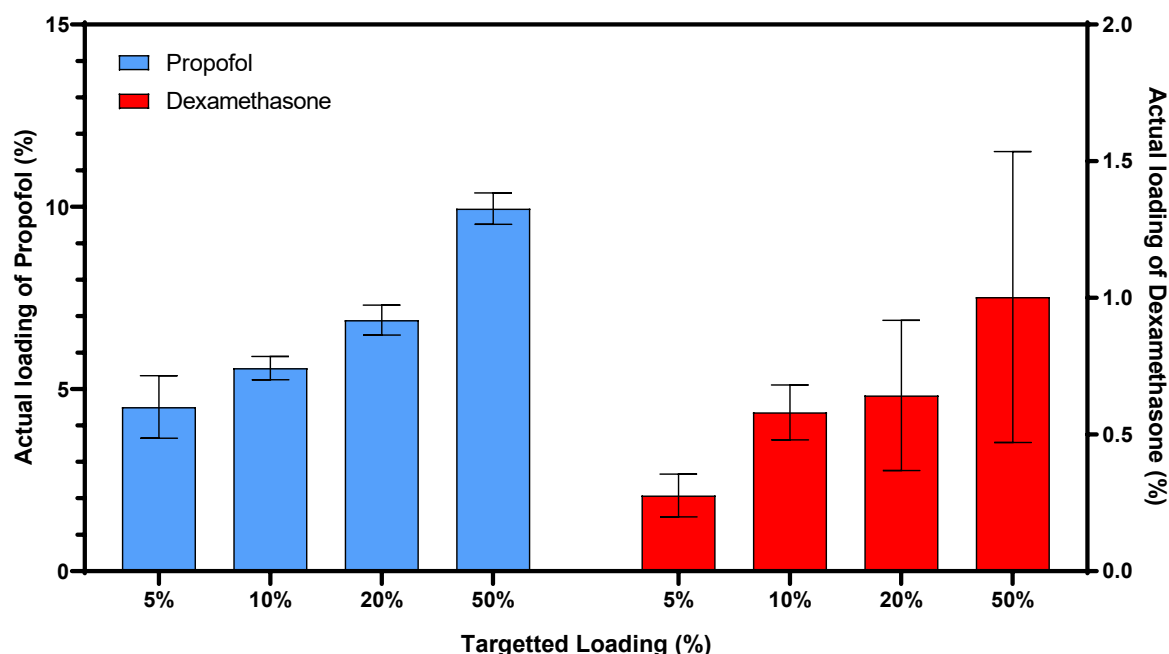
Figure 4.3.10: Effect of increasing proportion of Propofol and Dexamethasone on measured loading (w/w% API: GMO) of fabricated liquid crystalline particles (300 mg Cithrol™, 50 mg Synperonic™ F127 and 5.65 mL water, with 15, 30, 60 and 150 mg of Propofol or dexamethasone). Actual loading was quantified through HPLC. N=3 ± S.D.

In addition to analysing the effect of the physicochemical properties of APIs on their loading, the loading of two different APIs was analysed with increasing initial API: lipids weight ratios in the encapsulation experiments. Here the targeted API loading was increased as a function of weight of API per weight of GMO. In the case of Propofol there was a significant increase (Figure 4.3.10) in the amount of API being loaded when the targeted loading was increased, furthermore there is a significant undesirable decrease in encapsulation efficiency with higher targeted loading. In the case of dexamethasone although there was an increase in the averages of API loading there was high variability within the repeats of each sample

and so a statistically significant trend is not possible to prove; this higher variability may be attributed to higher levels of flocculation in dexamethasone samples relative to Propofol. Dexamethasone has a lower water solubility compared to Propofol and so one possible scenario here is that the poor solubility of dexamethasone was prohibitive for API loading due to the rapid precipitation of Dexamethasone. When producing the high dexamethasone formulations there was some visible precipitation, presumably of dexamethasone. Therefore, in subsequent instances the formulator should find the desirable offset between a higher targeted API loading and a subsequent loss of higher encapsulation efficiency. The desirable point of increased API loading relative to the decrease in encapsulation efficiency may be variable between the desired parameters of the final medicine i.e., dose volume, and the cost and availability of the API. As a limited number (5 APIs were examined in total however the data for these additional APIs was inaccessible due to the Covid-19 pandemic, all APIs however did display a similar trend) of APIs were explored at a variety of targeted loading concentrations it is not possible to draw conclusions between the API physicochemical properties and the ability to increase the maximum achievable API loading.
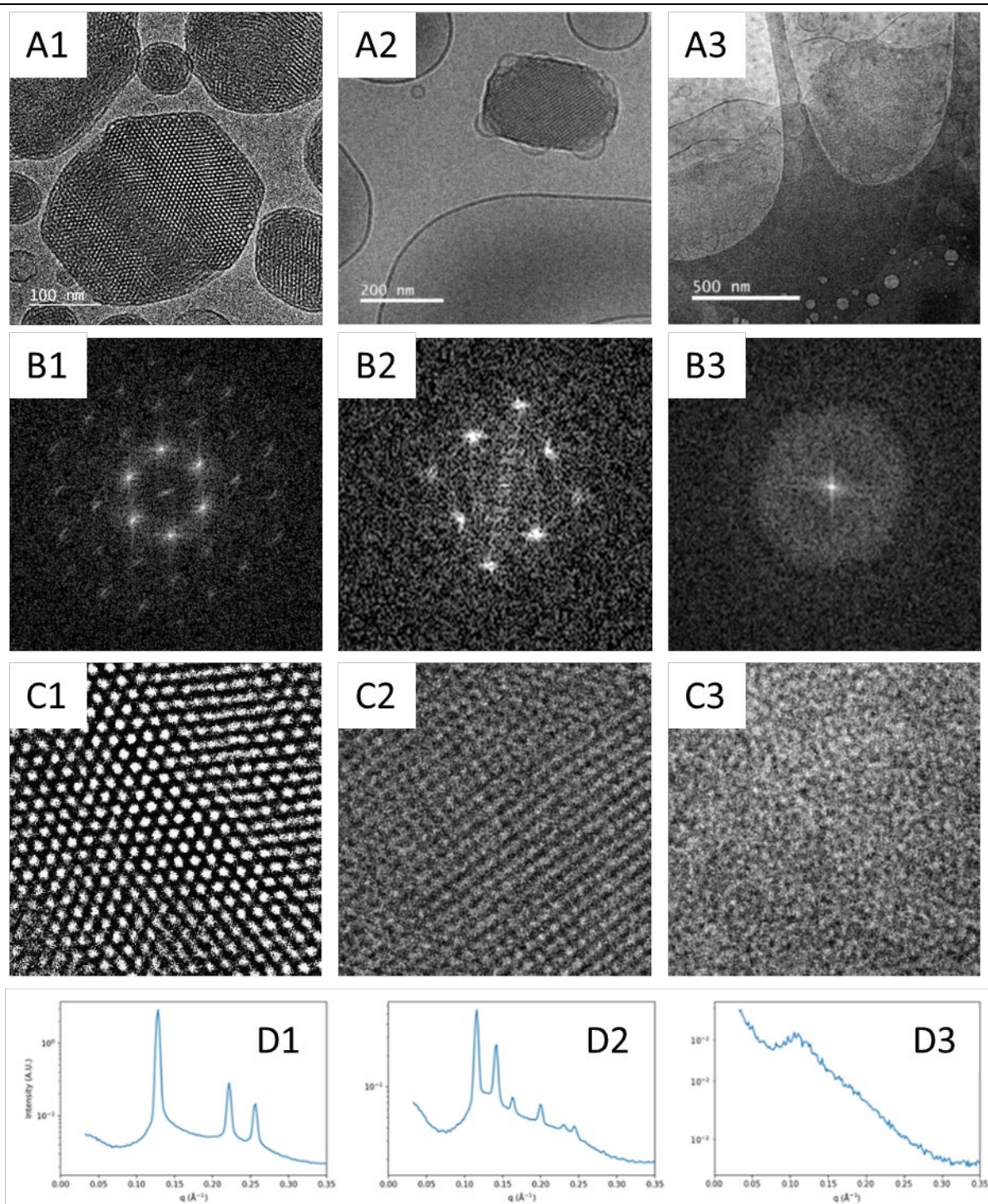
Figure 4.3.11. A) Cryo-TEM micrographs of 1) Hexasomes, 2) Cubosomes and 3) Spongisomes with corresponding B) fast Fourier transforms (FFTs) and C) inverse FFTs. D) shows representative SAXS profiles for 1) hexagonal, 2) cubic and 3) sponge phases. All samples consisted of 300 mg of Cithrol^{TM} GMO, 50 mg of Synperonic^{TM} F127, 5.65 ml Milli-Q water and A) 5% theoretical loading

Progesterone B) 5% theoretical loading Dexamethasone C) 5% theoretical loading Amitriptyline.

The inclusion of APIs has been found to induce changes in the mesophase produced by the Cithrol / Synperonic, API formulation in this work. This was found through cryo-TEM analysis (Figure 4.3.11) where the inclusion of various APIs induced changes in the liquid crystalline phase (this is further discussed in greater detail in Chapter 5). This matches observations from the literature that found that dioleoyl phosphatidic acid incorporation into a GMO based formulation induced the phase change in this direction: $Pn_3m \rightarrow Im_3m \rightarrow L_\alpha$, tetradecane incorporation induced the phase change: $Im3m \rightarrow H_{II}$ (135) and bacteriorhodopsin incorporation induced the phase change: $Q_{II} \rightarrow L_\alpha$ (136). While in our work the nature of the API influenced the LC phase formed, it is not clear how the API properties relate to the formed phase.

The phase shifts in API containing formulations consist primarily of cubic, hexagonal and sponge phase particles (cubosome, hexasome and spongisome), representative cryo-TEM and SAXS profiles are shown in Figure 4.3.11 and Chapter 5. The more API incorporated the larger the structural change, this can be seen in the cryo-TEM micrographs of formulations containing increasing ratios of Amitriptyline (Figure 4.3.12). Shown is the phase shift from hexagonal to cubic; increased API loading may induce further phase shifts, or the system may become saturated with API, leading to multiple possibilities such as complete or partial disruption of the LC phase, or a lack of encapsulation leading to no further change in

the nature of the phase. This is discussed in detail and explored experimentally in Chapter 5.
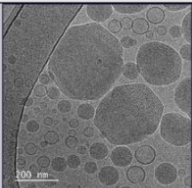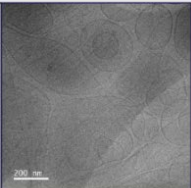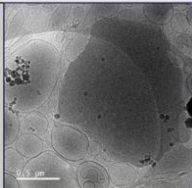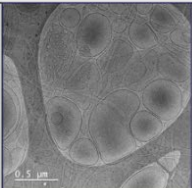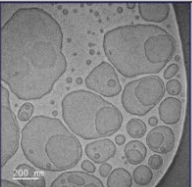
Theoretical Amitriptyline loading	0%	5%	10%	20%	50%
Cryo-TEM					
Mesophase/ Particle Assignment	Hexasomes	Bulk Sponge	Spongisomes	Spongisomes & Vesicles	Spongisomes & Multi Lamella Vesicles
Photographs of Samples					

Figure 4.3.12. Nanoscale and visible observations of formulations (300 mg CithrolTM, 50 mg SynperonicTM F127 and 5.65 mL water, with 15, 30, 60 and 150 mg of Amitriptyline). prepared at increasing concentrations of Amitriptyline (targeted loading). A transition from a hexagonal, to sponge to bilayer phase can be observed through cryo-TEM; whilst visual observations show on increase in the opaqueness of the formulations. Formulations were not extruded or sonicated.

4.3.3. API Release Studies
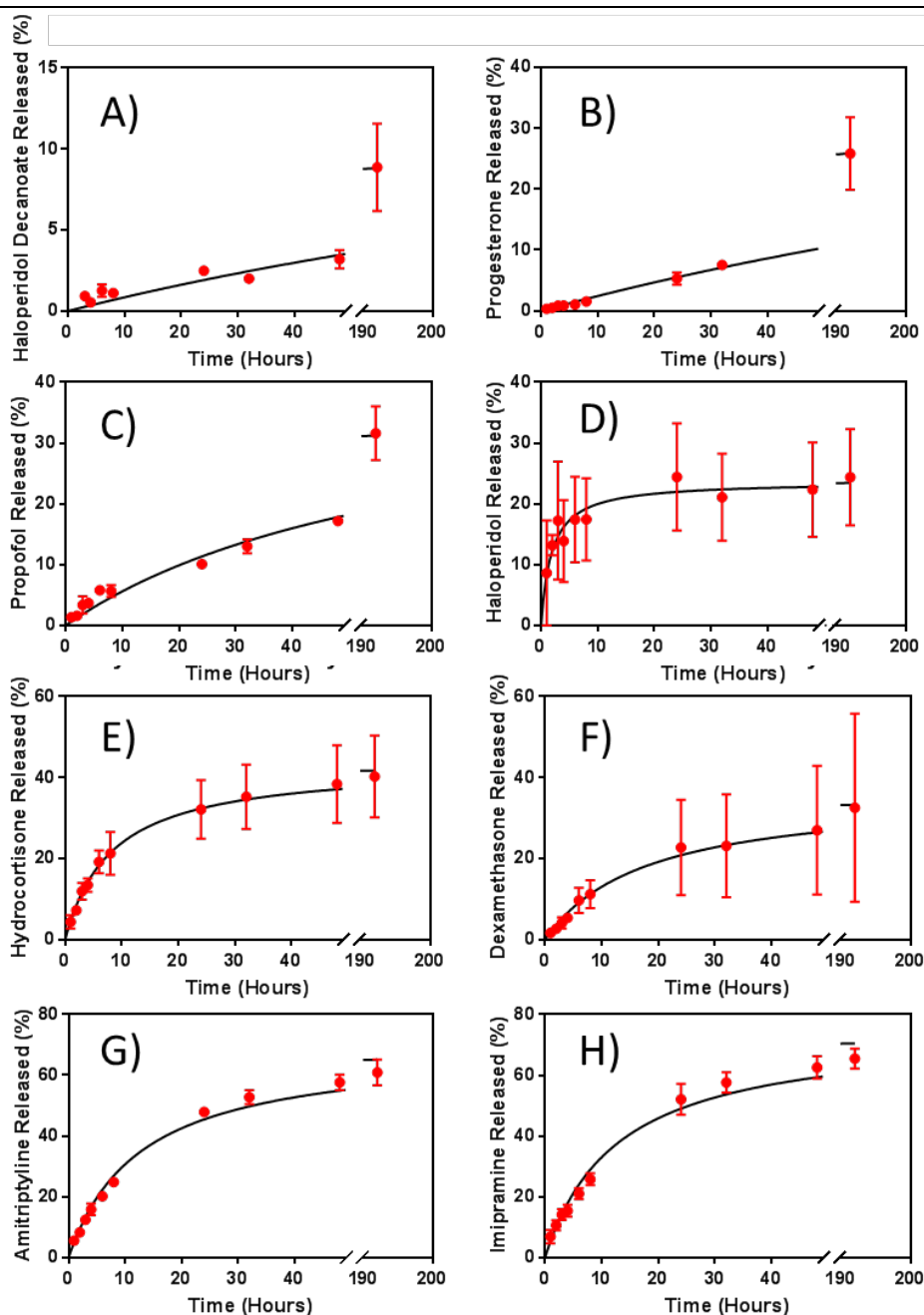
Figure 4.3.13. Cumulative API release profile of APIs, from liquid crystalline formulations, via dialysis into a 1% Tween 20 in water medium: A) Haloperidol decanoate, B) Progesterone C) Propofol, D) Haloperidol, E) Hydrocortisone F) Dexamethasone, G) Amitriptyline HCl, and H) Imipramine HCl. N=3 n=3 ± S.D. Lines represent model fits.

API release studies were performed over an 8-day period via dialysis, using a 1% Tween 20 water solution as a receptor medium. Samples were taken periodically, and the amount of API released was quantified via HPLC. When comparing the physiochemical properties of the APIs (Table 4.1.1) to elucidate a relationship between the API properties and release profile there appeared to be a correlation between the release profiles and an API's logD. API with a lower logD (Table 4.1.1, Figure 4.3.13) exhibit rapid release in the first 8 hours before reaching a low rate of sustained API release. The APIs with the highest LogDs of 8.12, 3.82 and 3.66, Haloperidol decanoate, Progesterone and Propofol respectively, did not reach plateau within the 8 days analysed, additionally the rate of API release remained consistent throughout.

Whereas release studies (Figure 4.3.13) of APIs with logD values 2.93 to -4.64 from the cubosomes, hexasomes and spongisomes follow a highly similar release pattern to the cubosome release studies in the literature (72,133), with initial drug release being rapid before slowing to a sustained rate of release. Kulkarni investigated aspirin release from cubosomes aspirin has a logD of -1.68 and so the release profile fits within the logD relationship that has been identified. Both in our studies, Rizwan's and Kulkarni, incomplete drug release was observed; with apparent plateau in cumulative release profile being achieved at significantly below 100% (72,133). Depending on route of administration the LC structure would likely disassemble under biological conditions e.g., lipases. Haloperidol and Haloperidol decanoate LC formulations may offer great potential for the treatment of schizophrenia (138,139). Haloperidol intramuscular injections exhibit rapid uptake and metabolism (within minutes). By utilising this LC formulation, the sustained release over the initial 3 hours may enable a reduced dosing frequency.

4.4. <u>Conclusion</u>

Encapsulation of a panel of APIs have been achieved with our LC phase particle fabrication procedure whilst achieving encapsulation efficiencies up to 98% and API loading up to 9.8%, a value highest with amphiphilic APIs (Figure 4.3.7). Upon comparing with the literature, instances were identified where LC particles produced throughout this work display a higher encapsulation efficiency and/or higher API loading, depending on the physicochemical properties of the API.

The properties most closely related to higher or lower API loading are the API's: structure, molecular weight, hydrogen bonding opportunities. Some correlation can be identified between these properties and the liquid crystalline phase characterisation, notably both amphiphilic APIs form sponge liquid crystalline phases. Further work was carried out to understand this relationship between an API's physicochemical properties and the liquid crystalline phase formed is reported in Chapter 5.

Release of APIs from liquid crystalline phases occurs over an extended period of days (more investigation required) and has a correlation with logD; APIs with LogDs between 8.12 and 3.66 (Haloperidol decanoate, Progesterone and Propofol) exhibit sustained API release over a period of days, whilst APIs with LogDs between 2.93 to -4.64 exhibit initial rapid release in the first 8 hours – this does not exceed >30% release of total API encapsulated, formulations then exhibit sustained release; which may offer further advantages of liquid crystalline phase particles over simple lipid particles, such as liposomes. Except for Haloperidol, where the API release

occurs within 8 hours then plateaus. These indications show that complete API release is not achieved in a simple dialysis system.

4.5. Supplementary Information
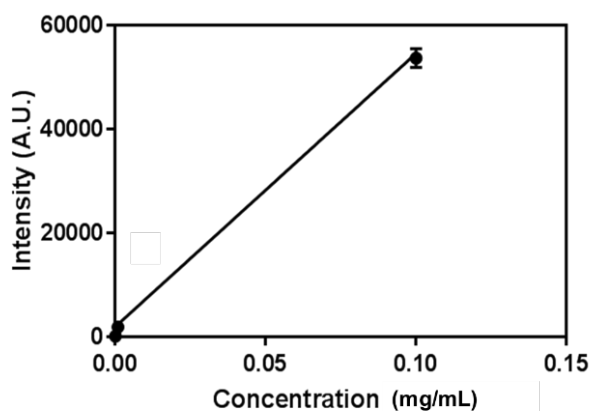
 Figure 4.5.1. Calibration curve for Riboflavin in water. N=3, R^2=0.9561 and Y = 526732 X + 2033. Graph consist of 6 data points.

Table 4.5.1. Solubility and LogP values of APIs as reported in the www.drugbank.com .

Active Pharmaceutical Ingredient	MW (g/mol)	LogP	Water Solubility (mg/mL)
Progesterone	314.469	3.87	0.00881
Dexamethasone	392.467	1.83	0.089
Mometasone	427.362	2.1	Insoluble
Hydrocortisone	362.466	1.61	0.32
Haloperidol	375.868	4.3	0.014
Haloperidol Decanoate	530.121	7.9	Insoluble
Cyclosporine	1202.635	7.5	Slightly
Propofol	178.275	3.79	0.124
Amitriptyline Hydrochloride	313.869	4.92	0.00971
Imipramine Hydrochloride	316.873	4.8	0.0182
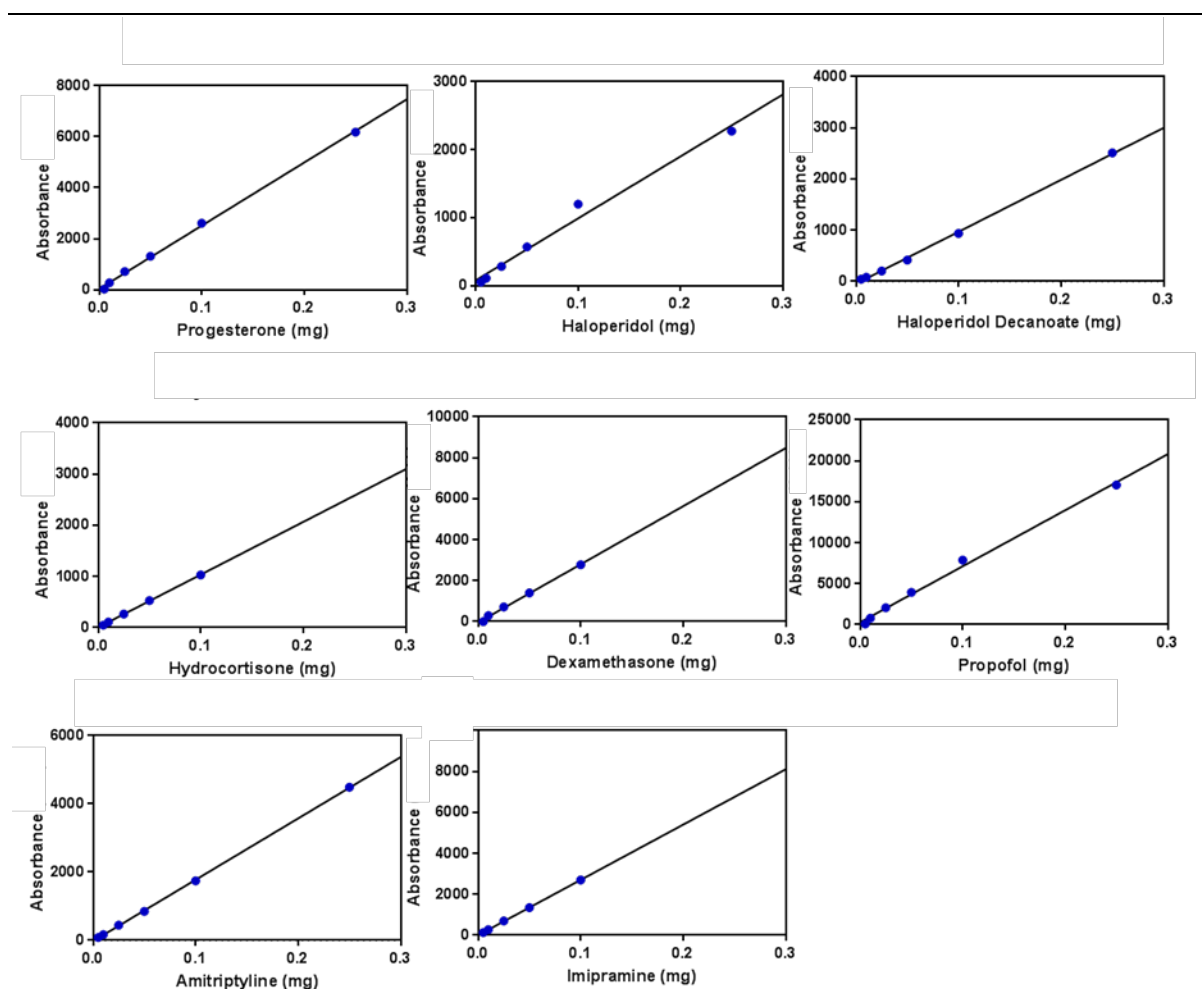
Figure 4.5.2: HPLC calibration graphs for API quantification. For all graphs R²>0.95.

Remaining graphs unavailable due to Covid-19. HPLC was performed at Croda Plc on a non-networked PC, as such data was unable to be accessed throughout the course of the pandemic.

Chapter 5: Influence of guest molecule incorporation upon the self-assembly of liquid crystalline structures.

Cithrol ^{TM} GMO and Synperonic ^{TM} F127 combined at a 6:1 ratio, in excess water, forms an inverse hexagonal nanoparticle suspension, commonly known as hexasomes (as shown in Chapter 3). The inverse hexagonal phase is formed due to the critical packing parameter (CPP) of the system. Upon the encapsulation of an active pharmaceutical ingredient (API) the CPP of the system will be manipulated by the API (as shown Chapter 4, where for example Amitriptyline incorporation resulted in a transition from the hexagonal phase to the sponge phase). Investigated are which API properties will result in the highest manipulation of the CPP, as well as how the API concentration will affect this manipulation. The change in the CPP is characterised through the changes in the liquid crystalline phase, these changes are analysed through small angle x-ray scattering experiments. These experiments showed an inverse relationship between API concentration and the CPP. As the API concentration is increased, the CPP decreased, with the decrease in the CPP the liquid crystalline phase has been shown shift from an inverse hexagonal phase towards a cubic or a sponge phase, with the sponge phase having the lowest associated CPP. A variety of API physicochemical properties have been identified

throughout this work as affecting the CPP. LogS is the most significant (p<0.02)

physicochemical factor affecting the CPP, as LogS increases the CPP decreases.

Decreasing CPP will result in the conversion of the inverse hexagonal phase, to a

cubic phase to a sponge phase. Other significant physicochemical properties have

been shown to decrease the CPP and the said physicochemical property parameter

decreases, these parameters include: Van der Waals surface area and volume, drug

loading (mol/mol), polar surface area and polarizability with a significance of p<0.05.

Less significantly (p<0.10) impacting the CPP is the number of hydrogen bonds,

solvent surface area, and drug loading (mg/mg).

5. Influence of guest drug incorporation upon the self-assembly of liquid crystalline structures.

Covid-19 Impact Statement

Scheduled HPLC analysis to complement data reported in this Chapter was interrupted due to the COVID19 pandemic.

5.1. Introduction

This Chapter considers how the CPP will enable the prediction of how the glycerol monooleate, and any guest molecules, will pack together in the presence of water, based primarily upon hydrophobic and hydrophilic interactions (Figure 1.2.2). The nature of this phase is dependent upon a formulation's constituent molecules CPP. That is, all the molecules that will form a part of the structure (Figure 1.2.1), and not solely the glycerol monooleate that forms the backbone of many liquid crystalline phase formulations.

The addition of guest molecules into the system will induce changes to the CPP, these changes may in turn alter the liquid crystalline phase formed, for example this may induce a conversion of a hexagonal phase structure into a diamond cubic phase (Figure 5.1.1).

As seen in Chapter 3, the glycerol monooleate used in this body of work, Cithrol GMO, will form a hexagonal phase in the presence of water in combination with Synperonic F127 with the given experimental conditions (Chapter 2). Investigated in this Chapter is the influence of active pharmaceutical ingredient (API) incorporation upon the nature of the liquid crystalline phase formed.

Influence of guest drug incorporation upon the self-assembly of liquid crystalline structures.

125

The aim is to understand: (i) the effect of each of the 23 APIs encapsulated (15 of which were analysed via HPLC, as detailed in Chapter 4) on the liquid crystalline phase; (ii) the relationships between API concentration and degree of change in the CPP, and (iii) to elicit the impact of specific API physicochemical properties on the change in the CPP. The latter will indicate which physicochemical properties are most consequential in inducing a change in the CPP and subsequent liquid crystalline phase.
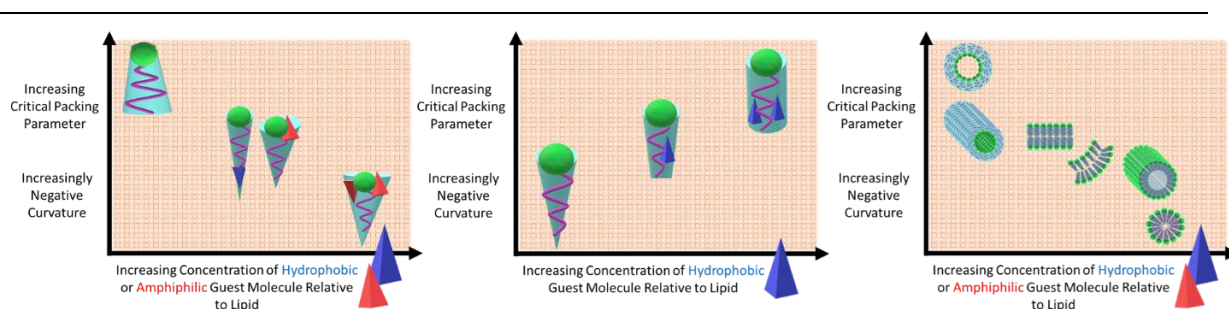
Figure 5.1.1. Effect of guest molecule incorporation upon the critical packing parameter of the system: Influence of hydrophobic guest molecule/API incorporation upon the critical packing parameter of the system. As a hydrophobic molecule will pack within the hydrophobic tail region the tail length will increase, leading to a decrease in the critical packing parameter, and a decrease in the negativity of curvature. The higher the concentration of API the greater the influence upon the tail length, and subsequently decrease the critical packing parameter.

5.1.1. Comparison of techniques to determine liquid crystalline phase properties.

To determine the effect of API loading upon the liquid crystalline phase it is first important to identify the most appropriate way in which one may characterise the phase present. Reviewing the literature, as discussed in Chapter 1, clearly identifies SAXS as the most appropriate technique in phase identification. SAXS therefore is the backbone analytical technique utilised in this Chapter, with supplementary techniques where appropriate. Although cryo-TEM has been identified as enabling phase identification in several cases it was not selected as the main characterisation method here due to:

- The low sample throughput.

- The limitations in gaining data representative across the whole sample.

- The requirement of very high micrograph quality to undertake phase identification through FFT analysis.

SAXS overcomes above disadvantages of cryo-TEM, under the condition of instrument accessibility. SAXS instruments fall under two brackets: lab based, or synchrotron based. Lab-based SAXS instruments are becoming more common and accessible, whereas the synchrotron based SAXS instruments are significantly less common, with the only instrument in the UK 'Diamond' housed at The Harwell Campus, Oxford. The primary differences between these synchrotron instruments are in the x-ray source. Synchrotron x-ray sources enable high-throughput data acquisition, particularly in the cases of the instrument having auto-sampling capabilities, as is the case with the B21 beamline at Diamond. This instrument is equipped with the BioSAXS auto-sampling robot; this enables the sampling of up to

Influence of guest drug incorporation upon the self-assembly of liquid crystalline structures.

127

96 samples (from a 96 well plate) in rapid succession, with the time for each sample to be processed being around 2 minutes. Synchrotron-based SAXS instruments with auto sampling capabilities allow high-throughput measurements. Instruments without auto sampling capabilities greatly increases the time taken to acquire data for multiple samples due to the requirement of samples to be analysed under vacuum, therefore sample exchange takes some time due to decommission and reinstatement of vacuum conditions. When comparing the lab based and synchrotron instruments there is a significant difference in data acquisition time. For example, a sample may be analysed for 30 minutes on a GANESHA SAXLAB instrument but to acquire data with a similar signal to noise ratio may take 30 seconds on a synchrotron based SAXS instrument. Advantages of SAXS over cryo-TEM data originate from SAXS being more representative of the entire sample, along with data sets possessing a higher resolution.

Discussing first the improved representativeness of SAXS compared to the alternative cryo-TEM technique. SAXS analyses a window of sample, although variable this is typically around 1 μm by 1 μm by the width of the capillary or cell holding the sample. The sample is maintained in its native state i.e., in suspension in the case of liquid crystalline formulations. Conversely, with cryo-TEM one may observe a single area dependent upon the magnification, but for example would be no more than 1 μm by 1 μm to achieve the resolution required, with a minimal depth/height of no greater than 1 μm; with a typical 3 μl of sample being applied to a sample grid for analysis (much of which is blotted away from the grid prior to analysis). This significantly reduces the amount of sample being analysed at one time, even with movement across the grid. Introduced also is biased through the

manual operator dependence of a cryo-TEM instrument to select of location on the grid for imaging. Additionally, SAXS allows the analysis of a sample in its native state, whereas cryo-TEM requires sample freezing. There is much discussion within the field of microscopy as to the effect, or lack of effect, sample freezing may have on the observable characteristics of a sample; the most prominent effect that may influence the desired observations would be due to structural swelling or shrinking upon freezing, or other changes due to osmotic stress. Such an effect would likely hinder sizing measurements rather than phase identification efforts. Similarly, the freezing process would likely not lead to changes in the phase.

Secondly, discussing the improved resolution of SAXS over cryo-TEM, and an improved accuracy compared to cryo-TEM and other readily accessible techniques such as polarising light microscopy which may be used to identify the presence and nature of liquid crystalline phases (16). Both SAXS, cryo-TEM and polarising light microscopy can identify the presence of liquid crystalline structure; however, in the case of polarising light microscopy, only non-isotropic liquid crystalline phases may be observed. This means polarising light microscopy may be used to identify the presence of for example a hexagonal phase, and not a cubic phase. Furthermore, minimal supplementary information, such as lattice parameter, can be gained with polarising light microscopy beyond confirming phase presence. Due to these limitations, polarising light microscopy will not be included hence forth. SAXS can identify liquid crystalline structures with better discrimination than cryo-TEM for two main reasons. The first being SAXS enables background subtraction, removing nearly all noise from the final data set. Such noise or non-sample signal may be generated from the medium in which particles are suspended in or from the sample

Influence of guest drug incorporation upon the self-assembly of liquid crystalline structures.

129

holder. In general background subtraction is not possible with cryo-TEM and so the background may interfere with the ability to interpret a cryo-TEM micrograph, and subsequently run an FFT analysis. FFT analysis identifies repeating patterns in micrographs, and hence can identify the repeating pattern produced by the presence of a liquid crystalline phase. FFT analysis is the most crucial aspect in identifying a particular liquid crystalline phase.

The most notable way in which a variance in resolution between cryo-TEM and SAXS can be appreciated is during lattice parameter calculations. The lattice parameter, also known as a lattice constant, is the measure of the size of a single unit of structure. In most liquid crystalline phases, the lattice parameter is in the order of 5 to 10 nm. The resolution of SAXS is reported to be around 0.5 to 2 nm, whilst cryo-TEM resolution is reported to be sub-1 nm. Yet, the acquisition of micrographs achieving sub 1nm resolution is less frequently. In practical terms however the method in which one may calculate the lattice parameter from SAXS investigations is based in mathematics and does not rely on manual interpretation making it a robust measure. Lattice parameter calculations from cryo-TEM micrographs require manual distance measurements, either of a single unit or structure, or preferably multiple units of structures measured and divided to find an average lattice parameter, limiting manual error. It is important to highlight that although multiple units of structure may be measured and averaged from cryo-TEM micrographs, lattice parameter calculations from SAXS will determine a lattice parameter from all units of structure that was within the beam window during the measurement.

5.1.2. SAXS utilisation for liquid crystalline particle determination

The effect of API incorporation upon the liquid crystalline phase was determined through SAXS analysis, as that was the most robust method identified here and within the literature (38,76) as being able to inform the investigator as to the nature of the liquid crystalline phase.

SAXS operates by directing x-rays through a sample. In the case of examining liquid crystalline particle formulations samples are typically held within a borosilicate glass capillary. The x-rays will pass through this capillary where they interact with the sample. X-rays will be scattered upon the interaction with structures within the sample. Scattered x-rays are collected by a detector on a 2-dimensional screen. X-rays scattered by uniform repeating units of structure will scatter to the same degree, producing rings of high x-ray intensity on the detector as shown in Figure 1.2.5. The intensity plot from the detector is converted into a spectrum which may be interpreted to gain a variety of information about particles in suspension. The information gathered is dependent upon the q range (angle of scattering) being investigated. The range to be investigated enables the identification of Bragg peaks, allowing for phase assignment and information to calculate a lattice parameter.
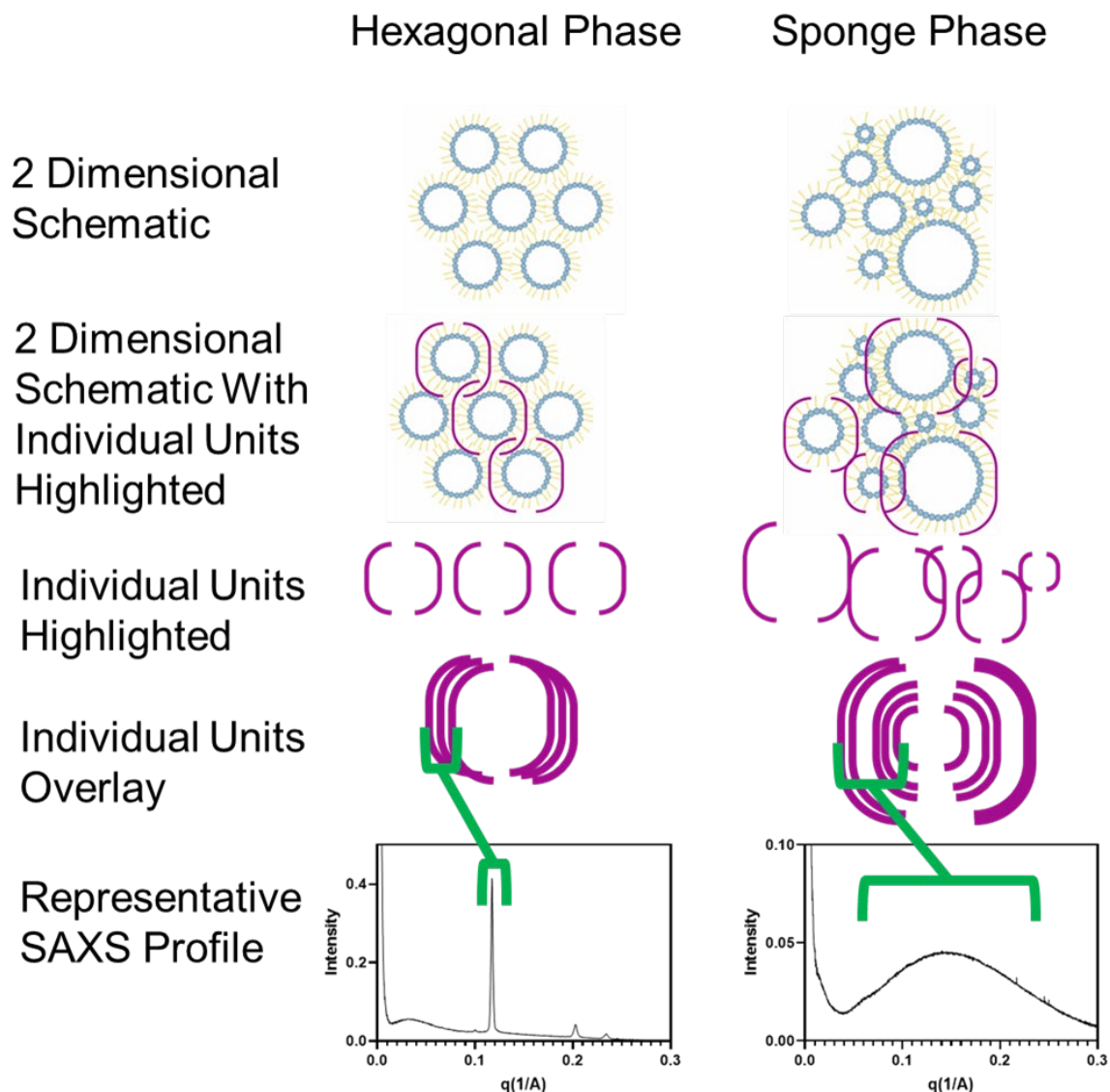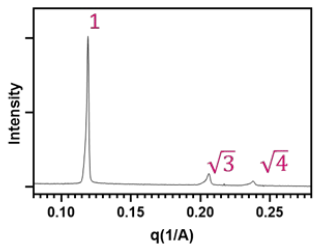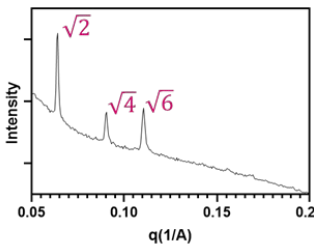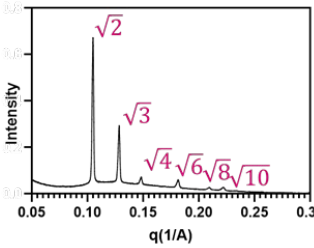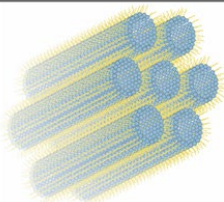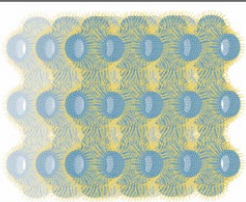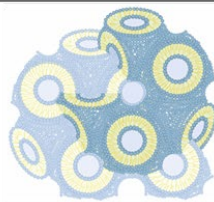
Figure 5.1.2. Simplistic representation of how SAXS converts sample structures into defined Bragg peaks, as with a hexagonal phase, or hump/broad peak, as with a sponge phase: Ordered repeating structures (hexagonal phase example here) will produce defined peaks known as Bragg peaks due to a large proportion of x-rays being scattered in the same manner and so the signals align into a narrow peak. In non-uniform repeating structures, such as the sponge phase the scattering is more variable, this results in peak broadening, producing a hump in the scattering spectrum.

In SAXS analysis of liquid crystalline structures it is typical that one would seek to identify Bragg peaks. Bragg peaks are formed from repeating units of structure, at repeating distances. Such repeating structure is seen in a range of phases, including hexagonal, cubic, and lamellar phases. However, although sponge phases have repeating units of structure the units are non-identical with no consistency between unit of structure distances; the repeating structure is much more random in nature than the previously mentioned hexagonal, cubic, and lamellar phases, as shown in Table 5.1.1 and Figure 1.2.3. In sponge phases, the water channels, or pores of different sizes with different distances between these pores which will interact with the X-rays from SAXS experiments, leading to a broader scattering of X-rays, producing a broad peak such, better identified as a hump. Whereas, in for example the hexagonal phase, the scattering of the x-rays is uniform, mimicking the uniformity of the hexagonal phase structure, producing the defined Bragg peaks. Some of the common uniform phases and their associated Bragg peaks are presented in Table 5.1.1.

One possible phenomenon to consider in the analysis of any Bragg peak scattering data is the possibility of the co-occurrence of different liquid crystalline phases. For example, it may be possible to identify those peaks belonging to a hexagonal phase and additional peaks belonging to a diamond cubic phase within the same sample.

Table 5.1.1. Liquid crystalline phases and Bragg peaks: Table of three commonly occurring liquid crystalline phases formed by glycerol monooleate upon self-assembly into particles. The hexagonal (H$_{II}$), the diamond cubic

(Pn3m) and the primitive cubic (Im3m). Detailed in the Bragg peak spacing that may be used to identify each phase. An example SAXS profile. And a pictorial representation as to each phase's appearance.

Liquid Crystalline Phase	(Inverse) Hexagonal	Primitive	Diamond
Peak Spacing	$1 \ \sqrt{3} \ \sqrt{4}$ ...	$\sqrt{2} \ \sqrt{4} \ \sqrt{6} \ \sqrt{8} \ \sqrt{10}$ ...	$\sqrt{2} \ \sqrt{3} \ \sqrt{4} \ \sqrt{6} \ \sqrt{8} \ \sqrt{10}$ ...
SAXS Profile			
Representation of the phase			

5.2. <u>**Methodology**</u>

The full methodology for liquid crystalline particle fabrication, including API incorporation can be found in Chapters 2 and 4.

To summarise this fabrication procedure, a molten mixture of our Cithrol, Synperonic F127 and API was formed before water addition to produces a particle in water suspension. Variables here were differing APIs at a range of target concentrations. These concentrations were 5%, 10%, 20% and 40% w/w percentages of API to Cithrol. Ratios of Cithrol: Synperonic: water were consistent with the ratios set out in the Chapters 2 and 4 Methodology sections.

Analysis of these formulations was primarily formed was primarily conducted through SAXS analysis with some supplementary cryo-TEM. All SAXS data shown in this Chapter was acquired through the B21 beamline at Diamond (The Harwell campus, Oxford, U.K.). Detailed analysis methodology can be found in Chapter 2.

5.2.1. Pearson regression analysis

The Pearson regression analysis was carried out as described Chapter 4. To perform this a numerical value had to be attributed to liquid crystalline phases, these are described in Table 5.2.1. As the control/innate phase of the system is hexagonal it was given a value of 1 to indicate no change, other phases of increasing change away from the hexagonal phase have been assigned as such. The value given to indicate the changing phases has an inverse relationship to the CPP. Highly heterogeneous samples containing both hexagonal and cubic phases were excluded from the analysis as non-homogenous drug loading makes attribution of changing phases to specific properties incompatible with the data analysis process.

Table 5.2.1. Values assigned to individual liquid crystalline phases during Pearson regression analysis.

Phase	Hexagonal	Diamond	Primitive	Sponge
Value attributed	1	2	3	4
		2.5		
	Excluded due to high heterogeneity			

5.3. <u>Results and Discussion</u>

The following figures show scattering data indicating the effect of API incorporation upon the liquid crystalline phase. This data was collected through SAXS experiments at the UK Diamond scattering facility. Each sample was prepared in triplicate, with each triplicate analysed once. Each graph shows the scattering profile for each sample in its triplicate. In some events scattering data was not obtained, this is indicated by the lack of a profile present and is further indicated at the end of each figure legend. A scattering profile may not have been obtained due to the auto sampling machinery failing. If the three profiles obtained per sample vary from one another there is the probability the concentration is sitting on a phase-phase border. If 2 or more phase profiles are congruent then this phase/profile is taken to be representative. In the case of no scattering data being seen for example in the case of Glipizide at the 10% concentration then the data interpretation relies on the single sample in which is scattering was observed. Phases were assigned using mathematical process discussed in the method section, more detail as to these phase assignments can be found within the supporting information.

As discussed in previous Chapters, the base or template formulation, that is the formulation containing no API, will form an inverse hexagonal, or H_{II} phase. The inverse hexagonal phase is more common than the normal hexagonal H_I phase, as such often within the literature when the writer refers to a hexagonal phase it is the inverse hexagonal phase that they are referencing (85,106,140). Hence forth, and as in previous Chapters, the inverse hexagonal phase will be referred to as a hexagonal phase (omitting inverse). The base formulation contains 53 mg Cithrol and 8.8 mg of Synperonic F127 per ml of water. These form a self-assembled structure with a

critical packing parameter of ~1.05-1.10 (57). An example SAXS profile for the base formulation is shown below in Figure 5.3.1.

Peaks of an inverse hexagonal phase
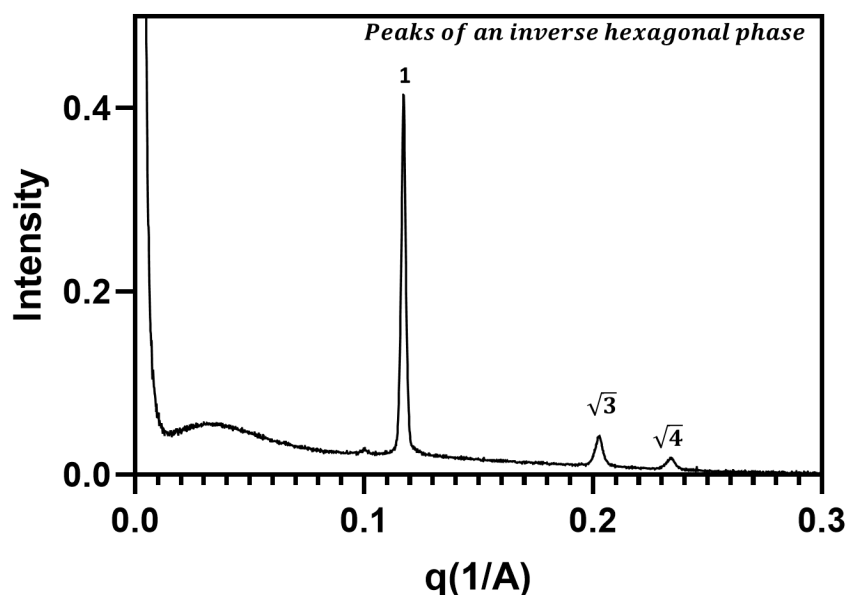
Figure 5.3.1. SAXS profile, showing a hexagonal phase, for the template formulation consisting of Cithrol^{TM} (300 mg) and Synperonic^{TM} F127 (50 mg) in a water suspension (5.65 mL).

Upon the incorporation of a guest molecule, such as an API, the critical packing parameter may be altered. Figure 5.1.1 describes how the incorporation of a drug may influence the critical packing parameter of the system. The APIs encapsulated all possessed a hydrophobic or amphiphilic nature. These APIs therefore may be expected to pack within the tail region of the self-assembled structures; packing here would increase the tail length, subsequently decreasing the critical packing parameter. The degree of change in the CPP will be multifactorial, the primary analysis here however will examine the physicochemical properties of the API, as this will determine how and where the API molecules will pack, and the

Influence of guest drug incorporation upon the self-assembly of liquid crystalline structures.

137

concentration of the API. API concentrations of 5 to 40% weight per weight of API to glycerol monooleate were investigated.

5.3.1. SAXS Results and Discussion for the Analysis of Changing API Concentration upon the Liquid Crystalline Phase

Figure 5.5.1 to Figure 5.5.21 (Shown in the Supplementary Section to this Chapter) show the changes through SAXS analysis in the liquid crystalline phases of the base formulation upon drug encapsulation. With discussion as to any inferences possible how the API is interacting, and subsequently contributing, along with the GMO, to the liquid crystalline structure. Summarising this section of the results and discussion is Table 5.3.1 which details the nature of the liquid crystalline phase at each concentration, accompanied with a summary of an observable trend.

Acknowledged here is the limitation that exact drug loading figures are unknown, therefore, discussion and conclusions are based upon theoretical drug loading, i.e., the amount of drug that was put into the system. The actual drug loading for several samples is discussed in Chapter 4; however, the data in Chapter 4 is incomplete due to experimental limitations in relation to Covid-19. As such only trends are discussed here. Future work here would be to confirm drug loading (w/w, API to GMO), to determine the exact effect of drug concentration on the CPP. As well as to better understand the relationship between an API's physiochemical properties and API loading.
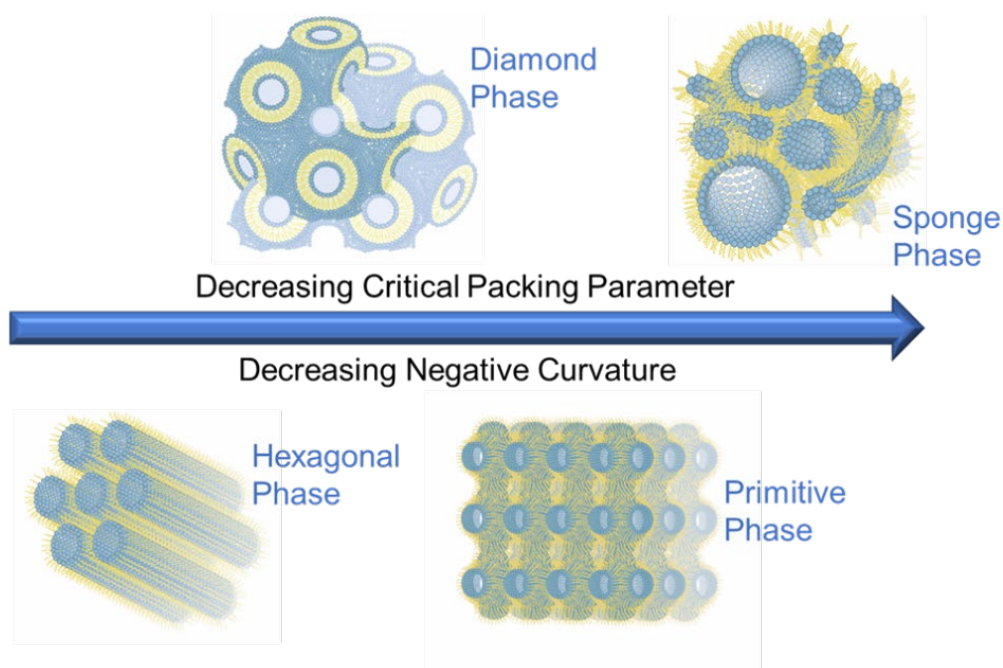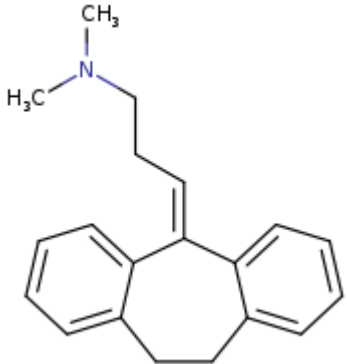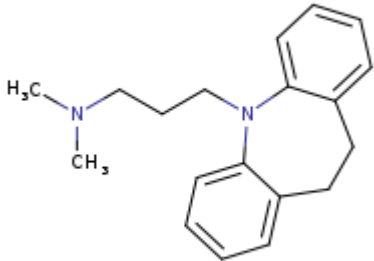
Figure 5.3.2. Transition between differing liquid crystalline phases dependent upon the associated CPP and negative curvature of the system. Shown is the transition from the inverse hexagonal phase, which has the most negative curvature, to the diamond then primitive cubic phases, through to the sponge phase. Sponge phases are proceeded by lamellar phases.
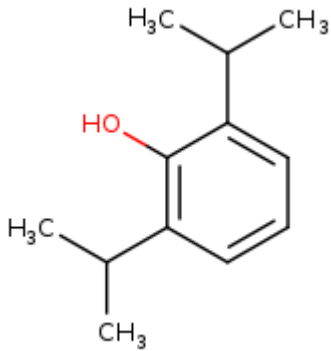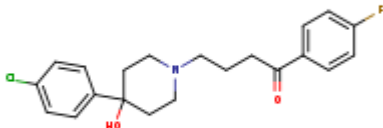
5.3.1.1. *Summary of the observations upon API incorporation*
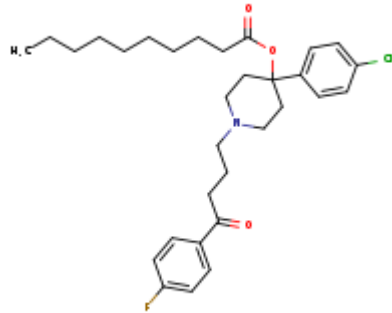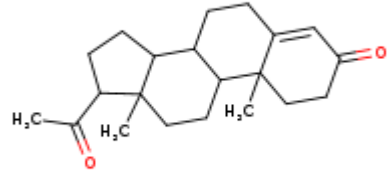
Table 5.3.1. Summary of the effect of API addition upon the liquid crystalline phase.
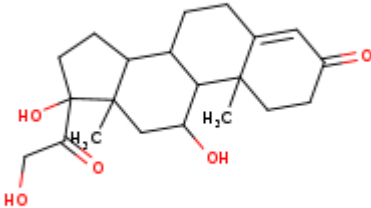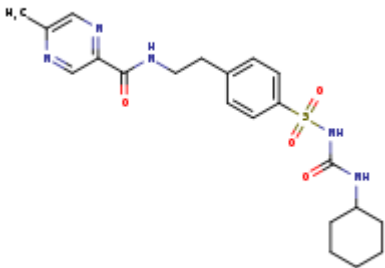
The table summarizes changes from the hexagonal phase of starting formulation (formed in absence of API) to phase present on addition an individual API into formulation. information is provided on nature of the change in the liquid crystalline structure of the system and change in the critical parking parameter was indicated. SAXS spectra showed and discussed in the later sections. Multiple phases are named where they were found to be co-existing.
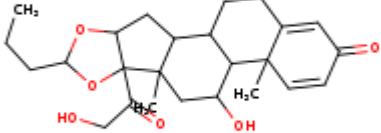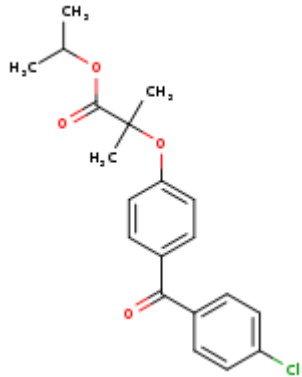
API	Encapsulation Efficiency at a targeted 10% Drug Loading	API Chemical Structure	Observations from SAXS profiles at targeted API (w/w API: GMO) concentrations of: (%)				Observations
			5	10	20	40	
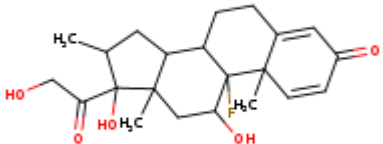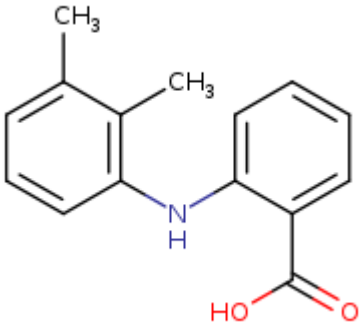
Amitriptyline	96.4 ± 7.7		Single peak from possible hexagonal phase	Lamellar and possible sponge phase	Lamellar and possible sponge phase	Lamellar and possible sponge phase	No distinctive trend/differences
Imipramine	88.3 ± 14.2		Hexagonal phase and peaks indicative of a cubic phase	Lamellar and possible sponge phase	Lamellar and possible sponge phase	Lamellar and possible sponge phase	No distinctive trend/differences
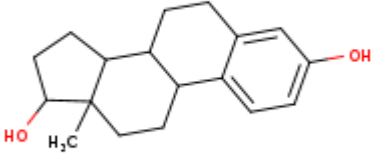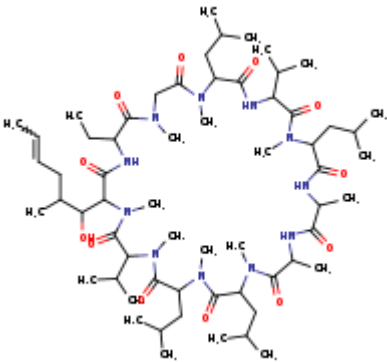
Propofol	66.2 ± 12.6		Hexagonal, Diamond, Primitive	Hexagonal	Hexagonal	No Bragg peaks, possible sponge phase	No linear trend in evident **could be explained by how Propofol may pack**
Haloperidol	57.0 ± 23.4		Diamond, Primitive	Diamond, Primitive	Diamond, Primitive	Diamond, Primitive	No change across the concentration range
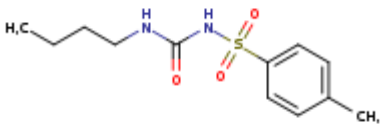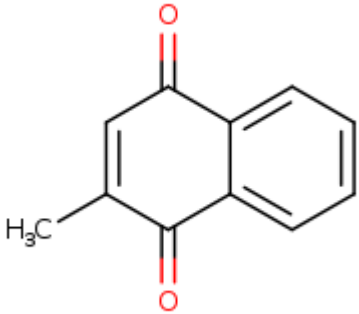
Haloperidol Decanoate	55.5 ± 19.1		Hexagonal	Hexagonal	Hexagonal	Hexagonal, Diamond, Primitive	Linear movement along the curvature scale with the emergence of cubic phases at the 40% concentration of Haloperidol decanoate
Progesterone	55.3 ± 11.0		Hexagonal	Hexagonal	Hexagonal	Hexagonal, Diamond, Primitive	Bragg peak intensity of the hexagonal phase decreases with an increasing concentration of Progesterone, indicating that Progesterone may disrupt the hexagonal phase at higher concentrations
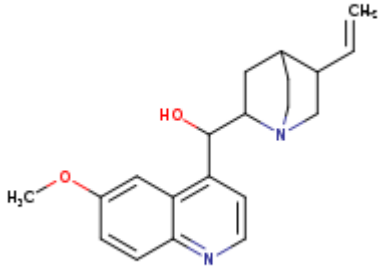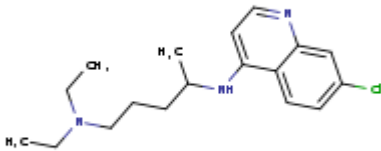
Hydrocortisone	52.3 ± 17.8		Diamond, Primitive	Diamond, Primitive	Diamond, Primitive	Diamond, Primitive	At the lower 5%, and higher 40% concentration the primitive cubic phase is predominant over the diamond phase, however at the two central concentrations of 10 and 20% Hydrocortisone the diamond phase is more predominant.
Glipizide	50.2 ± 9.7		Hexagonal, Diamond, Primitive	Hexagonal, Diamond, Primitive	Hexagonal, Diamond, Primitive	Hexagonal, Diamond, Primitive	No distinctive trend/differences
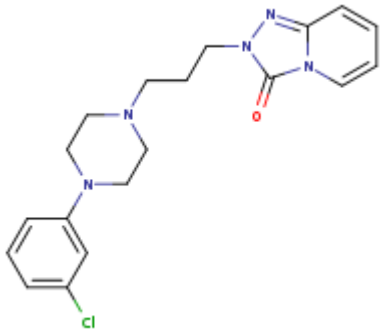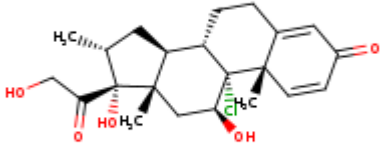
Budesonide	37.4 ± 29.6		Diamond, Primitive	Diamond, Primitive	Diamond, Primitive	No samples successfully ran	No distinctive trend/differences
Fenofibrate	37.3 ± 16.2		Hexagonal	Hexagonal	Hexagonal	Hexagonal	No distinctive trend/differences
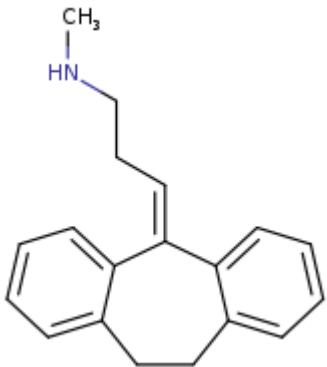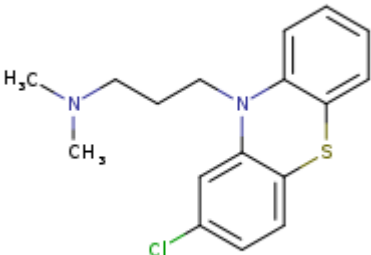
| Dexamethasone | 19.6 ± 7.2 | | Diamond, Primitive | Diamond, Primitive | Diamond, Primitive | Diamond, Primitive | No distinctive trend/differences |
| Mefenamic Acid | 14.5 ± 2.6 | | Diamond, Primitive, Hexagonal | Diamond, Primitive, Hexagonal | Diamond, Primitive, Hexagonal | Diamond, Primitive, Hexagonal | The hexagonal phase becomes more dominant at a lower concentration of Mefenamic acid. The diamond phase also decreases in prevalent as the concentration decreases |
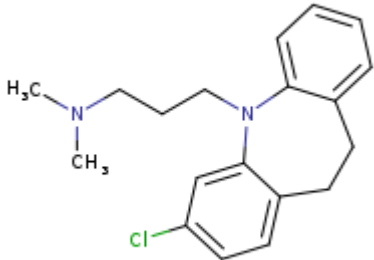
Estradiol	6.0 ± 1.6		Hexagonal, Diamond, Primitive	Hexagonal, Diamond, Primitive	Hexagonal, Diamond, Primitive	No data collected	No distinctive trend/differences
Cyclosporine	0.1 ± 0.0		Diamond, Primitive	Diamond and Primitive phases coexisting with a likely sponge phase	Single peak from an unidentifiable phase coexisting with a likely sponge phase	Single peak from an unidentifiable phase coexisting with a likely sponge phase	With increasing concentration of Cyclosporine there is an increasing movement away from the hexagonal phase

			Hexagonal, Diamond	Hexagonal, Diamond	Hexagonal, Diamond	Hexagonal, Diamond	
Tolbutamide	Unavailable		Hexagonal, Diamond	Hexagonal, Diamond	Hexagonal, Diamond	Hexagonal, Diamond	The diamond phase is most prevalent at 20%, the hexagonal phase becomes more prevalent with decreasing concentration. At 40% the prevalence of the 2 phases appears equal, this does not fit with the trend observable in the 3 other concentrations. This may indicate non-linearity in drug encapsulation
Menadione	Unavailable		Diamond, Primitive, Hexagonal	Diamond, Primitive, Hexagonal	Diamond, Primitive, Hexagonal	Diamond, Primitive, Hexagonal	Cubic phases become more prevalent at increasing concentrations of menadione. The hexagonal phase is present at all concentrations

Quinine	Unavailable		Primitive, $\sqrt{2}$ and $\sqrt{3}$ peaks present, indicative of a diamond phase	Primitive	Primitive	No Bragg peaks, possible sponge phase	The primitive phase is clearly observable at the 20% and 10% concentration. The intensity of the primitive phase at 5% proportional to the base line, the high baseline likely accounts for only 2 peaks being present for the secondary phase.
Chloroquine	Unavailable		Diamond, Hexagonal	Peak 1 of hexagonal	Peak 1 of hexagonal	Diamond, Hexagonal	5% exhibits a strong diamond phase, 40% has a strong hexagonal phase.

Trazodone	Unavailable		Primitive	Primitive	No Bragg peaks, possible sponge phase	No Bragg peaks, possible sponge phase	With increasing concentration of Trazodone there is an increasing movement away from the hexagonal phase
Beclomethasone	Unavailable		Hexagonal, Diamond, Primitive	Hexagonal, Diamond, Primitive	Hexagonal, Diamond, Primitive	Hexagonal, Diamond, Primitive	All samples appear to be comparable to one another

			Single peak from a possible hexagonal phase	Lamellar and possible sponge phase	Lamellar and possible sponge phase	Lamellar and possible sponge phase	No distinctive trend/differences
Nortriptyline	Unavailable						
Chlorpromazine	Unavailable		Lamellar and possible sponge phase	Lamellar and possible sponge phase	No Bragg peaks, possible sponge phase	No Bragg peaks, possible sponge phase	Reducing intensity with reducing chlorpromazine concentration

Clomipramine	Unavailable		Lamellar phase	Lamellar phase	Lamellar phase	Lamellar and possible sponge phase	No distinctive trend/differences

The data compiled within Table 5.3.1. is presented in full in the supplementary section 5.5 with in-depth analyses as to the influence of API incorporation.

When examining the negative curvature there is a linear scale in which the sample's curvature will be moving along, as depicted in Figure 5.3.2. It is expected to observe a movement along this scale upon drug incorporation - if the drug indeed significantly affects the critical packing parameter. If the system's curvature is very significantly affected, it may be the case that some phases on the scale are skipped; this may be due to the skipped phase falling between the concentrations examined; for example, with Imipramine that is an immediate jump from the hexagonal phase to the sponge phase with minimal indications of a cubic phase being present as the drug input increased to 10%. This is believed to be the case because there is a narrow frame in which the cubic phase may be formed (Table 5.3.1). A cubic phase is typically formed when the critical packing parameter falls between 1.00 and 1.05, which lies between the 5% and 10% loading of Imipramine; therefore, the cubic phase is not seen as a its upper and lower phase boundary falls between 5 and 10% targeted API loading.

SAXS analysis indicates that with increasing concentrations of API within the system, a greater influence on the liquid crystalline phase is observed. This is clearly seen when examining the APIs Trazodone and Quinine, however, concentration seems less consequential with Fenofibrate in altering the phase behaviour (Table 5.3.1).

It is observable that an increase in API concentration for all APIs, apart from Progesterone and Fenofibrate, increases the transition away from the innate hexagonal phase of the system (when no drug is encapsulated). Although this analysis is limited due to theoretical, rather than actual, drug loading being available,

Influence of guest drug incorporation upon the self-assembly of liquid crystalline structures.

153

it is still possible to conclude some trends as to what is influence of a theoretically increasing API concentration. The clear example here may be Trazodone. In this case there is a very clear inverse relationship between the theoretical concentration of Trazodone and the CPP. As the theoretical concentration of Trazodone increases, the CPP decreases (Figure 1.2.2, Figure 1.2.1and Figure 5.5.17). An overarching statement can be made for majority of tested APIs, excluding Propofol, that with an increasing API concentration, there is a decrease in the critical packing parameter and a decrease in the negative curvature of the system. The decrease in negative curvature leads to the system being much more linear in nature, as depicted in Figure 1.2.1. This results in the change of a hexagonal phase to a cubic, to a sponge and then to a micellar suspension.

In the case of Fenofibrate, no such trend or change in the phase is observed. Possibilities causing this include is the drug packing in such a way the critical packing parameter is not influenced, or the drug concentration within the system is maintained within the same phase window i.e., the critical packing parameter is not changed significantly with the addition of extra drug; a further possibility to acknowledge is that increasing the targeted drug concentration does not increase necessarily increase encapsulated drug concentration. However, in the instance of Fenofibrate the actual drug loading data is available which does indicate that with increasing concentration there is an increased encapsulation of the API. This is discussed more in later sections.

The 23 API formulations investigated, and as listed in Table 4.1.1, can be categorised based on the result of their influence on the liquid crystalline phase of the formulation. In the following sections APIs have been categorised into sponge phase forming APIs, hexagonal phase forming APIs, cubic phase i.e., primitive or

diamond phase forming APIs, APIs that form coexisting phases, and some examples that do not fit into one of these categories.

5.3.1.2. *Sponge and Lamellar Phased Formulations*

Sponge phases are characterised by water channels/pores of a variable size, distributed randomly through a lipid structure. Of the four phases seen throughout the formulations reported here the sponge phase has the lowest CCP and least negative curvature.

A lamellar (Lα) phase is characterised by evenly spaced peaks with the peak ratio pattern 1, 2, 3, 4… (141). In the case of Amitriptyline and the alike APIs (Imipramine, Nortriptyline, Clomipramine and Chlorpromazine) the lattice parameter of the lamellar phase is 31 nm ± 5 nm (Figure 5.5.1 to Figure 5.5.5), with the increased error primarily resulting from broad peaks. Broad peaks represent variance within the structure, as discussed in Figure 5.1.2.. A 31 nm lattice parameter of a lamellar phase may be expected to result from multi-lamellar vesicles. This idea correlates nicely with the cryo-TEM micrographs shown for Amitriptyline containing formulations (Figure 4.3.12) where vesicle particles can be seen inside one another.

Table 5.3.2. Phase assignments of sponge phase forming formulations (given percentage of API to GMO (w/w), 300 mg GMO, 50 mg Synperonic™ F127) at different theoretical API loading concentrations. Corresponding SAXS profiles can be found within the supplementary information 5.5.

	Percentage target of API (w/w API/GMO)	0 %	5 %	10 %	20 %	40 %
Liquid Crystalline Phase Present	Amitriptyline	Hexagonal	Lamellar/ Sponge	Lamellar/ Sponge	Lamellar/ Sponge	Lamellar/ Sponge
	Imipramine	Hexagonal	Lamellar/ Hexagonal Cubic	Lamellar/ Sponge	Lamellar/ Sponge	Lamellar/ Sponge
	Nortriptyline	Hexagonal	Lamellar/ Sponge	Lamellar/ Sponge	Lamellar/ Sponge	Lamellar/ Sponge
	Clomipramine	Hexagonal	Lamellar	Lamellar	Lamellar	Lamellar/ Sponge
	Chlorpromazine	Hexagonal	Lamellar/ Sponge	Lamellar/ Sponge	Sponge	Sponge

These APIs will all pack in a similar manner due to their similar physicochemical properties and structure, which will result in a similar effect upon the system's phase. From the effect they exert, one would assume that these APIs pack in a way to either increase tail length or head area relative to the tail volume. In some cases, such as with Imipramine the transition from hexagonal to cubic to a lamellar sponge co-existing phase can be observed, yet in most cases with this class of API the transition to the lamellar sponge co-existing phase occurs at the lower 5 to 10% API concentration percentages (API % relative to GMO w/w). Reported in Chapter 4 is that Amitriptyline and Imipramine have an encapsulation efficiency of

96.4 ± 7.7% and 88.3 ± 14.2% respectively at a targeted 10% mg/mg loading (28.9 and 26.5 mg respectively of Amitriptyline and Imipramine with 300 mg of Cithrol, 50 mg of Synperonic F127 and 5.65 mL of water). The variation in at which point a phase shift occurs between the APIs listed in Table 5.3.2 may be due to slight changes in the API's physicochemical properties or due to varying encapsulation efficiencies.

5.3.1.3. *Hexagonal Phase Formulations*

The innate phase of the Cithrol, Synperonic F127 liquid crystalline system is hexagonal. The minimal or lack of change in the hexagonal phase indicates one of two scenarios. Either the APIs in question have very low drug loading, or these APIs pack in a way in which the CPP of the system does not change. This later scenario could occur if an API packs in a way to proportionally increase the tail length and the tail volume and is likely the more probable explanation. This is because it is known a certain amount of API is known to be loaded in the cases of Haloperidol decanoate loading at 10% mg/mg to have an encapsulation efficiency of 55.5 ± 19.1%; and so, this indicates that Haloperidol decanoate packs in a way to not change the confirmation of the GMO packing within the system.

In some which cases, such as Progesterone, at the higher concentrations the conversion from the hexagonal phase to cubic is observed. However, this conversion, in the cases of Progesterone and Haloperidol decanoate with the 40% targeted API loading (API: GMO, w/w), is heterogeneous, with the diamond and primitive cubic phases co-existing with the hexagonal phase. This indicates packing of the API is non-uniform, resulting in varying CPP values throughout the formulation.

Table 5.3.3. Phase assignments of hexagonal phase forming formulations (given percentage of API to GMO (w/w), 300 mg GMO, 50 mg Synperonic™ F127) at different theoretical API loading concentrations. Corresponding SAXS profiles can be found within the supplementary information 5.5.

Percentage target of API (w/w API/GMO)		0 %	5 %	10 %	20 %	40 %
Liquid Crystalline Phase Present	Haloperidol Decanoate	Hexagonal	Hexagonal	Hexagonal	Hexagonal	Hexagonal Diamond Primitive
	Progesterone	Hexagonal	Hexagonal	Hexagonal	Hexagonal Diamond	Hexagonal Diamond Primitive
	Fenofibrate	Hexagonal	Hexagonal	Hexagonal	Hexagonal	Hexagonal

5.3.1.4. *Cubic Phase forming formulations.*

The cubic phase and cubosomes are the most discussed liquid crystalline phase in the literature. The cubic phase is formed from a decrease in the CPP of the system, as compared to the innate hexagonal phase of the system (Figure 1.2.1). Of the two cubic phases present the primitive phase has the lower CPP. The APIs that instigate a transition to the cubic phases are Haloperidol, Hydrocortisone, Budesonide, and trazadone. Haloperidol, Hydrocortisone, and Budesonide have encapsulation efficiencies at the 10% mg/mg drug loading concentration of 57.0 ± 23.4 %, 52.3 ± 17.8 % and 37.4 ± 29.6% respectively. These APIs pack in a way that increases the tail length or head area relative to the tail volume. Due to the hydrophobic nature of these APIs, it is likely that they pack in a way to increase the tail length. The most probable way in which these APIs (e.g., Haloperidol and

Trazodone) pack, which may be confirmed through small angle neutron scattering, is that the API molecules packs between opposite lipids in the bilayer.

The presence of fall our drugs named induces a transition of the LC system through the linear CPP scale, where the hexagonal phase transitions to diamond, to primitive, to a sponge phase (the sponge phase transition was only observed for Trazodone). In some of the cases detailed in Table 5.3.1. there is a co-existence of diamond and primitive phases across a range of concentrations; upon review of the scattering profiles as the targeted API loading increases, the prevalence of the primitive phase increases over the diamond phase. The co-existence of the diamond and primitive phases is due to discrete differences in API packing throughout the system (i.e., local inhomogeneity in the API packing) as the diamond and primitive phases are very closely related in terms of CPP and degree of negative curvature. This shows the slow transition towards the phases with a lower degree of negative curvature. In the case of Trazodone, the transition from the primitive cubic phase to a sponge phase is seen. The encapsulation efficiency for Trazodone is yet to be analysed by HPLC. There are two possibilities therefore as to why Trazodone stronger influence upon the induction of a phase transition compared to the other cubic phase forming APIs. Firstly, there is the possibility of that Trazodone has a higher encapsulation efficiency than the other drugs, or, alternatively Trazodone may have physicochemical properties that cause a more rapid induction of a phase shift. It may be expected that as the APIs with a known encapsulation efficiency all have an encapsulation efficiency that are statistically indifferent. It would be reasonable to presume that API concentration is a significant factor in the formation of the cubic phase, and hence it may be the case that Trazodone achieved a higher

encapsulation efficiency than the Haloperidol, Hydrocortisone, and Budesonide; hence resulting in the altered phase behaviour.

Table 5.3.4. Phase assignments of cubic phase forming formulations (given percentage of API to GMO (w/w), 300 mg GMO, 50 mg Synperonic™ F127) at different theoretical API loading concentrations. Corresponding SAXS profiles can be found within the supplementary information 5.5.

Concentration of API (w/w API/glycerol monooleate)		0 %	5 %	10 %	20 %	40 %
Liquid Crystalline Phase Present	Haloperidol	Hexagonal	Diamond Primitive	Diamond Primitive	Diamond Primitive	Diamond Primitive
	Hydrocortisone	Hexagonal	Diamond Primitive	Diamond Primitive	Diamond Primitive	Diamond Primitive
	Budesonide	Hexagonal	Diamond Primitive	Diamond Primitive	Diamond Primitive	NA
	Trazodone	Hexagonal	Primitive	Primitive	Sponge	Sponge

5.3.1.5. *Formulations containing coexisting hexagonal and cubic phases.*

Table 5.3.5. Phase assignments of coexisting hexagonal and cubic phase forming formulations (given percentage of API to GMO (w/w), 300 mg GMO, 50 mg Synperonic™ F127) at different theoretical API loading concentrations. Corresponding SAXS profiles can be found within the supplementary information 5.5.

	Percentage target of API (w/w API/GMO)	0 %	5 %	10 %	20 %	40 %
Liquid Crystalline Phase Present	Dexamethasone	Hexagonal	Hexagonal Diamond Primitive	Hexagonal Diamond Primitive	Hexagonal Diamond Primitive	Hexagonal Diamond Primitive
	Glipizide	Hexagonal	Hexagonal Diamond Primitive	Hexagonal Diamond Primitive	Hexagonal Diamond Primitive	Hexagonal Diamond Primitive
	Mefenamic acid	Hexagonal	Hexagonal Diamond Primitive	Hexagonal Diamond Primitive	Hexagonal Diamond Primitive	Hexagonal Diamond Primitive
	Estradiol	Hexagonal	Hexagonal Diamond Primitive	Hexagonal Diamond Primitive	Hexagonal Diamond Primitive	NA
	Menadione	Hexagonal	Hexagonal Diamond Primitive	Hexagonal Diamond Primitive	Hexagonal Diamond Primitive	Hexagonal Diamond Primitive
	Beclomethasone	Hexagonal	Hexagonal Diamond Primitive	Hexagonal Diamond Primitive	Hexagonal Diamond Primitive	Hexagonal Diamond Primitive
	Tolbutamide	Hexagonal	Hexagonal Diamond	Hexagonal Diamond	Hexagonal Diamond	Hexagonal Diamond

Reported in Chapter 4 is the encapsulation efficiency for dexamethasone, Glipizide and Estradiol at 19.6 ± 7.2 %, 50.2 ± 9.7 % and 6.0 ± 1.6 % respectively, at the 10% mg/mg targeted API loading. Encapsulation data is unavailable for the

remaining APIs. The variability in encapsulation efficiency for the known APIs would indicate that the resulting occurrence of coexisting phases is not due to a specific drug loading, but due to inhomogeneity in the API loading into the lipid structures. The pockets of higher API presence may have induced phase shift, producing cubic phases, with regions of primitive phase possibly containing the most drug. Hexagonal phase particles likely contain no or minimal drug and hence there is no change in the liquid crystalline phase. In most of the APIs in this category, as the API concentration increased the prevalence of the cubic phases increased relative to the presence of the hexagonal phase. This is shown by a change in peak intensity, observable in the SAXS profiles presented in the Supplementary information (Section 5.5).

5.3.1.6. *Quinine and Chloroquine*

Table 5.3.6. Phase assignment of Quinine and Chloroquine-containing formulations, (given percentage of API to GMO (w/w), 300 mg GMO, 50 mg Synperonic™ F127) at different theoretical API loading concentrations. Corresponding to the scatter profiles shown in Figure 5.5.19 and Figure 5.5.20

Percentage target of API (w/w API/GMO)	0 %	5 %	10 %	20 %	40 %
Liquid Crystalline Phase Present — Quinine	Hexagonal	Diamond Primitive	Primitive	Primitive	Sponge
Liquid Crystalline Phase Present — Chloroquine	Hexagonal	Hexagonal Diamond	Hexagonal Diamond	Hexagonal Diamond	Hexagonal Diamond

At a 40% concentration there are no Bragg peaks observable (Figure 5.5.19 and Figure 5.5.20), however there is solution scattering, indicating a possible sponge phase, or alternative disordered structures. Observed at the 20% and 10% targeted

API loading (API: GMO, w/w) of Quinine is a primitive phase, at the 5% concentration there is the co-occurrence of an additional phase, likely to be a diamond phase showing $\sqrt{2}$ and $\sqrt{3}$ peaks.

A clear trend in decreasing negative curvature, and associated decrease in the critical packing parameter can be identified here from the transition of hexagonal (0% Quinine) > diamond (5% Quinine) > primitive (5-20% Quinine) > sponge (40% Quinine). This is due to either a relative increase in the head area or tail length compared to the tail volume. Due to the hydrophobicity of Quinine, it is likely that this molecule packs between the tails of the glycerol monooleate molecules.

As has been observed for many of the APIs there is a co-existence of phases when resultant phases are cubic in nature. The range of CPP values that forms a diamond or primitive phase is relatively narrow compared to the hexagonal or sponge phase. Therefore, a slight variation in API loading throughout a formulation can result in the formation of co-existing cubic and hexagonal phases. But Quinine shows a single primitive phase being present at the 10 and 20% concentrations; this indicates highly uniform API loading throughout the system. Highly uniform API loading is highly desirable as it may aid predicting the ADME profile of the API containing formulation. If a formulator desired specifically a uniform cubic phase formulation further work in understanding the specific properties of this Quinine formulation would be important.

Observed here is a co-existence of both hexagonal and diamond phases, as the concentration of Chloroquine increases the prevalence of the hexagonal phase increases. This may suggest that initially the Chloroquine packs between opposite glycerol monooleate tails, increasing the tail length and subsequently decreasing the

critical packing parameter. At concentrations above 5% there is an increase in the critical packing parameter, indicating an increase in the tail volume, this suggests the Chloroquine packs between the tails of neighbouring glycerol monooleate molecules at concentrations above 5%. Further investigation would be required to confirm this theory.

5.3.1.7. *Cyclosporine*
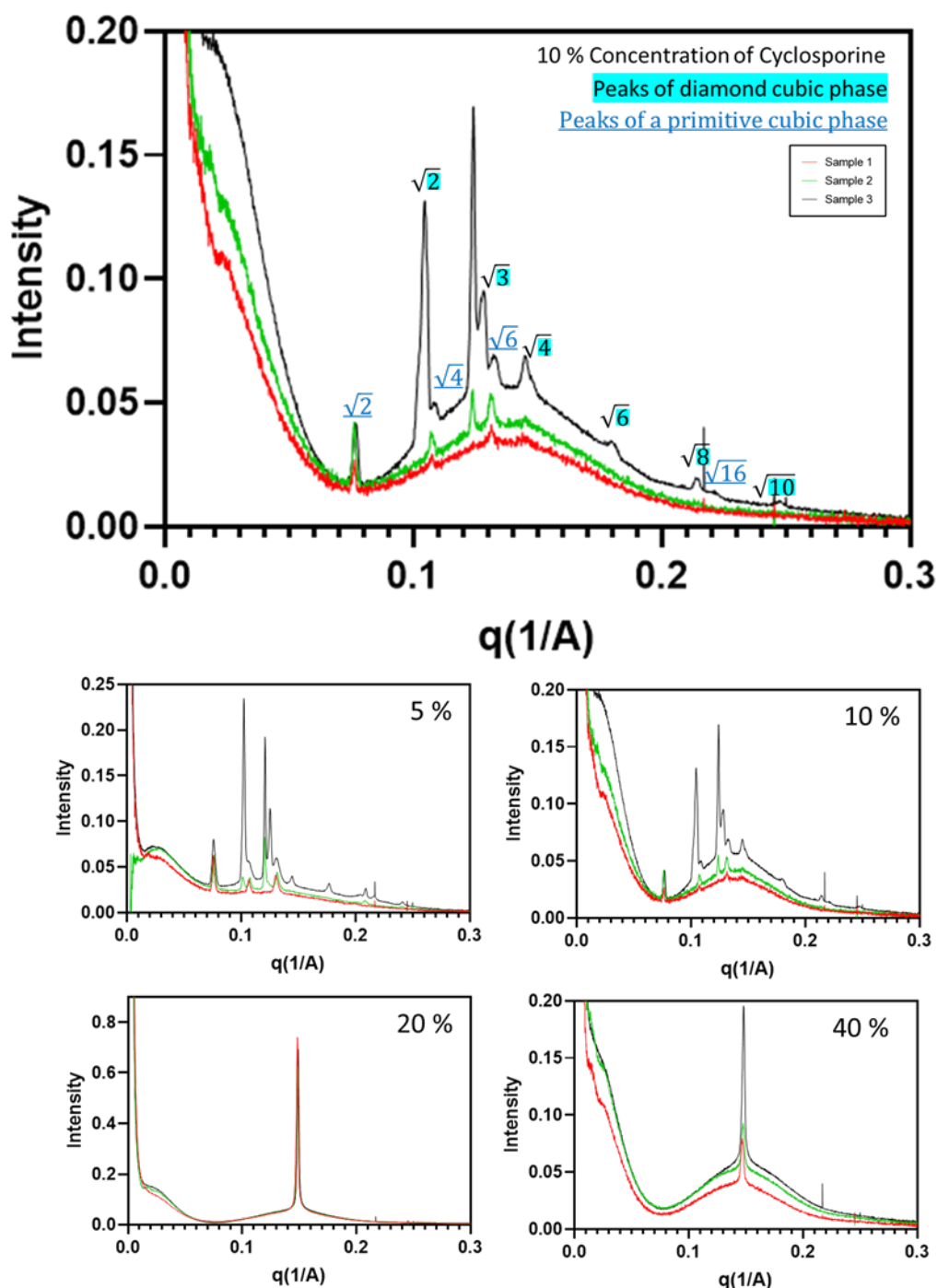
Figure 5.3.3. Cyclosporine: SAXS profiles of liquid crystalline phases with Cyclosporine incorporated at a range of weight per weight concentrations of 5%, 10%, 20% and 40%. 3 independent samples were analysed by SAXS and plotted individually above.

Influence of guest drug incorporation upon the self-assembly of liquid crystalline
structures.

165

**Table 5.3.7. Phase assignment of Cyclosporine containing formulations,
corresponding to the scatter profiles shown in Figure 5.3.3.**

Concentration of Cyclosporine (w/w API/glycerol monooleate)	0 %	5 %	10 %	20 %	40 %
Liquid Crystalline Phase Present	Hexagonal	Diamond Primitive	Diamond Primitive	Sponge	Sponge

Chapter 4 demonstrates that at a 10% w/w loading of an encapsulation efficiency of 0.1 ± 0.0 % (1 d.p.).

Cyclosporine is the largest of the APIs encapsulated, with a molecular weight of 1200 gmol^{-1}, making it approximately 4 times larger than GMO. Furthermore, it is a cyclic peptide, introducing more structural variation in how the molecule may interact and pack within a liquid crystalline system. At the lower theoretical Cyclosporine loading concentrations of 5 and 10% both diamond and primitive cubic phases are observable. Additionally, there is a relatively high intensity peak at ~0.122, this is a lone peak not corresponding to the diamond or cubic phase and so it is not possible to positively identify this phase. One possible explanation for this peak is that it is the 1st peak of a Lα phase. Few examples of the Lα phase can be found in the literature, however, Fong *et al*. reports the Lα phase model to be √1, √4. Furthermore, it is shown in Fong *et al*. that the √1 peak has a significantly higher intensity than the √4 peak (141). This may therefore provide an explanation for the presence of a high intensity peak, whilst the lack of a clear √4 peak could be explained high scattering from other sample components. overshadowing this typically low intensity peak . The corresponding Lα phase would have a lattice parameter of approximately 5 nm, due

to only the single peak being presence this calculation has a higher degree of error than if multiple peaks were observable. Consistently throughout all samples there is scattering in the range of 0.08 to 0.25 q. This scattering, forming a hump in the profile, is indicative of a sponge phase, with its intensity increasing between the 5 and 10% concentrations. The intensity of the 'hump' does not significantly change over the 10 to 40 % concentration range.

Possible explanations for the phase behaviour would be that there is heterogeneous packing of Cyclosporine, accounting for the consistent presence of hexagonal phase where incorporation of Cyclosporine is absent, in addition to a phase shift by decreasing the CPP of the system and reducing the negative curvature where the Cyclosporine does pack into GMO structure - first causing the formation of cubic phases, and subsequently a sponge phase.
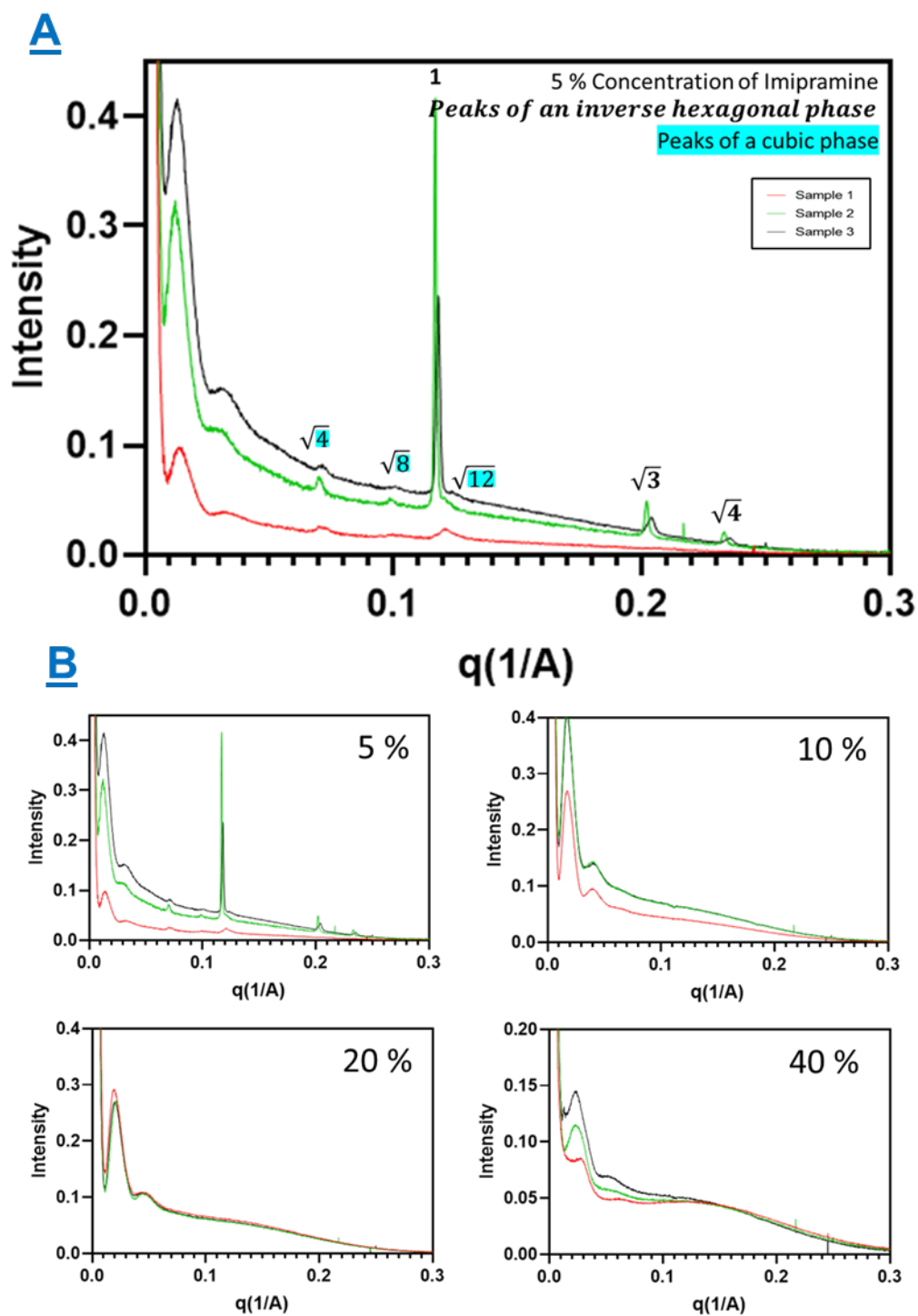
5.3.1.8. *Propofol*
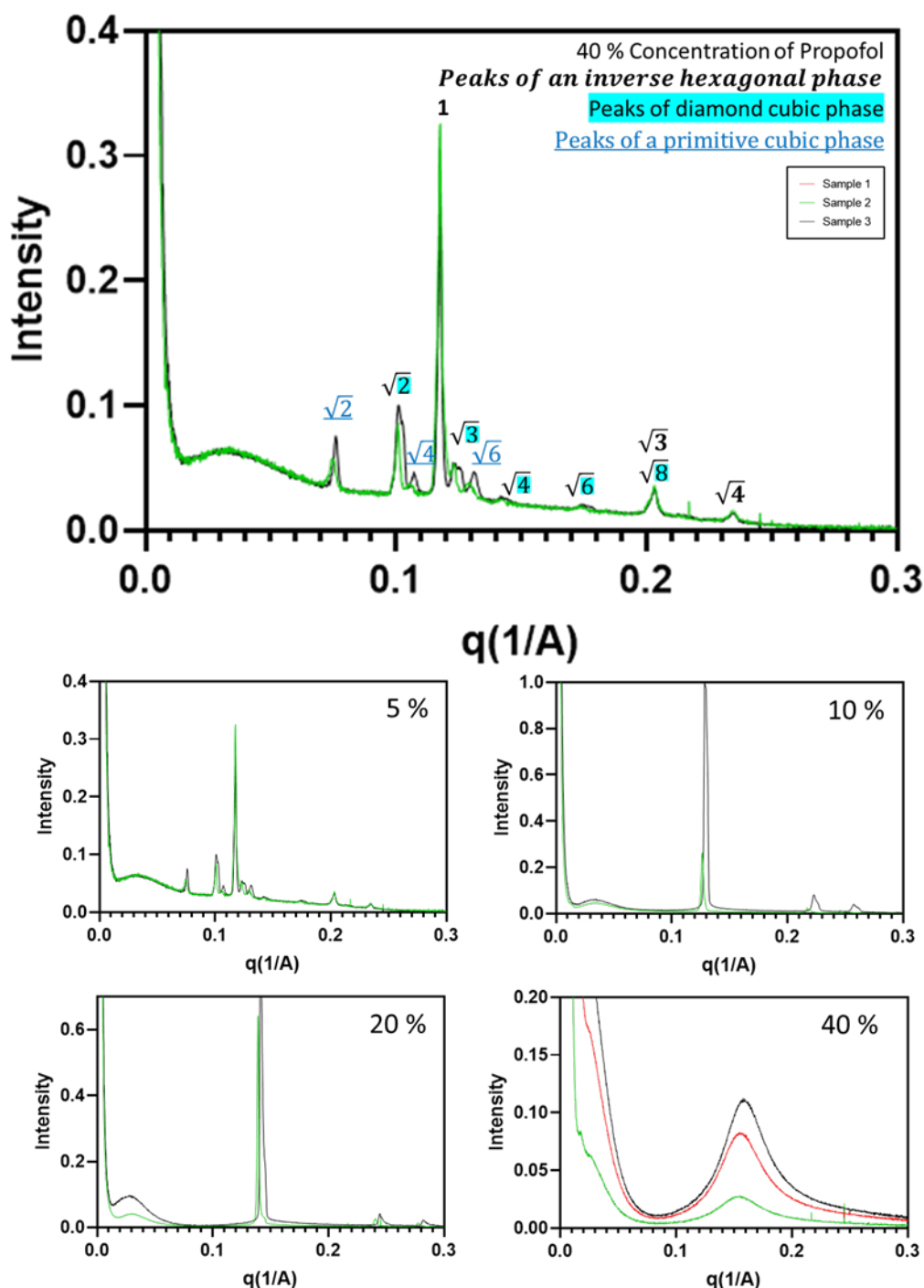
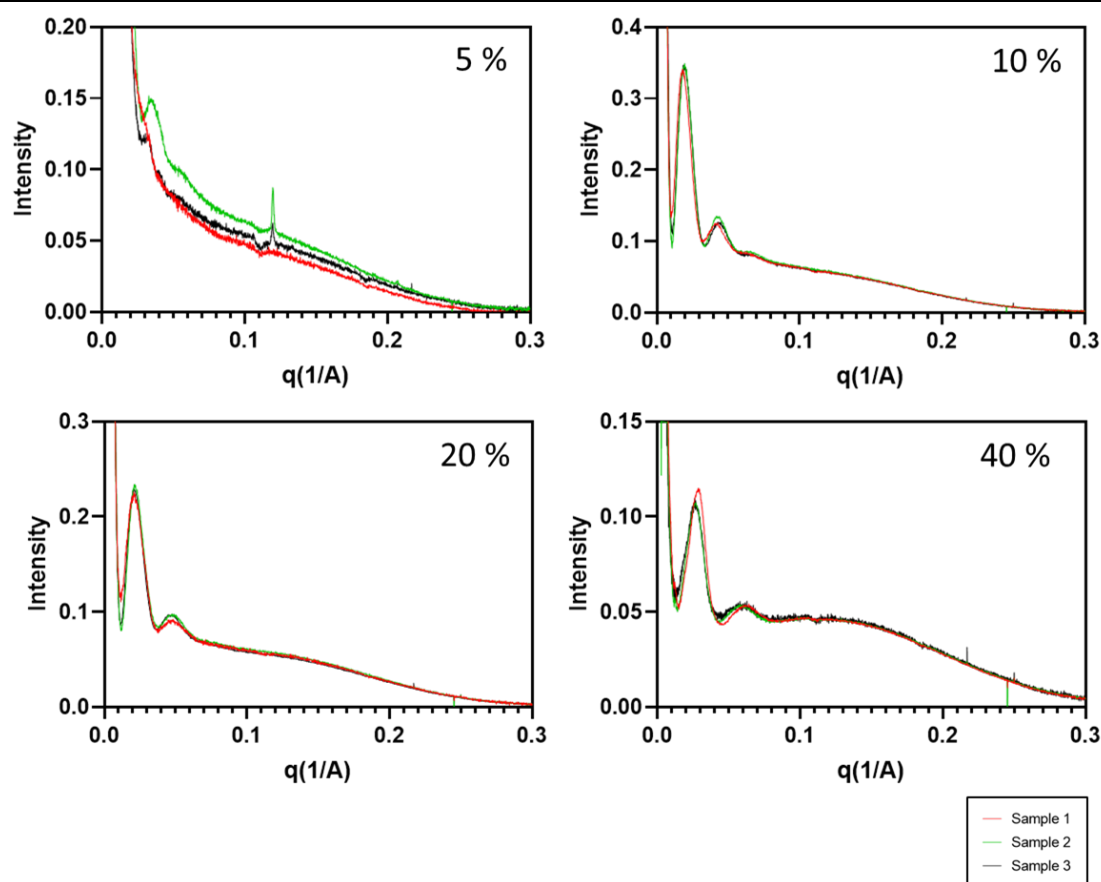**Figure 5.3.4. Propofol: SAXS profiles of liquid crystalline phases with Mefenamic acid incorporated at a range of weight per weight concentrations of 5%, 10%, 20% and 40%. 3 independent samples were analysed by SAXS and plotted individually above.**

Table 5.3.8. Phase assignment of Propofol containing formulations, corresponding to the scatter profiles shown in Figure 5.3.4.

Concentration of Propofol (w/w Propofol/glycerol monooleate)	0 %	5 %	10 %	20 %	40 %
Liquid Crystalline Phase Present	Hexagonal	Hexagonal Diamond Primitive	Hexagonal	Hexagonal	Sponge

Propofol has a unique affect upon the nature of the liquid crystalline phase, based on observations in this study. It behaves unlike the other studied APIs, where the addition of which into a formulation appears to either move the assembly structure linearly along the scale of CPP, curvature and hence liquid crystalline phase i.e., hexagonal < diamond < primitive < sponge. However, in the case of Propofol a non-linear movement along the curvature of the system can be observed; with the CPP decreasing (hexagonal to hexagonal, diamond and primitive), to then increase (back to the hexagonal phase) and then again decrease to a sponge phase. This may indicate that at increasing concentrations of Propofol added to the system the nature of its packing is altered. One possible scenario is that initially Propofol packs in the space between the tails of opposite lipid molecules at lower concentrations (5%) decreasing the CPP by increasing the tail length, whilst at the middle concentrations (10 and 20%) the Propofol packs between the tails of neighbouring lipid molecules, increasing the CPP by increasing the tail volume. Between the 20% and 40% concentration there is again a decrease in the CPP leading to the formation on a sponge phase, this results from either an increase in tail length or an increase in the head area. Due to the hydrophobic nature of Propofol

it is likely the Propofol packs in a way to increase the tail length without increasing

the tail volume significantly, perhaps this is possible due to the relative flatness of

Propofol molecules.

5.3.2. Correlation Analysis Results and Discussion for the effect of API Physicochemical Properties upon the Liquid Crystalline Phase

To allow comparison which determine the API's physiochemical properties-LC phase relationship, it was necessary to select the formulations at the same targeted API loading to enable a direct comparison. The formulations prepared at a targeted API loading of 10% (w/w, API: GMO) was selected as the majority of HPLC analysis (Chapter 4) was performed at this targeted loading. A representative phase (Table 5.2.1) was selected for each API at the 10% concentration and based on the reported phases in Table 5.3.1. This was done at a theoretical 10% loading due to incomplete HPLC analysis.

Future work (not performed here due to the Covid-19 pandemic) would entail comparing API effect on the liquid crystalline phase as a known concentration, with a fixed weight per weight ratio supplementary to this the analysis of the effect at the same mol to mol ratio would be of interest due to the differences between weight/weight and mol/mol. The phases present for all APIs at this 10% targeted loading correlate to CPP values. An assignment of a numerical value was placed on each phase (Table 5.2.1), this numerical assignment was used for principal component analysis along with the differing physicochemical properties values (Table 4.1.1). This analysis allowed us to elicit that the following physiochemical properties have an influence on the CPP and subsequent LC phase.
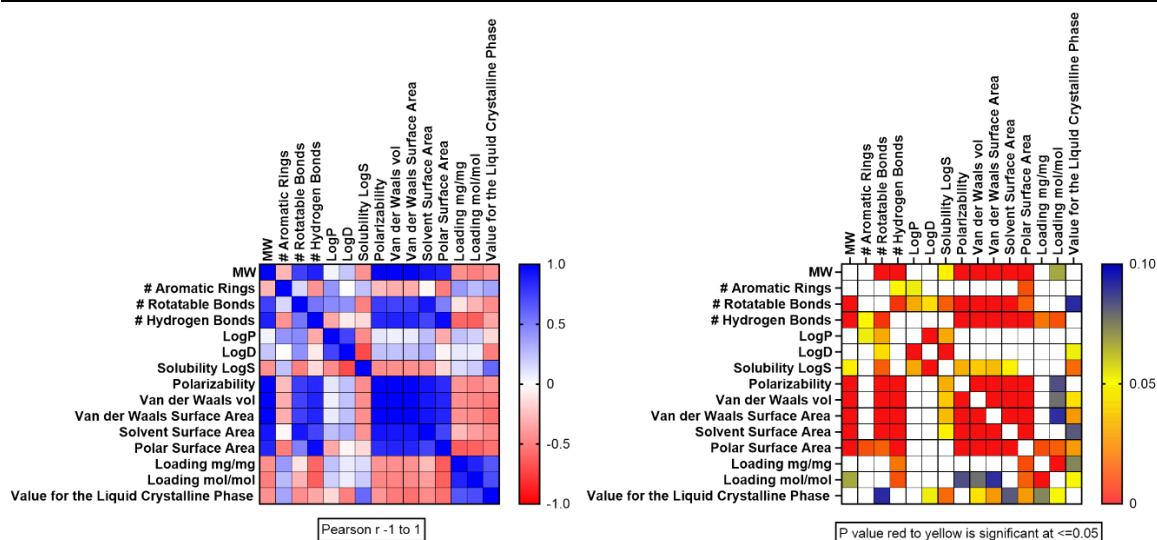
Figure 5.3.5. Pearson correlation coefficient analysis API loading (w/w and mol/mol) (left) and corresponding P values (right).

The Pearson correlation coefficient analysis highlights any trend, and the strength of trends amongst data sets. Being examined here to identify any possible trends between the physicochemical properties of encapsulated APIs, the amount encapsulated (as reported in Chapter 4), and a given value for the liquid crystalline phase. Excluded from this analysis were those samples where 3 phases were identified by SAXS to be present in a sample: for example, menadione formulation. Correlations between the liquid crystalline phase and API loading is limited to those APIs with loadings that were experimentally determined as reported in Figure 4.3.7 in Chapter 4. In the interpretation of the Pearson plot, the extreme values indicate as to if the trend is proportional (+1, indicated as blue) or inversely proportional (-1, red). The P value plot additionally indicates the significance of the identified trends, yellow to red colouring indicates a statistically significant trend with a p-value of 0.05, with blue to yellow colouring indicating a statistical significance of p = 0.10.

The analysis shows that LogS is the most significant physicochemical property of an API to impact upon the nature of the liquid crystalline phase. LogS has a positive relationship with the influence on the liquid crystalline phase, with the APIs with the lowest LogS value. LogS is a measure of the solubility of a molecule and equates to the log of the solubility at room temperature in mol/L at pH 7.4. The LogS values may therefore aid in understanding where the molecule in question may pack inside of a lipid liquid crystalline phase. To support this, one can review two examples from earlier in this section to illustrate this relationship. Taking first Fenofibrate with a LogS of -5.86. Fenofibrate incorporation into formulation has overall a minimal effect in influencing the liquid crystalline phase present. This would indicate that it packs in a manner that will proportionally increase the tail volume to the same degree as any increase in tail length, maintaining the same CPP of the system. The second example is Amitriptyline. It has a LogS of -2.56, the one of the highest investigated here. Amitriptyline shows a significant effect on the liquid crystalline formulation, converting it from a hexagonal phase to a sponge phase. This drastic change indicates that Amitriptyline molecules pack with GMO molecules in a way that disproportionately increases the head area or tail length compared to the tail volume. Drugs with a higher solubility (less negative LogS values) may be more likely to pack around the hydrophilic head groups of the glycerol monooleate. This would decrease the CPP, eliciting the conversion towards a sponge phase.

Polar surface area and Van der Waals surface area are two highly similar measures, both of which quantify the 3-dimensional space a molecule occupies. The polar surface area is the proportion of a molecules surface area arising from polar atoms. Whilst the Van der Waals surface area considers the surface area from all the atoms within the structure. The APIs with the smaller polar surface areas and

Van der Waals surface area, such as Amitriptyline (PSA: 3.2 $Å^2$ VWSA: 457.21 $Å^2$) and Clomipramine (PSA: 6.48 $Å^2$ VWSA: 494.38 $Å^2$) both have significant impact in the liquid crystalline phase formed, with the encapsulation of these two APIs producing a sponge phase. On the contrary, incorporation into formulations of Fenofibrate (PSA: 52.6 $Å^2$ and VWSA: 533.56 $Å^2$) and Haloperidol decanoate (PSA: 46.6 $Å^2$ and VWSA: 856.54 $Å^2$) maintains the original template hexagonal phase produced when no API is encapsulated. This may indicate that the spatially larger APIs pack in a way that will increase the tail length and tail volume of the system equally, negating any change in the CPP, whilst the smaller APIs may pack in a way as to disproportionately increase one of the variables used to calculate the CPP. This trend is also observed, to a less significant extent, for the Van der Waals volume property of APIs, with the same reasoning being considered as for the Van der Waals surface area and polar surface area.

Further physicochemical properties that influence the liquid crystalline phase formed include the logD, and less significantly the number of rotatable bonds, the solvent surface area, and the drug loading.

The API loading, particularly in the case of loading being expressed as mol/mol of API to GMO, has significant bearing on the phase behaviour upon API incorporation. As the values for these parameters increase the difference in the phase away from the native hexagonal phase increases as shown by the Pearson correlation coefficient analysis shown in Figure 5.3.5. Further supporting this are the APIs Progesterone, trazadone, and Quinine. Their incorporation drives the systems to move along the scale shown in Figure 1.2.1, where a proportional decrease in the CPP results in the transition from hexagonal to diamond to primitive to sponge.

An exception to this trend of increasing concentration, increasing influence on the liquid crystalline phase is the drug Propofol. As discussed in section 5.3.1.8 Propofol does not follow a linear shift in the bearing it has on the liquid crystalline phase when the concentration of Propofol is increased.

5.4. **<u>Conclusions</u>**

The SAXS data presented and discussed in this Chapter provide a firm foundation in understanding the effect that addition of APIs with differing physicochemical properties will have upon the innate hexagonal lipid liquid crystalline phase. Highlighted throughout section 5.3. (with additional supplementary information in section 5.5) and summarised in Table 5.3.1. is the effect of given drugs, at given concentrations, on the innate hexagonal phase.

Confirmed is the relationship between an increasing (targeted) API concentration and its increasing effect on the liquid crystalline phase, i.e., with increased incorporation of API there is a greater movement of the lipid liquid crystalline phase along the hexagonal to diamond to primitive to sponge phase scale. Found also is that there may be a coexistence of phases in a formulation, but even in this case there still generally appears to be a linear movement along the phase scale, with a shifting proportionality of the co-existing phases towards the later phases in the scale. Propofol, however, has found to be an exception to this rule. One distinctive difference between Propofol and the other APIs investigated is that Propofol is the only liquid form drug investigated and this may have some baring on this difference in behaviour. This would require further investigation to understand if

the liquid nature of an API has any bearing on its interaction and incorporation into liquid crystalline phases.

The most significant conclusions from this Chapter arise from the statistical analysis reported in section 5.3.2. This analysis highlights the significance of LogS, LogD, Van der Waals volume and surface area, polar surface area and API loading on the phase behaviour. LogS has the most significant bearing on the liquid crystalline phase. As LogS increases there is a greater movement away from the hexagonal phase towards the sponge phase. This analysis and data set will guide any formulator wanting to use this research to produce a liquid crystalline phase formulation containing a novel API with a predictable liquid crystalline phase. In the future this analysis and data set may enable the development of a predictive tool to understand the effect an API may have on a liquid crystalline phase formulation.

5.5. <u>**Supplementary Information**</u>

5.5.1.1. *Amitriptyline*
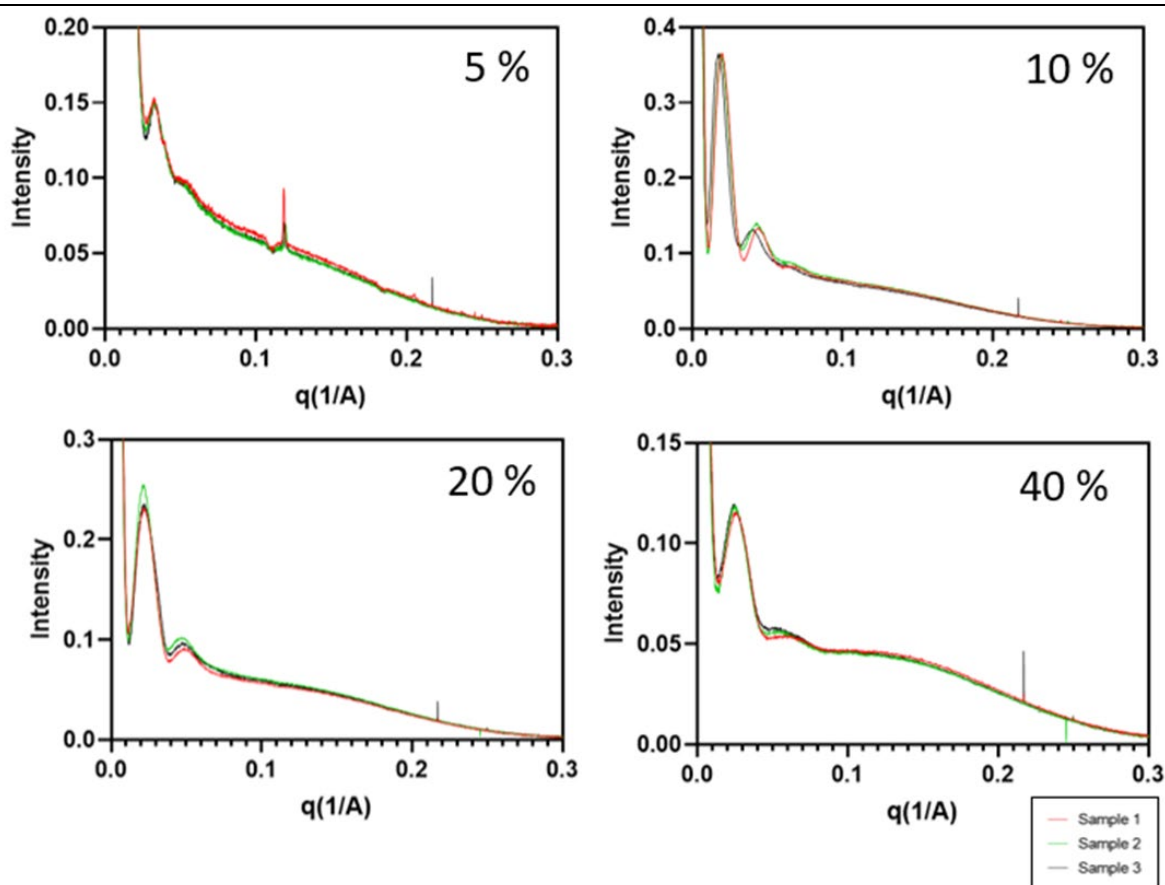
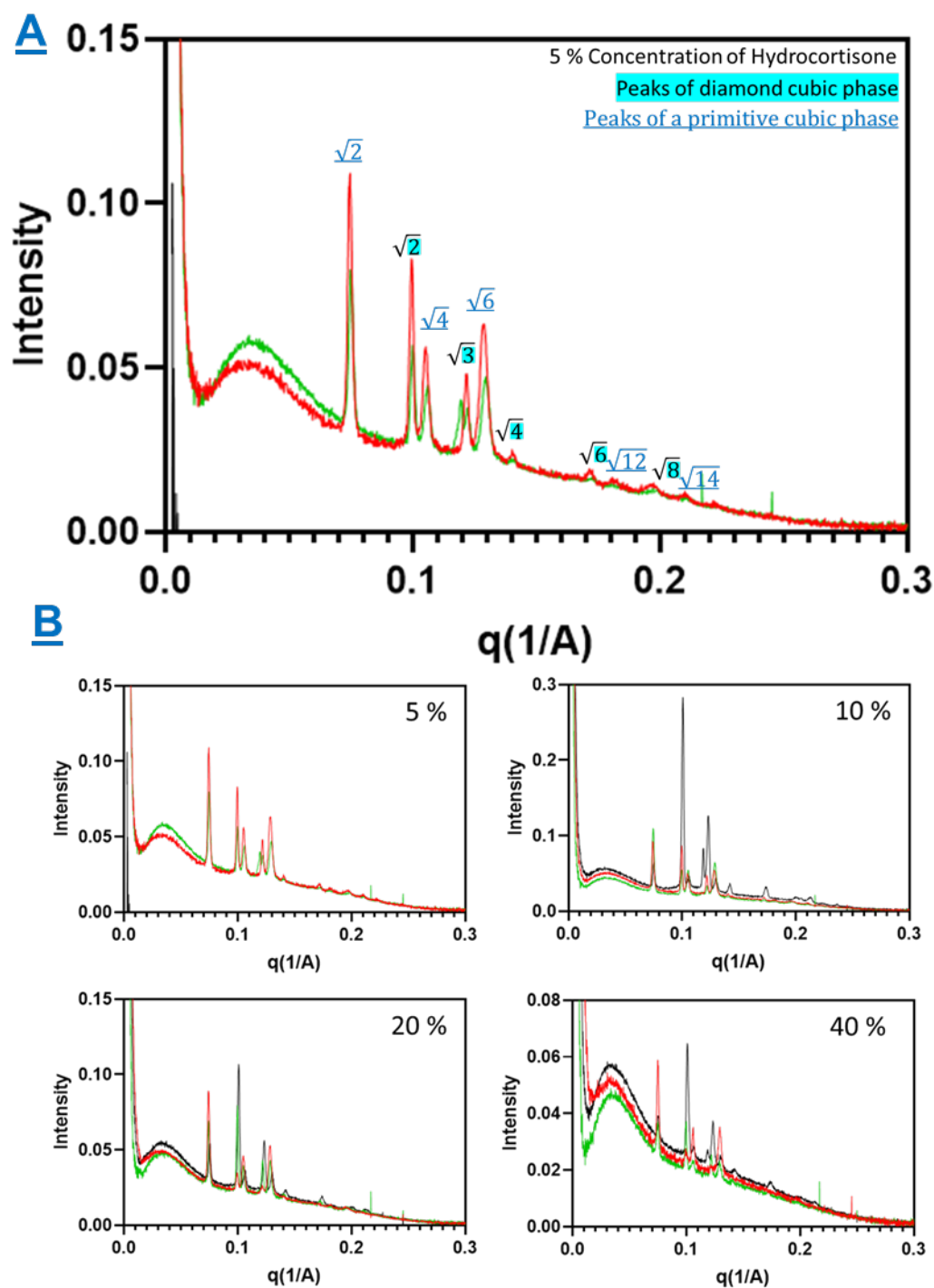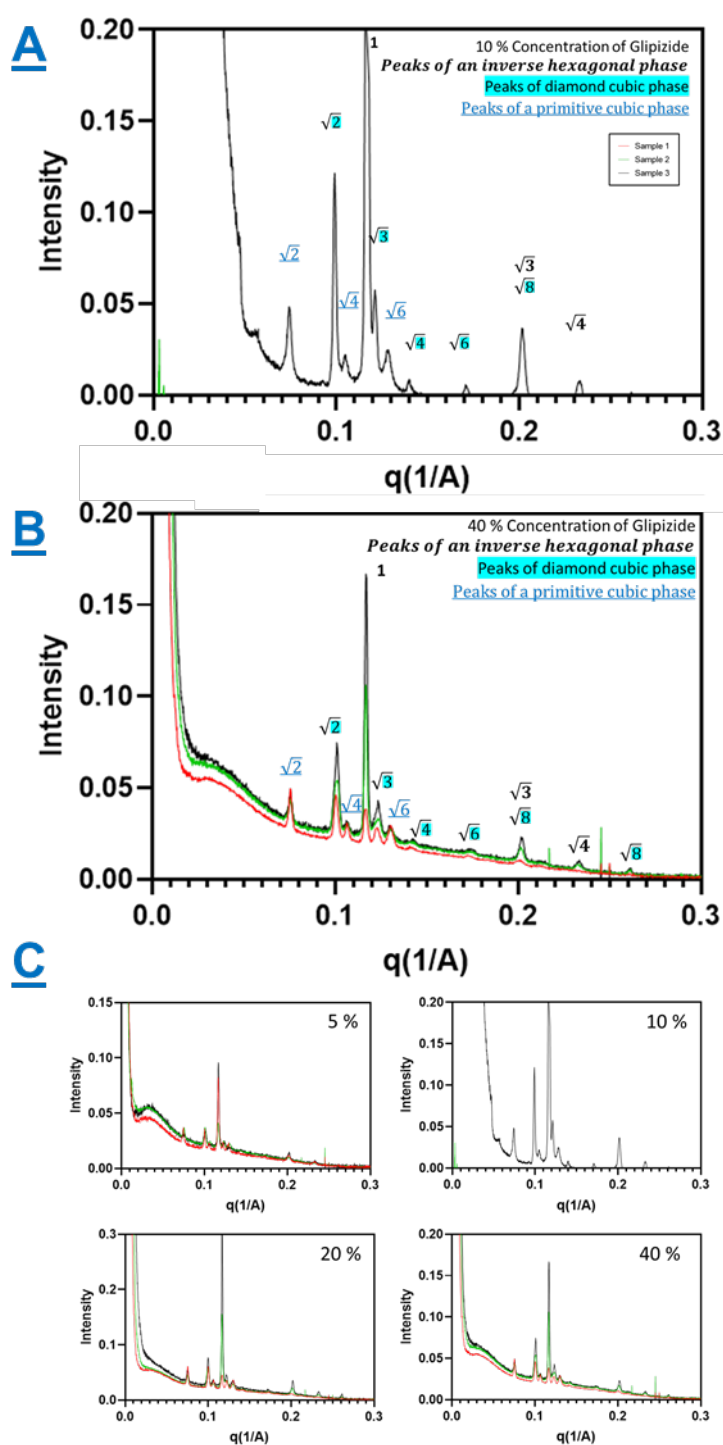**Figure 5.5.1. Amitriptyline: SAXS profiles of liquid crystalline phases with Amitriptyline incorporated at a range of weight per weight concentrations of 5%, 10%, 20% and 40%. 3 independent samples were analysed by SAXS and plotted individually above.**

Table 5.5.1. Phase assignment of Amitriptyline containing formulations, corresponding to the scatter profiles shown in Figure 5.5.1.

Concentration of Amitriptyline (w/w API/glycerol monooleate)	0 %	5 %	10 %	20 %	40 %
Liquid Crystalline Phase Present	Hexagonal	Lamellar/ Sponge	Lamellar/ Sponge	Lamellar/ Sponge	Lamellar/ Sponge

Observed here are broad peaks in the low q range of all the samples. As only two peaks are distinguishable it does pose difficulties in identifying the resulting liquid crystalline phase. However, these peaks would fit with the peak 1and peak 2 of the lamellar model. Further supporting this is that in formulations containing other APIs of a similar nature to Amitriptyline present the same peak pattern with a third peak visible (sections 5.5.1.2 Imipramine, 5.5.13 Nortriptyline, 5.5.1.4 Clomipramine and 5.5.1.5 Chlorpromazine). In the case of Amitriptyline and the alike APIs (Imipramine, Nortriptyline, Clomipramine and Chlorpromazine) the lattice parameter of the lamellar phase is 31 nm ± 5 nm, with the increased error primarily resulting from broad peaks. Broad peaks represent variance within the structure, as discussed in Figure 5.1.2.. A 31 nm lattice parameter of a lamellar phase may be expected to result from multi-lamellar vesicles. This idea correlates nicely with the cryo-TEM micrographs shown for Amitriptyline containing formulations (Figure 4.3.12) where vesicle particles can be seen inside one another. Although there is some variance in the SAXS profiles for the alike APIs (sections 5.5.1.2 Imipramine, 5.5.13 Nortriptyline, 5.5.1.4 Clomipramine and 5.5.1.5 Chlorpromazine) the structuring detailed here and phase properties would most likely apply.

In the 5% API loading sample, when comparing the q value of this peak to control samples and other API containing samples it would correlate to the peak 1 of an inverse hexagonal phase (Figure 5.5.1).

Chapter 4 demonstrates that at a 10% w/w loading of Amitriptyline an encapsulation efficiency of 96.4 ± 7.7 % is achievable, this would confirm API loading at the 10% theoretical concentration and support the assumption that all concentrations have API loaded. The loading of Amitriptyline clearly influences the liquid crystalline phase self-assembly as the hexagonal phase is no longer observable. However, there is still a significant amount of scattering observable. Proposed here, with increasing concentrations of Amitriptyline is the formation of a sponge phase. At the highest concentration of 40% the lower intensity scattering may indicate a loss in structure of the system, likely due to the significant dispersion effect of Amitriptyline on the self-assembled glycerol monooleate system. A combined overview of the effect of Amitriptyline on liquid crystalline phases is that Amitriptyline packs in a manner which decreases the critical packing parameter, leading to a reduced negative curvature, hence leading to the formation of a lamellar and then sponge phase. At the higher concentrations of Amitriptyline examined there is an interfering/disruptive effect of Amitriptyline on the self-assembly of the glycerol monooleate forming a liquid crystalline phase, reducing the scattering observed in samples with a theoretical loading of 40%. Although there is some variance in the SAXS profiles for the alike APIs (sections 5.5.1.2 Imipramine, 5.5.13 Nortriptyline, 5.5.1.4 Clomipramine and 5.5.1.5 Chlorpromazine) the structuring detailed here and phase properties would most likely apply.
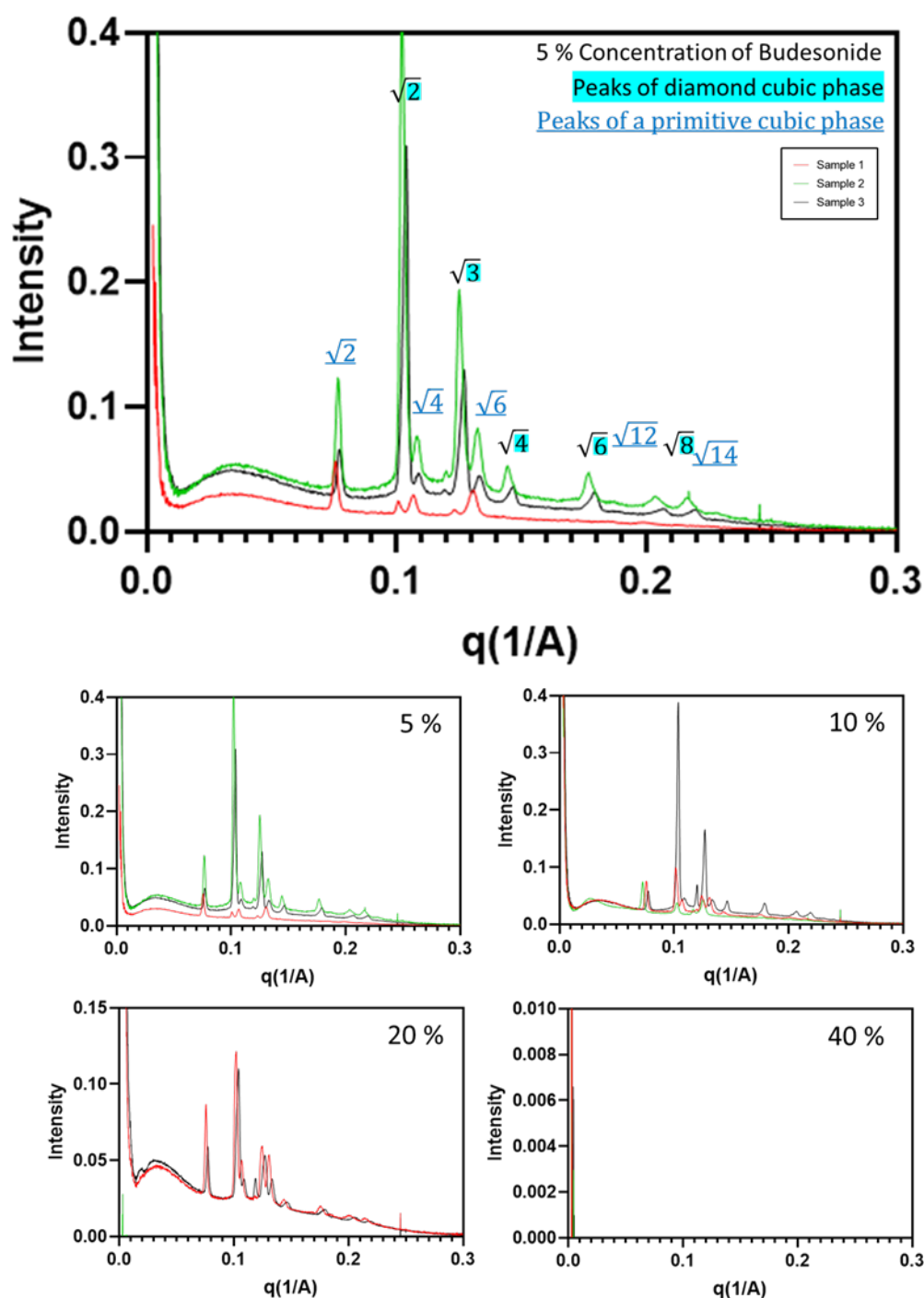
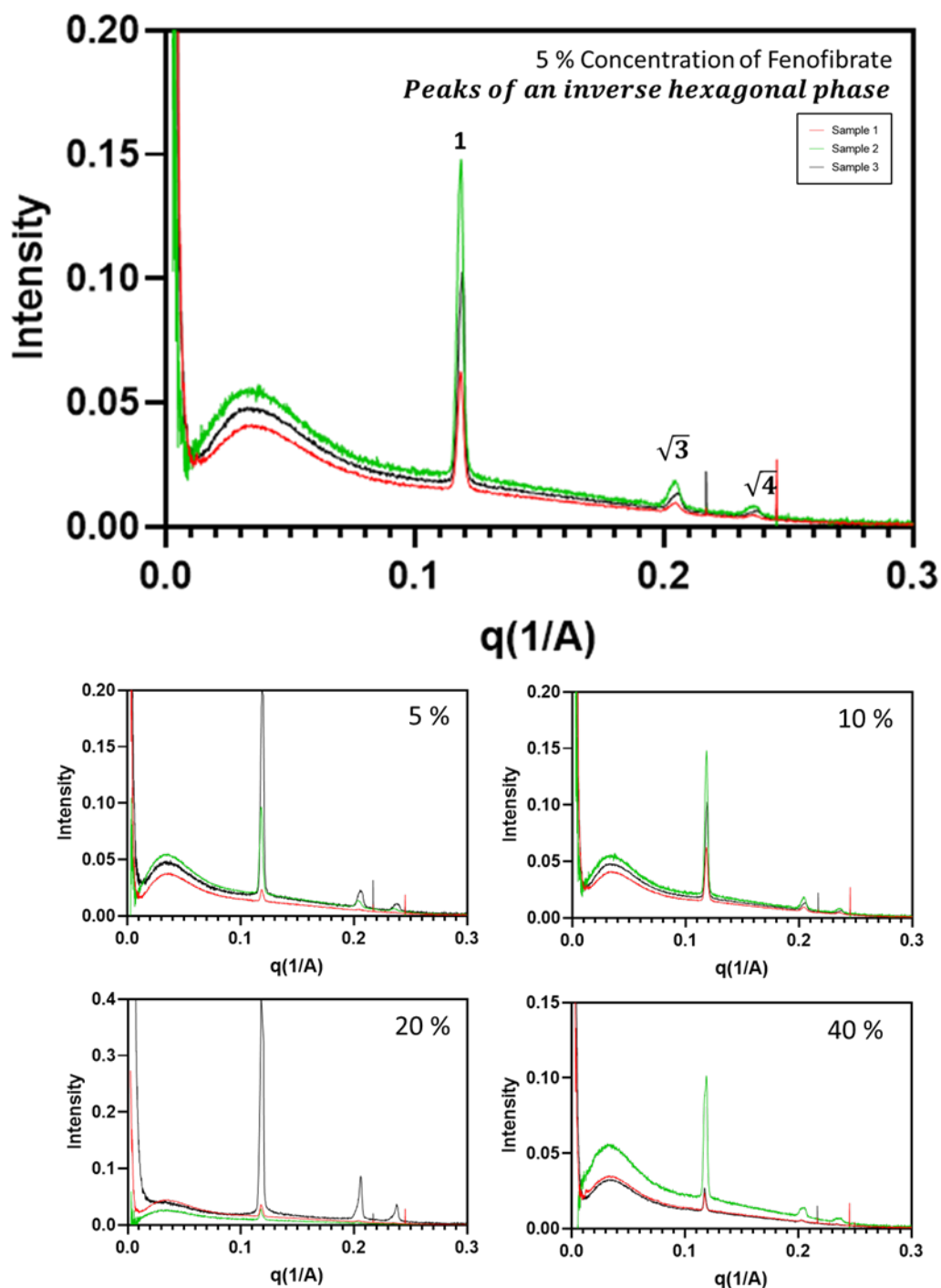### 5.5.1.2. *Imipramine*

Figure 5.5.2. Imipramine: SAXS profiles of liquid crystalline phases with

Nortriptyline incorporated at a range of weight per weight concentrations of

5%, 10%, 20% and 40%. 3 independent samples were analysed by SAXS and plotted individually above.

Observed here are no distinct peaks except for the 5% concentration where a single peak can be seen in samples 2 and 3. At 5% Imipramine concentration there is the presence of hexagonal phase peaks and cubic phase peaks indicative of a diamond or primitive phase.

Table 5.5.2. Phase assignment of Imipramine containing formulations, corresponding to the scatter profiles shown in Figure 5.5.2.

Concentration of Imipramine (w/w API/glycerol monooleate)	0 %	5 %	10 %	20 %	40 %
Liquid Crystalline Phase Present	Hexagonal	Lamellar/ Hexagonal Cubic	Lamellar/ Sponge	Lamellar/ Sponge	Lamellar/ Sponge

Chapter 4 demonstrates that at a 10% w/w loading of Imipramine an encapsulation efficiency of 88.3 ± 14.2 % is achievable, this would confirm API loading at the 10% theoretical concentration and support the assumption that all concentrations have API loaded. The loading of Imipramine clearly influences the liquid crystalline phase self-assembly as the hexagonal phase is no longer observable at the concentrations above 10% loading. Yet a significant amount of scattering is still observable. Proposed here, with increasing concentrations of Amitriptyline is the formation of a sponge phase. At the highest concentration of 40% the lower intensity scattering may indicate a loss in structure of the system, likely due

to the significant dispersion effect of Imipramine on the self-assembled glycerol monooleate system. A combined overview of the effect of Imipramine on liquid crystalline phases is that   Imipramine packs in a manner which decreases the critical packing parameter, leading to a reduced negative curvature, hence leading to the formation of a sponge phase. At the higher concentrations of Imipramine examined there is an interfering/disruptive effect of Imipramine on the self-assembly of the glycerol monooleate forming a liquid crystalline phase, reducing the scattering observed in samples with a theoretical loading of 40%.

5.5.1.3. *Nortriptyline*

Figure 5.5.3. Nortriptyline: SAXS profiles of liquid crystalline phases with Nortriptyline incorporated at a range of weight per weight concentrations of 5%, 10%, 20% and 40%. 3 independent samples were analysed by SAXS and plotted individually above.

Table 5.5.3. Phase assignment of Nortriptyline containing formulations, corresponding to the scatter profiles shown in Figure 5.5.3.

Concentration of Nortriptyline (w/w API/glycerol monooleate)	0 %	5 %	10 %	20 %	40 %
Liquid Crystalline Phase Present	Hexagonal	Lamellar/ Hexagonal/ Sponge	Lamellar/ Sponge	Lamellar/ Sponge	Lamellar/ Sponge

Observed here are broad peaks in the low q range of all the samples. As only two peaks are distinguishable it does pose difficulties in identifying the resulting liquid crystalline phase. However, these peaks would fit with the peak 1and peak 2 of the lamellar model. Further supporting this is that in formulations containing other APIs of a similar nature to Nortriptyline present the same peak pattern with a third peak visible (sections 5.5.1.4 Clomipramine and 5.5.1.5 Chlorpromazine). In the 5% API loading sample, when comparing the q value of this peak to control samples and other API containing samples it would correlate to the peak 1 of an inverse hexagonal phase (Figure 5.5.3).

With an increasing concentration of Nortriptyline there is a loss of Bragg peak forming structures and the emergence of sponge phase. At the highest concentration of 40% the lower intensity scattering may indicate a loss in structure of the system,

likely due to the significant dispersion effect of Nortriptyline on the self-assembled glycerol monooleate system.
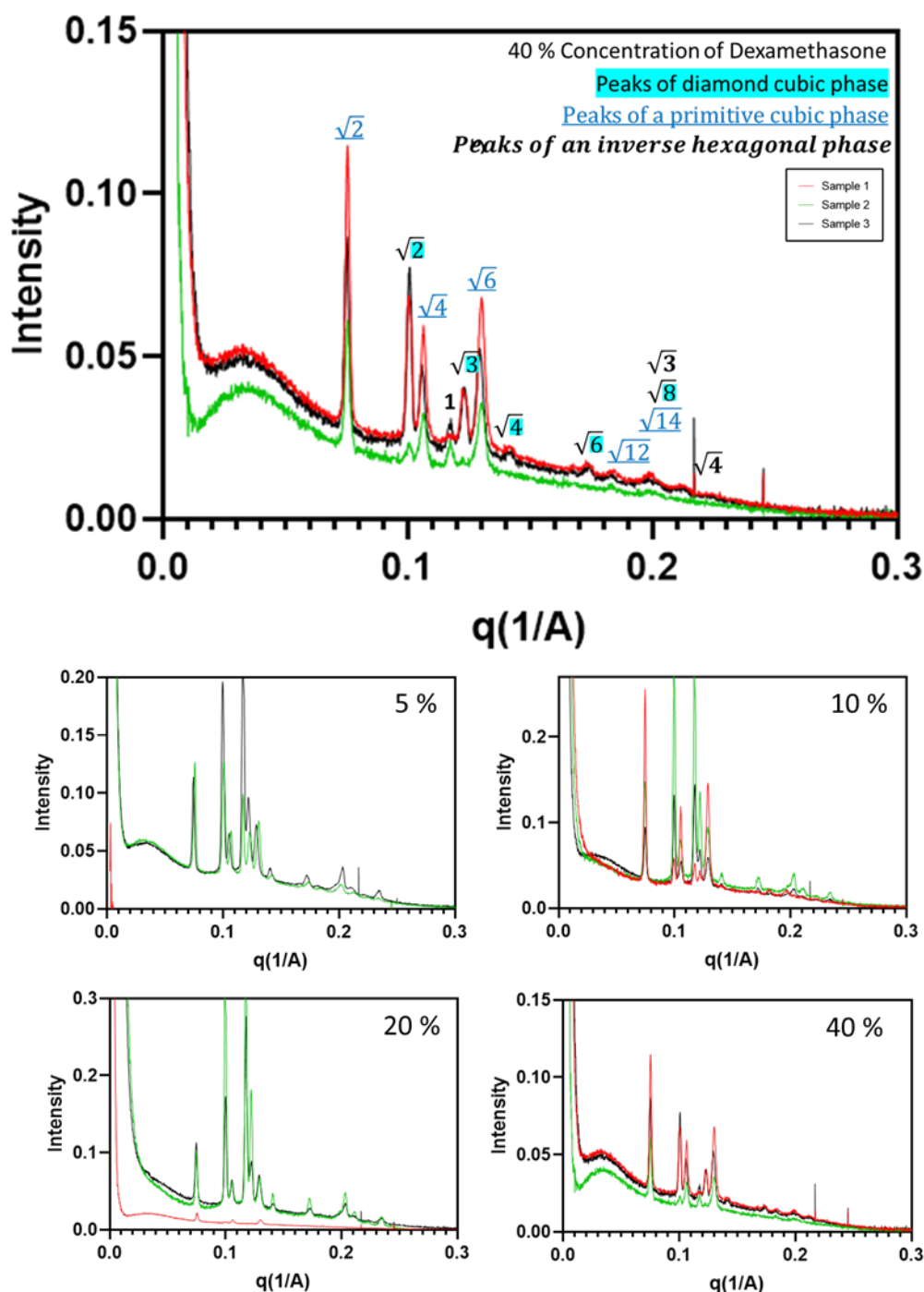
5.5.1.4. *Clomipramine*
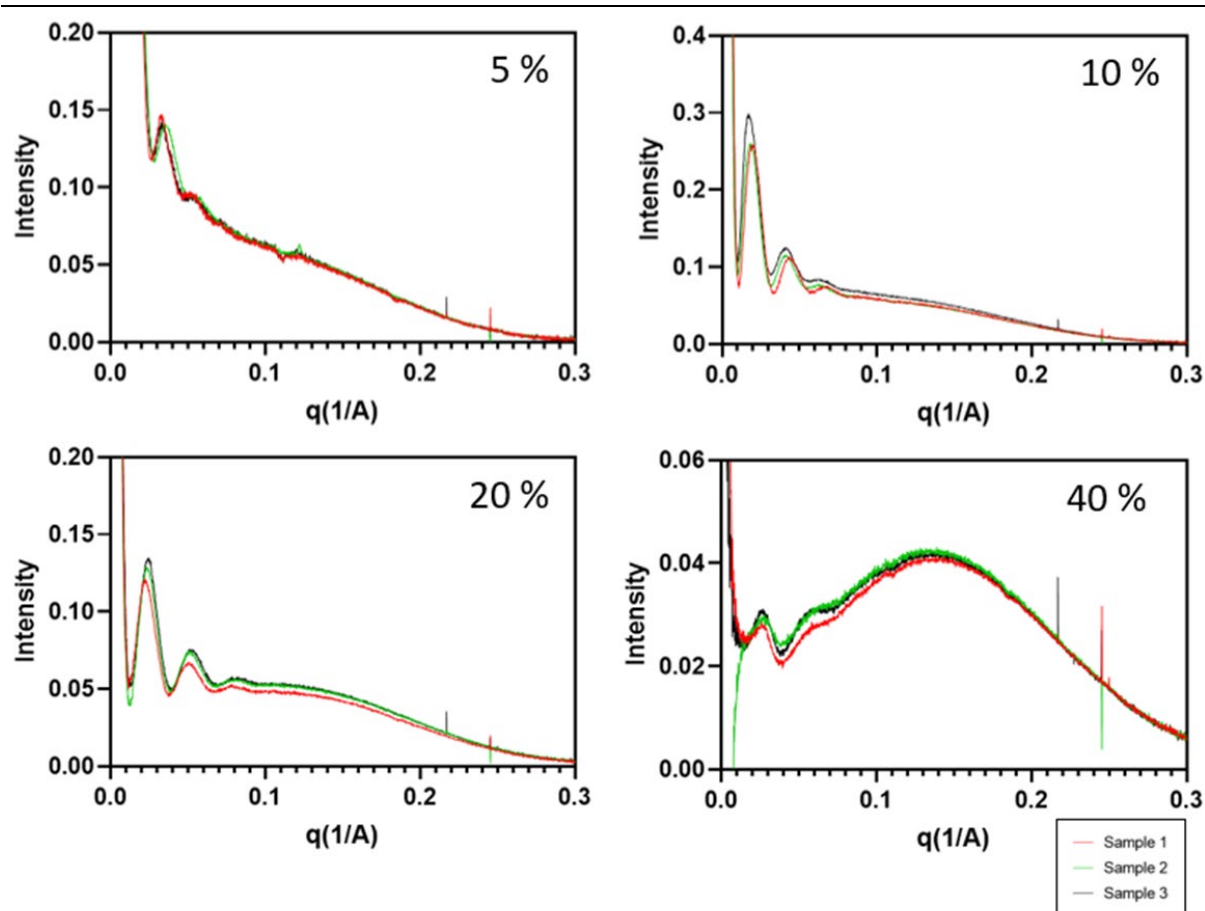
Figure 5.5.4. Clomipramine: SAXS profiles of liquid crystalline phases with Clomipramine incorporated at a range of weight per weight concentrations of 5%, 10%, 20% and 40%. 3 independent samples were analysed by SAXS and plotted individually above.

Table 5.5.4. Phase assignment of Clomipramine containing formulations, corresponding to the scatter profiles shown in Figure 5.5.4.

Concentration of Clomipramine (w/w API/glycerol monooleate)	0 %	5 %	10 %	20 %	40 %
Liquid Crystalline Phase Present	Hexagonal	Lamellar	Lamellar	Lamellar	Lamellar/ Sponge

Broad Bragg peaks can be seen in the low q range correlating to the 1, 2, 3 peaks typical of a lamellar phase. The lamellar phase exhibits a lattice parameter of 31 nm ± 5 nm. In the 40% API loaded sample there is clear sample scattering consistent with a sponge phase across all concentrations.

5.5.1.5. *Chlorpromazine*
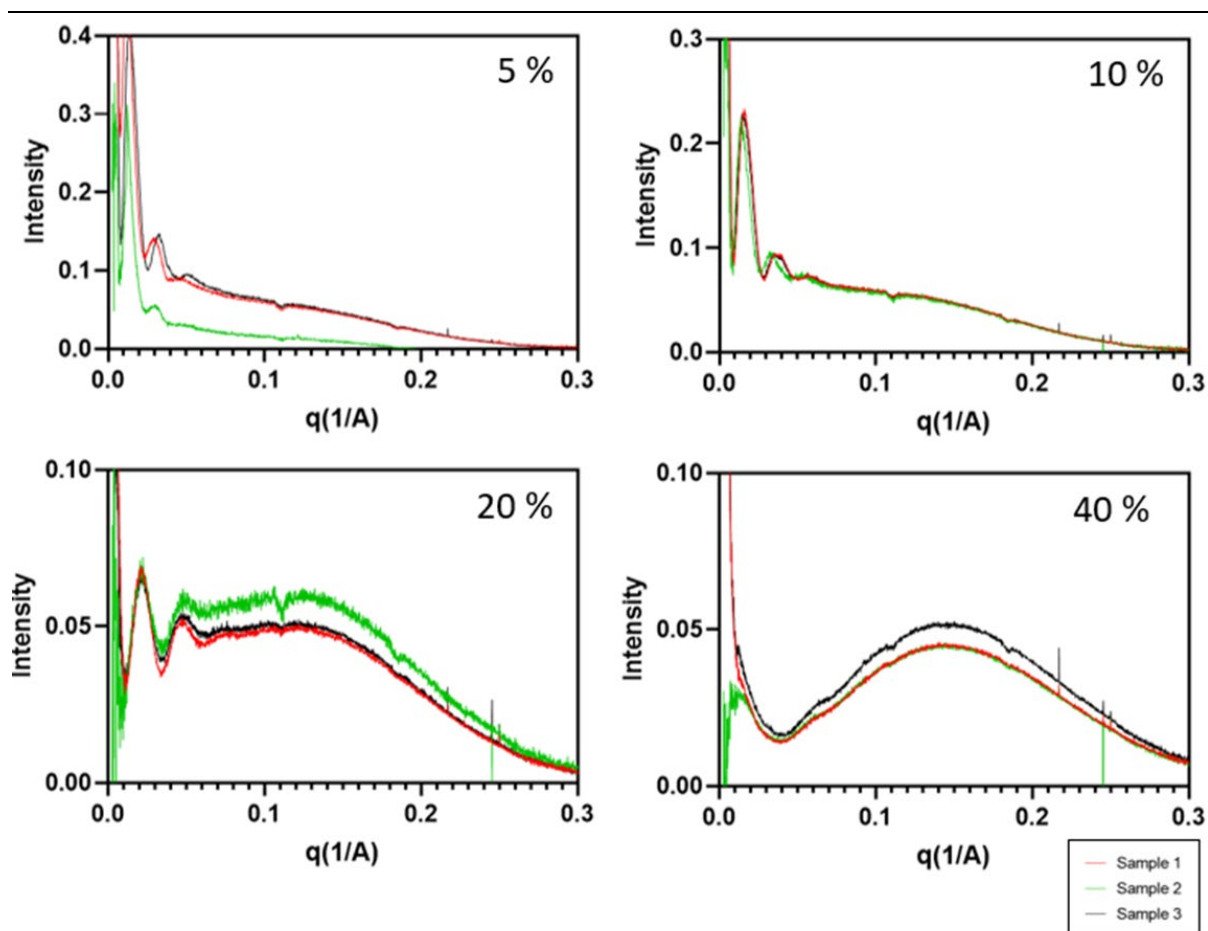
Figure 5.5.5. Chlorpromazine: SAXS profiles of liquid crystalline phases with Nortriptyline incorporated at a range of weight per weight concentrations of 5%, 10%, 20% and 40%. 3 independent samples were analysed by SAXS and plotted individually above.

Table 5.5.5. Phase assignment of chlorpromazine containing formulations, corresponding to the scatter profiles shown in Figure 5.5.5.

Concentration of chlorpromazine (w/w API/glycerol monooleate)	0 %	5 %	10 %	20 %	40 %
Liquid Crystalline Phase Present	Hexagonal	Lamellar/ Sponge	Lamellar/ Sponge	Sponge	Sponge

Broad Bragg peaks can be seen in the low q range correlating to the 1, 2, 3 peaks typical of a lamellar phase. The lamellar phase exhibits a lattice parameter of 31 nm ± 5 nm. The similarities with Clomipramine in the previous section are likely due to these two APIs having very similar physicochemical properties (Table 4.1.1). For 20% and 40% there is sample scattering consistent with a sponge phase across all concentrations, there is also likely the co-existence of a lamellar phase, however the peaks are less clearly defined as with other samples.

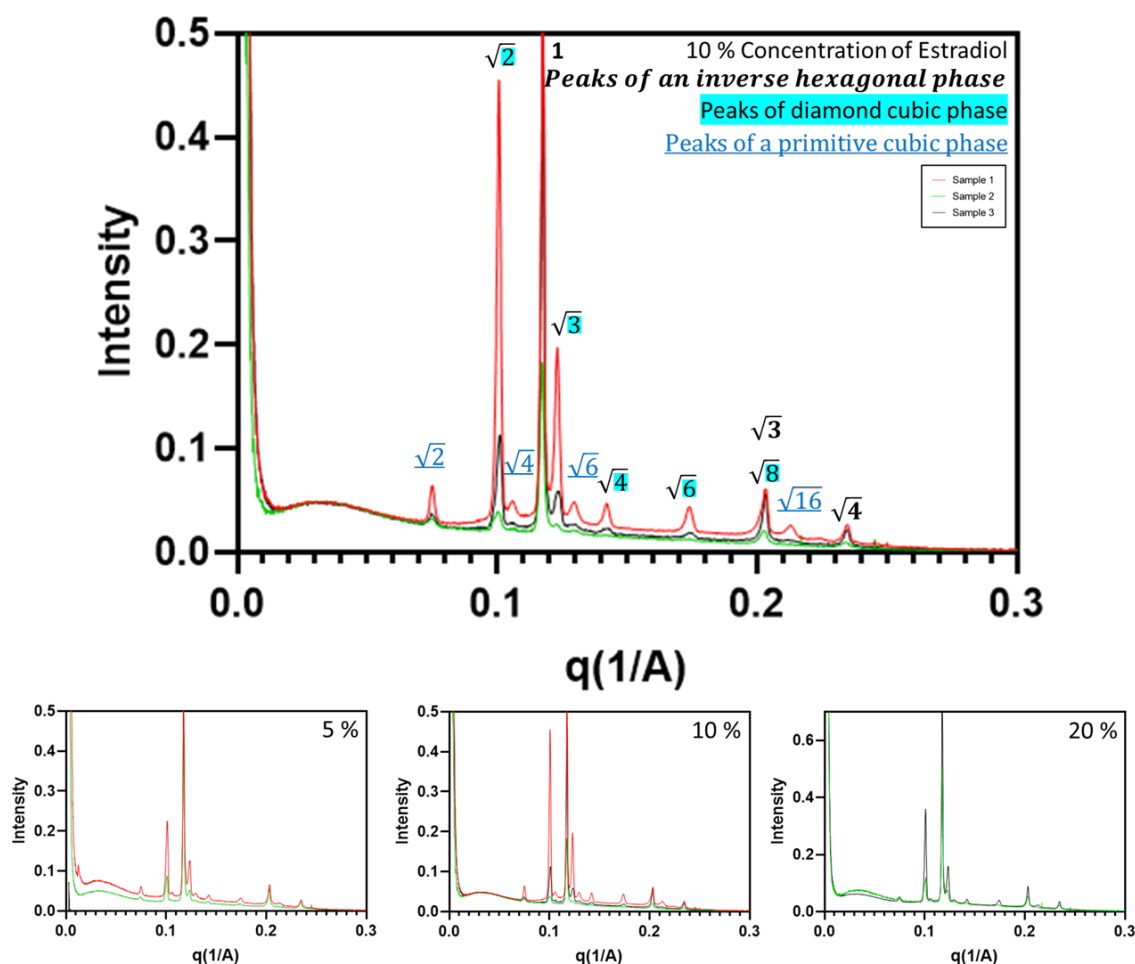### 5.5.1.6. *Haloperidol*
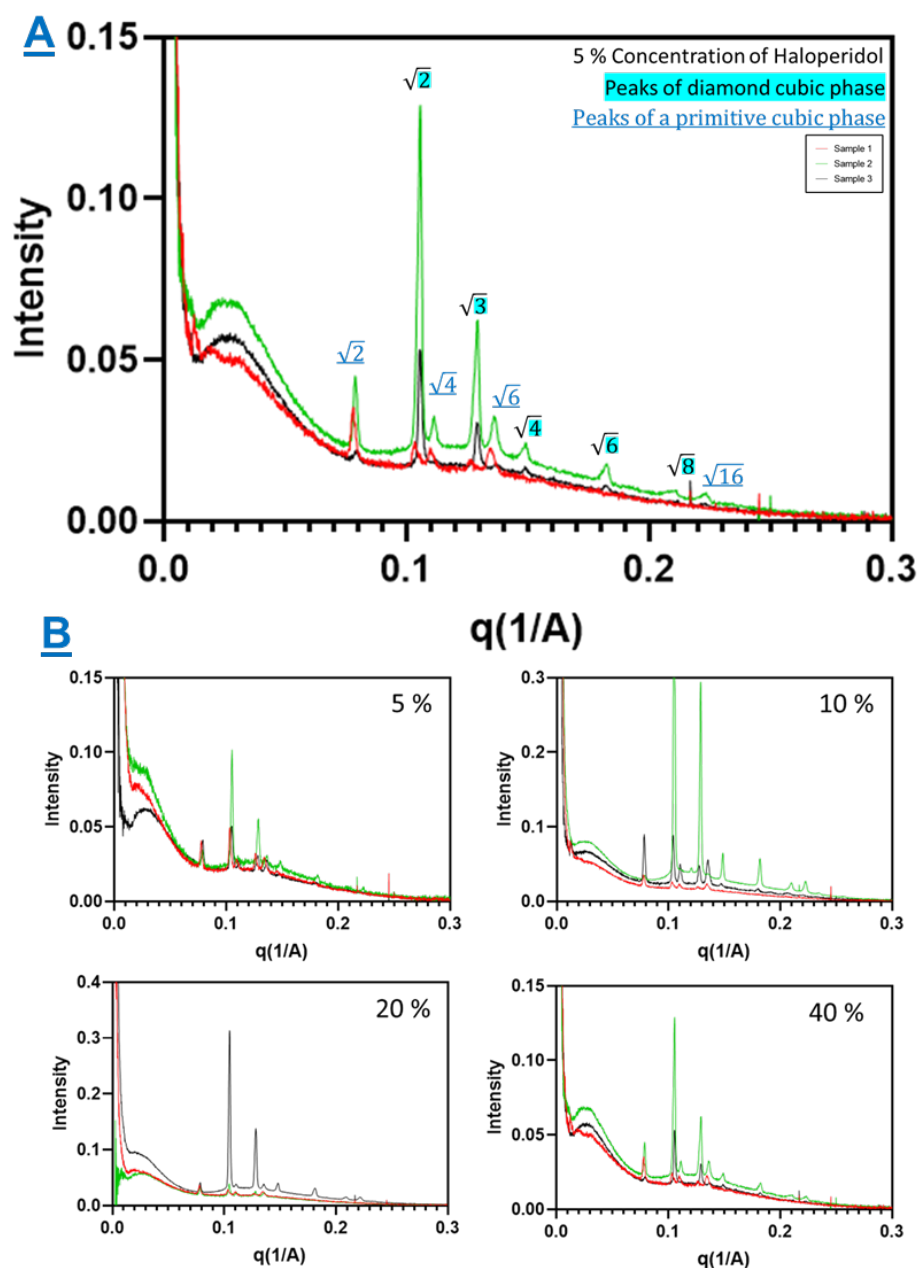
Figure 5.5.6. Haloperidol: SAXS profiles of liquid crystalline phases with Haloperidol incorporated at a range of weight per weight concentrations of 5%, 10%, 20% and 40%. Observed here are both the diamond and primitive. Thus, showing that the presence of Haloperidol induces a phase shift from the hexagonal phase to the cubic phases. No distinctive trend can be observed

with the increasing concentration of Haloperidol 3 independent samples were analysed by SAXS and plotted individually above.

Table 5.5.6. Phase assignment of Haloperidol containing formulations, corresponding to the scatter profiles shown in Figure 5.5.6.

Concentration of Haloperidol (w/w API/glycerol monooleate)	0 %	5 %	10 %	20 %	40 %
Liquid Crystalline Phase Present	Hexagonal	Diamond Primitive	Diamond Primitive	Diamond Primitive	Diamond Primitive

Chapter 4 reports a targeted 10% loading of Haloperidol achieved an encapsulation efficiency of 57.0 ± 23.4%, with an associated loading of 5.7 ± 2.3%.

Observed here is at all concentrations of Haloperidol is the co-existence of hexagonal, diamond and primitive phases. Due to variability between repeat samples at the different concentrations it is not possible to determine any trends in relative peak intensities with varying concentrations. Furthermore, there is no clear change in the relative amount of scattering between samples. Explanations include: a maximum drug loading has been reached at the lower concentrations of Haloperidol, with excess Haloperidol remaining in the buffer not affecting the liquid crystalline structures; or, Haloperidol packs in such a way that the change in the CPP between the actual loading at the theoretical loading of 5-40% is negligible and so does not significantly affect the negative curvature of the system, leading to the same phases being formed and the generation of highly similar scattering profiles.
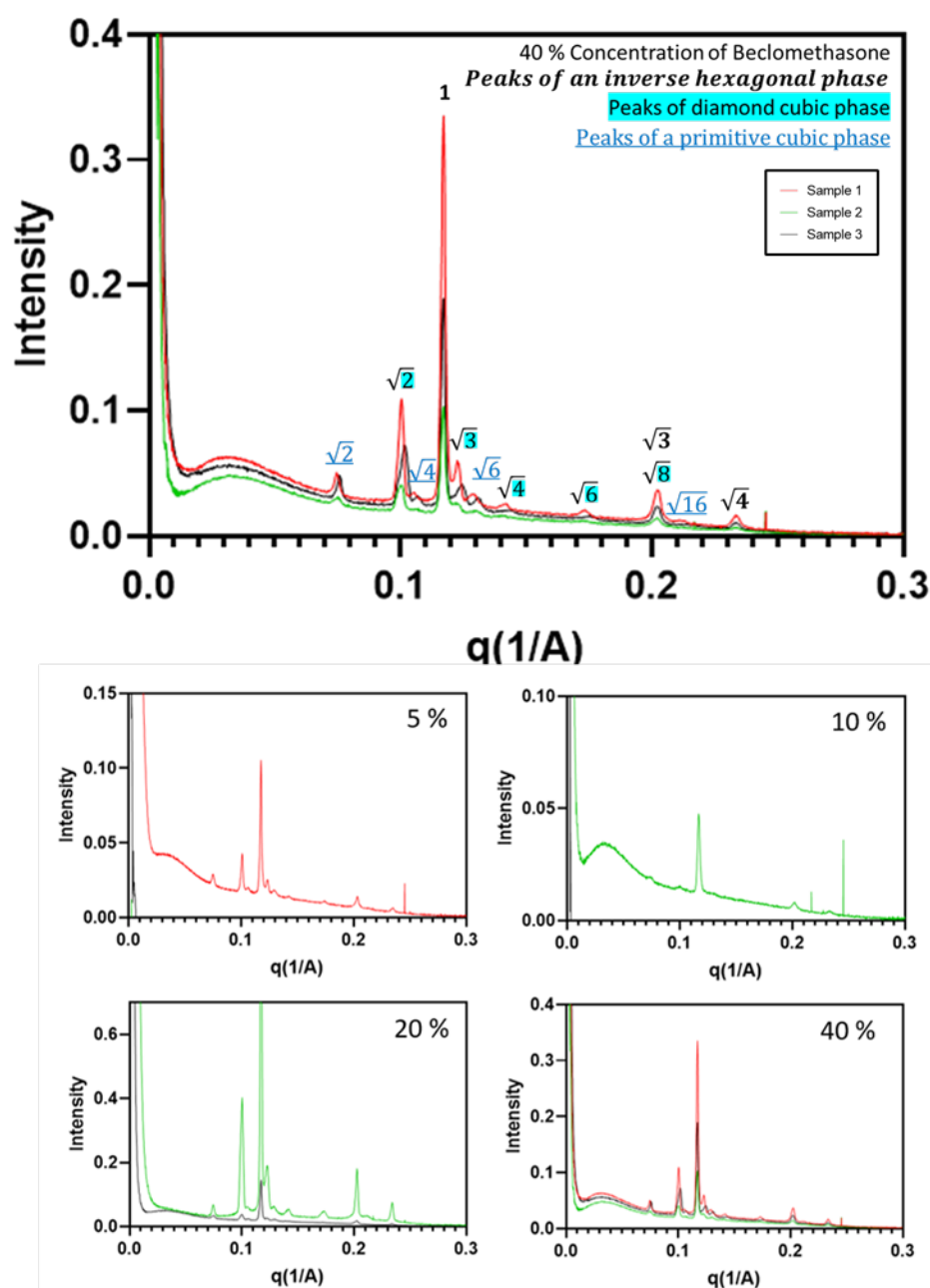
5.5.1.7. *Haloperidol Decanoate*
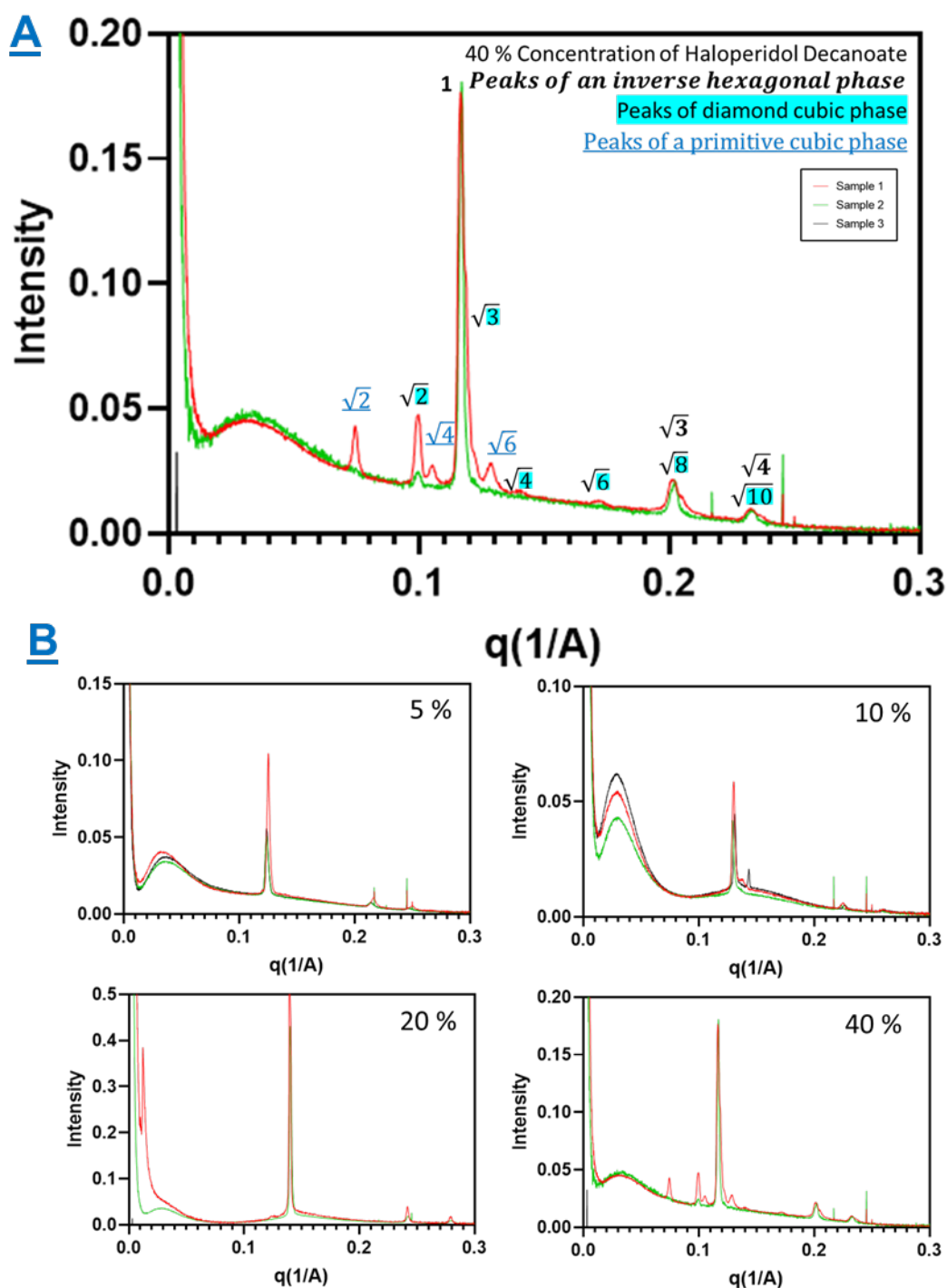
Figure 5.5.7. Haloperidol Decanoate: SAXS profiles of liquid crystalline phases with Haloperidol decanoate incorporated at a range of weight per weight

concentrations of 5%, 10%, 20% and 40%. 3 independent samples were analysed by SAXS and plotted individually above.

Table 5.5.7. Phase assignment of Haloperidol decanoate containing formulations, corresponding to the scatter profiles shown in Figure 5.5.7.

Concentration of Haloperidol decanoate (w/w API/glycerol monooleate)	0 %	5 %	10 %	20 %	40 %
Liquid Crystalline Phase Present	Hexagonal	Hexagonal	Hexagonal	Hexagonal	Hexagonal Diamond Primitive

Chapter 4 reports a targeted 10% loading of Haloperidol decanoate achieved an encapsulation efficiency of 55.5 ± 19.1% and associated API loading of 5.5 ± 1.9%.

Observed here is a hexagonal phase at all concentrations with the emergence of primitive and diamond phases at the higher 40% concentration. Some Bragg peaks, likely from cubic phases are randomly present at the 10 and 20% concentration, however they are not present at sufficient intensity or with additional Bragg peaks from cubic phases to allow for the positive identification of a cubic phase. Thus, the trend present may be described as showing that with an increasing concentration of Haloperidol decanoate there is a decrease in the degree of negative curvature, and hence an increase in the prevalence of the diamond and primitive cubic phases.
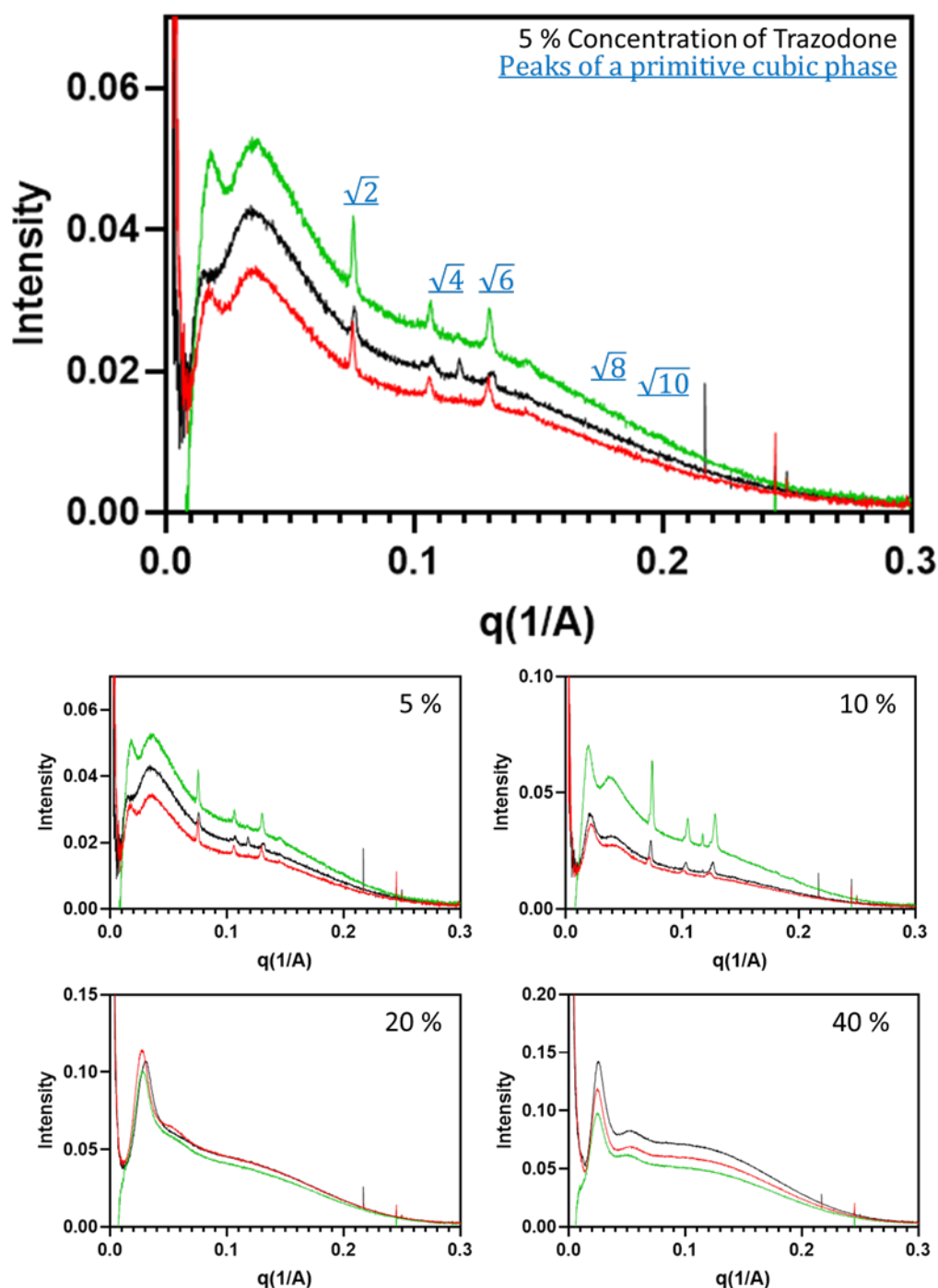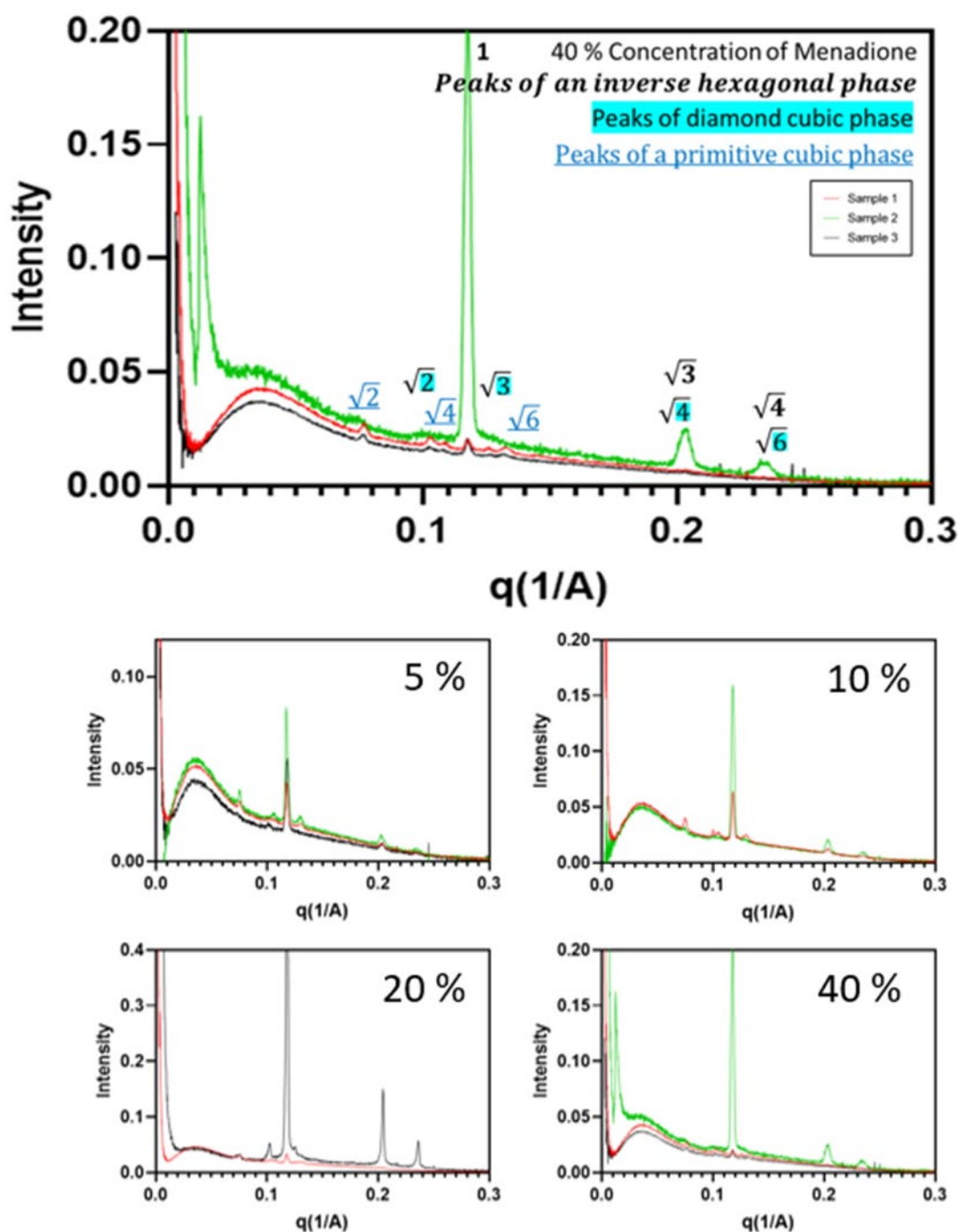
5.5.1.8. *Progesterone*
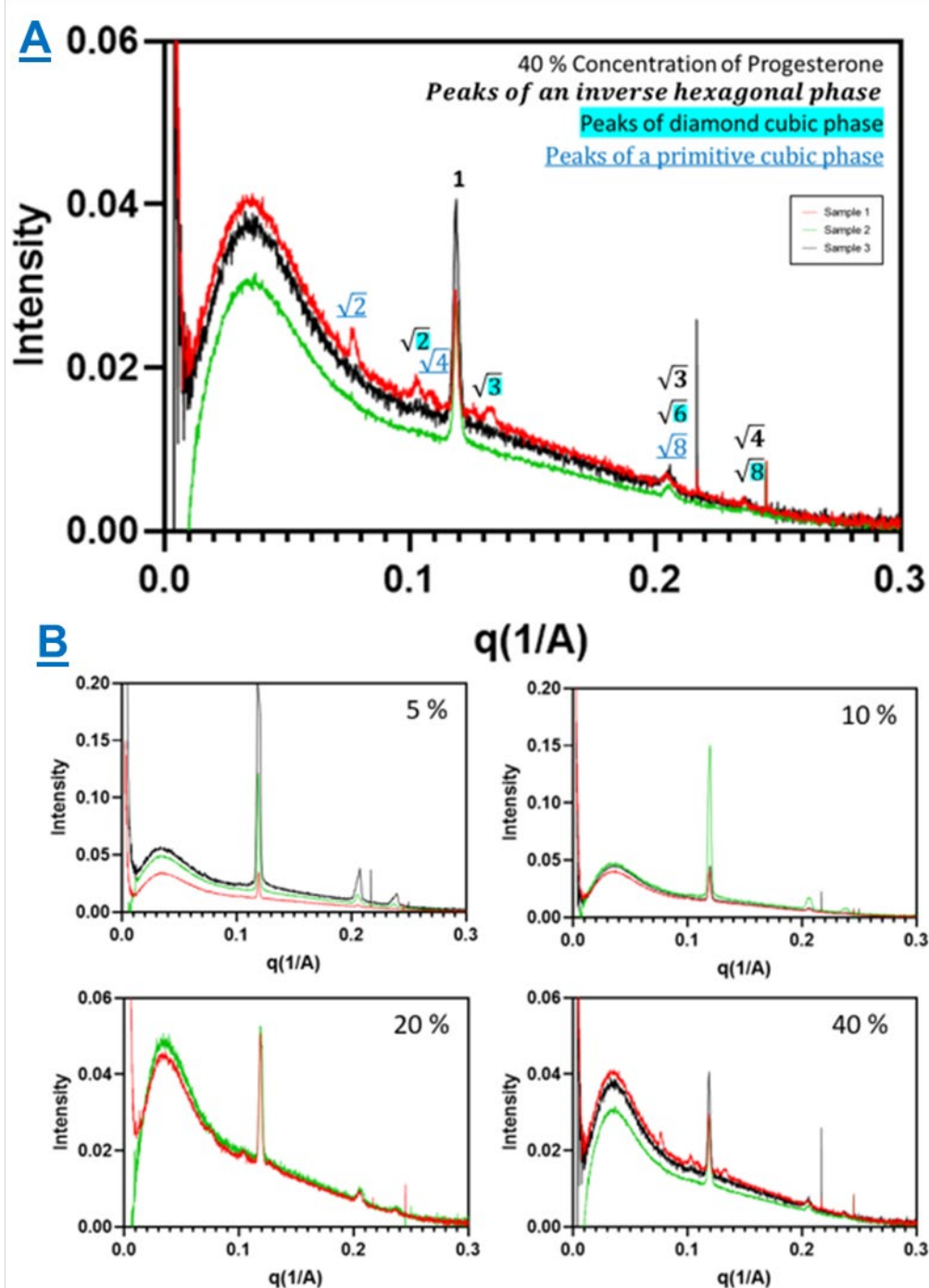
Figure 5.5.8. Progesterone: SAXS profiles of liquid crystalline phases with Progesterone incorporated at a range of weight per weight concentrations of 5%, 10%, 20% and 40%. 3 independent samples were analysed by SAXS and plotted individually above.

Table 5.5.8. Phase assignment of Progesterone containing formulations, corresponding to the scatter profiles shown in Figure 5.5.8.

Concentration of Progesterone (w/w API/glycerol monooleate)	0 %	5 %	10 %	20 %	40 %
Liquid Crystalline Phase Present	Hexagonal	Hexagonal	Hexagonal	Hexagonal Diamond	Hexagonal Diamond Primitive

At all concentrations, a hexagonal phase is formed. At the higher 40% concentration (and sample 1 at the 20% concentration) of Progesterone there are Bragg peaks of the diamond and primitive cubic phases. As these peaks are only distinctive in sample 1 this may indicate that the degree of Progesterone loading at the 40% concentration falls close to a phase boundary. Additionally, as shown by drug loading analysis in Chapter 4 demonstrates that at a 10% w/w loading of Progesterone an encapsulation efficiency of 55.3 ± 11.0 %, there is some variability in the actual drug loading at a given concentration. As most samples feature a hexagonal phase, it may be concluded that the presence of Progesterone in a formulation has a minimal effect upon the critical packing parameter of the system, and it is only with the higher concentrations where an effect can be seen. At the higher concentrations of drug loading, where the emergence of the primitive and diamond cubic phases can be observed, it may be inferred that the Progesterone is making in such a way as to reduce the critical packing parameter and negative curvature of the system. However, it can still be observed that the hexagonal phase at all concentrations, regardless of the presence of the cubic phase, it is indicated that Progesterone packs heterogeneously. Examining sample 1 at the 40%

concentration more in depth and comparing it to its sample 2 and 3 counterparts, the peak 1 of the hexagonal phase decreases in intensity relative to the other two samples. This indicates the direct conversion of some of that hexagonal phase into cubic phases, further aiding the postulation as to the activity of Progesterone in phase formation.

5.5.1.9. *Hydrocortisone*

Figure 5.5.9. Hydrocortisone: SAXS profiles of liquid crystalline phases with

Mefenamic acid incorporated at a range of weight per weight concentrations of

5%, 10%, 20% and 40%. 3 independent samples were analysed by SAXS and plotted individually above.

Table 5.5.9. Phase assignment of Hydrocortisone containing formulations, corresponding to the scatter profiles shown in Figure 5.5.9.

Concentration of Hydrocortisone (w/w API/glycerol monooleate)	0 %	5 %	10 %	20 %	40 %
Liquid Crystalline Phase Present	Hexagonal	Diamond Primitive	Diamond Primitive	Diamond Primitive	Diamond Primitive

Diamond and primitive phase co-exist at all concentrations of Hydrocortisone investigated. Upon referral to Chapter 4 an encapsulation efficiency of 52.3 ± 17.8 % of Hydrocortisone at a 10% w/w drug loading could indicate a reason as to variability between scattering intensities of samples at the same concentration of Hydrocortisone. With other APIs it has been possible to identify a trend in peak intensities that may aid determination as to the impact of drug incorporation upon the nature of the liquid crystalline phases formed, here however the variability between samples at each concentration is inhibitive. However, some determinations may be made as to the overall amount of scattering at each concentration. As the concentration of Hydrocortisone increases the overall degree of scattering decreases. This indicated that at increasing concentrations of Hydrocortisone the Hydrocortisone behaves in a manner as to disrupt the self-assembly of the liquid crystalline phases. But maintained at all concentrations investigated is the influence of Hydrocortisone on the phase(s) being formed. At all concentrations, the Hydrocortisone induces the formation of primitive and diamond cubic phases. A

possibility here that would require further investigation is that the self-assembled structures reach a maximum loading of Hydrocortisone around the 5-10% concentration and the addition of excess Hydrocortisone serves only to disrupt the formation of a liquid crystalline phase as opposed to manipulate it into forming another phase with decreasing curvature. To determine the probability of this further drug loading analysis would be required.
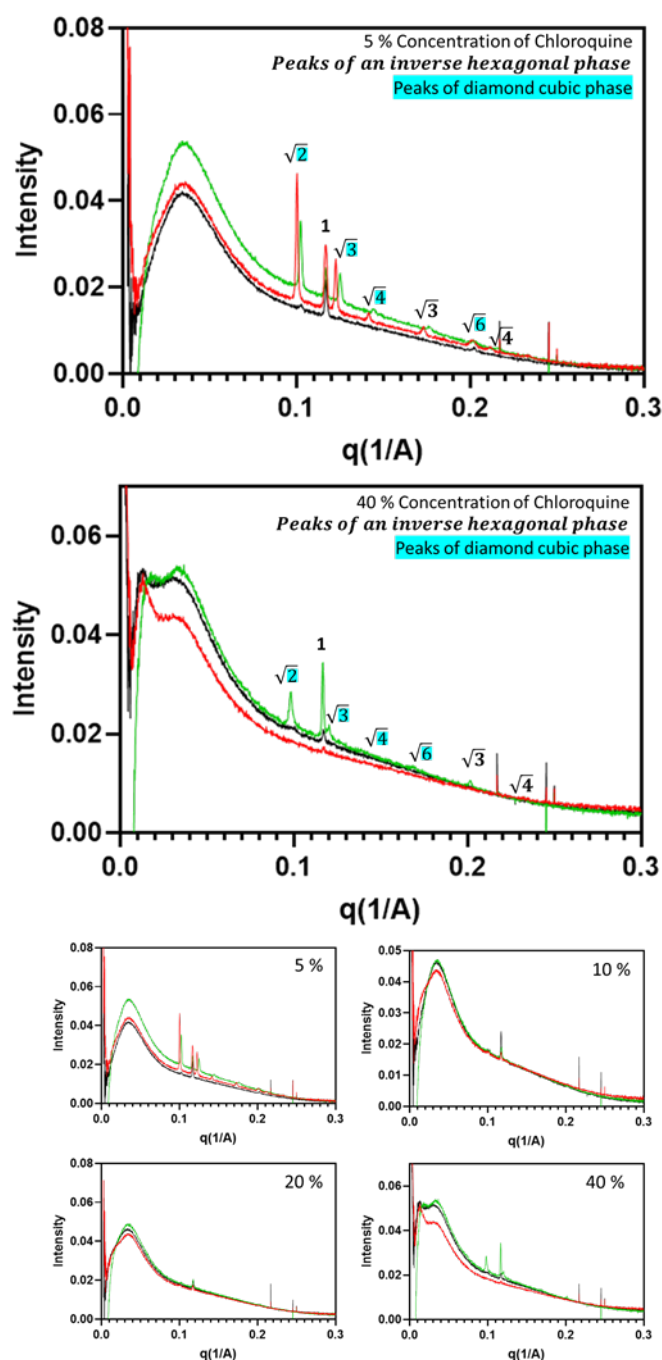
5.5.1.10. *Glipizide*

Figure 5.5.10. Glipizide: SAXS profiles of liquid crystalline phases with

Glipizide incorporated at a range of weight per weight concentrations of 5%,

10%, 20% and 40%. 3 independent samples were analysed by SAXS and plotted individually above.

Table 5.5.10. Phase assignment of Glipizide containing formulations, corresponding to the scatter profiles shown in Figure 5.5.10.

Concentration of Glipizide (w/w API/glycerol monooleate)	0 %	5 %	10 %	20 %	40 %
Liquid Crystalline Phase Present	Hexagonal	Hexagonal Diamond Primitive	Hexagonal Diamond Primitive	Hexagonal Diamond Primitive	Hexagonal Diamond Primitive

Chapter 4 demonstrates that at a 10% w/w loading of Glipizide an encapsulation efficiency of 50.2 ± 9.7 % was achieved with an associated API loading of 5.0 ± 1.0 %

Observed here is at all concentrations of Glipizide is the co-existence of hexagonal, diamond and primitive phases. Due to variability between repeat samples at the different concentrations it is not possible to determine any trends in relative peak intensities with varying concentrations. Furthermore, there is no clear change in the relative amount of scattering between samples. Explanations include: a maximum drug loading has been reached at the lower concentrations of Glipizide, with excess Glipizide remaining in the buffer not affecting the liquid crystalline structures; or, Glipizide packs in such a way that the change in the CPP between the actual loading at the theoretical loading of 5-40% is negligible and so does not significantly affect the negative curvature of the system, leading to the same phases being formed and the generation of highly similar scattering profiles.
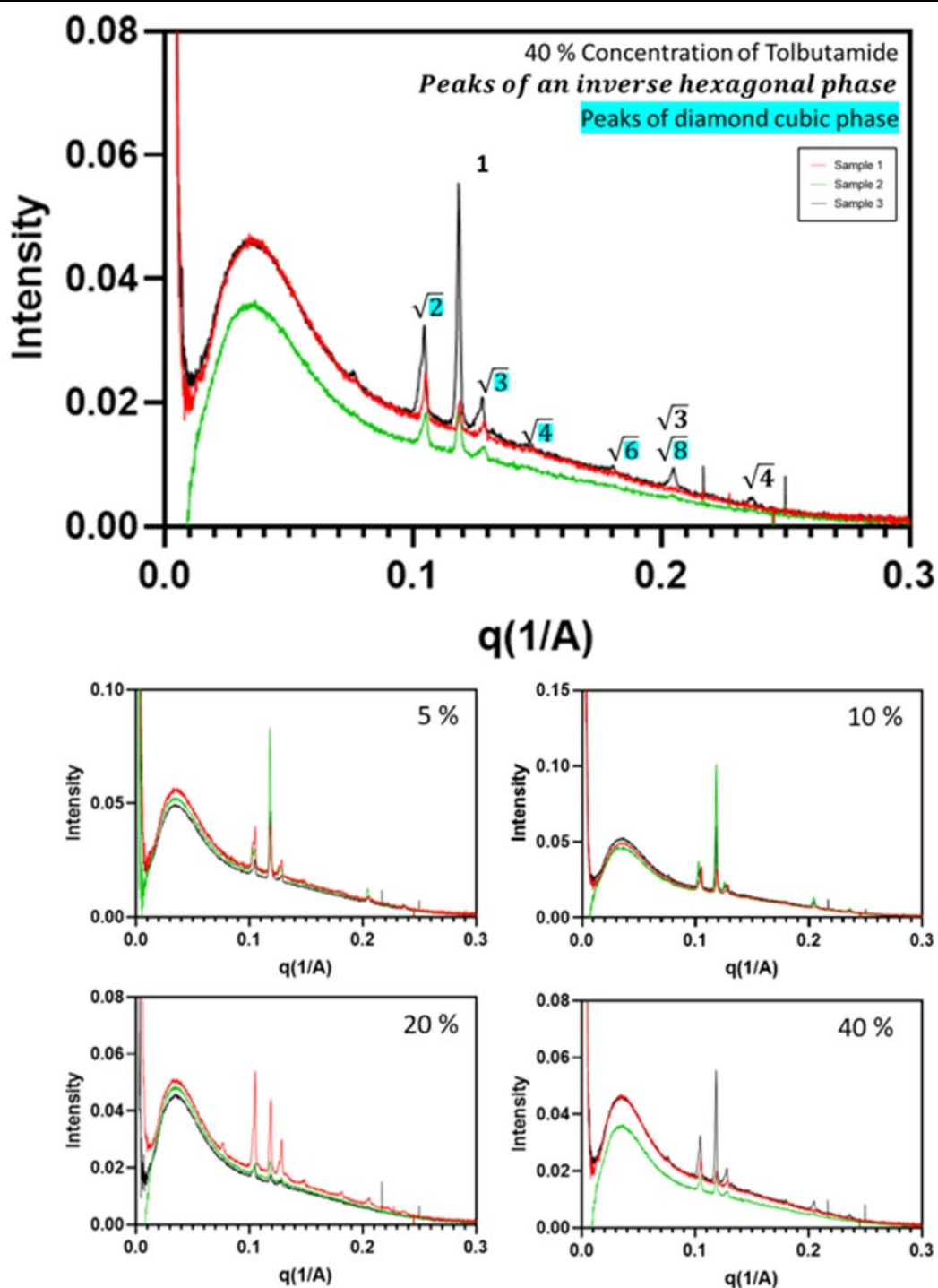
5.5.1.11. *Budesonide*

Figure 5.5.11. Budesonide: SAXS profiles of liquid crystalline phases with Hydrocortisone incorporated at a range of weight per weight concentrations of 5%, 10%, 20% and 40%.

Table 5.5.11. Phase assignment of Budesonide containing formulations, corresponding to the scatter profiles shown in Figure 5.5.11.

Concentration of Budesonide (w/w API/glycerol monooleate)	0 %	5 %	10 %	20 %	40 %
Liquid Crystalline Phase Present	Hexagonal	Diamond Primitive	Diamond Primitive	Diamond Primitive	NA

At the theoretical loading of 40% Budesonide w/w the Budesonide completely disrupts the formation of any structures or caused the sample to behave in such a way that the sample was incompatible with the auto-sampling technology and so no sample was present in the sampling chamber at the time of measurement, as shown by the lack of sample scattering.

At concentrations of Budesonide between a 5% and 20% there are Bragg peaks showing the presence of both diamond and primitive cubic phases. In the samples with a lower concentration of Budesonide comparison of the √2 Bragg peak intensities shows the diamond phase to be the more prominent phase, however, as the concentration of Budesonide increases (apart from sample 3 at the 10% concentration) the relative intensities of the two √2 Bragg peaks alter with the √2 Bragg peak of the primitive phase increasing in intensity, whilst the √2 Bragg peak of the diamond phase decreases. This suggests that within the 5% to 20% window, an increasing concentration of Budesonide decreases the critical packing parameter and reduces the negative curvature of the system, as would be indicated by the transition of the dominance of the diamond phase toward the primitive phase. Further evidence for this effect of Budesonide lies in the transition from a hexagonal

phase when no Budesonide is present to the cubic phases present in the Budesonide containing samples. Chapter 4 reports Budesonide loading at 10% to have an encapsulation efficiency of 37.4 ± 29.6%, this high standard deviation may account for variability in intensity and peak ratios between samples at the same concentration. At the 40% Budesonide loading and sample 2 at the 20% loading no scattering can be observed. This is due to either a complete disruption of any structure, or the formation of a sample not compatible with the BIOSAXS auto-sampling robot. Such non-compatibility may have been due to the formation of sample aggregates or bulk phase formation. Both instances may have inhibited the auto-sampler from drawing liquid sample into the sample chamber of the SAXS instrument, leading to the sampling of air or buffer, either of which would not give measurable scattering after the automated background subtraction.

5.5.1.12. *Fenofibrate*

Figure 5.5.12. Fenofibrate: SAXS profiles of liquid crystalline phases with Fenofibrate incorporated at a range of weight per weight concentrations of 5%, 10%, 20% and 40%. 3 independent samples were analysed by SAXS and plotted individually above. At all concentrations, a hexagonal phase is

observed, without the indication of Bragg peaks from any of the alternative liquid crystalline phases.

Table 5.5.12. Phase assignment of Fenofibrate containing formulations, corresponding to the scatter profiles shown in Figure 5.5.12.

Concentration of Fenofibrate (w/w API/glycerol monooleate)	0 %	5 %	10 %	20 %	40 %
Liquid Crystalline Phase Present	Hexagonal	Hexagonal	Hexagonal	Hexagonal	Hexagonal

At all concentrations of Fenofibrate a hexagonal phase is formed. Showing that at the concentrations analysed Fenofibrate loading has a minimal, or no, effect of the self-assembly of the hexagonal liquid crystalline phase. Chapter 4 demonstrates that at a 10% w/w loading of Fenofibrate an encapsulation efficiency of 37.3 ± 16.2 % was achieved. This informs us of two things: 1) Fenofibrate is present within our structures at the 10 % theoretical loading, and therefore likely present at all the concentrations, albeit at a reduced concentration due to lower encapsulation. 2) Fenofibrate loading is variable within structures upon different repeats. This variability in loading between repeats may account for the variability that can be observed in this figure between the 3 samples at the same theoretical Fenofibrate loading. This variability however also gives evidence that regardless of the degree of Fenofibrate loading a hexagonal phase is still formed. This hence indicates that Fenofibrate packs in such a manner that the CPP is not affected, meaning regardless of Fenofibrate concentration (within the examined range) the CPP will determine a hexagonal phase should be formed.

5.5.1.13. *Dexamethasone*

Figure 5.5.13. Dexamethasone: SAXS profiles of liquid crystalline phases with dexamethasone incorporated at a range of weight per weight concentrations of

5%, 10%, 20% and 40%. 3 independent samples were analysed by SAXS and plotted individually above.

Table 5.5.13. Phase assignment of dexamethasone containing formulations, corresponding to the scatter profiles shown in Figure 5.5.13.

Concentration of dexamethasone (w/w API/glycerol monooleate)	0 %	5 %	10 %	20 %	40 %
Liquid Crystalline Phase Present	Hexagonal	Hexagonal Diamond Primitive	Hexagonal Diamond Primitive	Hexagonal Diamond Primitive	Hexagonal Diamond Primitive

At all concentrations of dexamethasone there is the coexistence of hexagonal, diamond and primitive phases. There is no definitive trend between the ratios of intensity for diamond and primitive associated peaks; however, it is observable that for many samples at a 5-20% concentration of dexamethasone the diamond phase peaks have a greater intensity, but at the 40% concentration the primitive phase peaks have the greater intensity. Peaks corresponding to the hexagonal phase, particularly peak 1, reduces in intensity with an increasing concentration of dexamethasone. These patterns suggest the following suppositions: dexamethasone packs within the self-assembled system in a manner that reduces the CCP, resulting in the conversion of a hexagonal phase to a diamond phase to a primitive phase that is generally observed. The packing of dexamethasone is heterogeneous in nature, this is supported by the large standard deviation reported in Chapter 4 in that at a 10% w/w loading of dexamethasone an encapsulation efficiency of 19.6 ± 7.2 % was achieved. The coexistence of the phases further supports the supposition of heterogeneous packing.

5.5.1.14. *Mefenamic Acid*
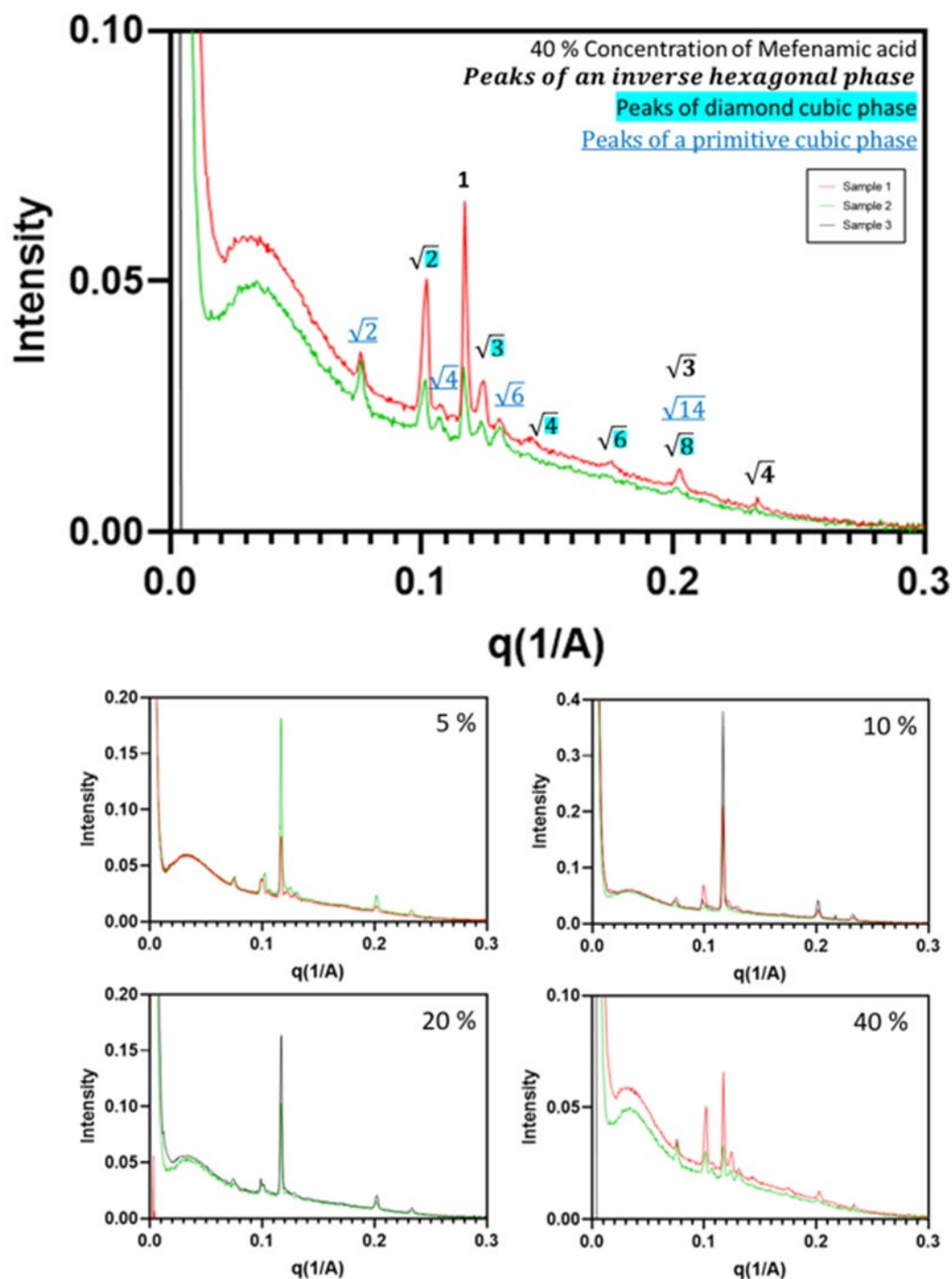
Figure 5.5.14. Mefenamic Acid: SAXS profiles of liquid crystalline phases with Mefenamic acid incorporated at a range of weight per weight concentrations of

5%, 10%, 20% and 40%. 3 independent samples were analysed by SAXS and plotted individually above.

Table 5.5.14. Phase assignment of Mefenamic acid containing formulations, corresponding to the scatter profiles shown in Figure 5.5.14.

Concentration of Mefenamic acid (w/w API/glycerol monooleate)	0 %	5 %	10 %	20 %	40 %
Liquid Crystalline Phase Present	Hexagonal	Hexagonal Diamond Primitive	Hexagonal Diamond Primitive	Hexagonal Diamond Primitive	Hexagonal Diamond Primitive

Observed here is at a concentration of 40% is the coexistence of hexagonal phase, primitive cubic phase, and diamond cubic phase. As the concentration of Mefenamic acid decreases there is a decrease in the intensity of the Bragg peaks associated with the cubic phases present, limiting the ability to identify the cubic phases at Mefenamic acid concentrations below 20% due to Bragg peaks falling below the baseline of non-Bragg peak sample scattering. The 1, $\sqrt{3}$ and $\sqrt{4}$ peaks of the hexagonal phase remain clear in all the scattering profiles containing Mefenamic acid. At the 40% concentration of Mefenamic acid there is a clear shift in intensity away from the hexagonal phase towards the cubic phase. To summarise the observable trend; with an increasing concentration of Mefenamic acid there is an increased prevalence of cubic phase increases, but at this concentration range the overall self-assembled system is not altered to the extent that the hexagonal phase is lost.

Influence of guest drug incorporation upon the self-assembly of liquid crystalline structures.

208

This shift towards the cubic phase is due to a decreased in the critical packing parameter and subsequent decrease in the negative curvature of the system. This is due to either a relative increase in the head area or tail length compared to the tail volume. Due to the hydrophobicity of Mefenamic acid it is likely that this molecule packs between the tails of the glycerol monooleate molecules.

5.5.1.15. *Estradiol*

Figure 5.5.15. Estradiol: SAXS profiles of liquid crystalline phases with Estradiol incorporated at a range of weight per weight concentrations of 5%,

**10%, 20% and 40%. 3 independent samples were analysed by SAXS and
plotted individually above.**

**Table 5.5.15. Phase assignment of Estradiol containing formulations,
corresponding to the scatter profiles shown in Figure 5.5.15.**

Concentration of Estradiol (w/w API/glycerol monooleate)	0 %	5 %	10 %	20 %
Liquid Crystalline Phase Present	Hexagonal	Hexagonal Diamond Primitive	Hexagonal Diamond Primitive	Hexagonal Diamond Primitive

Chapter 4 demonstrates that at a 10% w/w loading of Estradiol an
encapsulation efficiency of 6.0 ± 1.6 % with an associated API loading of 0.6 ± 0.2 %.

Observed here is at all concentrations of Estradiol is the co-existence of
hexagonal, diamond and primitive phases. Due to variability between repeat samples
at the different concentrations it is not possible to determine any trends in relative
peak intensities with varying concentrations. Furthermore, there is no clear change in
the relative amount of scattering between samples. Explanations include: a
maximum drug loading has been reached at the lower concentrations of Glipizide,
with excess Estradiol remaining in the buffer not affecting the liquid crystalline
structures; or, Estradiol packs in such a way that the change in the CPP between the
actual loading at the theoretical loading of 5-40% is negligible and so does not
significantly affect the negative curvature of the system, leading to the same phases
being formed and the generation of highly similar scattering profiles.

Influence of guest drug incorporation upon the self-assembly of liquid crystalline structures.

210

5.5.1.16. *Beclomethasone*

Figure 5.5.16. Beclomethasone: SAXS profiles of liquid crystalline phases with beclomethasone incorporated at a range of weight per weight concentrations of 5%, 10%, 20% and 40%. 3 independent samples were analysed by SAXS and plotted individually above.

Table 5.5.16. Phase assignment of beclomethasone containing formulations, corresponding to the scatter profiles shown in Figure 5.5.16.

Concentration of Glipizide (w/w API/glycerol monooleate)	0 %	5 %	10 %	20 %	40 %
Liquid Crystalline Phase Present	Hexagonal	Hexagonal Diamond Primitive	Hexagonal Diamond Primitive	Hexagonal Diamond Primitive	Hexagonal Diamond Primitive

Observed here is at all concentrations of beclomethasone is the co-existence of hexagonal, diamond and primitive phases. Due to variability between repeat samples at the different concentrations it is not possible to determine any trends in relative peak intensities with varying concentrations. Furthermore, there is no clear change in the relative amount of scattering between samples. Explanations include: a maximum drug loading has been reached at the lower concentrations of beclomethasone, with excess beclomethasone remaining in the buffer not affecting the liquid crystalline structures; or, beclomethasone packs in such a way that the change in the CPP between the actual loading at the theoretical loading of 5-40% is negligible and so does not significantly affect the negative curvature of the system, leading to the same phases being formed and the generation of highly similar scattering profiles.

Influence of guest drug incorporation upon the self-assembly of liquid crystalline structures.

212

5.5.1.17. *Trazodone*

Figure 5.5.17. Trazodone: SAXS profiles of liquid crystalline phases with Trazodone incorporated at a range of weight per weight concentrations of 5%, 10%, 20% and 40%. 3 independent samples were analysed by SAXS and plotted individually above.

Influence of guest drug incorporation upon the self-assembly of liquid crystalline structures.

213

Table 5.5.17. Phase assignment of Trazodone containing formulations, corresponding to the scatter profiles shown in Figure 5.5.17.

Concentration of Trazodone (w/w API/glycerol monooleate)	0 %	5 %	10 %	20 %	40 %
Liquid Crystalline Phase Present	Hexagonal	Primitive	Primitive	Sponge	Sponge

A diamond phase is observed at concentrations of 5% and 10% Trazodone. No Bragg peaks are present at 20% and 40% concentrations, but the presence of sample scattering indicates a sponge phase. The increasing concentration of Trazodone hence appears partnered with a decrease in the negative curvature of the system.

5.5.1.18. *Menadione*

Figure 5.5.18. Menadione: SAXS profiles of liquid crystalline phases with menadione incorporated at a range of weight per weight concentrations of 5%, 10%, 20% and 40%. 3 independent samples were analysed by SAXS and plotted individually above.

Table 5.5.18. Phase assignment of menadione containing formulations, corresponding to the scatter profiles shown in Figure 5.5.18.

Concentration of menadione (w/w API/glycerol monooleate)	0 %	5 %	10 %	20 %	40 %
Liquid Crystalline Phase Present	Hexagonal	Hexagonal Diamond Primitive	Hexagonal Diamond Primitive	Hexagonal Diamond Primitive	Hexagonal Diamond Primitive

Observed here is at a concentration of 40% is the coexistence of a hexagonal phase, a primitive phase, and a diamond cubic phase (sample 2 at this concentration shows only the hexagonal phase). As the concentration of menadione decreases there is a decrease in the intensity of the Bragg peaks associated with the cubic phases present, limiting the ability to identify the cubic phases at menadione concentrations below 20%. The 1, $\sqrt{3}$ and $\sqrt{4}$ peaks of the hexagonal phase remain clear in all the scattering profiles containing menadione, with their relative intensity compared to the cubic phases increasing with a decrease in the concentration. Increasing concentration of menadione increases the prevalence of cubic phases, at this concentration range the overall self-assembled system is not altered to the extent that the hexagonal phase is lost. In the instance of sample 2 at the 40% concentration and sample 3 at the 20% concentration the hexagonal phase is predominant, this is likely due to poor API encapsulation in the specific samples, either due to an anomaly, or at the higher concentration of menadione the menadione may have precipitated out of suspension.

This shift towards the cubic phase is due to a decreased in the critical packing parameter and subsequent decrease in the negative curvature of the system. This is

due to either a relative increase in the head area or tail length compared to the tail volume. Due to the hydrophobicity of menadione it is likely that this molecule packs between the tails of the glycerol monooleate molecules.

5.5.1.19. *Quinine*
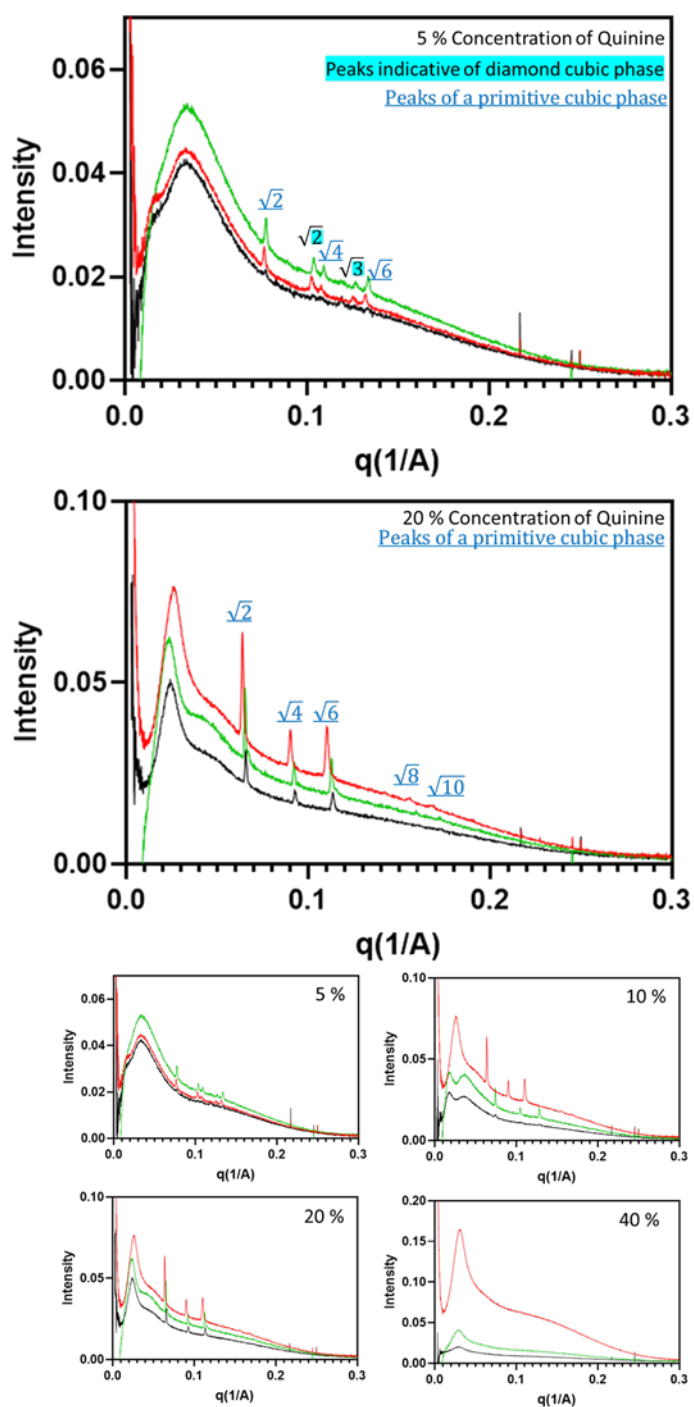
Figure 5.5.19. Quinine: SAXS profiles of liquid crystalline phases with Quinine incorporated at a range of weight per weight concentrations of 5%, 10%, 20% and 40%. 3 independent samples were analysed by SAXS and plotted individually above.

Table 5.5.19. Phase assignment of Quinine containing formulations, corresponding to the scatter profiles shown in Figure 5.5.19.

Concentration of Quinine (w/w API/glycerol monooleate)	0 %	5 %	10 %	20 %	40 %
Liquid Crystalline Phase Present	Hexagonal	Diamond Primitive	Primitive	Primitive	Sponge

At a 40% concentration there are no Bragg peaks observable, however there is solution scattering, indicating a possible sponge phase, or alternative disordered structures. Observed at the 20% and 10% concentrations of Quinine is a primitive phase, at the 5% concentration there is the co-occurrence of an additional phase, likely to be a diamond phase showing $\sqrt{2}$ and $\sqrt{3}$ peaks.

A clear trend in decreasing negative curvature, and associated decrease in the critical packing parameter can be identified here from the transition of hexagonal (0% Quinine) > diamond (5% Quinine) > primitive (5-20% Quinine) > sponge (40% Quinine). This is due to either a relative increase in the head area or tail length compared to the tail volume. Due to the hydrophobicity of Quinine, it is likely that this molecule packs between the tails of the glycerol monooleate molecules.

Influence of guest drug incorporation upon the self-assembly of liquid crystalline structures.

218

5.5.1.20. *Chloroquine*

Figure 5.5.20. Chloroquine: SAXS profiles of liquid crystalline phases with Mefenamic acid incorporated at a range of weight per weight concentrations of 5%, 10%, 20% and 40%. 3 independent samples were analysed by SAXS and plotted individually above.

Table 5.5.20. Phase assignment of Chloroquine containing formulations, corresponding to the scatter profiles shown in Figure 5.5.20.

Concentration of Chloroquine (w/w API/glycerol monooleate)	0 %	5 %	10 %	20 %	40 %
Liquid Crystalline Phase Present	Hexagonal	Hexagonal Diamond	Hexagonal Diamond	Hexagonal Diamond	Hexagonal Diamond

Observed here is a co-existence of both hexagonal and diamond phases, as the concentration of Chloroquine increases the prevalence of the hexagonal phase increases. This may suggest that initially the Chloroquine packs between opposite glycerol monooleate tails, increasing the tail length and subsequently decreasing the critical packing parameter. At concentrations above 5% there is an increase in the critical packing parameter, indicating an increase in the tail volume, this suggests the Chloroquine packs between the tails of neighbouring glycerol monooleate molecules at concentrations above 5%. Further investigation would be required to confirm this theory.

5.5.1.21. *Tolbutamide*

Figure 5.5.21. Tolbutamide: SAXS profiles of liquid crystalline phases with Tolbutamide incorporated at a range of weight per weight concentrations of 5%, 10%, 20% and 40%. 3 independent samples were analysed by SAXS and plotted individually above.

Table 5.5.21. Phase assignment of Tolbutamide containing formulations, corresponding to the scatter profiles shown in Figure 5.5.21.

Concentration of Tolbutamide (w/w API/glycerol monooleate)	0 %	5 %	10 %	20 %	40 %
Liquid Crystalline Phase Present	Hexagonal	Hexagonal Diamond	Hexagonal Diamond	Hexagonal Diamond	Hexagonal Diamond

Observed here is at all concentrations is the coexistence of a hexagonal phase and a diamond cubic phase. As the concentration of Tolbutamide decreases there is a decrease in the intensity of the Bragg peaks associated with the diamond cubic phase, limiting the ability to identify the cubic phases at Tolbutamide concentrations below 20% due to some peaks having an intensity below the baseline. The 1, $\sqrt{3}$ and $\sqrt{4}$ peaks of the hexagonal phase remain clear in all the scattering profiles containing Tolbutamide. An increasing concentration of Tolbutamide correlates to an increased prevalence of cubic phase (at the 40% concentration of Tolbutamide 2 of 3 samples fit this trend), but at this concentration range the overall self-assembled system is not altered to the extent that the hexagonal phase is lost.

This shift towards the cubic phase is due to a decreased in the critical packing parameter and subsequent decrease in the negative curvature of the system. This is due to either a relative increase in the head area or tail length compared to the tail volume.

Chapter 6: Conclusions and Future work

This Chapter summarises the outcome of this work and details the future work possible following the data set and conclusions established here.

6. Conclusions

A liquid crystalline formulation has been developed here with the capabilities of being used for the drug delivery applications. Liquid crystalline particles were identified through a review of the literature as an option for the encapsulation of hydrophobic APIs using lipid-based nanoparticle system. Certain limitations identified within the literature are possible to overcome through the work discussed here. These limitations include: the high energy – high shear fabrication techniques used within the literature. Little comparison of the encapsulation of different guest molecules was found, with a limited understanding of the phase behaviour upon guest molecule encapsulation and encapsulation capabilities, i.e., API encapsulation to system saturation, as potentially identified in the case of Amitriptyline (HPLC studies are required to show this). The aim of this body of work was to identify a formulation and fabrication methodology capable of forming liquid crystalline phase nanoparticles and to subsequently explore API encapsulation and develop an understanding of the interplay between APIs and the molecular structure of liquid crystalline particle.

The primary aim of developing a robust, scalable, and low energy input formulation based on the utilisation of Cithrol GMO was achieved. Differing Synperonics (i.e., F17, P108, L92), Synperonic: Cithrol ratios, and water: Cithrol ratios were explored. It was found that a range of different Synperonics, specifically F127, F108, F88, F87, F68, F38 and P105, had the ability to act as a stabilising agent for formulations without disrupting the liquid crystalline phase. It was found that Synperonic L92 did disrupt formation of the liquid crystalline phase. This surfactant has the highest PPO:PEO ratio amongst tested Synperonics, and this

molecular structure, highly skewed towards hydrophobic PPO, may be the reason for its disruptive properties.

The concentration (w/w compared to GMO) of Synperonic in the formulation relative to the amount of Cithrol was optimised to achieve two goals: 1) to have a stable formulation (i.e., stable during storage, stable to dilution, stable against changing temperatures (15-65 ˚C)) of liquid crystalline nanosized particles. and 2) to not have significant excess free Synperonic in the formulation (Chapter 3, Figure 3.3.3). Here SAXS studies were used to as analytical method to assess the formation of Synperonic micelles in the presence of excess Synperonic. These experiments showed a preferable Synperonic to Cithrol ratio of 1:6 in w/w. For the water to Cithrol ratios, examined in the range from 4 - 20% solid material to water by w/w (Chapter 3, Figure 3.3.2), there was no clear difference in the liquid crystalline structures formed. Any differences seen in Chapter 3 may be considered insignificant as SAXS analysis has a concentration dependence, i.e., SAXS data will show more defined structures at higher concentrations due to higher signal to noise ratios. Therefore, a lipid to water ratio (w/w) was selected based on practicality and usability, particularly in relation to the sample viscosity.

Tailoring of the particle size of fabricated lipid liquid crystalline phase particles was found to be possible by extrusion. Other methods of particle size manipulation were explored, including the alteration of the rate of water addition and mixing speed. Manipulation of particle size through the rate of component addition, as shown in Chapter 3 was found (complete works not shown). Mixing and controlling mixing parameters is highly scalable and used in currently used in industry for LNP formulations, as such it offers a good alternative to extrusion as extrusion has not been established on a large commercial basis (i.e., for the extrusion for litres of

formulation). Future work here could be to examine the use of microfluidics to better control mixing and hence the particle formation kinetics. Of note is that these post-fabrication size manipulation techniques removed the occurrence of sample flocculation.

In subsequent experiment, encapsulation of a range of APIs with different physicochemical properties has been achieved using the established LC phase particle fabrication procedure and template formulation composition. This achieved encapsulation efficiencies of up to 96.4% and API loading of up to 9.6% for Amitriptyline; values were achieved with a targeted loading of 10% w/w (Figure 4.3.7). At higher targeted API loading it was possible to surpass the 9.6% drug loading for Amitriptyline, a maximum API loading however this corresponded to a decreased encapsulation efficiency.

The properties most closely related to API loading are its molecular structure, molecular weight, and hydrogen bonds potential (Figure 4.3.9 in Chapter 4). Additionally, SAXS experiments confirmed the relationship between an increasing API concentration and an increasing effect on the nature of the liquid crystalline phase. The data illustrates that with more API present in the formulation, there is a greater movement of the liquid crystalline phase formed along the hexagonal to diamond to primitive to sponge phase scale, attributed to a decrease in the CPP of the system (Section 5.5). Pearson correlation analysis highlighted the significance of LogS, LogD, Van der Waals volume, as well as surface area and polar surface area of molecules and drug loading upon the phase behaviour. LogS was identified to have the most significant effect upon the nature of liquid crystalline phase formed. As the LogS of an API increases there is a greater movement away from the hexagonal phase towards the sponge phase.

Finally, the release of APIs from the LC particles was assessed with a selection of the APIs. This identified an API release profile, for examined APIs (e.g., Amitriptyline, Propofol, Progesterone, Imipramine, dexamethasone, Hydrocortisone, Haloperidol, and Haloperidol decanoate) that extended over a period of days (more investigation required). A correlation between an API's logD and its release profile was identified. Generally, APIs with logD values between 8.12 and 3.66 (Haloperidol decanoate, Progesterone and Propofol) exhibit sustained release, whilst APIs with logD between 2.93 to -4.64 exhibit initial rapid release in the first 8 hours. This does not exceed 30% release of total API encapsulated, and formulations after the first 8 hours show gradual release. Further API release studies would be required to support this identified trend with release studies performed on addition APIs.

In summary, presented here is the groundwork showing the potential to produce liquid crystalline formulations using a methodology avoiding the use of solvent or high energy homogenisation. It has been shown that a range of small molecular APIs can be encapsulated using this protocol, and that encapsulated APIs. Statistical analysis has then been utilised to show which physicochemical properties of APIs have the greatest influence upon API encapsulation. Structural SAXS studies and subsequent statistical analysis has developed an understanding as to the effect API encapsulation has upon the nature of liquid crystalline phases.

6.1. __Future Work__

There is scope for different streams of research from this body of work. In the first instance the completion of this work should be achieved through the quantification of API's loading in outstanding formulations. This can be achieved through HPLC analysis. A HPLC sample preparation protocol has been established along with many of the protocols required for the various APIs. The data obtained from further studies would allow the better understanding of the links between an API's physicochemical properties and API loading. Additionally, this could aid the analysis of the relationship between API loading and the nature of LC phase, as analysed and discussed in Chapter 5. Further to Chapter 5, it would be advantageous to explore a broader range of API concentrations (for example a 1% to 80% theoretical loading, however only APIs showing high encapsulation at the already formulated 50% should be explored at higher loading percentages) with smaller increments to better understand the location of phase boundaries. This would enable future investigators to have a better understanding of the relationships and interactions between APIs and the liquid crystalline phase. Additionally, examining a broader range of APIs would be desirable, as this would give more data points to ascertain trends and correlations between specific drug physiochemical properties and the resultant effect on the lipid liquid crystal phases and encapsulation capabilities of the formulation. In the future this additional data would, with currently available data, enable the development of a robust model to predict

phase behaviour upon API encapsulation, in addition to allowing the forecasting of API loading values. This may become vital if any distinct differences between the drug delivery capabilities of cubosomes, hexasomes, or spongisomes are identified.

From the literature and investigations here, there is an indication that the encapsulation of hydrophobic or amphiphilic biologics is possible, however a poor encapsulation efficiency was achieved with the lone biologic studied here i.e., Cyclosporine. There is an identified need for this due to the inherent sensitivity and instability of biologics. The gentle fabrication protocol developed in this thesis allows for incorporation of biologics that show sensitivity to high temperatures, sonication, or water/organic solvent interface; future work should be performed to show the application of this process to biological APIs to be successful and appropriate. In doing so, overcoming the drawbacks of liquid crystalline particle fabrication found within the literature that would not be appropriate for the encapsulation of biologics; for example, the heat cycles used in Spicer *et al*.'s cubosome fabrication procedure (and subsequently used by many other researchers) would inevitably lead to protein and RNA degradation. Therefore, it would be highly interesting to investigate the possibility of encapsulating biologics, such as: proteins, peptides, DNA and RNA (142,143). Such investigations would require further physiochemical characterisation of the liquid crystalline phases, with additional analysis as to if the biologic maintains its activity post-encapsulation. If successful this may lead to the ability to safely deliver biological APIs, whilst protecting the API by using a biologically safe nanoparticle carrier.

Current formulations are primed to progress into *in vivo* and *in vitro* testing. This would enable understanding of how the systems may behave if administered to a patient. Crucially this may aid formulation decisions as to using different

Synperonics. As discussed in Sections 1.2.4 and 3.1, different Synperonics have different abilities in facilitating cellular up-take. *In vitro* investigations into different cell lines and *in vivo* experiments will aid in the understanding of the Synperonics up-take facilitation of liquid crystalline particle up-take and if the Synperonic could alter any particle localisation to specific organs. *In vitro* and *in vivo* investigations will allow for an examination as to the formulation's toxicity, immunogenicity and ultimately the formulation's ADME profile. The ADME profile has so far not been fully investigated in the literature to show the metabolism and excretion of the liquid crystalline particles. This would be significant in the application of this formulation for purposes such as RNA vaccines.

There is the potential to select a specific disease indication, or a specific API to progress with, optimising specific formulations to take forward into *in vitro* and *in vivo* testing. It would be practical to examine an optimised formulation, example optimisations may entail reducing particle size to achieve liver targeting, decreasing the surface charge for spleen targeting, or altering the API encapsulation process to achieve higher encapsulation efficiencies. Further investigation is required for the most appropriate route of delivery; however, this may be dependent upon the disease indication and target site. Investigations into formulation stability and bulk behaviour would be required to understand the formulations suitability for delivery via various routes; for example, to ascertain stability in the gastrointestinal tract stability would need to be assessed at different pH.

Chapter 7: References

7. **References**

1. Kulkarni C V., Wachter W, Iglesias-Salto G, Engelskirchen S, Ahualli S. Monoolein: A magic lipid? Vol. 13, Physical Chemistry Chemical Physics. Phys Chem Chem Phys; 2011. p. 3004–21.

2. Salah S, Mahmoud AA, Kamel AO. Etodolac transdermal cubosomes for the treatment of rheumatoid arthritis: Ex vivo permeation and *in vivo* pharmacokinetic studies. Drug Deliv. 2017;24(1):846–56.

3. Peng X, Zhou Y, Han K, Qin L, Dian L, Li G, *et al*. Characterization of cubosomes as a targeted and sustained transdermal delivery system for capsaicin. Drug Des Devel Ther [Internet]. 2015 Aug 3 [cited 2021 Mar 13];9:4209–18. Available from: /pmc/articles/PMC4529266/

4. Barriga HMG, Holme MN, Stevens MM. Cubosomes: The Next Generation of Smart Lipid Nanoparticles? Vol. 58, Angewandte Chemie - International Edition. Wiley-VCH Verlag; 2019. p. 2958–78.

5. Evans DF, Pye G, Bramley R, Clark AG, Dyson TJ, Hardcastle JD. Measurement of gastrointestinal pH profiles in normal ambulant human subjects. Gut. 1988 Aug;29(8):1035–41.

6. Huang Y, Furuno M, Arakawa T, Takizawa S, de Hoon M, Suzuki H, *et al*. A framework for identification of on- and off-target transcriptional responses to drug treatment. Sci Reports 2019 91 [Internet]. 2019 Nov 26 [cited 2021 Nov 7];9(1):1–9. Available from: https://www.nature.com/articles/s41598-019-54180-4

7. Montellano PRO de. Cytochrome P450-activated prodrugs. Future Med Chem [Internet]. 2013 Feb [cited 2021 Oct 11];5(2):213. Available from: /pmc/articles/PMC3697796/

8. Wang Y, Cheetham AG, Angacian G, Su H, Xie L, Cui H. Peptide–Drug Conjugates as Effective Prodrug Strategies for Targeted Delivery. Adv Drug Deliv Rev [Internet]. 2017 Feb 1 [cited 2021 Nov 7];110–111:112. Available from: /pmc/articles/PMC5199637/

9. Han HK, Amidon GL. Targeted prodrug design to optimize drug delivery. AAPS PharmSci [Internet]. 2000 [cited 2021 Nov 7];2(1):48. Available from: /pmc/articles/PMC2751001/

10. De Keizer RJW, De Wolff-Rouendaal D, Van Delft JL. Topical application of 5-Fluorouracil in premalignant lesions of cornea, conjunctiva and eyelid. Doc Ophthalmol. 1986 Dec;64(1):31–42.

11. Naguib YW, Kumar A, Cui Z. The effect of microneedles on the skin permeability and antitumor activity of topical 5-fluorouracil. Acta Pharm Sin B. 2014 Feb 1;4(1):94–9.

12. Benson HAE, Grice JE, Mohammed Y, Namjoshi S, Roberts MS. Topical and Transdermal Drug Delivery: From Simple Potions to Smart Technologies. Curr Drug Deliv [Internet]. 2019 Feb 4 [cited 2021 Nov 7];16(5):444. Available from: /pmc/articles/PMC6637104/

13. Zhi D, Yang T, Zhang T, Yang M, Zhang S, Donnelly RF. Microneedles for gene and drug delivery in skin cancer therapy. J Control Release [Internet]. 2021 Jul 10 [cited 2021 Nov 7];335:158–77. Available from: https://pubmed.ncbi.nlm.nih.gov/33984344/

14. Khan I, Saeed K, Khan I. Nanoparticles: Properties, applications and toxicities. Arab J Chem. 2019 Nov 1;12(7):908–31.

15. Samaridou E, Heyes J, Lutwyche P. Lipid nanoparticles for nucleic acid delivery: Current

perspectives. Vols. 154–155, Advanced Drug Delivery Reviews. Elsevier B.V.; 2020. p. 37–63.

16. Dong Y Da, Larson I, Hanley T, Boyd BJ. Bulk and dispersed aqueous phase behavior of phytantriol: Effect of vitamin E acetate and F127 polymer on liquid crystal nanostructure. Langmuir. 2006 Nov;22(23):9512–8.

17. Rangelov S, Almgren M. Particulate and bulk bicontinuous cubic phases obtained from mixtures of glyceryl monooleate and copolymers bearing blocks of lipid-mimetic anchors in water. J Phys Chem B. 2005 Mar;109(9):3921–9.

18. Silindir-Gunay M, Karpuz M, Ozturk N, Yekta Ozer A, Erdogan S, Tuncel M. Radiolabeled, folate-conjugated liposomes as tumor imaging agents: Formulation and *in vitro* evaluation. J Drug Deliv Sci Technol. 2019 Apr;50:321–8.

19. Man F, Gawne PJ, T.M. de Rosales R. Nuclear imaging of liposomal drug delivery systems: A critical review of radiolabelling methods and applications in nanomedicine. Vol. 143, Advanced Drug Delivery Reviews. Elsevier B.V.; 2019. p. 134–60.

20. Parhiz H, Shuvaev V V., Pardi N, Khoshnejad M, Kiseleva RY, Brenner JS, *et al*. PECAM-1 directed re-targeting of exogenous mRNA providing two orders of magnitude enhancement of vascular delivery and expression in lungs independent of apolipoprotein E-mediated uptake. J Control Release. 2018 Dec;291:106–15.

21. Patel J. Liposomal doxorubicin: Doxil®. J Oncol Pharm Pract. 1996 Dec;2(4):201–10.

22. Barenholz Y. Doxil® - The first FDA-approved nano-drug: Lessons learned. Vol. 160, Journal of Controlled Release. Elsevier; 2012. p. 117–34.

23. Vogel AB, Kanevsky I, Che Y, Swanson KA, Muik A, Vormehr M, *et al*. Immunogenic BNT162b vaccines protect rhesus macaques from SARS-CoV-2. Nature. 2021 Feb;1–7.

24. Baden LR, El Sahly HM, Essink B, Kotloff K, Frey S, Novak R, *et al*. Efficacy and Safety of the mRNA-1273 SARS-CoV-2 Vaccine. N Engl J Med. 2021 Feb;384(5):403–16.

25. Jackson LA, Anderson EJ, Rouphael NG, Roberts PC, Makhene M, Coler RN, *et al*. An mRNA Vaccine against SARS-CoV-2 — Preliminary Report. N Engl J Med. 2020 Nov;383(20):1920–31.

26. Markovic M, Ben-Shabat S, Aponick A, Zimmermann EM, Dahan A. Lipids and lipid-processing pathways in drug delivery and therapeutics. Int J Mol Sci. 2020 May;21(9).

27. Maier MA, Jayaraman M, Matsuda S, Liu J, Barros S, Querbes W, *et al*. Biodegradable lipids enabling rapidly eliminated lipid nanoparticles for systemic delivery of RNAi therapeutics. Mol Ther. 2013 Aug;21(8):1570–8.

28. Wisse E, Jacobs F, Topal B, Frederik P, De Geest B. The size of endothelial fenestrae in human liver sinusoids: Implications for hepatocyte-directed gene transfer. Gene Ther. 2008;15(17):1193–9.

29. Basha G, Novobrantseva TI, Rosin N, Tam YYC, Hafez IM, Wong MK, *et al*. Influence of cationic lipid composition on gene silencing properties of lipid nanoparticle formulations of siRNA in antigen-presenting cells. Mol Ther. 2011;19(12):2186–200.

30. Ali MA, Kataoka N, Ranneh AH, Iwao Y, Noguchi S, Oka T, *et al*. Enhancing the solubility and oral bioavailability of poorly water-soluble drugs using monoolein cubosomes. Chem Pharm Bull. 2017;65(1):42–8.

31. Elnaggar YSR, Etman SM, Abdelmonsif DA, Abdallah OY. Novel piperine-loaded Tween-integrated monoolein cubosomes as brain-targeted oral nanomedicine in Alzheimer's disease:

Pharmaceutical, biological, and toxicological studies. Int J Nanomedicine. 2015 Aug;10:5459–73.

32. Boyd BJ, Whittaker D V., Khoo SM, Davey G. Hexosomes formed from glycerate surfactants-Formulation as a colloidal carrier for irinotecan. Int J Pharm. 2006 Aug;318(1–2):154–62.

33. Kaasgaard T, Drummond CJ. Ordered 2-D and 3-D nanostructured amphiphile self-assembly materials stable in excess solvent. Vol. 8, Physical Chemistry Chemical Physics. The Royal Society of Chemistry; 2006. p. 4957–75.

34. Kim H, Leal C. Cuboplexes: Topologically Active siRNA Delivery. 2015;9(10):10214–26.

35. Rizwan SB, Assmus D, Boehnke A, Hanley T, Boyd BJ, Rades T, *et al*. Preparation of phytantriol cubosomes by solvent precursor dilution for the delivery of protein vaccines. Eur J Pharm Biopharm. 2011 Sep;79(1):15–22.

36. Wadsäter M, Barauskas J, Nylander T, Tiberg F. Formation of highly structured cubic micellar lipid nanoparticles of soy phosphatidylcholine and glycerol dioleate and their degradation by triacylglycerol lipase. ACS Appl Mater Interfaces. 2014 May;6(10):7063–9.

37. Nielsen LH, Rades T, Boyd B, Boisen A. Microcontainers as an oral delivery system for spray dried cubosomes containing ovalbumin. Eur J Pharm Biopharm. 2017 Sep;118:13–20.

38. Boyd BJ, Khoo S-M, Whittaker D V., Davey G, Porter CJH. A lipid-based liquid crystalline matrix that provides sustained release and enhanced oral bioavailability for a model poorly water soluble drug in rats. Int J Pharm. 2007;340(1):52–60.

39. Lopes LB, Ferreira DA, De Paula D, Garcia MTJ, Thomazini JA, Fantini MCA, *et al*. Reverse hexagonal phase nanodispersion of monoolein and oleic acid for topical delivery of peptides: *in vitro* and *in vivo* skin penetration of cyclosporin A. Pharm Res. 2006 Jun;23(6):1332–42.

40. Swarnakar NK, Jain V, Dubey V, Mishra D, Jain NK. Enhanced oromucosal delivery of progesterone via hexosomes. Pharm Res. 2007 Dec;24(12):2223–30.

41. Cherezov V. Lipidic cubic phase technologies for membrane protein structural studies. Vol. 21, Current Opinion in Structural Biology. Curr Opin Struct Biol; 2011. p. 559–66.

42. Azmi IDM, Moghimi SM, Yaghmur A. Cubosomes and hexosomes as versatile platforms for drug delivery. Vol. 6, Therapeutic Delivery. Future Science Ltd; 2015. p. 1347–64.

43. Borné J, Nylander T, Khan A. Effect of lipase on monoolein-based cubic phase dispersion (cubosomes) and vesicles. J Phys Chem B [Internet]. 2002 Oct 10 [cited 2021 Mar 13];106(40):10492–500. Available from: https://pubs.acs.org/doi/abs/10.1021/jp021023y

44. Ganem-Quintanar A, Quintanar-Guerrero D, Buri P. Monoolein: A review of the pharmaceutical applications. Vol. 26, Drug Development and Industrial Pharmacy. Taylor & Francis; 2000. p. 809–20.

45. Gan L, Han S, Shen J, Zhu J, Zhu C, Zhang X, *et al*. Self-assembled liquid crystalline nanoparticles as a novel ophthalmic delivery system for dexamethasone: Improving preocular retention and ocular bioavailability. Int J Pharm. 2010 Aug;396(1–2):179–87.

46. Shi X, Peng T, Huang Y, Mei L, Gu Y, Huang J, *et al*. Comparative studies on glycerol monooleate- and phytantriol-based cubosomes containing oridonin *in vitro* and *in vivo*. Pharm Dev Technol. 2017 Apr;22(3):322–9.

47. Hyde ST, Andersson S, Ericsson B, Larsson K. A cubic structure consisting of a lipid bilayer forming an infinite periodic minimum surface of the gyroid type in the glycerolmonooleat-water system. Zeitschrift für Krist. 1984 Jan;168(1–4):213–9.

48.   Qiu H, Caffrey M. The phase diagram of the monoolein/water system: metastability and equilibrium aspects. Biomaterials. 2000 Feb;21(3):223–34.

49.   Davidson P, Penisson C, Constantin D, Gabriel JCP. Isotropic, nematic, and lamellar phases in colloidal suspensions of nanosheets. Proc Natl Acad Sci U S A. 2018 Jun;115(26):6662–7.

50.   Larsson K. Cubic lipid-water phases: structures and biomembrane aspects. J Phys Chem. 1989 Oct;93(21):7304–14.

51.   Spicer PT, Hayden KL, Lynch ML, Ofori-Boateng A, Burns JL. Novel process for producing cubic liquid crystalline nanoparticles (cubosomes). Langmuir. 2001 Sep;17(19):5748–56.

52.   Akhlaghi SP, Ribeiro IR, Boyd BJ, Loh W. Impact of preparation method and variables on the internal structure, morphology, and presence of liposomes in phytantriol-Pluronic® F127 cubosomes. Colloids Surfaces B Biointerfaces. 2016 Sep;145:845–53.

53.   Salentinig S, Yaghmur A, Guillot S, Glatter O. Preparation of highly concentrated nanostructured dispersions of controlled size. J Colloid Interface Sci. 2008 Oct;326(1):211–20.

54.   Ahmed MZ, Khan UA, Haye A, Agarwal NB, Alhakamy NA, Alhadrami HA, *et al*. Liquid Crystalline Nanoparticles for Nasal Delivery of Rosuvastatin: Implications on Therapeutic Efficacy in Management of Epilepsy. Pharmaceuticals (Basel). 2020 Oct;13(11):1–15.

55.   Mehrabi K, Nowack B, Arroyo Rojas Dasilva Y, Mitrano DM. Improvements in Nanoparticle Tracking Analysis to Measure Particle Aggregation and Mass Distribution: A Case Study on Engineered Nanomaterial Stability in Incineration Landfill Leachates. Environ Sci Technol. 2017 May;51(10):5611–21.

56.   Gerritzen MJH, Martens DE, Wijffels RH, Stork M. High throughput nanoparticle tracking analysis for monitoring outer membrane vesicle production. J Extracell Vesicles. 2017 Dec;6(1).

57.   Sarkar S, Tran N, Rashid MH, Le TC, Yarovsky I, Conn CE, *et al*. Toward Cell Membrane Biomimetic Lipidic Cubic Phases: A High-Throughput Exploration of Lipid Compositional Space. ACS Appl Bio Mater. 2019 Jan;2(1):182–95.

58.   Angelov B, Angelova A, Filippov SK, Drechsler M, Štěpánek P, Lesieur S. Multicompartment lipid cubic nanoparticles with high protein upload: Millisecond dynamics of formation. ACS Nano. 2014 May;8(5):5216–26.

59.   Helvig S, Azmi IDM, Moghimi SM, Yaghmur A. Recent advances in Cryo-TEM imaging of soft lipid nanoparticles. AIMS Biophys. 2015;2(2):116–30.

60.   Barauskas J, Johnsson M, Tiberg F. Self-assembled lipid superstructures: Beyond vesicles and liposomes. Nano Lett. 2005 Aug;5(8):1615–9.

61.   Guillot S, Salentinig S, Chemelli A, Sagalowicz L, Leser ME, Glatter O. Influence of the stabilizer concentration on the internal liquid crystalline order and the size of oil-loaded monolinolein-based dispersions. Langmuir. 2010 May;26(9):6222–9.

62.   Hartnett TE, Ladewig K, Oconnor AJ, Hartley PG, McLean KM. Size and phase control of cubic lyotropic liquid crystal nanoparticles. J Phys Chem B. 2014 Jul;118(26):7430–9.

63.   Sagalowicz L, Acquistapace S, Watzke HJ, Michel M. Study of liquid crystal space groups using controlled tilting with cryogenic transmission electron microscopy. Langmuir. 2007 Nov;23(24):12003–9.

64.   Demurtas D, Guichard P, Martiel I, Mezzenga R, Hébert C, Sagalowicz L. Direct visualization of dispersed lipid bicontinuous cubic phases by cryo-electron tomography. Nat Commun. 2015

Nov;6.

65. Rizwan SB, Dong YD, Boyd BJ, Rades T, Hook S. Characterisation of bicontinuous cubic liquid crystalline systems of phytantriol and water using cryo field emission scanning electron microscopy (cryo FESEM). Micron. 2007 Jul;38(5):478–85.

66. Yaghmur A, Glatter O. Characterization and potential applications of nanostructured aqueous dispersions. Vols. 147–148, Advances in Colloid and Interface Science. 2009. p. 333–42.

67. Liu Z, Luo L, Zheng S, Niu Y, Bo R, Huang Y, *et al*. Cubosome nanoparticles potentiate immune properties of immunostimulants. Int J Nanomedicine. 2016 Jul;11:3571–83.

68. Chong JYT, Mulet X, Keddie DJ, Waddington L, Mudie ST, Boyd BJ, *et al*. Novel steric stabilizers for lyotropic liquid crystalline nanoparticles: PEGylated-phytanyl copolymers. Langmuir. 2015 Mar;31(9):2615–29.

69. Yavlovich A, Singh A, Blumenthal R, Puri A. A novel class of photo-triggerable liposomes containing DPPC:DC 8,9PC as vehicles for delivery of doxorubcin to cells. Biochim Biophys Acta - Biomembr. 2011 Jan;1808(1):117–26.

70. Briuglia ML, Rotella C, McFarlane A, Lamprou DA. Influence of cholesterol on liposome stability and on *in vitro* drug release. Drug Deliv Transl Res. 2015 Jun;5(3):231–42.

71. Chong JYT, Mulet X, Postma A, Keddie DJ, Waddington LJ, Boyd BJ, *et al*. Novel RAFT amphiphilic brush copolymer steric stabilisers for cubosomes: Poly(octadecyl acrylate)-block-poly(polyethylene glycol methyl ether acrylate). Soft Matter. 2014 Sep;10(35):6666–76.

72. Kulkarni C V., Vishwapathi VK, Quarshie A, Moinuddin Z, Page J, Kendrekar P, *et al*. Self-Assembled Lipid Cubic Phase and Cubosomes for the Delivery of Aspirin as a Model Drug. Langmuir. 2017 Sep;33(38):9907–15.

73. Mierzwa M, Cytryniak A, Krysiński P, Bilewicz R. Lipidic Liquid Crystalline Cubic Phases and Magnetocubosomes as Methotrexate Carriers. Nanomater (Basel, Switzerland). 2019 Apr;9(4).

74. Kim DH, Lim S, Shim J, Song JE, Chang JS, Jin KS, *et al*. A simple evaporation method for large-scale production of liquid crystalline lipid nanoparticles with various internal structures. ACS Appl Mater Interfaces. 2015 Sep;7(36):20438–46.

75. Schramm LL. Emulsions, Foams, and Suspensions: Fundamentals and Applications. Emuls Foam Suspens Fundam Appl [Internet]. 2006 Mar 29 [cited 2021 Nov 7];1–448. Available from: https://onlinelibrary.wiley.com/doi/book/10.1002/3527606750

76. Phan S, Fong WK, Kirby N, Hanley T, Boyd BJ. Evaluating the link between self-assembled mesophase structure and drug release. Int J Pharm. 2011 Dec;421(1):176–82.

77. Deshpande S, Venugopal E, Ramagiri S, Bellare JR, Kumaraswamy G, Singh N. Enhancing cubosome functionality by coating with a single layer of poly-ε-lysine. ACS Appl Mater Interfaces. 2014 Oct;6(19):17126–33.

78. Negrini R, Mezzenga R. PH-responsive lyotropic liquid crystals for controlled drug delivery. Langmuir. 2011 May;27(9):5296–303.

79. Wu C, Yang Z, Peng X, Tan Y, Chen M, Zhu X, *et al*. Optimization of the preparation process for an oral phytantriol-based Amphotericin B cubosomes. J Nanomater. 2011;2011.

80. Rarokar NR, Saoji SD, Raut NA, Taksande JB, Khedekar PB, Dave VS. Nanostructured Cubosomes in a Thermoresponsive Depot System: An Alternative Approach for the Controlled Delivery of Docetaxel. AAPS PharmSciTech. 2016;17(2).

81. Han S, Shen J, Gan Y, Geng H, Zhang X, Zhu C, *et al*. Novel vehicle based on cubosomes for ophthalmic delivery of flurbiprofen with low irritancy and high bioavailability. Acta Pharmacol Sin. 2010;31(8):990–8.

82. Liu M, Chen M, Xu P, Yang Z. Nanostructured Cubosomes as a Platform for Oral Drug Delivery. Curr Pharm Biotechnol. 2015 Feb;16(4):313–21.

83. Boyd BJ. Characterisation of drug release from cubosomes using the pressure ultrafiltration method. Int J Pharm [Internet]. 2003 Jul 24 [cited 2021 Nov 16];260(2):239–47. Available from: https://www.researchgate.net/publication/10677839_Characterisation_of_drug_release_from_ cubosomes_using_the_pressure_ultrafiltration_method

84. Chang C, Meikle TG, Drummond CJ, Yang Y, Conn CE. Comparison of cubosomes and liposomes for the encapsulation and delivery of curcumin. Soft Matter [Internet]. 2021 Apr 1 [cited 2021 Nov 16];17(12):3306–13. Available from: https://pubs.rsc.org/en/content/articlehtml/2021/sm/d0sm01655a

85. Libster D, Aserin A, Wachtel E, Shoham G, Garti N. An HII liquid crystal-based delivery system for cyclosporin A: physical characterization. J Colloid Interface Sci. 2007 Apr;308(2):514–24.

86. Libster D, Aserin A, Yariv D, Shoham G, Garti N. Soft matter dispersions with ordered inner structures, stabilized by ethoxylated phytosterols. Colloids Surfaces B Biointerfaces. 2009 Nov;74(1):202–15.

87. Wöhri AB, Johansson LC, Wadsten-Hindrichsen P, Wahlgren WY, Fischer G, Horsefield R, *et al*. A Lipidic-Sponge Phase Screen for Membrane Protein Crystallization. Structure. 2008 Jul;16(7):1003–9.

88. Wadsten P, Wöhri AB, Snijder A, Katona G, Gardiner AT, Cogdell RJ, *et al*. Lipidic Sponge Phase Crystallization of Membrane Proteins. J Mol Biol. 2006 Nov;364(1):44–53.

89. Barauskas J, Misiunas A, Gunnarsson T, Tiberg F, Johnsson M. "Sponge" nanoparticle dispersions in aqueous mixtures of diglycerol monooleate, glycerol dioleate, and polysorbate 80. Langmuir. 2006 Jul;22(14):6328–34.

90. Valldeperas M, Wiśniewska M, Ram-On M, Kesselman E, Danino D, Nylander T, *et al*. Sponge Phases and Nanoparticle Dispersions in Aqueous Mixtures of Mono- and Diglycerides. Langmuir. 2016 Aug;32(34):8650–9.

91. Merclin N, Bender J, Sparr E, Guy RH, Ehrsson H, Engström S. Transdermal delivery from a lipid sponge phase-iontophoretic and passive transport *in vitro* of 5-aminolevulinic acid and its methyl ester. J Control Release. 2004 Nov;100(2):191–8.

92. Rapoport N. Stabilization and activation of Pluronic micelles for tumor-targeted drug delivery. Colloids Surfaces B Biointerfaces. 1999 Nov;16(1–4):93–111.

93. Raval A, Pillai SA, Bahadur A, Bahadur P. Systematic characterization of Pluronic® micelles and their application for solubilization and *in vitro* release of some hydrophobic anticancer drugs. J Mol Liq. 2017 Mar;230:473–81.

94. Akash MSH, Rehman K. Recent progress in biomedical applications of pluronic (PF127): Pharmaceutical perspectives. Vol. 209, Journal of Controlled Release. Elsevier B.V.; 2015. p. 120–38.

95. Pitto-Barry A, Barry NPE. Pluronic® block-copolymers in medicine: From chemical and biological versatility to rationalisation and clinical advances. Vol. 5, Polymer Chemistry. Royal Society of Chemistry; 2014. p. 3291–7.

96. Yaghmur A, De Campo L, Sagalowicz L, Leser ME, Glatter O. Emulsified microemulsions and oil-containing liquid crystalline phases. Langmuir. 2005 Jan;21(2):569–77.

97.   Gagliardi A, Cosco D, Udongo BP, Dini L, Viglietto G, Paolino D. Design and Characterization of Glyceryl Monooleate-Nanostructures Containing Doxorubicin Hydrochloride. Pharmaceutics. 2020 Oct;12(11):1–20.

98.   Salentinig S, Tangso KJ, Hawley A, Boyd BJ. pH-driven colloidal transformations based on the vasoactive drug nicergoline. Langmuir. 2014 Dec;30(49):14776–81.

99.   Dong H, Qin Y, Huang Y, Ji D, Wu F. Poloxamer 188 rescues MPTP-induced lysosomal membrane integrity impairment in cellular and mouse models of Parkinson's disease. Neurochem Int. 2019 Jun;126:178–86.

100.   Sriadibhatla S, Yang Z, Gebhart C, Alakhov VY, Kabanov A. Transcriptional activation of gene expression by pluronic block copolymers in stably and transiently transfected cells. Mol Ther. 2006 Apr;13(4):804–13.

101.   Alakhova DY, Rapoport NY, Batrakova E V, Timoshin AA, Li S, Nicholls D, *et al*. Differential metabolic responses to pluronic in MDR and non-MDR cells: a novel pathway for chemosensitization of drug resistant cancers. J Control Release. 2010 Feb;142(1):89–100.

102.   Magnusson G, Olsson T, Nyberg J-A. Toxicity of pluronic F-68. Toxicol Lett. 1986 Mar;30(3):203–7.

103.   Johnston TP, Miller SC. Toxicological evaluation of poloxamer vehicles for intramuscular use. J Parenter Sci Technol. 1985;39(2):83–9.

104.   Nawaz S, Redhead M, Mantovani G, Alexander C, Bosquillon C, Carbone P. Interactions of PEO-PPO-PEO block copolymers with lipid membranes: A computational and experimental study linking membrane lysis with polymer structure. Soft Matter. 2012 Jul;8(25):6744–54.

105.   Redhead M, Mantovani G, Nawaz S, Carbone P, Gorecki DC, Alexander C, *et al*. Relationship between the affinity of PEO-PPO-PEO block copolymers for biological membranes and their cellular effects. Pharm Res. 2012 Jul;29(7):1908–18.

106.   Amar-Yuli I, Wachtel E, Shoshan E Ben, Danino D, Aserin A, Garti N. Hexosome and hexagonal phases mediated by hydration and polymeric stabilizer. Langmuir. 2007 Mar;23(7):3637–45.

107.   Cox F, Khalib K, Conlon N. PEG That Reaction: A Case Series of Allergy to Polyethylene Glycol. J Clin Pharmacol. 2021 Feb;2021(0):jcph.1824.

108.   Kim H, Song Z, Leal C. Super-swelled lyotropic single crystals. Proc Natl Acad Sci U S A. 2017 Oct;114(41):10834–9.

109.   Angelov B, Angelova A, Drechsler M, Garamus VM, Mutafchieva R, Lesieur S. Identification of large channels in cationic PEGylated cubosome nanoparticles by synchrotron radiation SAXS and Cryo-TEM imaging. Soft Matter. 2015 May;11(18):3686–92.

110.   Zhai J, Suryadinata R, Luan B, Tran N, Hinton TM, Ratcliffe J, *et al*. Amphiphilic brush polymers produced using the RAFT polymerisation method stabilise and reduce the cell cytotoxicity of lipid lyotropic liquid crystalline nanoparticles. Faraday Discuss. 2016;191:545–63.

111.   Zhai J, Waddington L, Wooster TJ, Aguilar MI, Boyd BJ. Revisiting β-casein as a stabilizer for lipid liquid crystalline nanostructured particles. Langmuir. 2011 Dec;27(24):14757–66.

112.   Chountoulesi M, Pippa N, Chrysostomou V, Pispas S, Chrysina ED, Forys A, *et al*. Stimuli-Responsive Lyotropic Liquid Crystalline Nanosystems with Incorporated Poly(2-Dimethylamino Ethyl Methacrylate)-b-Poly(Lauryl Methacrylate) Amphiphilic Block Copolymer. Polymers (Basel). 2019 Aug;11(9).

113. Cherezov V, Clogston J, Misquitta Y, Abdel-Gawad W, Caffrey M. Membrane protein crystallization in meso: Lipid type-tailoring of the cubic phase. Biophys J. 2002 Dec;83(6):3393–407.

114. Caltagirone C, Falchi AM, Lampis S, Lippolis V, Meli V, Monduzzi M, *et al*. Cancer-cell-targeted theranostic cubosomes. Langmuir. 2014 Jun;30(21):6228–36.

115. Duss M, Salvati Manni L, Moser L, Handschin S, Mezzenga R, Jessen HJ, *et al*. Lipidic Mesophases as Novel Nanoreactor Scaffolds for Organocatalysts: Heterogeneously Catalyzed Asymmetric Aldol Reactions in Confined Water. ACS Appl Mater Interfaces. 2018 Feb;10(5):5114–24.

116. Spicer PT, Small WB, Lynch ML, Burns JL. Dry powder precursors of cubic liquid crystalline nanoparticles (cubosomes). J Nanoparticle Res. 2002;4(4):297–311.

117. Zabara A, Chong JTY, Martiel I, Stark L, Cromer BA, Speziale C, *et al*. Design of ultra-swollen lipidic mesophases for the crystallization of membrane proteins with large extracellular domains. Nat Commun. 2018 Dec;9(1).

118. Kim H, Sung J, Chang Y, Alfeche A, Leal C. Microfluidics Synthesis of Gene Silencing Cubosomes. ACS Nano. 2018 Sep;12(9):9196–205.

119. Barauskas J, Johnsson M, Joabsson F, Tiberg F. Cubic phase nanoparticles (cubosome): Principles for controlling size, structure, and stability. Langmuir. 2005 Mar;21(6):2569–77.

120. Murgia S, Falchi AM, Mano M, Lampis S, Angius R, Carnerup AM, *et al*. Nanoparticles from lipid-based liquid crystals: Emulsifier influence on morphology and cytotoxicity. J Phys Chem B. 2010 Mar;114(10):3518–25.

121. Cytryniak A, Nazaruk E, Bilewicz R, Górzyńska E, Żelechowska-Matysiak K, Walczak R, *et al*. Lipidic Cubic-Phase Nanoparticles (Cubosomes) Loaded with Doxorubicin and Labeled with 177Lu as a Potential Tool for Combined Chemo and Internal Radiotherapy for Cancers. Nanomater 2020, Vol 10, Page 2272 [Internet]. 2020 Nov 16 [cited 2021 Nov 7];10(11):2272. Available from: https://www.mdpi.com/2079-4991/10/11/2272/htm

122. Zhang A, Citation Zhang YD. Atomic-resolution transmission electron microscopy of electron beam-sensitive crystalline materials Item Type Article.

123. Martiel I, Sagalowicz L, Mezzenga R. Phospholipid-based nonlamellar mesophases for delivery systems: Bridging the gap between empirical and rational design. Vol. 209, Advances in Colloid and Interface Science. Elsevier; 2014. p. 127–43.

124. Bardag-Gorce F. Effects of ethanol on the proteasome interacting proteins. World J Gastroenterol. 2010 Mar;16(11):1349–57.

125. Brasnett C, Longstaff G, Compton L, Seddon A. Effects of Cations on the Behaviour of Lipid Cubic Phases. Sci Rep. 2017 Dec;7(1).

126. Fraser SJ, Mulet X, Hawley A, Separovic F, Polyzos A. Controlling nanostructure and lattice parameter of the inverse bicontinuous cubic phases in functionalised phytantriol dispersions. J Colloid Interface Sci. 2013;408(1):117–24.

127. Faria AR, Silvestre OF, Maibohm C, Adão RMR, Silva BFB, Nieder JB. Cubosome nanoparticles for enhanced delivery of mitochondria anticancer drug elesclomol and therapeutic monitoring via sub-cellular NAD(P)H multi-photon fluorescence lifetime imaging. Nano Res. 2019 May;12(5):991–8.

128. Boge L, Hallstensson K, Ringstad L, Johansson J, Andersson T, Davoudi M, *et al*. Cubosomes for topical delivery of the antimicrobial peptide LL-37. Eur J Pharm Biopharm. 2019 Jan;134:60–7.

129. Karami Z, Hamidi M. Cubosomes: Remarkable drug delivery potential. Vol. 21, Drug Discovery Today. Elsevier Ltd; 2016. p. 789–801.

130. Eiríksdóttir E, Konate K, Langel Ü, Divita G, Deshayes S. Secondary structure of cell-penetrating peptides controls membrane interaction and insertion. Biochim Biophys Acta - Biomembr. 2010;1798(6):1119–28.

131. Aleandri S, Bandera D, Mezzenga R, Landau EM. Biotinylated Cubosomes: A Versatile Tool for Active Targeting and Codelivery of Paclitaxel and a Fluorescein-Based Lipid Dye. Langmuir. 2015;31(46).

132. Lee J, Kellaway IW. Combined effect of oleic acid and polyethylene glycol 200 on buccal permeation of [D-ala2, D-leu5]enkephalin from a cubic phase of glyceryl monooleate. Int J Pharm. 2000 Aug;204(1–2):137–44.

133. Rizwan SB, McBurney WT, Young K, Hanley T, Boyd BJ, Rades T, *et al*. Cubosomes containing the adjuvants imiquimod and monophosphoryl lipid A stimulate robust cellular and humoral immune responses. J Control Release. 2013 Jan;165(1):16–21.

134. Tran N, Mulet X, Hawley AM, Fong C, Zhai J, Le TC, *et al*. Manipulating the Ordered Nanostructure of Self-Assembled Monoolein and Phytantriol Nanoparticles with Unsaturated Fatty Acids. Langmuir. 2018 Feb;34(8):2764–73.

135. Li SJ, Yamashita Y, Yamazaki M. Effect of electrostatic interactions on phase stability of cubic phases of membranes of monoolein/dioleoylphosphatidic acid mixtures. Biophys J. 2001 Aug;81(2):983–93.

136. Chupin V, Killian JA, de Kruijff B. Effect of phospholipids and a transmembrane peptide on the stability of the cubic phase of monoolein: implication for protein crystallization from a cubic phase. Biophys J. 2003 Apr;84(4):2373–81.

137. Tandon H, Ranjan P, Chakraborty T, Suhag V. Polarizability: a promising descriptor to study chemical–biological interactions. Mol Divers. 2020 Feb;25(1):249–62.

138. Hanafi I, Arafat S, Al Zayed L, Sukkar M, Albeirakdar A, Krayem D, *et al*. Haloperidol (route of administration) for people with schizophrenia. Cochrane Database Syst Rev [Internet]. 2017 Oct 19 [cited 2021 Nov 7];2017(10). Available from: /pmc/articles/PMC6485536/

139. Quraishi SN, David A, Brasil MA, Alheira F V. Depot haloperidol decanoate for schizophrenia. Cochrane database Syst Rev [Internet]. 2000 Jan 25 [cited 2021 Nov 7];1999(2). Available from: https://pubmed.ncbi.nlm.nih.gov/10796438/

140. Astolfi P, Giorgini E, Gambini V, Rossi B, Vaccari L, Vita F, *et al*. Lyotropic Liquid-Crystalline Nanosystems as Drug Delivery Agents for 5-Fluorouracil: Structure and Cytotoxicity. Langmuir. 2017 Oct;33(43):12369–78.

141. Fong WK, Negrini R, Vallooran JJ, Mezzenga R, Boyd BJ. Responsive self-assembled nanostructured lipid systems for drug delivery and diagnostics. J Colloid Interface Sci. 2016 Dec 15;484:320–39.

142. Stevenson HS, Wang Y, Muller R, Edelman DC. Long-term stability of total RNA in RNAstable® as evaluated by expression microarray. Biopreserv Biobank. 2015 Apr;13(2):114–22.

143. Bischof JC, He X. Thermal stability of proteins. Vol. 1066, Annals of the New York Academy of Sciences. Ann N Y Acad Sci; 2006. p. 12–33.

Identifying lipid mesophases from a set of Small-Angle X-Ray Scattering (SAXS) peaks

Christopher Brasnett[1] and Annela Seddon[1,2]

[1]H.H. Wills Physics Laboratory, Tyndall Avenue, University of Bristol, Bristol BS8 1FD
[2]Bristol Centre for Functional Nanomaterials, HH Wills Physics Laboratory, Tyndall Avenue, University of Bristol, Bristol BS8 1FD

January 18, 2018

Abstract

A statistical method of identifying lipid mesophases from Small-Angle X-ray Scattering (SAXS), is described, having been implemented in python code at `https://github.com/csbrasnett/lipidsaxs`

1 Introduction

High-throughput methods of SAXS to identiying the mesophase behaviour of aggregated lipid systems necessarily produce a lot of data. In general - or at least most often - the SAXS patterns such systems produce belong to one of five mesophases: Lamellar, Inverse Hexagonal, and the Primitive, Diamond, and Gyroid cubic phases. They are distinguished through the characteristic spacings of the Bragg peaks present in the SAXS patterns [1]. A consequence of the combination of subtle differences in the characteristic peak spacings, combined with rigorously identifying peaks in 1D azimuthally-integrated SAXS data is that the initial analysis of lipid mesophase data is both time-consuming, and repetitive. The methods described in this paper have been developed and implemented so that less time has to be spent analysing phase behaviour of SAXS data, and more time can be spent on designing experiments.

The Github repository has 4 python scripts: *finder.py*, *detect_peaks.py*, *phase_ID.py*, and *complete.py*. *finder* and *detect_peaks* are responsible for the finding and fitting of Bragg peaks in 1D I vs. q SAXS data, whilst *phase_ID* tries to assign a phase to the collection of Bragg peaks found. *complete* is an example script calling the others in order to demonstrate the type of results that can be expected from the analysis. *complete* has some example parameters in, and only requires a folder of text files of I vs q data in order to run. The exact description of the parameters is contained in this document.

2 Peak identification

The first stage of identifying the mesophase behaviour of lipid systems is necessarily finding the position in q of the Bragg peaks of the scattering pattern. The peak positions are found using the script *finder.py*. *finder.py* requires five variables to be passed to it:

file_name : The location of a text file of the q and Intensity data, formatted into two columns, the first of which is the q data, and the second the I(q).

lo_lim, hi_lim : Cut offs in values of q for the q range to be searched for peaks, and, later, for confirming permitted mesophase assignments.

fig : A switch for whether a graph is produced at the end of the finding routine, showing the data with overlaid lines of the positions in q of where the peaks in the returned array have been found. The figure will only be returned if this value is 1.

1
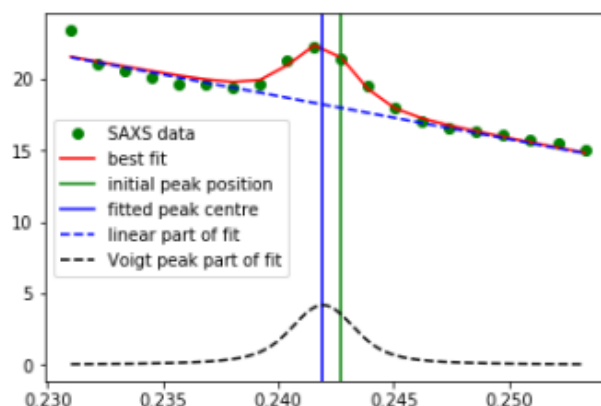
Figure 1: An example of the fitting performance of a Bragg peak. Axes of q vs. I(q). As labeled in the figure, the vertical green line is the initial peak position found by the *detect_peaks.py* script. This initial peak position is passed to the fitting function, along with the data shown as discrete green points. The data are fitted with a convolution of a linear background and a voigt peak, the individual contributions of which are shown as dotted black lines, and shown as a convolution in solid red. The new, 'true' centre of the peak to be returned in an array of total peak positions, at the centre of the fitted Voigt peak, is shown as a vertical solid blue line.

The programme has two functions, finder and fitting. The variables for the fitting function are entirely determined by the routine of the finder. In the first instance, the function uses the *detect_peaks.py* script, written by Marcos Duarte, and made available at `http://nbviewer.jupyter.org/github/demotu/BMC/blob/master/notebooks/DetectPeaks.ipynb`. These are subsequently refined so that the peaks for consideration only lie within the user-defined accepted q range, as given by the **lo_lim** and **hi_lim** variables. However, as the function only finds peaks in discrete values of q, and not always successfully. Therefore, the key aspect of the finding script is using a range of points around the discrete point to fit the data using a peak and background model. The fitting is performed using the *lmfit* library [2]. *lmfit* is not installed as a default library on some common distributions of python (eg. Anaconda), so should be installed or checked for installation before the scripts are used.

The peak and background model used is a convolution of a Voigt peak model, and a linear background, as demonstrated in Fig. 1. The peak model has been found not to work well on its own, due to the fact that the form factor of the SAXS pattern means there is a significant background aspect to the data. Additionally to note is the fact that the gamma parameter of the Voigt peak fit is set to equal the sigma parameter by default. These parameters are used to determine aspects of the peak width in the fit of the data. They can, however, be set to not equal each other to improve the fit, but extensive testing of the free variation of the gamma parameter has not proved fruitful in improving the fitting of SAXS data. Most commonly, it has resulted in the centre of the peak being found very far away from where the true centre is. When the free variation of the gamma parameter is turned off, the data are usually found to fit very well. For more information of the fit, the *lmfit* results table can be returned at each instance of fitting, if so desired, by changing the value of the final **plot** variable in the fitting function, as called in the finding function, to 1. The fitting function then simply returns where the centre of the peak has been found to be.

The set of initial peaks are fitted over a range of fitting widths, so to try to maintain as much information as possible about the data. The set of peak centres found in this way are subsequently tested for degeneracy, to remove peaks very close to each other. The peaks established in this way are then used as the final set of peaks for the data passed to the module, returned as a numpy array. At this point, if the **fig** variable has been set to 1, then a figure of the data with the peak positions overlaid as vertical lines is shown.

The peaks obtained by this module can now be used by the *Phase_ID.py* script to try to determine the mesophase of the sample from which the SAXS data came.

3   Phase Identification

The 5 most common mesophases described earlier have characteristic peak spacings like so:

Lamellar (L$_\alpha$) : 1,2,3

Inverse Hexagonal (H$_{II}$) : 1, $\sqrt{3}$, $\sqrt{4}$

Primitive Cubic (Q$_{II}^P$) : $\sqrt{2}$, $\sqrt{4}$, $\sqrt{6}$, $\sqrt{8}$, $\sqrt{10}$, $\sqrt{12}$, $\sqrt{14}$

Diamond Cubic (Q$_{II}^D$) : $\sqrt{2}$, $\sqrt{3}$, $\sqrt{4}$, $\sqrt{6}$, $\sqrt{8}$, $\sqrt{9}$, $\sqrt{10}$, $\sqrt{11}$

Gyroid Cubic (Q$_{II}^G$) : $\sqrt{6}$, $\sqrt{8}$, $\sqrt{14}$, $\sqrt{16}$, $\sqrt{20}$, $\sqrt{22}$, $\sqrt{24}$

If a set of peaks can be said to belong to a particular mesophase, then the lattice parameter (that is, repeat unit cell spacing) of the mesophase can be subsequently calculated:

Lamellar : $a_{[hkl]} = \frac{2\pi}{q_{[hkl]}}$

Inverse Hexagonal $a_{[hk]} = \frac{2}{\sqrt{3}} \frac{\sqrt{h^2+k^2-hk}}{q_{hk}}$

Cubic phases $a_{[hkl]} = \frac{\sqrt{h^2+k^2+k^2}}{q_{[hkl]}}$

Indeed, most easily, a mesophase can be identified by finding a set of peaks which, when used for the above calculations, and indexed correctly, produce the same value. However, and especially in the case of coexisting systems, this is a laborious method to tackle the identification problem. It is therefore useful to have a process of automatically indexing peaks to identify the mesophase.

Two facts are useful to note at this point:

- The cubic phases more readily scatter to higher-order Bragg peaks, and thus it is useful to know the characteristic ratios to higher order

- Within the characteristic ratios of the cubic phases, there is a good degree of overlap with regards to the Miller indicies that peaks may be assigned.

With respect to these factors, the first step that is taken is to discriminate the possibilities of the phase to assign to any set of peaks by the number of peaks provided to the phase_ID.py programme. If 3 or fewer peaks have been identified, then it is more likely that the data are from a L$_\alpha$ or H$_{II}$ phase than a cubic one[1]. As noted previously, distinguishing between cubic mesophases is a greater challenge than other possibilities, and so the method used for clarification there will be described first.

The entire *phase_ID.py* script can be called from the main function. main expects two variables:

peaks : An array of peak positions

lo_q : The same lo_q value previously used to define the region in which to search for Bragg peaks.

main firstly discriminates what kind of phase to search for by the number of peaks that have been passed to it. This is run in a *while* loop. The *while* loop accounts for the possibility of cubic/non-cubic phase coexistence. If such a situation has arisen, then a greater number of peaks will have been found, of which a subset may be successfully assigned as cubic, but leaving the non-cubic ones. Once the number of peaks is used to determine which sort of phases to search for, the separate functions are called, whose variables and methods are detailed in the following sections. Subsequently, if the number of peaks left unassigned through this search is still greater than 1, the remaining peaks are re-investigated, until either all peaks have been assigned, or until the *while* loop has been run 10 times. Ultimately, the main programme returns a dictionary of the phases found, along with any unassigned peaks.

---

[1] Of course from single crystalline mesophase structures, such as those of the Kim and coworkers [3], there is the possibility of systematic Bragg extinctions, resulting in fewer peaks present anyway
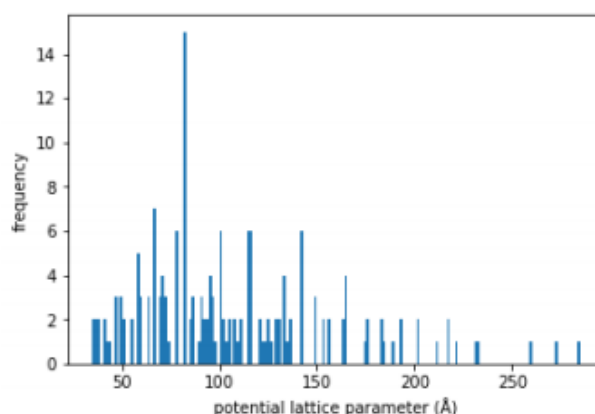
Figure 2: A histogram of all possible lattice constants of a set of input peaks, as a result of indexing every peak with every possible index. There are higher peaks where the same lattice constant has been found more often: one of these will be the correct indexing of the peaks provided.

3.1 The cubic phases

(NB for this section: if a programme variable is described as 'x_', x is being used to describe the set of identical variables at the same stage of the method to separate the P, D, and G variables.)

The function Q_main is used to identify cubic mesophases from the SAXS Bragg peaks found. The Q_main function runs two other functions: Q_possible_phases, and Q_projection_testing, both of whose variables are passed from the Q_main. Q_main expects four variables:

peaks : The array of peaks found in the data, from as determined by the

bin_factor : A factor to determine the widths of the bins in a historgram used for finding lattice parameters of cubic phases. Doesn't have to be big, 2 should suffice.

threshold : A value for which a histogram bin has to be populated more than for confirming that a phase is valid.

lo_q : should be the same as the lo_q value in the finder.py.

Q_main begins by passing all the **peaks**, **bin_factor**, and **threshold** variables to the Q_possible_phases function. Q_possible_phases begins exploring the entire range of possible lattice parameters that could be found from the data, by creating x_init: a set of multidimensional arrays which simulta-neously index all peaks as all x indices. These arrays are then concatenated together. Additionally, n_x are created, along with n. These are arrays of integers running the length of the individual arrays, and the concatenated array. They are later used in order to track back where values in the x_init have originated from: the specific peak and index from which the value arose.

At this point, the frequency of the possible lattice parameters are examined by a histogram: this is where the variable **bin_factor** is used. **bin_factor** is used to determine the widths of the bins, which is defined as the product of the number of possible values and the variable. A value of 2 should suffice for this purpose. As Fig. 2 demonstrates, when a peak has been correctly indexed to calculate the lattice parameter, there are more peaks present in the bin, and therefore the frequency count is higher. It is for this reason a **threshold** variable is passed to Q_possible_phases: if the number of potential lattice parameters in a bin is lower than the threshold, then the bin is discarded, as the indexing has not been correct.

If the number of values in the bin exceeds the **threshold** parameter, then the contents of the bin are examined further. The factors contributing to the height of the bin are traced back to the phase array, peak, and indexing from which they arose. That is to say, across the three cubic phases, it is inevitable that the 'correct' index has been used for a peak: as noted previously, the factors $\sqrt{6}$ and $\sqrt{8}$ appear in all three cubic phase indexings, and consequently, regardless of whichever cubic phase the set of peaks has arisen from, they will both make a 'correct' contribution.

The individual factors are collected separately. At this point, the number of contributing correct indices is used as the comparison for which phase it is most likely to have arisen from. As a result

4
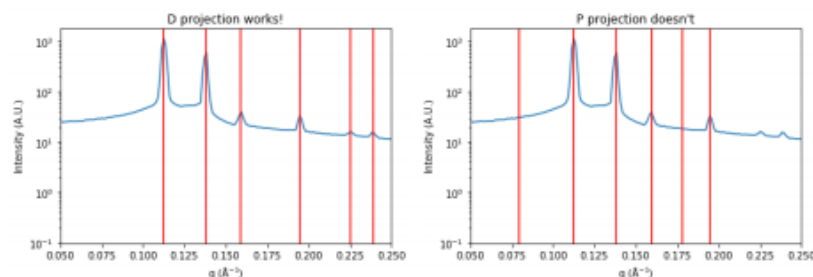
(a) The projected peaks from a Q_{II}^D phase proposed by Q_possible_phases match those found in the data. Note here that for this example, the $\sqrt{4}$ peak was not actually found by the finder.py module, and nor has it been found by the projection shown in this figure, which must be taken care of when considering the acceptable threshold of missing peaks.

(b) The projected peaks of a Q_{II}^P phase fall into gaps in the data, and do not index the final two peaks at all.

Figure 3: Projections of peaks from the proposed phases by the Q_possible_phases function across the data being tested.

of the high coincidence between the factors of the Q_{II}^D and Q_{II}^P phases, they are examined slightly separately. Firstly, it is assumed that 4 peaks is the minimum number required to assign a phase by this point, for any phase. Subsequently, if this condition is met by both the Q_{II}^D and Q_{II}^P contributing factors, they are examined. It would be expected that:

1. The correct assignment of the peaks contains more correct peak indices.

2. The incorrect assignment of index and peak pairs is entirely contained in the correct assignment.

These factors are tested for, and the correct assignment between the Q_{II}^D and Q_{II}^P phases is made based on which conditions are met.

The function described above, Q_possible_phases, returns a dictionary of possible phase assignments back to the Q_main function of the *phase_ID* script. At this point, another check is made, cross referencing the set of assigned peaks with the peaks actually present in the data, by the Q_projection_testing function. The function firstly generates a set of peaks based on the lattice parameter and assigned phase, as worked out from the first Q_possible_phases routine. The function then firstly checks that the first peak of this generated set of peaks falls within the user-determined q search range as initially defined. Secondarily, the function cross references the generated set of peaks (all or most of which will be completely coincidental with the 'real' peaks in the data) with the peaks present in the data.

That is, there are two sets of peaks to consider: one from the actual data itself, and a set of peaks that can be generated by knowing both the phase and lattice parameter of an assigned set of peaks. These latter set of peaks are tested against the peaks that have been similarly assigned to the phase. By identifying where the generated peaks match up to the data, the number of peaks that have been correctly assigned to the phase can be identified. This is apparent in Fig 3, where it can be seen the there is a single Q_{II}^D phase in the data, which has been identified as either Q_{II}^D or Q_{II}^P by the Q_possible_peaks function. The $\sqrt{2}$, $\sqrt{3}$, $\sqrt{6}$, $\sqrt{8}$, and $\sqrt{9}$ peaks were found in the data by the finder.py script, and have been correctly indexed in the case of the Q_{II}^D possible assignment. In the Q_{II}^D projection, the $\sqrt{4}$ peak has additionally been projected, so that visually it matches up in Fig 3a, but is not actually identified for comparison purposes. However, as the first peak is within the accepted search range, and all but one of the peaks are present in the data, the phase assignment (complete with peak indexing) has been confirmed as correct. In the case where the Q_{II}^P phase has been tested, as shown in Fig 3b, it can be seen the there are visual matches on four of the peaks, whilst the proposed $\sqrt{10}$ peak of the Q_{II}^P phase falls at a point where the isn't a peak either in the data, let alone by visual inspection. Notably in this case, it is the $\sqrt{4}$, $\sqrt{6}$, and

5

$\sqrt{16}$ peaks that have been correctly assigned - and matching up with the correctly assigned peaks a factor of $\frac{1}{\sqrt{2}}$ less.[2]

Therefore, the entire set of possible cubic phases have been tested and checked for correct assignment, so if any are present in the dataset of peaks provided to the respective functions, then they should have hopefully been identified by this point.

3.2   Lamellar and Hexagonal phases

As previously highlighted, it might reasonably be expected that for powder scattering, the number of peaks identified in the data will be fewer for non-cubic phase patterns than for cubic-phase structures. If this condition is met in the first instance, then instead of the cubic-phase routines being carried out, a shorter, separate, routine for identifying either L_α or H_{II} mesophases is used. The La_HII_possible_phases function expects only two variables:

peaks : The array of peak positions

bin_factor : A factor to determine bin width of the histogram used for finding lattice parameters of phases.

Overall, the function uses a similar statistical frequency method to the cubic phase routines, but simply distinguishes between which phase has been used by which is the more common value. The incidence between the possible L_α and H_{II} peak assignments coincide such that this statement should always be true if the phase provided to the routine is indeed one of those phases.

4   Acknowledgements

References

[1] C. V. Kulkarni, W. Wachter, G. Iglesias-Salto, S. Engelskirchen, and S. Ahualli, "Monoolein: a magic lipid?," *Phys. Chem. Chem. Phys.*, vol. 13, pp. 3004–3021, 2011.

[2] M. Newville, T. Stensitzki, D. B. Allen, and A. Ingargiola, "LMFIT: Non-Linear Least-Square Minimization and Curve-Fitting for Python," Sept. 2014.

[3] H. Kim, Z. Song, and C. Leal, "Super-swelled lyotropic single crystals," *Proceedings of the National Academy of Sciences*, vol. 114, no. 41, pp. 10834–10839, 2017.

---

[2]In fact, in the case of these data, the Q_{II}^P test failed at the first hurdle: the first peak was outside of the search range.

Table of Figures

Table of Tables

Table of Equations